Aus dem

Institut für Schlaganfall- und Demenzforschung (ISD)

Klinikum der Ludwig-Maximilians-Universität München

Unexpected mechanisms of the MIF/receptor network in activated T cells and neutrophils

Dissertation
zum Erwerb des Doctor of Philosophy (Ph.D.)
an der Medizinischen Fakultät
der Ludwig-Maximilians-Universität München

vorgelegt von

Lin Zhang

aus

Henan / China

Jahr

2025

_____

Erstes Gutachten:	Prof. Dr. Jürgen Bernhagen
Zweites Gutachten:	Priv. Doz. Dr. Dr. Patrick Scheiermann
Drittes Gutachten:	Priv. Doz. Dr. Naoto Kawakami
Viertes Gutachten:	Prof. Dr. Rainer Glaß

Dekan:	Prof. Dr. med. Thomas Gudermann

Tag der mündlichen Prüfung: 25.06.2025

Affidavit

Zhang, Lin
_____

Surname, first name

I hereby declare, that the submitted thesis entitled

Unexpected mechanisms of the MIF/receptor network in activated T cells and neutrophils

is my own work. I have only used the sources indicated and have not made unauthorised use of services of a third party. Where the work of others has been quoted or reproduced, the source is always given.

I further declare that the dissertation presented here has not been submitted in the same or similar form to any other institution for the purpose of obtaining an academic degree.

Munich 29.07.2025
_____

Place, Date

Lin Zhang
_____

Signature doctoral candidate

LUDWIG-
MAXIMILIANS-
UNIVERSITÄT
MÜNCHEN

Dean's Office Medical Faculty
Doctoral Office

Confirmation of congruency between printed and electronic version of the doctoral thesis

Zhang, Lin

Surname, first name

I hereby declare that the electronic version of the submitted thesis, entitled

Unexpected mechanisms of the MIF/receptor network in activated T cells and neutrophils

is congruent with the printed version both in content and format.

Munich 29.07.2025

Place, Date

Lin Zhang

Signature doctoral candidate

Table of contents

List of figures

List of tables

List of abbreviations

ABC	ATP-binding cassette
ACKR3	Atypical chemokine receptor 3
A*t*MDL	*A. thaliana* MIF/*D*-dopachrome-tautomerase-like protein
AMPK	Adenosine monophosphate-activated protein kinase
AIDS	Acquired immunodeficiency syndrome
AhR	Aryl hydrocarbon receptor
APC	Antigen-presenting cell
Bcl 6	B cell lymphoma 6
CD74	Cluster of differentiation 74
CS	Chondroitin sulfate
CXCL	CXC-type chemokine ligand
CXCR	CXC-motif chemokine receptor
DC	Dendritic cell
D-DT	*D*-dopachrome-tautomerase
DN	Double-negative
DP	Double-positive
ER	Endoplasmic reticulum
ELR	Glutamic acid-leucine-arginine
ERK	Extracellular signal-regulated kinase
GPCR	G protein-coupled receptor
HsMIF	*Homo sapiens* macrophage migration inhibitory factor
HVEM	Herpes virus entry mediator
JAB1	c-Jun activation domain-binding protein-1
IRF4	IFN-regulatory factor 4
Ii	Invariant chain

MDL	MIF and D-dopachrome tautomerase-like
MHC	Major histocompatibility complex class
MIF	Macrophage migration inhibitory factor
mTOR	Mammalian target of rapamycin
NF-κB	Nuclear factor-κB
PBMCs	Peripheral blood mononuclear cells
PI3K/Akt	Phosphatidylinositol 3-kinase/protein kinase B
RNA seq	RNA sequencing
TCR	T-cell receptor
Tfh	Follicular helper T cell
Th1	T-helper 1
Th2	T-helper 2
Th9	T-helper 9
Th17	T-helper 17
TGFβ	Transforming growth factor-β
Tr1	Type 1-regulatory T cell
Treg	Regulatory T cell
TRX	Thioredoxin
iTreg	Induced regulatory T cell
pTreg	Peripheral regulatory T cell
tTreg	Thymic regulatory T cell
SNP	Single nucleotide polymorphism
SOJIA	Systemic-onset juvenile idiopathic arthritis
TLR4	Toll-like receptor 4

List of publications

Journal articles

- **Zhang, L.**, Woltering, I., Holzner, M., Brandhofer, M., Schaefer, C. C., Bushati, G., Ebert, S., Yang, B., Muenchhoff, M., Hellmuth, J. C., Scherer, C., Wichmann, C., Effinger, D., Hübner, M., El Bounkari, O., Scheiermann, P., Bernhagen, J., and Hoffmann, A. (2024) CD74 is a functional MIF receptor on activated CD4(+) T cells. *Cell Mol Life Sci* **81**, 296

- Spiller, L., Manjula, R., Leissing, F., Basquin, J., Bourilhon, P., Sinitski, D., Brandhofer, M., Levecque, S., Gerra, S., Sabelleck, B., **Zhang, L.**, Feederle, R., Flatley, A., Hoffmann, A., Panstruga, R., Bernhagen, J., and Lolis, E. (2023) Plant MDL proteins synergize with the cytokine MIF at CXCR2 and CXCR4 receptors in human cells. *Sci Signal* **16**, eadg2621

Poster presentation

- **Zhang, L.**, Abdyli, A., Zhang, Z., Kontos, C., Volta, B., Scheiermann, P., Kapurniotu, A., Bernhagen, J., and Hoffmann, A. Tackling acute lung injury by targeting the MIF inflammation axis. International Neutrophil Symposium 2024, Munich, Germany; 17-19 September, 2024.

1. Introduction

The integrated defense mechanisms of biological organisms comprise sophisticated networks, encompassing both innate and adaptive immune responses. (1-3). Acting as the body's primary protective barrier, the innate immune components against pathogens, providing a rapid but non-specific response to infections. Key players in this system include neutrophils, macrophages, monocytes, and others, which work together to initiate an inflammatory response (4). In contrast, the adaptive immune system is distinguished by its capacity to recognize specific antigens and develop immunological memory (5, 6). This system is facilitated by T and B lymphocytes, which mediate cellular and humoral immunity, respectively (3, 7). Central to both immune branches are cytokines (8, 9). These molecules regulate communication across immune cells, modulating the intensity and duration of immune activity to ensure an effective and coordinated defense (7, 10). One of these cytokines, macrophage migration inhibitory factor (MIF), has been identified as a crucial regulator within this network (11, 12). However, the precise function of MIF in T cells, particularly CD4$^+$ T cells, remains largely unexplored. This thesis seeks to elucidate the MIF/receptor signaling network in activated T cells, with a specific emphasis on its functions and implications in CD4$^+$ T cells.

1.1. CD4$^+$ T cells

CD4$^+$ T cells, also known as helper T cells, are fundamental elements of the adaptive immune system, coordinating the activities of various immune cells and driving diverse immune responses (13). Their defining characteristic lies in the presence of the T cell receptor (TCR), which engages with major histocompatibility complex class II (MHC-II) molecules on antigen-presenting cells (APCs) (14). Upon recognizing a specific antigen, CD4$^+$ T cells activate and subsequently differentiate into various functional categories that shape the immunological responses (13, 15). The profound impact of CD4$^+$ T cells on both protective immunity and immunopathology makes them an essential focus of study, particularly in understanding immune-related diseases and potential therapeutic interventions(16) .

1.1.1 CD4$^+$ T-cell development

T lymphocytes originally derived from hematopoietic stem cells located in the bone marrow and subsequently migrate to the thymus (17). In the initial stages of development, T cells within the thymus do not express the TCR or co-receptors CD4 and CD8, termed double-negative (DN) thymocytes. During multiple DN stages, thymocytes begin to express pre-TCR complex. Successful expression of the pre-TCR induces substantial proliferation of thymocytes, facilitating the transition toward the double-positive (DP) stage(CD4$^+$CD8$^+$) (18). The fate of DP thymocytes is determined by their interaction with cortical epithelial cells presenting MHC I and II molecules complexed with self-peptides (19). Only appropriate TCR signaling promotes positive selection, enabling thymocytes to mature (18, 20). Thymocytes binding self-peptide-MHC I molecules differentiate into CD8$^+$ T cells, whereas those binding self-peptide-MHC II molecules develop into CD4$^+$ T cells. Subsequently, negative selection in the thymic medulla eradicates thymocytes that demonstrate excessively strong affinities for self-antigens, ensuring the development of self-tolerance (21). Following this selection process, the surviving thymocytes are matured and prepared for export to peripheral lymphoid tissues, in which they are termed naive T cells.

1.1.2 CD4$^+$ T-cell activation and differentiation

Naive CD4$^+$ T cells remain quiescent within secondary lymphoid structures until they engage with their specific antigen presented by APCs. Major APC types of categories encompass B lymphocytes, macrophages, and dendritic cells (DCs), all of which can present antigens using MHC I or MHC II pathways (22, 23). The recognition of MHC class II-bound antigens by CD4$^+$ T lymphocytes occurs through their TCRs. This initial recognition event triggers the onset of lymphocyte activation (24). Nevertheless, TCR engagement alone is insufficient to trigger complete CD4$^+$ T cell activation. The activation process also needs co-stimulatory signals provided by stimulatory molecules. Without these essential accessory molecule-coreceptor interactions providing critical signals, this engagement may lead to unresponsiveness in naive lymphocytes (25). Among these interactions, the binding across T cell-expressed CD28 and APC-displayed B7 proteins (CD80/CD86) represents a crucial co-stimulatory pathway (26, 27). Upon activation, the T cell expresses various proteins that help sustain or modu-

late the co-stimulatory signals necessary for driving clonal expansion and differentiation. The CD40 ligand represents one such protein, which interacts with APC-expressed CD40 (28). This molecular partnership enhances T cell responses while promoting B7 expression on APCs. Additional pathways supporting T cell activation include the 4-1BB/4-1BBL axis and ICOS/LICOS interactions (29-32). However, cytotoxic T-lymphocyte associated protein 4 (CTLA-4) functions as a regulatory mechanism by competing for B7 molecules with an affinity 20 times stronger than that of CD28, delivering inhibitory signals that help maintain immunologic homeostasis (33, 34). Furthermore, T cell function and activation are also modulated by various membrane proteins, along with genetic and epigenetic mechanisms (35, 36). Upon achieving full activation status, T cells exhibit alterations in their surface protein expression profile. Several molecules serve as indicators of T-cell activation, including CD69, HLA-DR and CD25 (37-39) (Table 1).

Table 1. Main characteristics of T-cell activation markers. This table compiles data from various studies, presenting a detailed overview of key T-cell activation markers, their peak expression times, and functional roles (40-43).

Activation maker	Optimal expression time	Function
CD69	Peaks ~ 24 hours	Early activation marker; modulation retention in lymphoid tissues
CD25	Peaks ~ 96 hours	High-affinity IL-2 receptor; T-cell proliferation and survival; a marker for Treg cells
HLA-DR	Peaks ~ 120 hours	T-cell recognition and activation

The differentiation trajectory of activated helper T cells is orchestrated through an intricate interplay of multiple signaling cascades, encompassing TCR activation, cytokine signaling networks, costimulatory pathways, chemokine gradients, integrin-mediated adhesion, and metabolic cues (44). These signals collectively direct the development of distinct effector populations, including the canonical Th (T helper) 1 and Th2 subsets, along with more recently characterized lineages such as Th17, regulatory T cells (Tregs), follicular helper T cells (Tfh), Th9, and Th22 populations (44-47) (See Figure 1).

The initial classification of CD4 T$^+$ cells was established in mice built on patterns of lymphokine activity production, dividing them into two populations: Th1 and Th2. Th1 generated IFN-γ, IL-2, IL3 and GM-CSF, whereas Th2 cells produce IL-3, BSF-1 and mast cell growth factor 2 (MCGF2) (48). Subsequent research established the instrumental role of specific cytokines in directing lineage commitment. The presence of IL-4 alongside IL-2 emerged as crucial determinants in effector subset specification (49, 50). IL-4 is crucial for developing Th2-like effectors that produce IL-4 and IL-5. In contrast, IL-2 fosters Th1-like effector development, maintaining the secretion of IL-2 and IFN-γ (49). Moreover, heat-killed *Listeria monocytogenes* could induce Th1 differentiation in vitro through macrophage-derived interleukin-12 (IL-12), correlating with in vivo observations of Th1-predominant responses to *Listeria monocytogenes* (51). These findings underscore how innate immune responses to microbial challenges guide appropriate T helper cell polarization. Whether the Th1 and Th2 phenotypes also exist in humans has generated considerable scientific interest. In 1991, a study showed that T cells isolated from human peripheral blood could also develop into Th1 or Th2 in different infectious agents, and consistency maintains the functional phenotype in vitro (52). Moreover, in allergic respiratory disorder patients, inhaling grass pollen allergens leads to the activation of Th2 within the respiratory mucosa, which is verified that Th2 can be found in vivo in humans (53). The molecular control of these lineages involves specific transcriptional regulators. T-bet / Eomes directs Th1 development, while GATA3 regulates Th2 differentiation (54, 55). With the T-bet gene knocked out, Th1 differentiation is significantly compromised (56). Similarly, GATA3 absence completely abolishes Th2 differentiation (57-60). Moreover, GATA3 drives Th2 differentiation by directing Th2 lineage commitment, selectively stimulating Th2 cell growth, and simultaneously suppressing Th1 differentiation (61).

Th17 cells as a distinct CD4$^+$ T lymphocyte expanded the classical Th1/Th2 dichotomy (62, 63). Furthermore, Th17 cells release IL-21, enhancing interaction with other immune cells (64, 65). Additionally, in Th17 cell differentiation, cytokines play a sequential and multilayered role, with early signals from transforming growth factor β (TGF-β) and IL-6 initiating this process, followed by contributions of IL-21 and IL-23 at later stages to further facilitate and maintain the Th17 phenotype(13). The transcriptional regulation of Th17 differentiation centers on retinoid-related orphan receptor-

γt (RORγt), whose expression sufficiently induces IL-17 production in naive CD4$^+$ populations (66). The functional significance of RORγt is evidenced by marked IL-17 reduction in RORγt-deficient lymphocytes (66, 67). The cooperative activity of RORγt and RORα in driving IL-17 expression becomes apparent through their concurrent deletion, which completely abrogates IL-17 production (67, 68). Th17 cells demonstrate significant involvement across diverse pathological conditions, spanning autoimmune disorders, neuroinflammation, oncological processes, and allograft rejection (69, 70).

Tregs were found as the fourth lineage of CD4$^+$ T cells (71). Foxp3 positive Tregs can be produced in multiple locations: primarily in the thymus as thymic Tregs (tTregs), extrathymically at peripheral sites as peripheral Tregs (pTregs), or induced in vitro (iTregs) under the influence of TGFβ (72). A distinct regulatory population, type 1 regulatory T cells (Tr1 cells), lacks FOXP3 expression but maintains immunosuppressive function through IL-10 and TGF-β secretion (73). Their regulatory mechanism operates through direct suppression of effector responses and modulation of APC function (74). These regulatory populations maintain immune homeostasis and self-tolerance (47, 75).

The other three new CD4 T lineages are Tfh, Th9 and Th22. Tfh cells, distinguished by C-X-C motif chemokine receptor 5 (CXCR5) expression, localize within lymphoid follicles where they coordinate B cell responses and germinal center formation (76). Their developmental program requires IL-6 and IL-21, with Bcl6 serving as the master transcriptional regulator (75). Th9 cells, characterized by predominant IL-9 production, develop under combined TGF-β, IL-4, and IL-2 signals (44). Their transcriptional program depends on IFN regulatory factor 4 (IRF4) and PU.1 (77). Functionally, Th9 cells contribute to promoting antitumor immune activities, such as those against melanoma, and facilitating immune defenses against intestinal parasites (78-80). Meanwhile, they also contribute to allergic and autoimmune pathologies(81). Th22 cells are primarily recognized for producing IL-22 and TNF-α, without concurrent IFN-γ or IL-17 expression (82-84). Their differentiation requires TNF-α, IL-6, and IL-21 signals, coordinated by signal transducer and activator of transcription 3 (STAT3), aryl hydrocarbon receptor (AhR) and RORγt transcriptional activity (83, 85). In influenza and acquired immunodeficiency syndrome (AIDS), Th22 cells exhibit protective effects, whereas in hepatitis B infections, they play a pro-inflammatory role (86-88).
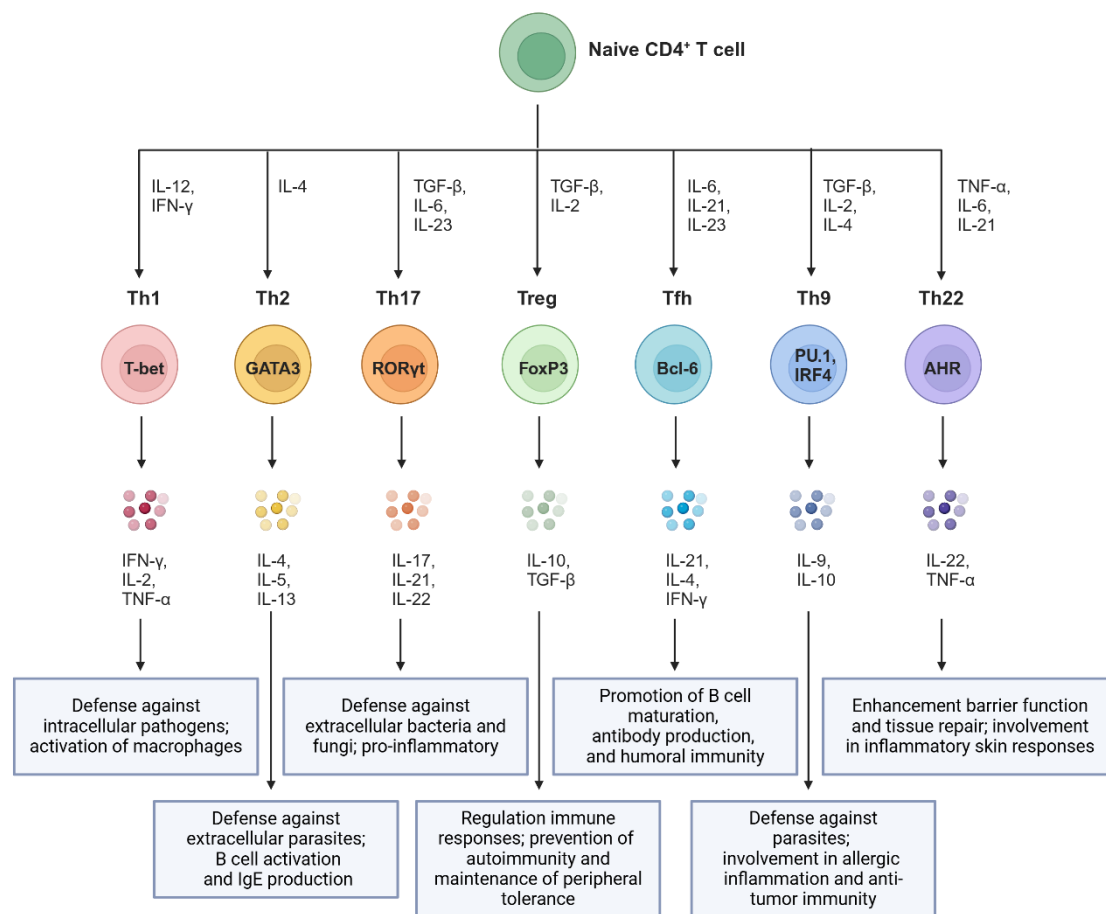
Figure 1. Main characteristics of T helper cell lineages. This figure integrates data from multiple studies, providing a comprehensive overview of T helper-cell subsets and their functions in the immune system(44, 89, 90). This graph was edited with BioRender (Created in BioRender. Bernhagen, L. (2025) https://BioRender.com/h51e818) and modified from Koh *et al,* Exp Mol Med 2023 (91).

After the initial immune response, most effector T lymphocytes undergo programmed cell death. In contrast, approximately 5-10% of activated CD4$^+$ T cells differentiate into memory T cells(92-94). The distinction between naive and memory populations can be characterized by differential expression of CD45 isoforms, which fluctuate throughout cellular development (95). The CD45RA isoform predominates expression in naive populations, while activated subsets (effector and memory T cells) preferentially express CD45RO (96, 97). Age influences the expression of CD45RA and CD45RO. In newborns, the T cell population predominantly expresses CD45RA, and aged individuals shift towards a higher expression of CD45RO (97, 98).

Memory CD4$^+$ T cells are pivotal in mounting a robust secondary response upon antigenic rechallenge, surpassing magnitude and speed of the primary response, and

thereby contributing significantly to long-term protective immunity (99, 100). This compartment comprises two principal subsets: central memory T cells (TCM) and effector memory T cells (TEM) (101). TCM cells, primarily located in lymphoid tissues, exhibit a high proliferative capacity, allowing them to respond efficiently upon re-encounter with the antigen (94). They function as a reservoir capable of generating new effector cells, thus contributing to sustained immune surveillance and response (102). In contrast, TEM cells are predominantly found in peripheral tissues like lungs, skin and bone marrow, where they provide immediate protection through rapid effector functions (94, 103-105). The functional heterogeneity between these populations manifests through distinct cytokine profiles: TCM cells characteristically produce IL-2, supporting their proliferative capacity, while TEM cells generate IFN-γ, IL-4, and IL-17 (101) (106). TEM populations further subdivide into specialized Th1, Th2, and Th17 memory subsets, reflecting distinct functional capabilities (93, 101, 107, 108). A novel subset of TEM, known as T effector memory cells re-expressing CD45RA (TEMRA), has been identified (109). These cells atypically re-express CD45RA. They exhibit unique phenotypic and functional properties, distinguishing them from TCM and TEM (110, 111). CD8$^+$ TEMRA were found in blood, spleen and lung, whereas CD4$^+$ TEMRA cells are rare (110). TEMRA is mainly studied on CD8$^+$ T cells, and CD8$^+$ TEMRA exhibits features of senescence or exhaustion, often associated with reduced telomere length and limited proliferative capacity (112, 113).

1.2 Macrophage migration inhibitory factor and MIF family proteins

MIF is a pleiotropic cytokine with extensive function in various pathological states (11). D-dopachrome tautomerase (D-DT), alternatively designated as MIF-2, exhibits significant structural and sequence homology to MIF, resulting in overlapping functional role (114). MIF and MIF/D-DT-like (MDL) proteins are evidenced by their conservation across diverse organisms, ranging from unicellular life forms to multicellular parasites, fungal species, and plant systems (100). The research in this PhD thesis primarily focused on elucidating the mechanisms and functions of MIF and MDL proteins in CD4+ T cells and neutrophils.

1.2.1 Macrophage migration inhibitory factor

MIF was initially identified during studies on delayed-type hypersensitivity reactions, where it was noted to inhibit macrophage migration (115). The field experienced significant advancement in the late 1980s and 1990s through human MIF cDNA isolation and its identification as a pituitary-derived inflammatory mediator (116). Subsequently, the generation of a *Mif*-knockout mouse model has significantly contributed to advancing research on this protein (117).

The human MIF gene is encoded on chromosome 22q11.2. It comprises three exons (107, 172, and 66 base pairs) separated by two introns (188 and 94 base pairs) (11). MIF gene expression is regulated not only by transcription factors but also by genetic polymorphisms within its promoter region. Notably, two polymorphisms significantly affect its expression: a -173 single nucleotide polymorphism (SNP) and a -794 CATT tetranucleotide repeat (114). These genetic variations impact the MIF transcriptional activity, thereby influencing MIF protein levels and impacting its biological functions. For instance, studies have linked the MIF -173 G/C polymorphism to enhanced risk of systemic-onset juvenile idiopathic arthritis risk (118). A comparable association has been mentioned with inflammatory bowel disease (119). Furthermore, a comprehensive analysis of 1171 COVID-19 cases revealed that the -794 CATT7 allele correlates with reduced symptomatic SARS-CoV-2 infection susceptibility but an elevated risk of disease severity in affected individuals (120). Additionally, the MIF-794 CATT5 allele has been identified as a genetic variant associated with enhanced diffusion capacity in Chronic Obstructive Pulmonary Disease individuals (121). Together, these findings highlight the significant impact of MIF gene polymorphisms on various disease conditions, emphasizing their potential as genetic markers for assessing disease risk and progression.

MIF exists as a 12.5 kDa non-glycosylated protein consisting of 114 amino acids, with a unique structure that includes a conserved tautomerase catalytic site (116, 122). The remarkable evolutionary conservation of MIF is demonstrated by the extensive homology between mouse and human variants, which exhibit 90% sequence identity at the amino acid level (123). Crystallographic analysis of human MIF demonstrates that the protein assembles into a homotrimer, comprising three identical subunits. In

its active conformation, this homotrimeric structure facilitates binding to MIF's cell surface receptor CD74, thereby initiating signaling cascades critical for its biological functions (124).

While initially identified in activated T lymphocytes, MIF expression extends across diverse cell populations, including monocytes, neutrophils, B lymphocytes, and others (115, 125-127). Additionally, MIF is also distributed differently across various tissues, including the lung, liver, kidney, and colon, highlighting its widespread physiological relevance (11, 12, 126). MIF production occurs through a non-classical pathway, unlike most cytokines that follow the conventional endoplasmic reticulum (ER)-Golgi route (128). MIF is continuously generated and stored in intracellular reservoirs, allowing for fast mobilization and release in response to stimulation, ensuring a quick response to reaction. Research indicates that ATP-binding cassette (ABC) transporters facilitate the direct transport of MIF from the cytosol to the extracellular environment, bypassing the ER-Golgi system (128). Additionally, recent studies suggest that MIF can be secreted via extracellular vesicles such as exosomes or microvesicles (129). This vesicular transport enables the targeted and concentrated delivery of MIF to recipient cells, enhancing its functional effectiveness. Various stimuli, including stress signals, mitogenic, hormonal and inflammatory mediators regulate MIF secretion process (130).

1.2.2 MIF receptors

MIF signals through several receptors, including CD74/invariant chain (Ii) and CXCR2, CXCR4 and atypical chemokine receptor 3 (ACKR3)/CXCR7, to regulate various immune cell functions, including proliferation, survival, and migration (131). Understanding the specific roles and mechanisms of MIF and its receptors provides valuable insights into therapeutic opportunities across numerous pathological conditions, including cancer, autoimmune and cardiovascular diseases and inflammatory disorders (132).

1.2.2.1 CD74

CD74, initially characterized as a protein co-immunoprecipitating with MHC class II molecules (133). CD74 exhibits expression patterns beyond conventional class II-expressing immune cells to include endothelial populations and cardiac myocytes under

inflammatory conditions (134). CD74 contains three domains: a cytoplasmic N-terminus, a single transmembrane domain, and a luminal region (135, 136) (shown in Figure 2). In mice, two isoforms of CD74 (p31 and p41) generate from alternative splicing (137). In humans, CD74 gives rise to four isoforms: p33 and p41, similar to the mouse counterparts, and two additional isoforms, p35 and p43, which are generated through an alternative start codon that extends the N-terminus by 16 amino acids (138, 139). These isoforms contribute to the functional diversity of CD74, enhancing its regulatory capacity in immune responses.
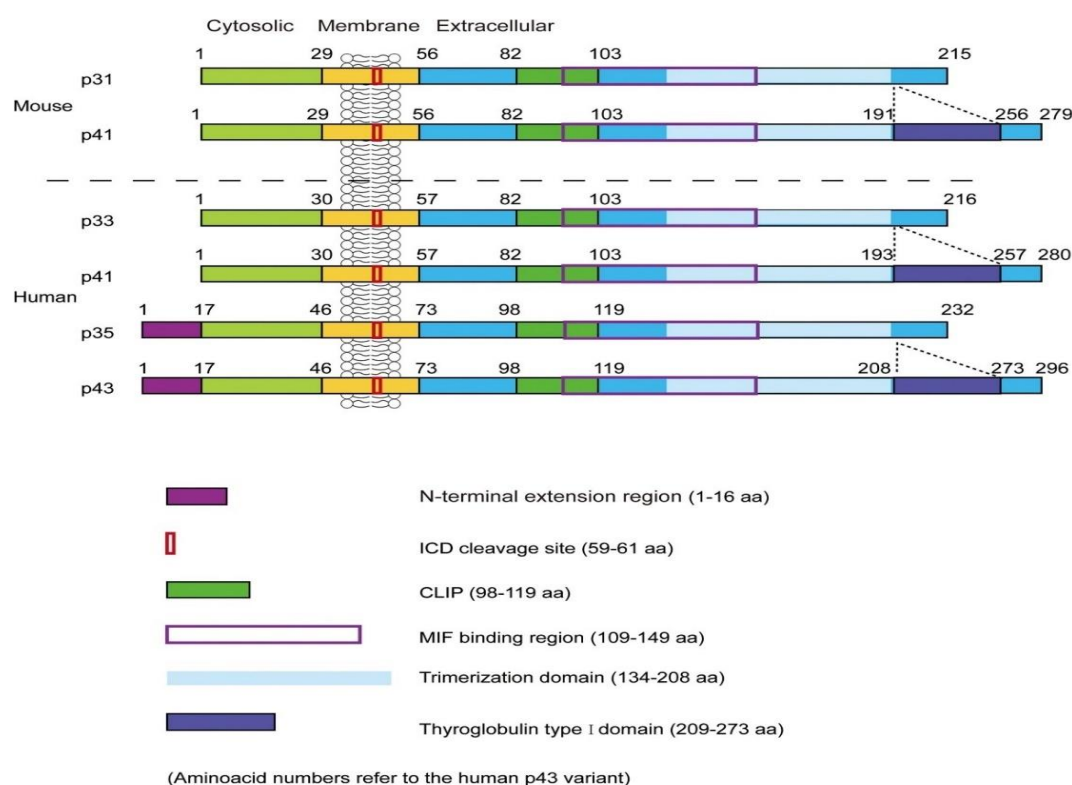
Figure 2. Structure and domains of CD74. The architecture of the murine isoforms and the human isoforms is illustrated, highlighting key functional regions. The positions of the CLIP segment, intracellular domain (ICD), MIF-binding region, trimerization domain, and thyroglobulin type I domain are marked. Taken from Li *et al*, Front Cardiovasc Med 2022 (140).

CD74 proteins undergo several post-translational modifications. Glycosylation is one of these crucial modifications (141). Chondroitin sulphate modification, a specific form of glycosylation, has been shown to enable CD74 to function in T-cell stimulation by facilitating its interaction with CD44 (142). However, the exact role and mechanism of this modification, particularly in CD4$^+$ T cells, remain unclear and warrant further

study. Phosphorylation is another important post-translational modification, occurring primarily in the cytoplasmic tail of CD74 (143). This modification is crucial for regulating signaling pathways and is essential for controlling CD74-mediated cell survival (144, 145). Furthermore, palmitoylation is a potential modification of CD74. Although it can influence the levels of the N-terminal fragment and modulate CD74 processing, it is not essential for intramembrane proteolysis (146).

CD74 serves as a critical molecular chaperone for MHC II molecules, ensuring their stability, proper folding, trafficking, and peptide loading in antigen-presenting cells (147, 148) (Figure 3). MHC class II molecules are heterodimers composed of two non-covalently associated transmembrane glycoproteins: the 34-kDa α chain and the 28-kDa β chain (149). In the ER, CD74 trimerizes and associates with MHC class II α/β heterodimers, forming nonameric structures that facilitate proper protein folding and stabilization (147). CD74 and MHC class II interaction occurs through the class II-associated invariant chain peptide (CLIP) segment, that binds to the peptide-binding groove of the MHC II complex (150). By occupying this groove, CD74 avoids premature peptide loading and protects the MHC II molecules from aggregation (151). Furthermore, CD74 facilitates the transport of the MHC II complex from the ER and guides it to the endosomal/lysosomal compartments via sorting signals in its cytoplasmic tail (152, 153). Within these compartments, CD74 undergoes proteolytic degradation, leaving behind the CLIP fragment (154). The chaperone human leukocyte antigen DM (HLA-DM), together with PH, subsequently facilitates CLIP release, allowing high-affinity, processed antigenic peptides to bind to MHC class II molecules(155). Finally, the peptide-loaded MHC class II complexes translocate to the cell surface, presenting the antigen to CD4$^+$ T lymphocytes and initiating an immune response. Through these functions, CD74 ensures the effective presentation of pathogen-derived peptides by MHC II, contributing to adaptive immune surveillance and activation. Notably, CD74 can also participate in cross-presentation through the MHC class I pathway on DCs, contributing to MHC class I-induced cytolytic T lymphocyte (CTL) responses (156).

Beyond the chaperone function of CD74, the intracellular domain of CD74 (CD74-ICD) was discovered to be involved in various cellular processes, particularly in transcriptional regulation. The CD74-ICD is generated through a process called regulated intramembrane proteolysis (RIP), involving sequential proteolytic events (157). In antigen-processing compartments, CD74 undergoes cleavage by different proteases like

cathepsins, removing most of the luminal domain and creating a truncated, membrane-bound fragment (154, 158, 159). This fragment is further cleaved by intramembrane proteases (IMPs) within the transmembrane region, releasing the CD74-ICD into the cytoplasm (160). A specific member of the IMP family, known as signal-peptide-peptidase-like 2a (SPPL2a), has been demonstrated to be essential for executing this proteolytic event (161, 162). This liberated domain translocates to nuclear regions, engaging with transcription factors, including nuclear factor kappa B(NF-κB), to modulate gene expression and promote cellular survival (157, 163, 164)This proteolytic processing highlights the function of CD74 in antigen presentation and intracellular signaling, linking its chaperone activity to more extensive cellular roles.
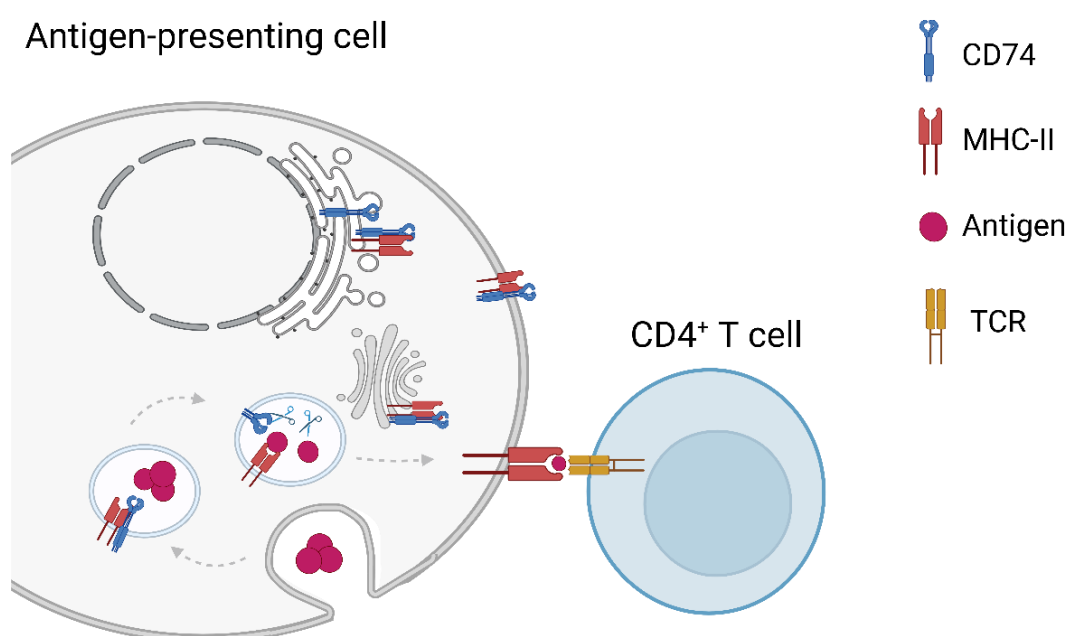
Figure 3. The role of CD74 in MHC II-antigen presentation. CD74 associates with MHC II α and β chains in the ER, aiding in their folding and dimer formation. Sorting signals in the N-terminus of CD74 facilitate its trafficking, either directly or via the plasma membrane. In the endosomal compartments, CD74 undergoes degradation, enabling MHC II to bind antigen-derived peptides for presentation. This graph was generated using BioRender (Created in BioRender. Bernhagen, L. (2025) https://BioRender.com/u47x538) and kindly provided by Dr. med. Adrian Hoffmann.

In 2003, CD74 was identified as the first receptor to exhibit high affinity for MIF (143). Upon binding to MIF, CD74 forms a complex with CD44, initiating downstream pathways, including NF-κB, mitogen-activated protein kinase/ERK (MAPK/ERK), and

phosphatidylinositol 3-kinase/protein kinase B (PI3K/AKT) (165, 166). The CD74/CD44 complex has an essential role in various disease conditions. In rheumatoid arthritis, CD74 acts as a co-receptor with CD44 for MIF binding, promoting synovial fibroblast adhesion and migration. This interaction triggers inflammatory signaling pathways, contributing to joint inflammation and progressive damage (167, 168). In ischemic heart disease, the infarct region showed marked elevation of both MIF and the CD74/CD44 complex expression (169). Cardiomyocytes secrete MIF, which triggers cardioprotective effects through CD74/CD44-dependent AMPK (adenosine monophosphate-activated protein kinase) pathway activation, reducing both ischemic damage and apoptosis (170, 171). In atherosclerosis, the interaction of MIF to CD74/CD44 on macrophages facilitates the recruitment of inflammatory cells to the atherosclerotic plaques and enhances macrophage survival (165, 172, 173). Additionally, elevated serum levels of soluble CD74 (sCD74) have elevated during active disease phases compared to remission, indicating its role in RA activity (167). Similarly, plasma sCD74 also increases in COVID-19 patients (174). Furthermore, CD74 demonstrates increased expression across multiple tumor types, suggesting therapeutic potential (175). In addition, it has been speculated that MIF may facilitate the translocation of CD74-ICD to the nucleus, although this has not been conclusively demonstrated (164, 176). Moreover, extracellular MIF also binds to CD74 and forms a heterocomplex with co-receptors such as CXCR2, CXCR4, or CXCR7, facilitating its functional activity (126, 172, 177) . Further details will be discussed in Chapters 1.2.2.2 and 1.2.2.3.

1.2.2.2 CXCR2

CXCR2, a G protein-coupled receptor (GPCR), is encoded on chromosome 2. CXCR2 demonstrates broad cellular distribution across granulocyte and macrophage progenitors, tumor cells, and retinal glial cells (178-180). CXCR2 primarily binds to CXC chemokines such as CXCL8 (IL-8), along with other CXC motif chemokines like CXCL1-3 and CXCL5-7 (181). The binding of the ligand CXCL8 to CXCR2 involves the glutamic acid-leucine-arginine (ELR) motif and N loop (182). Furthermore, the interaction between CXCR2 and MIF has been confirmed through receptor binding and internalization assays, with a dissociation constant of 1.4 nanomolar (172). Similar to

CXCL8, MIF interacts with CXCR2 through a pseudo-(E) LR motif, formed by the residues R12 and D45, which together establish a three-dimensional ELR-like structure (183). Additionally, an N-like loop within the sequence spanning residues 47–56 further contributes to the functional MIF/CXCR2 binding (182).

The MIF/CXCR2 axis regulates crucial immunological processes, influencing cell adhesion, survival, and migration (172, 184, 185) . Surface-associated MIF promotes monocyte arrest through CXCR2, which is further facilitated by CD74 (172, 186). This interaction contributes to inflammatory responses and the development of atherogenesis. Furthermore, blocking the MIF-CXCR2 interaction reduces monocyte adhesion and plaque formation in models of atherosclerosis (182). Additionally, CXCR2 supports MIF-induced arrest in Jurkat T cells, indicating its role in enhancing leukocyte sensitivity to MIF(185). In a PBMC-neutrophil coculture system, blocking CXCR2 on neutrophils prevented their survival when exposed to MIF-conditioned PBMC supernatants, while blocking CXCR2 on PBMCs abolished the inhibitory effect of their supernatants on neutrophil apoptosis (185). Moreover, the MIF/CXCR2 axis is also critical for the chemotactic migration of neutrophils towards inflammatory areas and tumor sites (185, 187).

1.2.2.3 CXCR4

CXCR4 is also a member of the seven-span transmembrane GPCR family. It shows extensive distribution across Tfh cells, central memory CD4 T cells, memory B cells, hematopoietic progenitor cells, neurons, and cancer cells (188-192). This receptor regulates diverse physiological processes, including cancer progression, immune system regulation, and stem cell trafficking (193, 194). The CXCR4-CXCL12 axis is crucial as it influences cell migration, proliferation, and survival, making it a key therapeutic target (193). MIF engages CXCR4 distinctly from CXCL12, it does not interact with the transmembrane cavity of CXCR4; instead, it binds to the extracellular loops (EL1 and EL2) and the N-terminal region, functioning as a partial allosteric agonist (195). This distinct mode of engagement results in partial receptor activation, leading to different signaling outcomes compared to the CXCL12-CXCR4 interaction. For instance, MIF-CXCR4 binding promotes pro-atherogenic processes, such as atherosclerosis, whereas the CXCL12-CXCR4 axis is known to exert athero-protective effects (172, 196, 197). A novel strategy for targeting the MIF-CXCR4 axis in

atherosclerosis uses engineered peptides called msR4Ms, which are designed to effectively block the MIF-CXCR4 interaction without disrupting the beneficial or dichotomous signaling pathways elicited by CXCL12-CXCR4 and MIF-CD74 (198). A study using a mouse model of early atherosclerosis applied msR4M-L1, the current lead peptide of the msR4M class, which was found to be targeted to atherosclerotic plaques, effectively reducing arterial leukocyte adhesion and mitigating atherosclerosis (198). This offers a promising chemokine-targeted therapeutic intervention for atherosclerosis and possibly other inflammatory conditions. Moreover, CXCR4 serves as the dominant MIF receptor, driving mesenchymal stem cell migration and invasion via the MAPK pathway (199). Furthermore, CXCR4, in conjunction with CD74, facilitates MIF-induced migration of B cells via the ZAP-70 signaling (177). Additionally, CXCR4 forms a complex with CD74, as observed in HEK293 cells and monocytes. The CXCR4-CD74 complex functionally mediates MIF-induced Akt activation in T lymphocytes (200).

1.2.2.4 CXCR7/ACKR3

CXCR7(ACKR3) is another member of the GPCR family. CXCR7 expression spans cardiac, neural, and immune tissues, influencing cardiovascular development, tumor progression, immune cell trafficking, and inflammation (201-204). CXCR7 serves as a receptor primarily for the chemokines CXCL11 and CXCL12 (205). Unlike classical chemokine receptors, CXCR7 does not engage G proteins to trigger typical intracellular signaling pathways. Instead, it functions mainly as a scavenger or decoy receptor for CXCL11 and CXCL12, modulating the activity of other chemokine receptors, such as CXCR4 (205-208).Furthermore, studies have identified CXCR7 as a novel receptor for MIF (209). Contrary to earlier findings, evidence indicates that MIF can directly interact with CXCR7. It has been demonstrated that MIF can induce the internalization of human CXCR7 independently of CXCR4. Furthermore, inhibition of CXCR7 resulted in the suppression of MIF-induced migration of mouse B cells (209). In platelets, MIF exerts a pro-survival function through binding with CXCR7, which activates the AKT signaling (202). In rhabdomyosarcoma, MIF secreted by tumor cells binds to CXCR7, enhancing cell adhesion and tumor vascularization while inhibiting the recruitment of cancer-associated fibroblasts (201). Moreover, CXCR7 was verified form complexes

with CXCR4 and CD74 (209). This dual role suggests that MIF-CXCR7 interaction is significant in tumor microenvironment modulation.

1.2.3 Non-mammalian MIF family proteins

The MDL protein family exhibits remarkable evolutionary conservation across diverse species. Beyond mammals, these proteins appear in numerous organisms, including fish, parasites, and even plants (210-212). In the plant kingdom, MDL expression has been observed in Arabidopsis thaliana, which is the focus of my thesis. MIF is a highly conserved protein, and recombinant Arabidopsis MDLs (AtMDLs) share 28-33% sequence identity and similar secondary structure with human MIF (HsMIF). In Arabidopsis, three MDL genes produce the proteins AtMDL1, AtMDL2, and AtMDL3, which retain minimal residual tautomerase activity compared to MIF (213, 214). AtMDL1 and AtMDL2 are localized in cytoplasmic regions, while AtMDL3 is found in peroxisomal spaces (215). AtMDLs not only bind to CD74, a known receptor for MIF, but also interact with CXCR4, triggering PI3K/Akt signaling cascades. Additionally, AtMDLs prompted human monocytes and T cells chemotaxis in a dose-dependent manner, further highlighting their functional similarities to human MIF (214). However, the underlying mechanisms of these interactions and their function on neutrophils remained unclear. It is also unknown whether AtMDLs interact with other known MIF receptors, and further research is necessary to clarify these interactions and their potential biological significance. Additionally, there is growing interest in understanding how MDL and hsMIF interact and exploring the functional roles of the MDL/hsMIF complex.

1.3 MIF family proteins in CD4$^+$ T cells

Initially discovered as a factor released by activated T lymphocytes, MIF expression occurs across Th0, Th1 and Th2 cells (11, 115, 125, 216). A research from 1996 using antibodies that neutralize MIF has demonstrated its crucial role in T-cell activation processes(216). Effective T-cell activation relies on three signals: antigen recognition via the TCR, co-stimulatory input from APCs, and cytokines that guide differentiation and promote cell expansion (127). APCs enhance CD4$^+$ T-cell responses by presenting antigens via MHC class II. MIF exhibits dual regulatory functions in CD4$^+$ T-cell activation during different conditions. In *vitro* studies show that MIF downregulates MHC

II levels in endothelial cells and macrophages, while upregulating co-stimulatory molecules (B7-2, CD40L and CD40) on astrocytoma cells and B cells (217). In *Schistosoma mansoni*-infected mice, MIF upregulated B7-1 on B cells alongside CD40L on T cells in the spleen (217). Conversely, MIF-deficient models of type 1 diabetes mellitus showed reduced levels of co-stimulatory molecules (CD80, CD86, and CD40) and MHC II on splenic macrophages and DCs, as along with decreased expression of TLR2 and TLR4 (218). Additionally, further research has shown that MIF enables CD4$^+$ T lymphocytes to mediate activation via TLR4 signaling (219).

Beyond activation, MIF influences CD4$^+$ T-cell differentiation. MIF can enhance Th1 and Th2 cytokine production (220-222). Moreover, in MIF-deficient colon carcinoma mice, there are fewer Tregs (both CD4$^+$ Tregs and CD8$^+$ Tregs) in the spleen, as MIF facilitates Treg development by modulating IL-2 production (223). On the contrary, the absence of MIF facilitated Treg accumulation in visceral adipose tissue (224). In healthy subjects, MIF-treated PBMCs induced a clear increase in the Th17 cytokine profile, which are IL-17A, IL-17F and IL-21 (225). In patients suffering from HIV infection, MIF-CD74 interactions in monocyte-derived macrophages impact CD4$^+$ T-cell populations, leading to an increase in Th17-like cells and thereby continuing to shape immune responses (226). In Hashimoto's thyroiditis, MIF promotes Th17 cell differentiation via the NF-κB pathway and enhances herpes virus entry mediator (HVEM) expression (227). In cancer, particularly nasopharyngeal carcinoma, MIF drives both the development and mobility of Th17 lymphocytes through mechanisms dependent on MIF-CXCR4 axis and reliant on the mammalian target of rapamycin (mTOR) pathway (228). Taken together, these findings highlight MIF's multifaceted regulatory functions in CD4$^+$ T cell activation, differentiation, and immune response modulation across a range of physiological and pathological conditions.

Naive and memory CD4$^+$ T lymphocytes both display the MIF receptor CXCR4 (229, 230). CD4$^+$ T-cell activation lead to a downregulation in surface CXCR4, partly due to receptor internalization (230). Functionally, CXCR4 facilitates HIV-1 entry, and its downregulation upon activation helps restrict the spread of X4 HIV by limiting viral access to CD4$^+$ T cells (230-232). Additionally, CXCR4 mediates T-cell migration through ZAP-70 signaling (233). On the contrary, CD74 was only descriptively described as expressing on CD4$^+$ and CD8$^+$ T cells, and its function as a MIF receptor in

T cells has remained poorly defined (174, 234, 235). The underlying receptor-related mechanisms activated by MIF in human T cells are still inadequately understood, highlighting a gap in current knowledge that requires further investigation.

1.4 MIF in acute respiratory distress syndrome (ARDS)

ARDS can cause severe pulmonary inflammation, leading to considerable morbidity, mortality, and substantial healthcare expenditures (236). The LUNG-SAFE study reports that ARDS affects 10% of intensive care unit (ICU) patients, and 23% of them require mechanical ventilation (237). The COVID-19 pandemic has highlighted the critical necessity for effective treatments for ARDS, as severe cases of COVID-19 frequently lead to ARDS development. As of October 27, 2024, there have been 776,754,317 confirmed global cases of COVID-19, including 7,073,466 fatalities, with infection cases continuing to escalate. In a study of 201 patients with SARS-CoV-2 infection, 41.8% developed ARDS, and 26.4% required intensive care (238). COVID-19 patients exhibit a sustained reduction in CD4$^+$ and CD8$^+$ T cells, with CD8$^+$ T cell counts gradually increasing after six weeks of hospitalization (238-241). Additionally, T-helper cell subsets exhibit shifts in proportion, with a reduced ratio of Th1 cells, an elevated ratio in Th2 cells, and no significant change in Th17 cells compared to healthy individuals (239). Neutrophils are strongly related to the development and progression of ARDS (242). In patients with COVID-19, raised levels of neutrophils and a higher neutrophil/lymphocyte ratio in the blood linked to increased mortality (238, 243, 244). Accumulating evidence has identified MIF as a crucial mediator in the pathogenesis of both ARDS and COVID-19 (120, 245-247). However, MIF receptors expression profiles on immune cells, particularly on CD4$^+$ T cells and neutrophils, remain inadequately characterized in the context of ARDS. Importantly, the precise functional roles and mechanistic actions of MIF and its receptors on CD4$^+$ T cells and neutrophils during ARDS pathogenesis require further elucidation.

2. Own contribution to the publications

This cumulative thesis is built on two publications that investigate different aspects of the interactions between MIF-family proteins and the CD4$^+$ T cell network. In this chapter, a comprehensive overview of my contributions to these studies will be presented.

2.1 Publication I: Zhang, L. *et al*, 2024

CD74 is a functional MIF receptor on activated CD4$^+$ T cells

Zhang, L.*, Woltering, I.*, Holzner, M., Brandhofer, M., Schaefer, C. C., Bushati, G., Ebert, S., Yang, B., Muenchhoff, M., Hellmuth, J. C., Scherer, C., Wichmann, C., Effinger, D., Hübner, M., El Bounkari, O., Scheiermann, P., Bernhagen, J., and Hoffmann, A. (2024) CD74 is a functional MIF receptor on activated CD4(+) T cells. *Cell Mol Life Sci* **81**, 296

(*: Lin Zhang and Iris Woltering are credited as co-first authors due to their equal contributions.)

DOI: 10.1007/s00018-024-05338-5

In this article (refer to Section 5 and Subsection 7.1 for supplementary data), the MIF receptor network during T-cell activation is characterized. We identified CD74 functions as a novel MIF receptor and activation marker without MHC II molecule dependence for primary human CD4+ T cells. As a joint first author, I conducted key experiments, analyzed and visualized the data, and revised the manuscript.

Specifically, I made significant contributions to the experiments investigating the roles of CD74 and CXCR4 in the chemotaxis of MIF-facilitated CD4$^+$ T-cells. Our findings established the functional involvement of both receptors in MIF-driven migration, as shown by the complete abrogation of this process when using the AMD3100 (CXCR4 inhibitor) and LN2 (CD74-neutralizing antibody). These results indicated that MIF-induced chemotaxis in activated CD4$^+$ T cells is mediated through a coordinated mechanism involving CD74/CXCR4 heterocomplex formation or synergistic/converging sig-

naling pathways. Using proximity ligation techniques, I observed CD74/CXCR4 complexes in activated CD4$^+$ T cells. The experiment demonstrated a dramatic decrease in proximity ligation assay (PLA) signals following MIF stimulation, indicating that MIF induces internalization of these receptor complexes during signal transduction, a previously undocumented phenomenon in activated T cells. Additionally, I conducted experiments that demonstrated enhanced CD74 presence on T cells (CD4$^+$ and CD8$^+$ T cells) and classical monocytes (CD14^{++}CD16$^-$) from severe COVID-19 patients versus mild cases, pointing to CD74's potential role in disease severity. In summary, I significantly contributed to Figures 5, 6, Supplementary Figures 2, 4, and 5. I was also involved in experiments related to MIF receptor expression on the surface and intracellular levels, verifying CD74 localization in CD4$^+$ T cells. Thus, I also partially contributed to Figures 1, 2, and Supplementary Figure 1. Additionally, I performed revision experiments for the paper.

For data analysis and interpretation, I consolidated and analyzed the data, presenting the results in graphical form. Regarding the manuscript, I prepared all figures, reviewed, and edited the final version, ensuring clarity and accuracy in the presentation of our findings.

2.2 Publication II: Spiller, L. *et al*, 2023

Plant MDL proteins synergize with the cytokine MIF at CXCR2 and CXCR4 receptors in human cells.

Spiller, L., Manjula, R., Leissing, F., Basquin, J., Bourilhon, P., Sinitski, D., Brandhofer, M., Levecque, S., Gerra, S., Sabelleck, B., **Zhang, L**., Feederle, R., Flatley, A., Hoffmann, A., Panstruga, R., Bernhagen, J., and Lolis, E. (2023) Plant MDL proteins synergize with the cytokine MIF at CXCR2 and CXCR4 receptors in human cells. *Sci Signal* **16**, eadg2621

DOI: 10.1126/scisignal. adg2621.

In this article (refer to Section 6 and Subsection 7.2 for supplementary data), I contributed to the revision phase of the manuscript. I examined the inhibitory impacts of MIF

and MDL1 on the chemotactic migration of human CD4$^+$ T cells. Results showed the combination of MIF and MDL1 exhibits distinct functions compared to either molecule alone, providing new perspectives on their impact on lymphocytes. Additionally, I further validated the synergistic effect of MIF and MDL1 in promoting inflammation-related gene expression in A549 (human lung epithelial cells) in a dose-responsive manner, offering insights into their combined role in inflammation. I also contributed to the establishment of the 3D neutrophil migration experimental set-up.

3. Summary

The first part of this cumulative thesis (corresponding to the study by Zhang, L. et al, *Cell Mol Life Sci* 2024) examined the MIF receptors functionality in CD4$^+$ T lymphocytes, with an emphasis on CD74. While traditionally recognized for its involvement in antigen presentation via MHC II molecules on APCs, CD74 has surprisingly been detected on CD4+ T lymphocytes (174, 234, 235). The investigation in my thesis aimed to clarify the functional capabilities of MIF receptor CD74 on CD4$^+$ T cells and to elucidate the regulatory mechanisms governing its expression, addressing a novel and unanticipated aspect of T cell biology.

Investigations uncovered distinctive patterns of MIF receptor distribution between quiescent and stimulated CD4$^+$ T lymphocytes. In their resting state, these cells exhibited minimal extracellular expression of CXCR2, ACKR3 and CD74, while CXCR4 appeared abundantly on approximately 90% of cellular surfaces. Upon activation of CD4$^+$ T cells, CD74 surface expression increased significantly, whereas CXCR4 expression declined. Notably, the upregulation of CD74 was independent of HLA-DR, indicating that CD74 functioned independently of MHC class II on CD4$^+$ T lymphocytes. Further investigations showed that CD74 was primarily localized intracellularly in both resting and activated states, mirroring the expression pattern observed on the cell surface. Transcriptomic and proteomic analyses supported these findings, providing the first comprehensive report on MIF receptor distribution on CD4$^+$ T cells across different states.

Additionally, the study revealed CD74 presence within ER and endolysosomal compartments, a distribution similar to that in B cells. Upon activation, CD74 underwent post-translational modification with CS, resulting in a new 55 kDa isoform. Previous studies have shown that CD74-CS rapidly translocated to the cell surface, subsequently undergoing immediate endocytosis, leading to its low surface detectability- a finding consistent with this study's observation of minimal surface CD74 in CD4$^+$ T lymphocytes.

Moreover, the study showed CD74 form complexes with CXCR4 upon CD4$^+$ T cells activation. MIF stimulation reduced surface presence of these heterocomplexes, indicating MIF-induced internalization. These complexes also enhanced the MIF-induced

migration of stimulated CD4$^+$ T lymphocytes, underscoring the significance of MIF-CD74/CXCR4 signaling in lymphocyte functions.

Furthermore, analysis of a COVID-19 study uncovered that heightened CD74 expression on CD4$^+$ and CD8$^+$ T cells during severe disease progression compared to mild cases. Notably, CXCR4 or HLA-DR remained constant between the groups, reinforcing that CD74 functions independently of MHC class II in CD4$^+$ T cells, even under infection conditions. These results positioned CD74 as a potential biomarker for assessing disease severity and as a promising target for therapeutic intervention in inflammation-driven disease.

The latter portion (corresponding to parts of the study by Spiller, L. et al, Sci Signal 2023) examined interactions between human MIF and plant-derived MDL proteins from the model plant *Arabidopsis thaliana*. High-resolution crystallographic analysis elucidation of the structure of all three MDL proteins at high resolution. The research also demonstrated that MDLs, despite evolutionary divergence, maintained structural similarities to mammalian MIF, allowing them to engage with human MIF receptors, specifically CXCR2 and CXCR4. Experimental findings showed that MDL1 and MDL2 from *Arabidopsis* bind to these receptors and could enhance immune signaling responses in human cells, particularly through hetero-oligomeric complexes with human MIF.

These complexes showed synergistic effects, promoting cellular responses such as chemotaxis in neutrophils and inflammatory gene expression in pulmonary epithelial cells. The study highlighted the evolutionary conservation in MIF-like proteins and proposed potential implications for human exposure to plant MDLs through dietary or environmental pathways.

4. Zusammenfassung

Der erste Teil dieser kumulativen Dissertation (entsprechend der Studie von Zhang et al., Cell Mol Life Sci 2024) untersuchte die Rolle von MIF-Rezeptoren in CD4^{+}-T-Zellen mit einem Schwerpunkt auf der Charakterisierung von CD74. Historisch war CD74 für seine Funktion in der MHC-II-vermittelten Antigenpräsentation auf Antigen-präsentierenden Zellen (APCs) bekannt. Neuere Studien zeigten jedoch eine unerwartete Expression von CD74 auf CD4^{+}-T-Zellen (174, 234, 235). Ziel dieser Arbeit war es, die funktionelle Relevanz des MIF-Rezeptors CD74 in CD4^{+}-T-Zellen sowie die zugrunde liegenden Regulationsmechanismen seiner Expression zu untersuchen und damit einen neuen, unerwarteten Aspekt der T-Zell-Biologie aufzuzeigen.

Die Ergebnisse zeigten distinkte Expressionsmuster der MIF-Rezeptoren auf CD4^{+}-T-Zellen in nicht aktivierten und aktivierten Zuständen. In nicht aktivierten CD4^{+}-T-Zellen zeigten CD74, CXCR2 und ACKR3 eine minimale Oberflächenexpression, während CXCR4 mit etwa 90 % stark auf der Zelloberfläche exprimiert wurde. Nach Aktivierung der CD4^{+}-T-Zellen nahm die Oberflächenexpression von CD74 signifikant zu, während die von CXCR4 abnahm. Bemerkenswert war, dass die Hochregulation von CD74 unabhängig von HLA-DR erfolgte, was darauf hinweist, dass CD74 unabhängig von MHC-II auf CD4^{+}-T-Zellen exprimiert wird. Weitere Untersuchungen zeigten, dass CD74 sowohl in nicht aktivierten als auch in aktivierten Zuständen vorwiegend intrazellulär lokalisiert war. Reanalysen von bereits veröffentlichten Transkriptom- und Proteom-Datensätzen bestätigten diese Befunde und lieferten erstmals einen umfassenden Überblick über die Expression von MIF-Rezeptoren auf CD4^{+}-T-Zellen in unterschiedlichen Aktivierungs- und Differenzierungszuständen. Zusätzlich wurde CD74 an seiner typischen Lokalisation im endoplasmatischen Retikulum und in endolysosomalen Kompartimenten nachgewiesen. Nach Aktivierung wurde eine posttranslationale Modifikation mit Chondroitinsulfat (CS) identifiziert, die zu einer neuen 55-kDa-Isoform führte. Frühere Studien zeigten, dass CD74-CS schnell zur Zelloberfläche transloziert wird, gefolgt von einer sofortigen Endozytose. Diese Befunde stimmen mit der in dieser Arbeit beobachteten niedrigen Oberflächenexpression von CD74 in CD4^{+}-T-Zellen überein.

Die Arbeit zeigte zudem, dass CD74 auf aktivierten CD4$^+$-T-Zellen einen Komplex mit CXCR4 bilden kann. Nach Stimulation mit MIF nahm die Präsenz des CD74/CXCR4-Heterokomplexes auf der Zelloberfläche ab, was darauf hinweist, dass MIF die Internalisierung des CD74/CXCR4-Komplexes vermittelt. Zudem wurde die funktionelle Rolle der MIF-CD74/CXCR4-Achse bei der MIF-induzierten T-Zell-Migration nachgewiesen.

Darüber hinaus zeigte die Analyse einer COVID-19-Patientenkohorte, dass die CD74-Expression auf CD4$^+$- und CD8$^+$-T-Zellen bei Patienten mit schwerem COVID-19 im Vergleich zu milderen Verläufen signifikant erhöht war. Dies deutet auf einen Zusammenhang zwischen CD74-Expression und der Schwere der Immunantwort bei COVID-19 hin. Bemerkenswerterweise gab es keine Unterschiede in der Expression von CXCR4 oder HLA-DR zwischen den Gruppen, was erneut die MHC-II-unabhängige Funktion von CD74 auf CD4$^+$-T-Zellen selbst unter Entzündungsbedingungen bestätigt. Diese Ergebnisse positionieren CD74 als potenziellen Biomarker zur Bewertung der Krankheitschwere und als vielversprechendes Ziel für therapeutische Interventionen bei entzündungsgetriebenen Erkrankungen.

Der zweite Teil dieser Dissertation (entsprechend Teilen der Studie von Spiller et al., Sci Signal 2023) untersuchte die Interaktionen zwischen humanem MIF und MIF-ähnlichen Proteinen (MDL) aus der Modellpflanze Arabidopsis thaliana. Diese Arbeit umfasste die röntgenkristallographische Aufklärung der Struktur aller drei MDL-Proteine und belegte, dass MDLs trotz evolutionärer Divergenz strukturelle Ähnlichkeiten mit humanem MIF aufweisen, was ihre Interaktion mit menschlichen MIF-Rezeptoren, insbesondere CXCR2 und CXCR4, ermöglicht. Experimentelle Befunde zeigten, dass MDL1 und MDL2 aus Arabidopsis an diese MIF-Rezeptoren binden und die Immunantwort in menschlichen Zellen durch heterooligomere Komplexe mit humanem MIF verstärken können. MIF/MDL-Komplexe zeigten synergistische Effekte auf zelluläre Reaktionen wie Chemotaxis in Neutrophilen und die Expression entzündungsfördernder Gene in Lungenepithelzellen. Die Studie hob die evolutionäre Konservierung von MIF-ähnlichen Proteinen hervor und diskutierte mögliche Implikationen für den menschlichen Kontakt mit pflanzlichen MDLs über Ernährung oder Umwelt.

5. Publication I: Zhang, L. *et al*, 2024

CD74 is a functional MIF receptor on activated CD4+ T cells

Zhang, L..*, Woltering, I.*, Holzner, M., Brandhofer, M., Schaefer, C. C., Bushati, G., Ebert, S., Yang, B., Muenchhoff, M., Hellmuth, J. C., Scherer, C., Wichmann, C., Effinger, D., Hübner, M., El Bounkari, O., Scheiermann, P., Bernhagen, J., and Hoffmann, A. (2024) CD74 is a functional MIF receptor on activated CD4(+) T cells. *Cell Mol Life Sci* **81**, 296

(*: Lin Zhang and Iris Woltering equally contributing first authors.)

ORIGINAL ARTICLE

CD74 is a functional MIF receptor on activated CD4+ T cells

Lin Zhang[1] · Iris Woltering[1] · Mathias Holzner[1] · Markus Brandhofer[1] · Carl-Christian Schaefer[1] · Genta Bushati[1] · Simon Ebert[1] · Bishan Yang[1] · Maximilian Muenchhoff[2,3,4] · Johannes C. Hellmuth[4,5] · Clemens Scherer[4,6] · Christian Wichmann[7] · David Effinger[8,9] · Max Hübner[8,9] · Omar El Bounkari[1] · Patrick Scheiermann[8] · Jürgen Bernhagen[1,10] · Adrian Hoffmann[1,8,10]

Abstract

Next to its classical role in MHC II-mediated antigen presentation, CD74 was identified as a high-affinity receptor for macrophage migration inhibitory factor (MIF), a pleiotropic cytokine and major determinant of various acute and chronic inflammatory conditions, cardiovascular diseases and cancer. Recent evidence suggests that CD74 is expressed in T cells, but the functional relevance of this observation is poorly understood. Here, we characterized the regulation of CD74 expression and that of the MIF chemokine receptors during activation of human CD4+ T cells and studied links to MIF-induced T-cell migration, function, and COVID-19 disease stage. MIF receptor profiling of resting primary human CD4+ T cells via flow cytometry revealed high surface expression of CXCR4, while CD74, CXCR2 and ACKR3/CXCR7 were not measurably expressed. However, CD4+ T cells constitutively expressed CD74 intracellularly, which upon T-cell activation was significantly upregulated, post-translationally modified by chondroitin sulfate and could be detected on the cell surface, as determined by flow cytometry, Western blot, immunohistochemistry, and re-analysis of available RNA-sequencing and proteomic data sets. Applying 3D-matrix-based live cell-imaging and receptor pathway-specific inhibitors, we determined a causal involvement of CD74 and CXCR4 in MIF-induced CD4+ T-cell migration. Mechanistically, proximity ligation assay visualized CD74/CXCR4 heterocomplexes on activated CD4+ T cells, which were significantly diminished after MIF treatment, pointing towards a MIF-mediated internalization process. Lastly, in a cohort of 30 COVID-19 patients, CD74 surface expression was found to be significantly upregulated on CD4+ and CD8+ T cells in patients with severe compared to patients with only mild disease course. Together, our study characterizes the MIF receptor network in the course of T-cell activation and reveals CD74 as a novel functional MIF receptor and MHC II-independent activation marker of primary human CD4+ T cells.

Keywords CD74/invariant chain · Macrophage migration inhibitory factor · MIF · T cells · Atypical chemokine · CXCR4

Introduction

CD74, also known as major histocompatibility complex class II (MHC II) invariant chain (Ii), is a type II transmembrane glycoprotein that plays a crucial role in MHC II-mediated antigen presentation mainly by acting as a class II chaperone [1]. Accordingly, CD74 expression is seen in antigen-presenting B cells, monocytes/macrophages, and dendritic cells. Beyond this canonical function, CD74 was discovered as a high affinity receptor for the cytokine and atypical chemokine MIF that has emerged as an upstream regulatory and inflammatory mediator in the pathogenesis of various cardiovascular, infectious, autoimmune and cancerous diseases [2–5]. Next to CD74, the currently known MIF receptors comprise the classical chemokine receptors CXCR2, CXCR4 and ACKR3/CXCR7. These are found to a varying degree on nearly all leukocyte subsets enabling MIF to shape the local immune cell profile in inflamed tissues [3, 4, 6–8]. In-depth investigations of the underlying molecular mechanisms including the detailed characterization of ligand/receptor interactions not only placed MIF in this complex ligand/receptor network, but also enabled the development of various MIF-targeted treatment strategies [9, 10].

Lin Zhang and Iris Woltering equally contributing first authors.

Extended author information available on the last page of the article

Springer

MIF-mediated signaling via CD74 has been shown to be dependent on receptor complex formation with CD44, CXCR2, CXCR4 and ACKR3/CXCR7, inducing downstream phosphatidylinositol 3-kinase/protein kinase B (PI3K/Akt), adenosine monophosphate-activated protein kinase (AMPK), nuclear factor-κB (NF-κB), calcium signaling, and extracellular signal-regulated kinase (ERK) pathways [4, 8, 11, 12]. Thereby, CD74 is critically involved in MIF-driven immune cell recruitment and activation of a variety of cellular responses, including cell proliferation and cell metabolism that have been found to play a role in cancer, metabolic and ischemic heart disease [4, 5, 13–17].

In T cells, MIF was previously shown to be secreted upon activation and to influence key immunological processes such as migration, proliferation, apoptosis and to promote a Th17-phenotype [18–24]. MIF-receptor pathways have been amply studied in numerous cell types, but despite its first description as a soluble T cell-derived mediator more than 50 years ago, our current understanding of the receptor mechanisms triggered by MIF in human T cells is still incomplete [25]. In particular, with only very few incidental descriptive reports on CD74 expression in human T cells available, the role of CD74 receptor activity in T cells is unclear. In fact, although CD74 upregulation in the context of inflammation and cell stress has previously been observed in MHC II-negative cell types such as endothelial cells, cancer cells, or cardiomyocytes, the occurrence of CD74 in T cells is surprising, as T cells, which are MHC class II-negative themselves, are best known for their role in MHC-based peptide recognition from MHC-II$^+$ antigen-presenting immune cells [21, 26–28]. Therefore, this study aimed to characterize the regulation of CD74 and its relevance for MIF-mediated functions in human CD4$^+$ T cells in the course of T-cell activation, with CD4$^+$ T cells representing the cornerstone of the adaptive immune system by mediating immune homeostasis, antigen-recognition, self-tolerance and immunological memory. CD4$^+$ T-cell activation occurs through binding of the T-cell receptor (TCR) to an MHC II-bound antigen in the presence of costimulatory signals and represents the crucial mechanism by which T cells respond to foreign or endogenous antigens and differentiate into effector T cells [29].

Here, we provide evidence that CD4$^+$ T cells constitutively express CD74 intracellularly, which upon T-cell activation, is significantly and rapidly upregulated, post-translationally modified by chondroitin sulfate (CS) and translocated to the cell surface to fulfil its function as MIF receptor. By exploiting flow cytometry, Western blot (WB), immunohistochemistry, and re-analysis of published RNA-sequencing (RNAseq) and proteomic data sets, our study identified CD74 as a novel activation marker of T cells that is regulated independent of MHC II. Functional studies revealed a significant involvement of both CD74

and CXCR4 in MIF-elicited CD4$^+$ T-cell chemotaxis. Proximity ligation assay (PLA) visualized CD74/CXCR4 complexes on activated T cells, which are internalized upon MIF-treatment.

With accumulating evidence pointing towards a critical role of MIF as a prognostic marker to predict disease severity and patient outcome in COVID-19 and observations of an impaired T cell response during Sars-CoV-2 infections often displayed by sustained T-cell activation, we aimed to confirm the translational relevance of our findings in the context of COVID-19 [30–32]. In a patient cohort of 30 patients with mild and severe COVID-19, we observed a significant upregulation of CD74 surface expression on CD4$^+$ and CD8$^+$ T cells in patients with severe (WHO grade $\geq$ 5) compared to patients with only mild disease (WHO grade 1–3), which was accompanied by CD74 upregulation on classical monocytes. Together, our data characterize CD74 as a relevant MHC II-independent functional MIF-receptor in activated human T cells.

Materials and methods

Proteins and reagents

Biologically active and endotoxin-free recombinant human MIF was prepared as previously described [9, 33]. Briefly, recombinant MIF was obtained by expression in the pET11b/*E. coli* BL21/DE3 system, followed by recovery of the supernatant of the bacterial lysate, centrifugation, filtration, purification by Mono Q anion exchange and C8 reverse-phase chromatography, as well as dialysis-based renaturation. The protein as purified by this procedure is essentially endotoxin-free (< 10–15 pg/μg) and exhibits a purity grade of ~ 98% as determined by SDS/PAGE/silver staining [9, 33].

Isolation of human peripheral blood-derived leukocyte subsets

Peripheral blood mononuclear cells (PBMCs) were isolated by density gradient centrifugation using Ficoll-Paque Plus (GE Healthcare, Freiburg, Germany) from peripheral blood (1:3 mixture with PBS) that was collected in conical chambers of a Leukoreduction System (LRS) during thrombocyte apheresis of anonymous and healthy thrombocyte donors at the Division of Transfusion Medicine, Cell Therapeutics and Haemostaseology of the LMU University Hospital. Red blood cells (RBCs) were lysed using RBC lysis buffer (BioLegend, San Diego, USA) for 3 min at room temperature (RT). Subsequently, cells were washed with RPMI 1640 media (Gibco, Karlsruhe, Germany) and supplemented with 10% fetal bovine serum

(FBS). Human CD4$^+$ T cells were isolated by negative depletion from the enriched PBMC fraction using the human CD4$^+$ T-cell isolation kit from Miltenyi Biotec (Bergisch Gladbach, Germany) according to the manufacturer's instructions. The purity of isolated CD4$^+$ T cells was analyzed by flow cytometry using anti-CD3 and anti-CD4 antibodies and estimated to be 95–98% (Supp. Fig. 1A).

Human neutrophilic granulocytes were isolated from blood that was obtained from healthy human volunteers with informed consent by dextran sedimentation followed by a density gradient centrifugation using Ficoll-Paque Plus. Cells were cultivated in RPMI 1640 medium supplemented with 10% FBS, 1% penicillin/streptomycin in a cell culture incubator at 37 °C and 5% CO_2. Studies abide by the Declaration of Helsinki principles and were approved by ethics approvals 18-104 and 23-0639 of the Ethics Committee of LMU Munich, which encompasses the use of anonymized tissue and blood specimens for research purposes.

Analysis of human COVID-19 clinical specimens

PBMCs that were purified by density centrifugation (Histopaque 1077 from Sigma-Aldrich, St. Louis, USA) from 30 patients with PCR-verified COVID-19 infection were obtained from the COVID-19 Registry of the LMU University Hospital Munich (CORKUM, WHO trial ID DRKS00021225). The study was approved by the local ethical committee of the University Hospital (project numbers: 20-245 and 23-0711) and was conducted according to the Guidelines of the World Medical Association Declaration of Helsinki. All patients provided informed consent. Baseline information like age, gender and laboratory status was provided. Patients were classified according to ordinal scale for clinical improvement of COVID-19 infection reported by the WHO (Blueprint W. Novel Coronavirus. COVID-19 Therapeutic Trial Synopsis. 2020. https://www.who.int/blueprint/priority-diseases/key-action/COVID-19_Treatment_Trial_Design_Master_Proto col_synopsis_Final_18022020pdf (accessed on 5 February 2021) [Internet] Available from: https://bsitd.com.bd/wp-content/uploads/2020/06/7_an-international-randomised-trial-of-candidate-vaccines-against-covid-19.pdf.) and grouped into two sub-cohorts based on disease severity in mild (18 patients, WHO grade I–III, mean age of 59.39 years ± 18.24 years, 5 female and 13 male patients) and severe disease (12 patients, WHO grade ≥ V, mean age of 67.50 years ± 11.26 years, 4 female and 8 male patients). Due to heterogeneity of available time-points for each patient, we chose the time-point closest to admission to the hospital. Using inflammation markers C-reactive protein (CRP) and Interleukin 6 (IL-6), we identified the inflammation peak for each patient, defined as the highest measured CRP or

IL-6 value. Human CD3$^+$ T cells were isolated by positive depletion from the enriched PBMC fraction using CD3$^+$ microbeads from Miltenyi Biotec (Bergisch Gladbach, Germany) according to the manufacturer's instructions. CXCR4 and CD74 expression was determined in CD3$^+$-selected cells that were further characterized by CD4, CD8, and HLA-DR surface expression and CD3$^-$-selected cells after identification of monocyte subpopulations by CD14, CD16 and HLA-DR surface expression as described by Marimuthu et al. via flow cytometry using a FACS Canto II (BD Biosciences, Franklin Lakes, USA). Quantification was performed using FlowJo V10 software, version 10.2 (Tree Star, Ashland, USA). (Supp. Figure 1B and 1C, Supp. Table 1) [34].

In vitro activation of peripheral blood-derived CD4$^+$ T cells

When indicated, purified CD4$^+$ T cells were cultivated and in vitro-activated using anti-CD3/CD28-coated magnetic beads (Dynabeads™ Human T Activator, ThermoFisher, Waltham, USA) for different time periods according to the manufacturer's protocol with a bead to cell ratio of 1:1.5 for flow cytometry experiments and 1:4 for WB, immunohistochemistry and functional studies. For following experiments, the activation beads were removed using magnetic separation.

Flow cytometry

The cell surface expression of immune cell markers or MIF receptors was analyzed by flow cytometry using antibodies directed against CD3, CD4, CD8, CD45RO/RA, CD74, CXCR4 or HLA-DR (details in Supp. Table 1). In brief, 2×10^5 cells were washed three times with ice-cold PBS supplemented with 0.5% BSA and then incubated with the above-mentioned antibodies for 1 h at 4 °C in the dark. For intracellular staining, cells were fixed and permeabilized using intracellular fixation and permeabilization buffer (ThermoFisher). After incubation, cells were washed thoroughly and analyzed using a BD FACSVerse™ (BD Biosciences). Quantification was performed using FlowJo V10 software, version 10.2 (Tree Star).

SDS-PAGE and Western blot

For WB analysis, cells were washed three times with PBS and resuspended in Pierce™ RIPA lysis and extraction buffer (ThermoFisher). Protein concentrations of the according cell lysates were determined using the Pierce™ BCA protein assay kit (ThermoFisher) and an EnSpire plate reader (PerkinElmer, Waltham, USA) according to the manufacturer's protocol. Samples were diluted in LDS

sample buffer (NuPAGE, ThermoFisher), boiled at 95°C for 15 min and equal amounts of protein were loaded onto 10% SDS–polyacrylamide gels (NuPAGE, ThermoFisher) and transferred to polyvinylidene difluoride (PVDF) membranes (Carl Roth, Karlsruhe, Germany). The CozyHi prestained protein ladder (highqu, Kraichtal, Germany) was used as a protein size marker. For antigen detection, membranes were blocked in PBS-Tween-20 containing 5% BSA (Roth) for 1 h and subsequently incubated overnight at 4 °C with the primary antibodies anti-β-actin (sc-47778, 1:1000, Santa Cruz, Dallas, Texas, USA) or anti-CD74 (LN1, 555317, 1:500, BD Biosciences) diluted in blocking buffer. On the next day, membranes were washed and incubated with the HRP-linked secondary antibody goat anti-mouse IgG2a (ab97245, abcam, Cambridge, UK) or goat anti-rat IgG (HAF005, R&D Systems, Minneapolis, USA). To reveal protein content, signals were detected by chemiluminescence on an Odyssey® Fc Imager (LI-COR Biosciences GmbH, Bad Homburg, Germany) using SuperSignal™ West Dura ECL substrate (ThermoFisher).

Chondroitinase treatment

To specifically cleave CS modifications of protein in 72 h-activated CD4+ T cells, cells were washed with PBS and resuspended in chondroitinase buffer (50 mM Tris–HCl, pH 8.0, 50 mM sodium acetate). Cells were lysed by 5 min of sonication in a water bath (Elmasonic S 40, Elma Schmidbauer GmbH, Singen, Germany), followed by brief homogenization using steel beads in a bead mill at 50 Hz (TissueLyser LT, QIAGEN, Hilden, Germany). To cleave CS from proteins, chondroitinase ABC from *Proteus vulgaris* (Sigma-Aldrich / Merck KgaA, Darmstadt, Germany) was added to a concentration of 0.6 U/ml. Samples were incubated for 2 h at the enzyme's temperature optimum of 37°C and directly prepared for analysis via SDS-PAGE and WB.

Re-analysis of RNA-seq and mass spectrometry datasets

For analysis of mRNA expression levels, single cell RNA-seq data published by Szabo et al. were re-analyzed [35]. The data is publicly available on the gene expression omnibus (GEO) with Accession Number GSE126030. Plots were generated using the Single Cell Expression Atlas of the European Bioinformatics Institute (EBI) of the European Molecular Biology Laboratory (EMBL) (https://www.ebi.ac.uk/gxa/sc/experiments/E-HCAD-8/results/tsne, last visited 20th of December, 2023). Secondly, a bulk-RNAseq data set together with the according proteomic data as recently published by Cano-Gamez et al. was re-analyzed [28]. The RNAseq raw data were accessed via the Open Targets

website (https://www.opentargets.org/projects/effectorness). Differential gene expression (DEG) analysis between the conditions was performed using R version 4.3.2 and the DESeq2 package [36]. Subsequently, differentially expressed genes (DEGs) were visualized using an EnhancedVolcano plot and ggplot2 [37, 38]. The full analysis code is published on GitHub (https://github.com/SimonE1220/CD74Tcelldiff). The available proteomic raw data were accessed via the Proteomics Identifications Database (PRIDE) under the accession number PXD015315 and analyzed using the Thermo Scientific Proteome Discoverer Software (Version 3.1.1.93). Additionally, proteomic data of resting and activated naive and memory CD4+ T cells published by Wolf et al. were re-analyzed [39]. The data-set is publicly accessible in the GEO with Accession Number GSE147229 and GSE146787 or via www.immunomics.ch (last visited 7th of December, 2023). Re-analysis was performed regarding protein abundance, protein renewal and protein degradation experiments. Graphs were generated using the annotation provided by the author.

Database investigation to evaluate transcriptional CD74 gene regulation

Potential transcription factor binding sites at a maximum distance of 500 base pairs (bp) from the *CD74* gene locus were identified in the Gene Transcription Regulation Database (GTRD) http://gtrd2006.biouml.org/bioumlweb/#de=databases/EnsemblHuman85_38/Sequences/chromosomes%20GRCh38&pos=5:150400041-150514325, last visited on the 25th of May 2024) [40]. The PathwayNet database (https://pathwaynet.princeton.edu/predictions/gene/?network=human-transcriptional-regulation&gene=15273, last visited on the 25th of May 2024) and the STRING network analysis tool (https://string-db.org/cgi/network?taskId=bVkllE1RJOb3&sessionId=b4C13zpxyaPE, last visited on the 25th of May 2024) were used to identify relevant and MHC II-independent CD74 transcriptional regulation [41, 42].

3D migration of human peripheral blood-derived CD4+ T cells by time-lapse microscopy

The three-dimensional (3D) migration behavior of 72 h-activated human CD4+ T cells was assessed by time-lapse microscopy and individual cell tracking using the chemotaxis μ-Slide system from Ibidi GmbH (Munich, Germany). Briefly, CD4+ T cells (4×10^6 cells) were seeded in rat tail collagen type I (Ibidi GmbH) gel in DMEM medium and subjected to a gradient of human MIF (concentration: 200 ng/ml) in the presence or absence of the neutralizing anti-CD74 antibody LN2 (sc-6262, Santa Cruz; 10 μg/ml) or the respective IgG control

(sc-3877, 10 μg/ml) and the CXCR4 receptor inhibitor AMD3100 (A5602, Sigma Aldrich, 10 μg/ml). Cell motility was monitored performing time-lapse imaging every 1 min at 37 °C for 2 h using a Leica inverted DMi8 Life Cell Imaging System equipped with a DMC2900 Digital Microscope Camera with CMOS sensor and live cell imaging software (Leica Microsystems, Wetzlar, Germany). Images were imported as stacks to ImageJ software and analyzed with the manual tracking and chemotaxis and migration tool (Ibidi GmbH) plugin for ImageJ.

Immunofluorescent staining

Cells were fixed with 4% paraformaldehyde (PFA) in PBS (Morphisto GmbH, Frankfurt a. M., Germany) for 15 min. For intracellular staining, cells were additionally permeabilized using TritonX-100 (Serva Electrophoresis, Heidelberg, Germany) in PBS for 10 min. After washing, T cells were blocked in 1% BSA in PBS for 1 h at RT. The blocking solution was removed and the cells incubated with primary antibodies against CD74 (LN2, sc-6262, 1:100, Santa Cruz), CXCR4 (PA3-305, 1:800, ThermoFisher), Bip (ab21685, 1:1000, abcam), or LAMP1 (H-228; 1:100, Santa Cruz) diluted in blocking buffer, at 4 °C overnight. After washing, secondary antibodies (goat anti-mouse Alexa-Fluor 647, A21235, Invitrogen; donkey anti-rabbit Cy3, 711–165-153, 1:300, Jackson ImmunoResearch) and, where indicated, 1 × DAPI was added to the sample and incubated in a humidity chamber for 1 h at RT. Samples were washed and prepared for microscopy using Vectashield® mounting medium (Vector Laboratories, H-1000), either stored at 4 °C in the dark or analyzed directly using a LSM880 AiryScan confocal microscope (Carl Zeiss Microscopy GmbH, Jena, Germany).

Proximity ligation assay (PLA)

For detection of CD74/CXCR4 protein complexes, 72 h-activated CD4$^+$ T cells were stimulated with MIF in indicated concentrations for 40 min following fixation and PLA using the Duolink™ InSitu Orange Starter Kit Mouse/Rabbit (DUO92102) from Sigma Aldrich. For immunofluorescent staining and PLA, the Duolink® PLA fluorescence protocol provided by the manufacturer was essentially followed, using primary antibodies against CD74 (sc-6262, 1:100, Santa Cruz) and CXCR4 (PA3-305, 1:800, ThermoFisher) as described above. Samples were then prepared for microscopy using Duolink® mounting medium with DAPI, and coverslips sealed with

commercially available nail polish and stored at − 20 °C until imaging on a Zeiss LSM880 AiryScan confocal microscope was performed. For quantification of complex formation, PLA dots per cell in four or more randomly selected fields of view were counted for each biological replicate.

Statistical analysis

Statistical analysis was performed using GraphPad Prism Version 8.4.3 software. Unless stated otherwise, data are represented as means ± standard deviation (SD). After testing for normal distribution (evaluated using D'Agostino–Pearson testing or Shapiro–Wilk testing for small sample sizes and QQ plotting), data were analyzed either by two-tailed Student's t-test or Wilcoxon matched-pairs signed-rank test, Mann–Whitney U test or unpaired t test with Welch's correction as appropriate. One-way ANOVA, Friedman test or Kruskal–Wallis test was performed, if more than two data sets were compared as appropriate. To account for multiple comparisons, either Dunnett's or Dunn's multiple comparisons tests were applied as appropriate. Differences with $P < 0.05$ were considered to be statistically significant.

Results

Differentially regulated surface expression of MIF receptors CXCR4 and CD74 in primary human CD4$^+$ T cells upon activation

In order to systematically investigate MIF receptor expression in the course of T-cell activation, we first performed a flow cytometry-based receptor profiling of the known MIF receptors CD74, CXCR4, CXCR2, and ACKR3 on freshly isolated primary human CD4$^+$ T cells. The analysis confirmed an abundant expression of CXCR4 close to 90% in CD4$^+$ T cells, whereas CD74, CXCR2, and ACKR3 showed no appreciable surface expression in non-activated CD4$^+$ T cells (Fig. 1A–D, Supp. Fig. 2D–2G). [43, 44]. However, in vitro T-cell activation with anti-CD3/anti-CD28-coated beads for 72 h revealed a significant upregulation of CD74 surface expression from 0.65 ± 0.95 to 5.93 ± 2.97% (Fig. 1A), accompanied by a significant downregulation of CXCR4 from 89.85 ± 6.43 to 78.03 ± 15.03% (Fig. 1B). CXCR2 and ACKR3 surface expression levels remained unchanged upon activation (Fig. 1C, D, Supp. Fig. 2F and 2G).

The effectiveness of in vitro activation was verified by flow cytometry analysis of the surface activation markers CD45RA, indicating naive T cells, and CD45RO as a marker of activated effector and memory T cells, as well as for HLA-DR, a subunit of the MHC class II complex
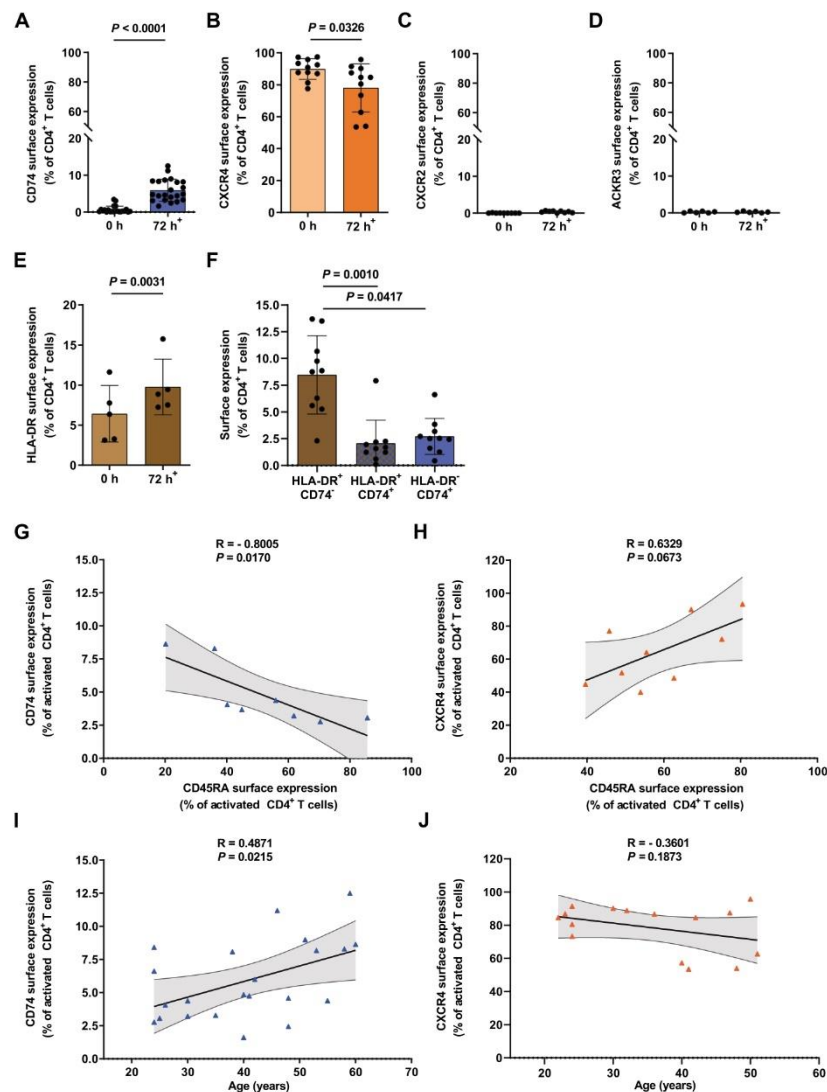
Fig. 1 Cell surface MIF receptor profiling reveals inverse regulation of CD74 and CXCR4 upon T-cell activation. **A–D** MIF receptor profiling on primary human CD4$^+$ T cells upon activation. Flow cytometry-based cell surface receptor profiling of the four MIF receptors CD74, CXCR4, CXCR2, and ACKR3, as indicated, on purified human CD4$^+$ T cells before (0 h) and after 72 h of in vitro T-cell activation. Cell surface receptor-positive cells are plotted for each of the four receptors as percentage of CD4$^+$ T cells. **E, F** MHC class II-independent expression of CD74 on activated CD4$^+$ T cells. HLA-DR surface expression on CD4$^+$ T cells before (0 h) and after 72 h of in vitro T-cell activation determined by flow cytometry. Comparison of percentages of HLA-DR$^+$CD74$^-$, HLA-DR$^+$CD74$^+$ and HLA-DR$^-$CD74$^+$ CD4$^+$ T cells after 72 h of activation. For **A–F**, values are shown as means ± SD with individual datapoints representing independent donors (**A**, n = 22; **B**, n = 11; **C**, n = 9; **D**, n = 6; **E**, n = 5; **F**, n = 10). Differences between the 0 h and 72 h time points were analyzed by paired student's t-test for **B, D, E**; by Wilcoxon matched-

pairs signed-rank test for **A** and **C** and Friedman test with Dunn post-hoc test for **F** as appropriate. 72 h$^+$ indicates time of in vitro T-cell activation in **A–E**. **G, H** Inverse correlation of CD74 and CXCR4 surface expression with the naive cell marker CD45RA. Correlation of surface CD74 and CXCR4 expression with the naive cell marker CD45RA in 72 h-activated CD4$^+$ T cells as evaluated by flow cytometry. Data is displayed as scatter diagrams with individual data points shown (**G**, n = 8; **H**, n = 9). Pearson correlation coefficient was calculated for percentage of CD74$^+$ and CXCR4$^+$ vs. CD45RA$^+$ cells. **I, J** Correlation between MIF receptor expression and donor age. Correlation between CD74 and CXCR4 surface expression and donor age after 72 h of T-cell activation. Data are depicted as scatter plots with individual data points shown (**I**, n = 22; **J**, n = 15). Pearson correlation coefficient was calculated for relation between the percentage of CD74$^+$ and CXCR4$^+$ T cells and donor age. For all panels statistical significance is indicated by actual *P* values.

and previously described T-cell activation marker [45–49]. Activation led to a profound disappearance of the proportion of naive CD4$^+$ T cells and shift towards the activated CD45RA$^-$RO$^+$ phenotype (Supp. Fig. 2A–2C). Consistent with previously published data, HLA-DR surface staining showed a significant activation-dependent increase in HLA-DR$^+$CD4$^+$ T cells from 6.43 ± 3.52 to $9.76 \pm 3.47\%$ after 72 h of activation (Fig. 1E). Co-analysis of both MHC-II related proteins CD74 and HLA-DR revealed that the majority of HLA-DR$^+$ cells were CD74$^-$. Focusing on the CD74$^+$ population, we observed both HLA-DR$^+$/CD74$^+$ ($2.07\% \pm 2.16\%$) double positive cells and a fraction of T cells ($2.71\% \pm 1.68\%$) that expressed CD74 independent of MHC-II (Fig. 1F).

The observed inverse regulation of CD74 and CXCR4 upon activation was further confirmed by analyses revealing a close-to-significant positive correlation between CXCR4 and the naive T-cell marker CD45RA ($r = 0.6329$, $P = 0.0673$) and a significant negative correlation between CD74 and the naive cell marker CD45RA ($r = -0.8005$, $P = 0.0170$) (Fig. 1G, H). Notably, correlation of CD74 and CXCR4 expression with donor age upon activation showed enhanced upregulation of CD74 ($r = 0.4871$, $P = 0.0215$), but only a non-significant trend towards a more pronounced downregulation of CXCR4 ($r = -0.3601$, $P = 0.1873$) with increasing age (Fig. 1I, J).

Abundant intracellular CD74 expression in resting CD4$^+$ T cells and upregulation upon activation

Only a small fraction of CD74 is known to be expressed on the cell surface, while most of CD74 is present in intracellular compartments. This prompted us to investigate intracellular CD74 and CXCR4 protein abundance in T cells via flow cytometry [50, 51]. Remarkably, in freshly isolated non-activated CD4$^+$ T cells, we detected a high percentage of CD74$^+$ cells ($67.30\% \pm 16.94\%$) after membrane permeabilization pointing towards abundant CD74 protein expression even in resting conditions (Fig. 2A). Upon a 72 h-T-cell activation regime, we observed a significant further upregulation of CD74$^+$ CD4$^+$ T cells (67.30 ± 16.94 vs. $91.65 \pm 6.178\%$) up to almost 100% (Fig. 2A). The initially observed variability of CD74 positivity most likely reflected individual donor characteristics, whereas in vitro T-cell activation aligned the T-cell populations leading to a more homogeneously increased percentage. Using the same experimental settings, the percentage of CXCR4$^+$CD4$^+$ T cells was determined before and after activation. CXCR4$^+$CD4$^+$ T cells were significantly diminished after 72 h activation from a baseline of nearly 100% in resting cells to approx. 85% ($99.56\% \pm 0.3386\%$ vs. $82.50\% \pm 8.965\%$) after activation. Nevertheless, CXCR4 remained abundantly expressed (Fig. 2B).

Intracellular localization of CD74 within the ER and endolysosome

CD74 is typically located in cytoplasmic membranes such as the endoplasmic reticulum (ER), the Golgi apparatus and in endosomal or lysosomal vesicles [50, 51]. To verify a potential intracellular localization in these compartments, immunofluorescent co-staining of CD4$^+$ T cells for CD74 together with the ER marker immunoglobulin binding protein (BiP) and the lysosomal marker lysosomal-associated membrane protein 1 (LAMP-1) were performed. Both the distribution pattern of CD74 signal surrounding the nucleus and the overlap of CD74 and BiP signals (yellow) indicate its presence primarily in the ER. Partial colocalization with LAMP-1 further suggests trafficking of CD74 within the endolysosomal compartment. Taken together, immunofluorescent staining of activated CD4$^+$ T cells provided additional proof for CD74 expression and confirmed its localization within the cell in the ER/endolysosomal compartments (Fig. 2C).

Upregulation of CD74 protein expression upon T-cell activation and identification of a chondroitin sulfate-modified p55 isomer

In order to verify and quantify CD74 protein expression in the course of T-cell activation, we performed additional time-dependent WB experiments from freshly isolated, 1 h-, 24 h- and 72 h-activated CD4$^+$ T cells with an antibody against CD74. As expected, we observed protein bands at approx. 33 kDa and 41 kDa, corresponding to the most abundant human isoforms p33 and p41 (Fig. 2D) [52]. Quantification of CD74 protein expression was performed using the most reliably obtained p33 isoform and confirmed an upregulation of CD74 protein expression upon CD4$^+$ T-cell activation (0 h: 0.35 ± 0.31 vs. 24 h: 0.53 ± 0.37 vs. 72 h: 0.82 ± 0.35) (Fig. 2E).

Surprisingly, further comparing non-activated and activated CD4$^+$ T cells in the time-dependent WB experiments revealed an emerging protein band at 55 kDa (p55), which was only present after T-cell activation for 24 h and 72 h (0 h: 0.06 ± 0.07 vs 24 h: 0.41 ± 0.30 vs 72 h: 0.78 ± 0.32) (Fig. 2F). Lysates of Jurkat cells, an immortalized T cell clone that shares many of the features of primary human T cells, were electrophorized for comparison and contained not only the p33 and p41 isoforms, but also the novel p55 variant [53].

It seemed unlikely that p55 band signal is non-specific, as the band pattern was reproducible and was not observed in isolated primary human neutrophils that were included as a negative control in the experiment. The data are in line with previous reports of a specific post-translational chondroitinylated CD74 isoform, CD74-CS, running at
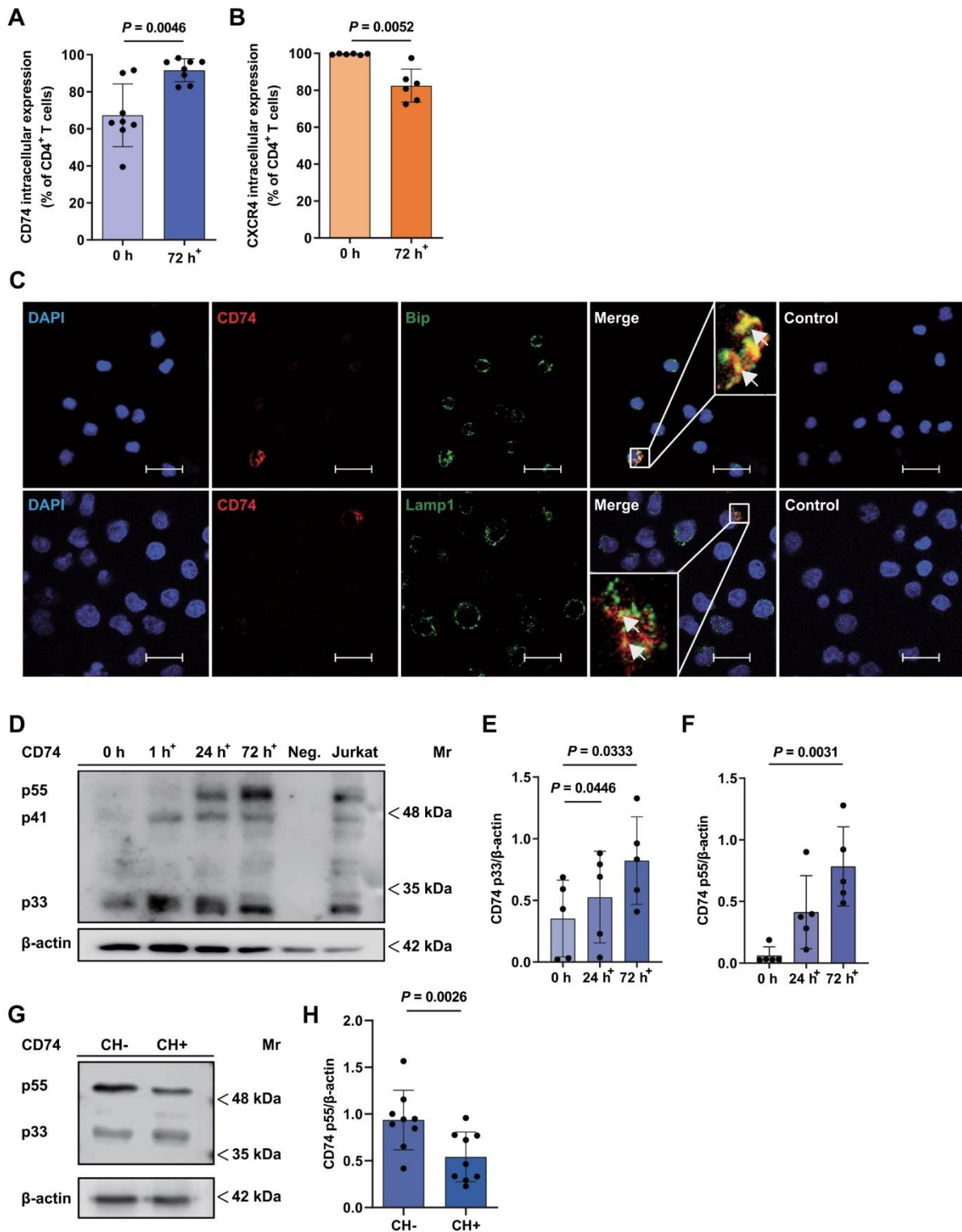
◄**Fig. 2** Constitutive expression and intracellular localization of CD74 in CD4$^+$ T cells. **A**, **B** CD74 and CXCR4 expression in permeabilized CD4$^+$ T cells before and after activation. Intracellular CD74 and CXCR4 expression was evaluated by flow cytometry of permeabilized freshly isolated (0 h) and 72 h-activated CD4$^+$ T cells. Percentages of CD74$^+$ (n = 8) and CXCR4$^+$ (n = 6) cells are shown as means ± SD with individual datapoints representing independent donors. Statistical differences between the 0 h and 72 h time points were analyzed by paired student's t-test. **C** Localization of CD74 in the endoplasmic reticulum (ER) and endolysosomal compartments. Immunofluorescent staining of CD74 (red) together with an ER (BiP, upper row, green) or lysosomal marker (LAMP1, bottom row, green) in 72 h in vitro activated and permeabilized CD4$^+$ T cells imaged via CLSM (scale bar = 20 μm). Cell nuclei were counterstained with DAPI (blue). Samples stained with secondary antibodies alone served as controls. Arrows mark exemplary overlapping signals (yellow). Images shown are representative of three separate experiments. **D**–**F** CD74 protein expression in the course of CD4$^+$ T-cell activation evaluated by SDS-PAGE/WB. CD4$^+$ T cells were purified and lysed before (0 h) or after 1 h, 24 h or 72 h of in vitro T-cell activation following SDS-PAGE and WB analysis for CD74 and β-actin protein expression. Neutrophil cell lysates served as a negative control (Neg.), CD74 protein content of the Jurkat cell line was assessed without prior activation. OD values of the detected p33 and p55 CD74 isoforms before and after 24 h and 72 h of T-cell activation were determined and normalized to β-actin. Upregulation of the p33 and p55 isoforms is displayed as columns (means ± SD) with individual data points (n = 5). For comparison of 24 h and 72 h timepoints to 0 h control, statistical differences were analyzed by one-way ANOVA with Dunnett post-hoc test for **E** and Friedman test with Dunn post-hoc test for **F**. 1 h$^+$, 24 h$^+$, 72 h$^+$ indicate the respective time of in vitro T-cell activation in **A**–**F**. **G**, **H** Evaluation of CD74 protein expression before and after chondroitinase treatment. 72 h-activated CD4$^+$ T cells were lysed and treated with (CH+) or without (CH–) chondroitinase. SDS-PAGE and WB was performed as before for detection of CD74 and β-actin protein expression. Quantification of OD values of CD74 p55 in CH+ s. CH- samples normalized to β-actin displayed as bar chart (means ± SD) with individual data points (n = 9). Statistical differences were analyzed by paired student's t-test. For all bar diagrams, statistical significance is indicated by actual *P* values.

about the same molecular weight [54–56]. Consistent with our observations on CD74 dynamics, previous studies showed a rapid and transient translocation of CD74-CS to the cell surface, followed by immediate endocytosis, so that only a small portion of CD74 was detected on the cell surface [54, 57–62]. Thus, the following experiment was designed to confirm the presence of a CD74-CS isoform. For this purpose, 72 h-activated CD4$^+$ T cells were subjected to either PBS (CH–) or chondroitinase (CH+) treatment. Indeed, following chondroitinase treatment, we noticed the p55 signal intensity to be significantly decreased in comparison to non-treated controls pointing towards a rapid post-translational modification of CD74 with CS, which mediates CD74 translocation to the cell membrane (0.94 ± 0.32 vs. 0.54 ± 0.27) (Fig. 2G, H).

In-depth confirmation of activation-dependent regulation of CD74 and CXCR4 by re-analysis of transcriptomic and proteomic data sets

To gain a deeper insight into the regulation of CD74 in CD4$^+$ T cells, we re-analyzed publicly available scRNA-seq data from Szabo et al. [35]. scRNA data was retrieved from data sets of resting and CD3/CD28-activated (16 h) blood, lung, lymph node and bone marrow-derived CD3$^+$ T cells from two deceased adult organ donors and PBMCs of two healthy blood donors. Ubiquitous expression of CD74 and CXCR4 was clearly evident in both activated and resting T-cell phenotypes (Fig. 3A). However, enhanced expression of CD74 was detected mainly in activated T-cell clusters, whereas enhanced CXCR4 expression was mainly observed in cells with a resting phenotype. Of note, a comparable inverse activation pattern for CD74 and CXCR4 was noted in CD8$^+$ T cells (Fig. 3B).

To verify these results and to assess whether CD74, CXCR4 and MIF expression is influenced by cytokine conditions driving CD4$^+$ T-cell differentiation towards T-cell effector phenotypes during CD3/CD28 activation, we further re-analyzed a publicly available data set of Cano-Gamez et al., who performed a bulk-RNAseq analysis of polarized (resting: no activation, no added cytokines; Th0: control with no added cytokines; Th1: IL-12, anti-human IL-4 antibody; TH2: IL-4, anti-human IFN-γ antibody, Th17: IL-6, IL-23, IL-1β, TGF-β1, anti-human IL-4 antibody, anti-human IFN-γ antibody; iTreg: TGF-β1, IL-2; IFN-β-stimulated group) naive CD4$^+$ T cells after 16 h and 5 d of stimulation (Fig. 3C, D) [28]. DEG analysis confirmed a significant upregulation of CD74 (log2fold change 16 h: 1.37; 5 d: 1.82) and MIF (log2fold change 16 h: 1.12; 5 d: 1.27) expression in 16 h- and 5 d-activated naive T cells, when comparing the resting and Th0 experimental groups. CXCR4 expression in turn was significantly downregulated after 16 h, but showed enhanced expression after 5 d of activation in Th0 vs. resting naive T cells (log2fold change 16 h: − 3.87; 5 d: 1.53). To analyze cytokine-induced polarization of T cells, we performed DEG analysis of 16 h- and 5 d-activated naive T cells (Th0) with the respective polarized experimental group. In fact, most of the cytokine conditions did not lead to any significant changes in CD74, CXCR4 or MIF expression. The only observed significant change regarding CD74 expression was a downregulation in Th17 cells at 5 d (log2foldchange: − 0.77986), accompanied by an upregulation of CXCR4 (log2foldchange: 0.553153) and MIF (log2foldchange: 1.130575). Overall, CD74 mRNA expression was markedly upregulated by T-cell activation in naive CD4$^+$ T cells, while the specific cytokine milieu only showed minor effects. Inverse regulation of the MIF receptors CD74 and CXCR4 during the early activation process was confirmed on mRNA level. Additionally,
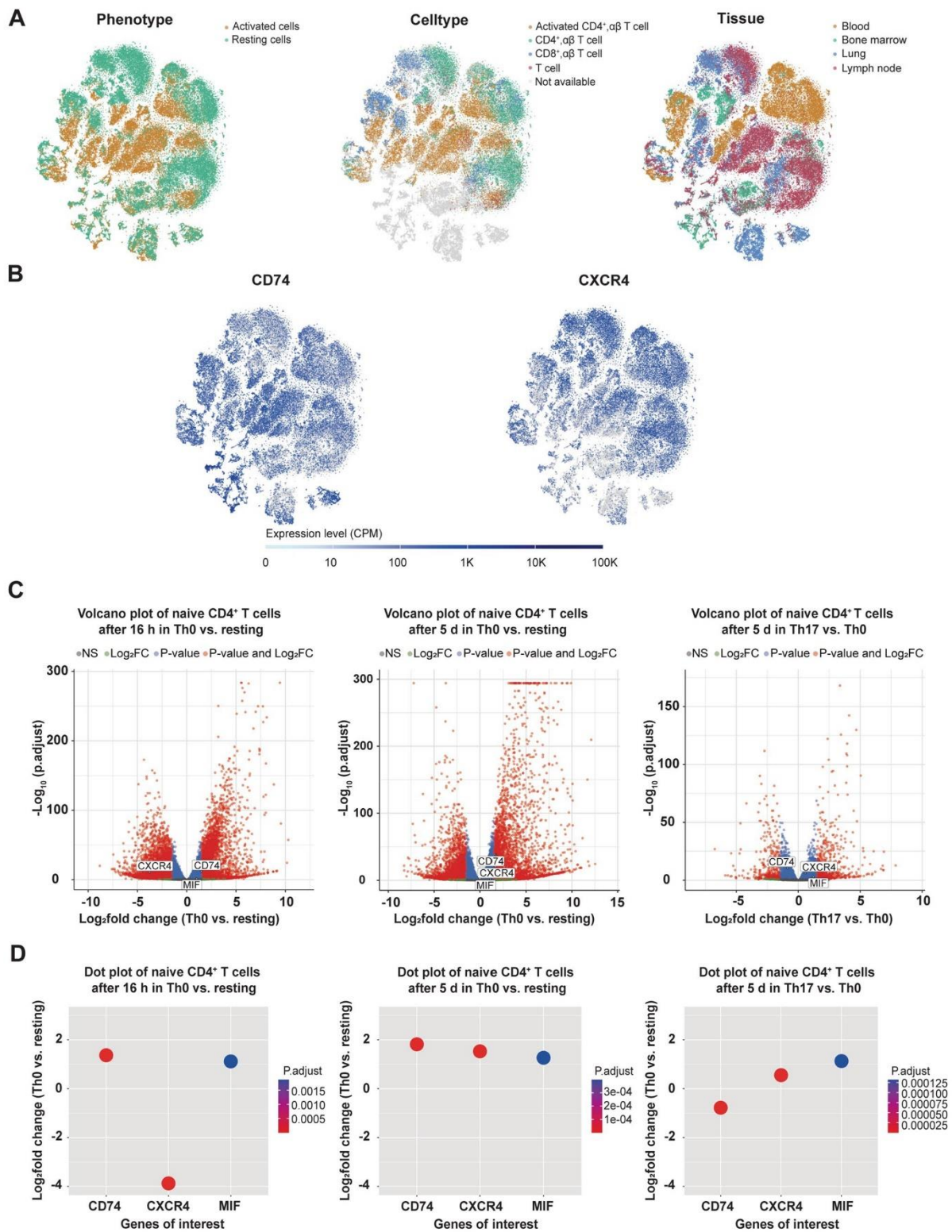
◄**Fig. 3** Evaluation of mRNA expression dynamics of CD74, CXCR4 and MIF in CD4+ T cells. **A**, **B** CD74 and CXCR4 mRNA expression in resting and activated CD4+ T cells. t-SNE embedding for the scRNAseq dataset obtained from Szabo et al. including scRNA data of CD3+ T cells from lung, lung draining lymph nodes and bone marrow of two deceased organ donors and PBMCs of two healthy volunteers [35]. Clusters depicted in the upper row colored by resting (green) vs. activated (orange) phenotype (left), by cell type (middle, orange: activated CD4+ αβ T cells, green: CD4+ αβ T cells, blue: CD8+ αβ T cells, red: T cells, gray: not available) or by tissue (right, orange: blood, green: bone marrow, blue: lung, red. lymph node). mRNA expression levels are depicted in copies per million (CPM) reads of CD74 and CXCR4. **C**, **D** DGE analysis of CD74, CXCR4 and MIF depending on T-cell activation and cytokine polarization in naive CD4+ T cells. Re-analysis of publicly available bulk-RNAseq data of naive CD4+ T cells from three healthy individuals in different activation and cytokine polarization conditions by Cano-Gamez et al. regarding DGE analysis of CD74, CXCR4 and MIF highlighted in volcano plots (upper row, red: genes with log2fold >|1,5| and adjusted $P < 0.05$ changes, blue: genes with log2fold <|1,5| and adjusted $P < 0.05$ changes, green: genes with log2fold >|1,5| but non-significant (ns) changes, grey: genes with log2fold <|1,5| and ns changes) and in dot blots (bottom row, dots highlight significant results between experimental groups with adjusted $P < 0.05$, color scale indicates the respective p-values) including comparison of Th0 (activated without cytokine polarization) vs. resting (non-activated controls) conditions after 16 h (left) and 5 d (middle) as well as Th0 vs. Th17 cytokine polarization after 5 d (right) [28].

obtained data provides further evidence of an increased MIF expression upon T-cell activation (Fig. 3D). To assess whether these smaller effects of additional cytokine polarization on CD74 and CXCR4 mRNA levels are also reflected on protein level, we re-analyzed the proteomic data of 5 d-polarized CD4+ memory T cells from the Cano-Gamez et al. study [28]. Re-analysis confirmed an upregulation of CD74 protein upon T-cell activation, whereas cytokine polarization to T-cell phenotypes did not have any significant impact on CD74 protein abundance (Supp. Fig. 3A). In contrast, CXCR4 protein abundance was markedly increased upon cytokine-driven polarization towards Treg and Th17 phenotypes (Supp. Fig. 3B).

Next, we re-analyzed the proteomic data set of Wolf et al., who studied mRNA translation kinetics, protein turnover and synthesis rates in human naive and activated T cells, to gain a better understanding on the dynamics of CD74 protein expression in CD4+ T cells [39]. At first, we assessed the data on protein turnover and renewal under resting conditions. For this experiment, Wolf et al. measured protein synthesis and turnover rates of non-activated naive and memory CD4+ T cells by applying stable isotope labeling of amino acids in cell culture (SILAC) and subsequent liquid-chromatography coupled mass spectrometry (LC–MS/MS) analysis. The protein synthesis rate was determined based on the proportion of newly synthesized, heavy isotope-labeled amino acid-containing proteins to total protein content after 6, 12, 24 and 48 h of cultivation. The study identified ETS1, a proto-oncogene associated with survival, activation and

proliferation in T cells as the most rapidly renewed transcription factor (renewal ratio of 0.99 after 24 h, estimated half-life of less than 1 h) [63, 64] (Supp. Fig. 3C). Of note, the retrievable data on CD74 renewal yielded comparable results (protein renewal ratio of 0.92 after 24 h, estimated half-life less than 1 h) and thus revealed that CD74 is among the proteins with fastest renewal and turnover rates in resting memory T cells (Fig. 4A). This effect was much less pronounced in naive T cells with a renewal ratio below 50% after 24 h, possibly linking CD74 to homeostasis and preparedness of memory T cells. Supp. Fig. 3C and 3D show protein renewal rates of selected other proteins for further comparison. Re-analysis of protein abundance in naive CD4+ T cells in the course of CD3/CD28 activation confirmed our previous findings showing an upregulation of CD74 and downregulation of CXCR4 protein levels upon activation (Fig. 4B). CD74 upregulation began at 12 h with peak expression of CD74 protein observed after 72 h of activation both in naive and memory T cells with an observed timespan of upregulation of up to 120 h. For comparison, we analyzed the proteomic time course of CD69, IL2Rα/CD25 and HLA-DR, i.e. well-established T-cell activation markers. CD74 upregulation occured between the 'early' marker CD69 and the 'intermediate' activation marker CD25 (Supp. Fig. 3E–3G) [65, 66]. The dynamics of CXCR4 protein expression in naive T cells confirmed the previously observed inverse profile and indicated an immediate down-regulation of CXCR4 protein with a minimum protein abundance seen after 48 h of activation with following protein reconstitution towards 96 h, supporting our above mentioned finding of initially downregulated and later-on induced mRNA expression. We also analyzed MIF in these data sets. Similar to the upregulation pattern seen for CD74, MIF protein was also markedly enhanced upon activation and showed elevated expression in resting naive and memory T cells starting from 24 h, with a peak observed at 96 h (Fig. 4B). In order to specifically address protein degradation, Wolf et al. quantified protein copy numbers by LC–MS/MS in naive CD4+ T cells after inhibition of mRNA translation by cycloheximide (CHX) alone or in combination with bortezomib (PS), a specific inhibitor of the 26S proteasome. CD74 protein levels were only mildly affected by blockade of protein synthesis, speaking in favor of a low protein degradation rate and consistent with a lower renewal in resting naive CD4+ T cells. As CD74 was previously described to be degraded strictly sequentially in the endolysosomal system, additional treatment with PS confirmed the expected proteasome-independent degradation of CD74, while CXCR4 is most likely partially degraded via the proteasome (Fig. 4C) [67]. Furthermore, inhibition of proteasomal degradation did not recover MIF protein levels, suggesting a proteasome-independent degradation of MIF in resting T cells (Fig. 4C).
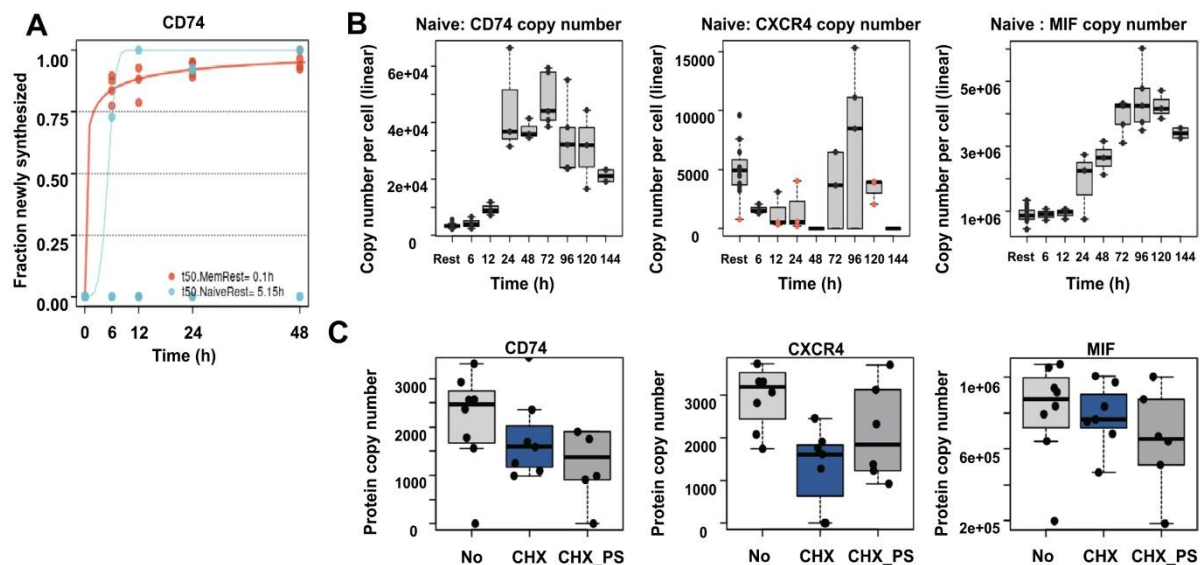
Fig. 4 Evaluation of protein dynamics of CD74, CXCR4 and MIF in CD4$^+$ T cells. **A** Rapid renewal of CD74 in resting memory CD4$^+$ T cells. CD74 protein renewal rates in naive (blue) vs. memory (orange) CD4$^+$ T cells. Fraction of newly synthesized protein calculated from LC–MS/MS analysis of pulsed SILAC of resting CD4$^+$ T cells. Analysis conducted after 0, 6, 12, 24 and 48 h in culture. n = 3–4. **B** Time course of CD74, CXCR4 and MIF protein expression upon activation in naive CD4$^+$ T cells. CD74 (left), CXCR4 (middle) and MIF (right) copy number per cell in naive CD4$^+$ T cells. Label-free quantification of proteins via the MaxQuant algorithm without and after 6, 12, 24, 48, 72, 96, 120 and 144 h of in vitro activation. Proteins identified by MS/MS (black dots) or matching (orange dots). Estimation of copy number per cell based on protein mass of cell. n = 7 for resting naive T cells; n = 3 for 6 h, 12, 48 h, 120 h T cells, n = 4 for 24 h, 72 h, 96 h activated T cells. **C** Analysis of protein degradation in naive CD4$^+$ T cells. Protein copy numbers of CD74 (left), CXCR4 (middle) and MIF (right) in naive CD4$^+$ T cells without treatment (No), with 24 h of cycloheximide treatment alone (CHX, 50 μg/ml) or in combination with 10 μM bortezomib (CHX_PS). Box plots depict median and interquartile range (IQR). Whiskers show lowest data point contained in the 1.5 IQR of lowest quartile and highest data point contained in the 1.5 IQR of highest quartile. n = 5 for No, n = 4 for CHX and n = 6 for CHX_PS. Data in **A**–**C** retrieved from Wolf et al. [39].

Exploring MHC II-independent CD74 transcriptional gene regulation

To explore potential MHCII-independent CD74 transcriptional gene regulation, we performed a database analysis using the Gene Transcription Regulation Database (GTRD) yielding 375 different transcription factor binding sites within a maximum distance of 500 bp from the *CD74* gene locus (Supp. Table 2) [40]. Relevant results were narrowed down by predicting the genes involved in the transcriptional regulation of CD74 using the PathwayNet database [41]. Genes with a relationship confidence of more than 0.1 were included for further consideration (Supp. Table 3). Of the 19 transcription factors identified, four lacked a binding site within 500 bp of the CD74 gene and were therefore excluded. Furthermore, STRING network analysis identified the seven transcription factors with the highest relationship confidence as MHC II transactivator (CIITA)-associated genes, representing the master regulator of MHC II class gene expression (Supp. Fig. 4) [42, 68]. Assuming a common transcriptional regulation of MHC II proteins and CD74 by these transcription factors,

we excluded these hits from our search as well [68, 69]. Among the remaining eight transcription factors, ETS1, a proto-oncogene associated with survival, activation and proliferation in T cells, seemed particularly noteworthy, as it was only recently identified by Wolf et al. as the most rapidly renewed transcription factor in T cells reflecting preparedness towards activating stimuli [39, 63, 64]. By performing an assay for transposase-accessible chromatin (ATAC) and ChIP sequencing, Wolf et al. further investigated genes regulated by ETS1 in CD4$^+$ T-cells [39]. Revisiting the ATAC and ChIP supplemental material of that study, we identified the *CD74* gene to be located in ETS-1-accessible chromatin regions in resting naive CD4$^+$ T cells and revealed actual ETS1 binding in the CD74 promoter region, both suggesting an ETS1 transcriptional regulation of *CD74* in CD4$^+$ T cells. Binding of ETS1 to other MHC II-associated genes was not observed. In conclusion, these data reflect an independent regulation of gene expression for CD74 and MHC II in resting naive CD4$^+$ T cells and identify ETS1 as an associated transcription factor.

Involvement of CD74 and CXCR4 in MIF-mediated CD4$^+$ T-cell chemotaxis

One key attribute of T cells is their ability to migrate towards sites of inflammation. MIF-mediated T-cell recruitment is a well characterized atherogenic MIF effect that has been assumed to be primarily mediated via CXCR4 [4, 70]. In order to determine the functional relevance of CD74 surface upregulation in activated human CD4$^+$ T cells, we assessed their migratory capacity in response to MIF applying a 3D chemotaxis assay that allows for tracking single cell migration trajectories via live cell imaging. MIF potently promoted chemotactic migration of activated CD4+ T cells in a bell-shaped dose–response behavior typically observed for chemokines, with maximal MIF-induced chemotaxis seen at 200 ng/ml of MIF (Supp. Fig. 5A and 5B). Therefore, this concentration was used for all subsequent migration assays. In a next step, we performed co-incubation experiments with AMD3100, a selective pharmacological CXCR4 inhibitor and the CD74-neutralizing antibody LN2. MIF-induced chemotaxis was fully abrogated when MIF was co-incubated with AMD3100 and LN2 either alone or in combination, while incubation of T cells with the inhibitors alone or isotype control immunoglobulin (IgG) showed no significant effects on cell motility (Fig. 5A, B, Supp. 5C and 5D). Taken together, we show involvement of CD74 and CXCR4 in MIF-elicited chemotaxis of activated CD4$^+$ T cells. Mechanistically, joint involvement of CD74 and CXCR4 may be explained by CD74/CXCR4 heterocomplex formation as previously observed in model cell lines after overexpression or by synergistic/converging signaling pathways [8].

CD74 and CXCR4 complex formation in activated CD4$^+$ T cells determined by proximity ligation assay

To evaluate whether CD74 and CXCR4 heterocomplex formation occurs in activated CD4$^+$ T cells, we first established immunofluorescent co-staining of CD74 and CXCR4 on 72 h-activated CD4$^+$ T cells. Stainings were performed without cell permeabilization to specifically detect cell surface-bound receptors. Widefield and confocal laser scanning microscopy (CLSM) provided initial evidence for a colocalization of CD74 and CXCR4 on 72 h-activated T cells (Fig. 5C). To investigate whether colocalized CD74 and CXCR4 indeed form heterocomplexes, a PLA was performed which detects inter-molecular interactions within a distance of < 40 nm and represents an established method to identify chemokine receptor heterocomplexes [12]. Specific PLA signals were detected in 72 h-activated T cells, demonstrating the occurrence of CD74 and CXCR4 heterocomplexes (Fig. 5D). Stimulation with 200 ng/ml MIF significantly decreased PLA-signal indicating a MIF-induced

signal transduction by internalization of CD74/CXCR4 receptor complexes (Fig. 5E). To our knowledge these results provide the first evidence of CD74/CXCR4 heterocomplex internalization in the context of MIF signaling.

CD74 surface upregulation in CD4$^+$ and CD8$^+$ T cells during severe COVID-19 infection

Finally, to explore the translational relevance of our findings, we assessed CD74 and CXCR4 surface expression in T cells and monocytes isolated from patients with mild (WHO 1–3) and severe (WHO grade $\geq$ 5) COVID-19 disease, which were obtained from the COVID-19 Registry of the LMU University Hospital Munich (CORKUM). Due to the retrospective approach of this study and heterogeneity of available time points for each patient, we chose to evaluate the MIF receptor profile at time points closest to admission to the hospital. As not all laboratory indices were available at any given time point, we identified the inflammation peak for each patient defined as the highest measured CRP or IL-6 value for additional comparison of both groups. As expected, the inflammation markers CRP (9.71 ± 9.07 vs. 21.58 ± 8.15) and IL-6 (215.1 ± 516.5 vs. 2464 ± 4654) were significantly increased in the severely affected patients (Fig. 6A).

In line with a recently published report by Westmeier et al., we observed a significant upregulation of CD74 surface expression on CD4+ ($5.71\% \pm 3.87\%$ vs. $23.75\% \pm 13.24\%$) and CD8$^+$ ($9.52\% \pm 6.95\%$ vs. $34.02\% \pm 17.80\%$) T cells in the severe disease group compared to patients with mild disease (Fig. 6C, E) [71]. Notably, CD74 expression was higher in the CD8$^+$ T cells ($34.02\% \pm 17.80\%$) compared to CD4$^+$ T cells ($23.75\% \pm 13.24\%$) among severe patients. In contrast, we observed no significant differences between both groups regarding CXCR4 and HLA-DR surface expression again pointing towards an HLA-DR-independent upregulation of CD74 (Fig. 6D, F, G). When comparing CD74 and CXCR4 surface expression on monocyte populations, we further observed a significant upregulation of CD74 in classical (CD14^{++}CD16$^-$) monocytes in the severe disease group compared to patients with mild disease (Supp. Fig. 6A–6E). Overall, we confirmed an upregulation of the MIF receptor CD74 in CD4$^+$ and CD8$^+$ T cells in critically ill COVID-19 patients.

Discussion

Here, we provide novel insights in constitutive and activation-dependent mRNA and protein dynamics of CD74 in CD4$^+$ T cells. Our analyses reveal CD74 upregulation, post-translational modification with CS and MHC II-independent translocation to the cell surface upon T-cell activation. Surface CD74 forms heterocomplexes with the

A

B

C

D

E
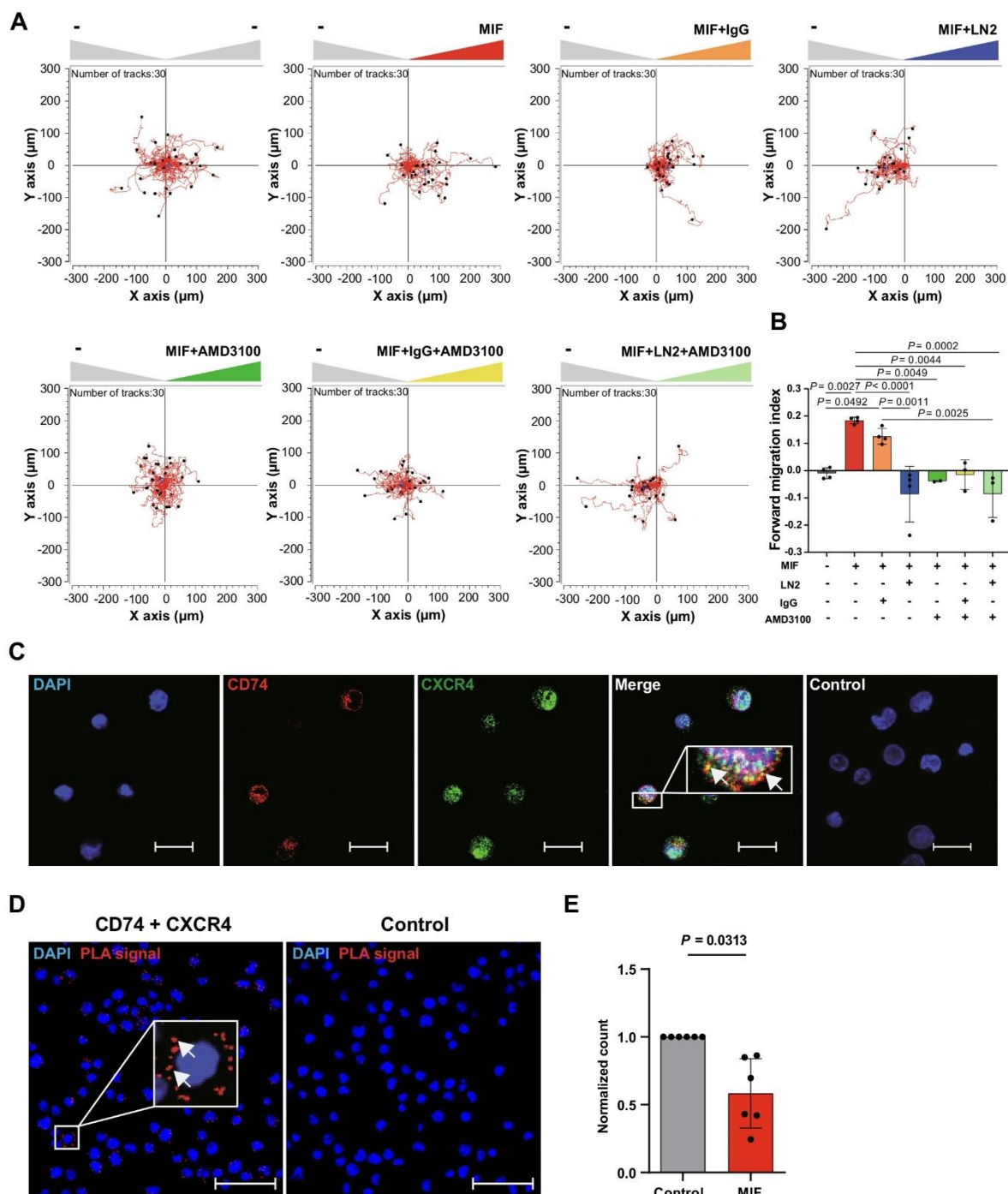
classical chemokine receptor CXCR4 and is mechanistically involved in MIF-elicited T-cell chemotaxis. Dysregulated CD74 expression in severe COVID-19 disease patients demonstrates the translational relevance of our findings.

Most likely due to its classical and well-established MHC II-related functions, CD74 was initially overwhelmingly studied in antigen-presenting cells, most notably monocytes/macrophages and B cells [1]. The discovery of CD74 as the cognate MIF receptor has partially changed this picture.

◄**Fig. 5** Involvement of CD74 and CXCR4 in MIF-mediated CD4$^+$ T-cell chemotaxis. **A** Both MIF receptors CXCR4 and CD74 are required for MIF-elicited migration of activated CD4$^+$ T cells as assessed by 3D chemotaxis assay. Representative trajectory plots (x, y = 0 at time 0 h) of migrated activated CD4$^+$ T cells (72 h) in a three-dimensional (3D) aqueous collagen-gel matrix towards a MIF chemoattractant gradient (MIF concentration: 200 ng/ml, –: control medium) that was established in presence or absence of a CD74 neutralizing antibody, a corresponding isotype control (IgG) or the CXCR4 receptor inhibitor AMD3100. Cell motility was monitored by time-lapse microscopy for 2 h at 37 °C, images were obtained every minute using the Leica DMi8 microscope. Single cell tracking was performed of 30 cells per experimental group. The blue cross-hair indicates the cell population's center of mass after migration. **B** Quantification of the 3D chemotaxis experiment in **A** showing inhibition of MIF-induced CD4$^+$ T-cell migration upon co-incubation with CD74 neutralizing antibody and AMD3100 either alone or in combination. Plotted is the calculated forward migration index (FMI, means ± SD) based on manual tracking of at least 30 individual cells per treatment (n = 2–4). Statistical differences were analyzed by one-way ANOVA with Tukey post-hoc test and indicated by actual *P* values. **C** Cell surface colocalization of the MIF receptors CD74 and CXCR4 on activated CD4$^+$ T cells. Immunofluorescent cell surface staining of CD74 (red) and CXCR4 (green) either alone or in combination on 72 h-activated CD4$^+$ T cells imaged via CLSM (scale bar = 20 μm). Cell nuclei were counterstained with DAPI (blue). Samples stained with secondary antibodies alone served as controls. Images shown are representative of two independent experiments. **D, E** Proximity ligation assay indicating CD74/CXCR4 heterocomplex formation and MIF dependent internalization. **D** Display of a representative PLA result visualizing the interaction of CD74 and CXCR4 on the cell surface of 72 h-activated CD4$^+$ T cells (red dots indicating positive PLA signal; imaged via CLSM; 40 × objective, DAPI, blue; scale bar: 50 μm). **E** Quantification of CD74/CXCR4 heterocomplexes on the cell surface of 72 h-activated CD4$^+$ T cells upon stimulation with MIF (200 mg/ml) prior to fixation (means ± SD of PLA dots /cell normalized to control, n = 6). Statistical differences were analyzed by Wilcoxon matched-pairs signed-rank test and indicated by actual *P* values

In the course of these studies, MIF/CD74 pathways were not only examined in monocytes and macrophages, but it turned out that CD74 can be abundantly expressed in several types of cancer cells and may be upregulated in certain other cell types such as endothelial cells or cardiomyocytes upon inflammatory stimulation or stress [21, 26–28]. However, MHC class II-negative T cells have mostly been neglected in this regard. Only a handful of descriptive reports on CD74 expression in human T cells exist, mainly in context of disease, and without scrutinizing any mechanisms. Yang et al. investigated CD74 surface expression in PBMCs after stroke and amongst other cell types found a significant increase in the number of CD74-expressing CD4$^+$ T cells but not CD8$^+$ T cells [26]. Fagone et al. showed an upregulation of CD74 gene expression in CD4$^+$ T cells upon activation, that was unchanged in T cells from healthy donors vs. patients with multiple sclerosis [27]. In contrast, in the chronic inflammatory context of rheumatoid arthritis, Sánchez-Zuno et al. observed the percentage of CD74 expressing T cells to be below 1% [72]. To our knowledge, Gaber et al. provided the

only functional evidence of CD74 in human CD4$^+$ T cells reporting on an inhibition of MIF-induced T-cell proliferation using a neutralizing CD74 antibody [21]. However, the relevance of this observation has remained unclear, as no isotype control immunoglobulin was used in that study. In contrast to CD74, regulation of CXCR4 in T cells has been studied comprehensively, also as it plays an important role in the docking-process of the human immunodeficiency virus and mediates CXCL12-driven co-stimulatory and migratory T cell responses [73–76].

Our MIF receptor profiling of freshly isolated primary human CD4$^+$ T cells revealed the expected abundant expression of CXCR4, whereas no substantial surface expression of CD74, CXCR2 and ACKR3 could be detected. This identifies non-activated human CD4$^+$ T cells as a suitable cell type to study the MIF/CXCR4 axis. In previous reports, CXCR4 expression was shown to be downregulated in the context of T-cell activation, which is confirmed by our study [73, 75]. Nevertheless, CXCR4 remained abundantly expressed also in activated T cells.

An unanticipated effect was the observation of a significant upregulation of CD74 surface expression upon T-cell activation. Of note, this upregulation was independent of HLA-DR pointing towards an MHC II-independent role of CD74 in CD4$^+$ T cells. Interestingly, CD74 surface expression correlated with donor age, indicating a potentially more pronounced CD74 upregulation in memory and effector T cells compared to naive T cells, due to physiologically increased abundance of these phenotypes upon enhanced antigen encounters during aging [77–79].

Our MIF receptor profiling of resting and activated CD4$^+$ T cells as well as re-analysis of CD4$^+$ T-cell proteome data from Wolf et al. revealed no expression of CXCR2 in T cells, which is in line with multiple literature reports, but stands in contrast to the recent finding of CXCR2/CD74 co-expression in T cells as reported by Westmeier et al. [80]. Expression of ACKR3 in T cells still remains controversial [81, 82].

As CD74 is known to be expressed only in small percentages on cell surfaces and is mainly stored in intracellular deposits, we next evaluated CD74 protein expression after membrane permeabilization via flow cytometry. Unexpectedly and to date unknown, we detected an abundant intracellular expression of CD74 in freshly isolated T cells, which was further enhanced by T-cell activation. WB experiments confirmed enhanced CD74 expression with detection of protein bands corresponding to the known p33 and p41 isoforms in humans [1, 52, 83, 84]. However, due to the small difference in size a clear differentiation between short and long isoforms of the protein regarding p33 vs. p35 and p41 vs. p43 isoforms was not possible. Interestingly, we observed an additional pronounced protein band at approximately 55 kDa, which appeared only after 24 h of T-cell activation and further
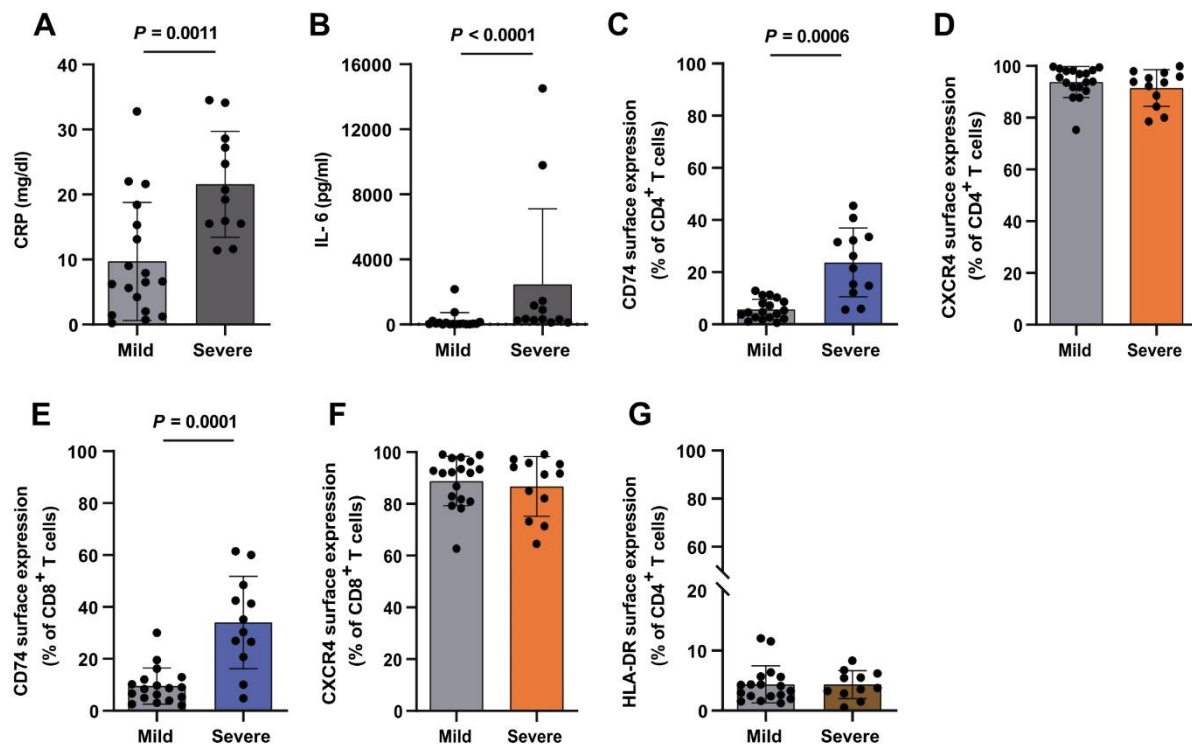
Fig. 6 MHC-II independent upregulation of CD74 in T cells of critically ill COVID-19 patients. **A**, **B** Increased inflammatory markers CRP and IL-6 in patients with severe COVID-19 disease. Serum peak concentrations of inflammatory markers CRP (mg/dl) and IL-6 (pg/ml) from laboratory results of patients with mild (WHO 1–3, n = 18) vs. severe (WHO ≥ 5, n = 12) COVID-19 disease. **C**–**F** CD74 and CXCR4 surface expression on CD4$^+$ and CD8$^+$ T cells from mild vs. severe disease patients. **G** No significant differences in HLA-DR surface expression in COVID-19 patient cohorts classified by disease severity. Results of a flow cytometry-based cell surface receptor profiling. Bar charts in **A**–**G** show means ± SD with individual datapoints representing independent patients. Cell surface receptor-positive cells are plotted as percentages of the respective T-cell phenotype. Statistical differences were analyzed by unpaired t test for **A** and **C** and Mann–Whitney U test for **B**, **D**, **E**, **F**, and **G** and indicated by actual *P* values.

increased in abundance during activation, even exceeding the most abundant p33 protein band. Previous reports identified a specific CD74 isoform, CD74–CS that is being reported to run at a similar molecular weight and is product of a post-translational modification with the glycosaminoglycan CS at Ser 201. The modification was shown to enable the translocation of CD74 molecules towards the cell surface, while due to following rapid endocytosis only a small proportion can be transiently detected on the cell surface [54–62]. In fact, when we treated our T-cell samples with chondroitinase, an enzyme that specifically cleaves CS, we noticed the signal intensity of the observed p55 isoform to be significantly decreased in comparison to untreated controls. Nevertheless, we acknowledge that treatment with chondroitinase did not lead to a complete disappearance of the observed band, which could be explained by sub-optimal buffer conditions due to the strong pH-dependency of the enzyme or non-sufficient incubation time. Furthermore, several other post-translational modifications, such as

O- and N-silylation, palmitoylation and phosphorylation, have been reported for CD74 that were not studied in this work [85–87]. Despite these limitations, we speculate that post-translational modification of CD74 with CS might be the underlying mechanism of CD74 translocation to the cell surface during the process of T-cell activation. Immunofluorescent co-staining of CD74 with ER and lysosomal markers verified the typical localization of CD74 in the ER and suggested a functional trafficking of CD74 within the endolysosomal compartment. Re-analysis of two independent RNAseq data sets from the Cano-Gamez et al. and Szabo et al. studies and two proteomic data sets from the Cano-Gamez et al. and Wolf et al. publications comparing resting and activated T-cell states, complemented our data and provided substantial corroborating evidence that CD74 is constitutively expressed in resting T cells and becomes rapidly upregulated upon T-cell activation in a sustained manner [28, 35, 39]. The proteome data suggested a maximum CD74 protein abundance after 72 h and again

identified a counter-regulation of CD74 and CXCR4 in the early activation phase. After the initial downregulation, CXCR4 expression was then found to be reconstituted after approximately 3 to 4 d. Of note, CD74 upregulation occurred after upregulation of the early activation marker CD69, but before the intermediate activation marker CD25 [65, 66]. Cytokine polarization to T-cell effector phenotypes had no additional effects on CD74 protein abundance. In contrast, CXCR4 protein expression was upregulated after 5 days of Treg and Th17 polarization, possibly linked to an already described TGF-β-induced CXCR4 expression mechanism [88].

The study by Cano-Gamez et al. caught our attention as CD74 incidentally appeared as a strong marker protein of natural Tregs and effector memory T cells re-expressing CD45RA (TEMRA) in their presented data, possibly linking CD74 protein expression to T-cell effectorness [28]. Since observations of CD74 expression have often been made under inflammatory conditions, as for instance IFN-γ-rich environments, or in a disease context, we compared DEGs of regularly activated T cells (Th0) with activated T cells that were additionally differentiated towards Th0, Th1, Th2, iTreg and Th17 phenotypes through established cytokine polarization protocols [89]. Notably, except for the observed reduction of CD74 in Th17 conditions, cytokine conditions did not trigger significant changes. Therefore, T-cell activation represents the main stimulus for CD74 upregulation independent of the surrounding inflammatory cytokine milieu. Interestingly, Th17-polarized cells were also the only phenotype with significantly upregulated MIF expression compared to non-polarized CD4⁺ T cells, fitting to previous data indicating a role of MIF in Th17 T-cell differentiation [18, 20, 24]. Re-analysis of proteomic data further identified CD74 to be rapidly renewed in resting memory CD4⁺ T cells, potentially pointing towards a role of CD74 in memory T-cell homeostasis.

We also aimed to identify potential MHC II-independent *CD74* transcriptional gene regulation. Combining a database analysis of the GTRD, PathwayNet and STRING network databases enabled us to narrow down relevant and potential MHC II-independent transcription factors within a 500 bp distance from the CD74 gene locus. However, we like to emphasize that the here provided database research approach mainly relies on the quality of the included pathway/protein interaction prediction tools and can only be interpreted as a first approximation to the subject. The list of eight CIITA-independent transcription factors with high confidence predictions included ETS1, a crucial transcription factor for T-cell survival and activation [63, 64]. In this context, Wolf et al. identified ETS1 as the most rapidly renewed transcription factor in T cells reflecting preparedness towards activating stimuli [39]. Accordingly, by performing

an ATAC assay, Wolf et al. found that the ETS1 transcription factor binding motif can be detected in accessible promoter regions of the resting naive CD4⁺ T-cell genome. About half of these binding sites were located in promoter regions, suggesting ETS1 as a transcriptional regulator of the promoter-associated genes. Interestingly, supplementary data of Wolf et al. shows that the CD74 gene is located in accessible chromatin regions in naive CD4⁺ T cells. Based on a ChIP analysis, showing actual ETS1 binding in the CD74 promoter region, transcriptional regulation of CD74 by ETS1, a transcription factor associated with T-cell preparedness for rapid activation, seems conceivable. Binding of ETS1 to other MHC II-associated genes was not observed, which may be either related to insufficient accessibility of the MHC II-related genes in resting naive CD4⁺ T cells or differential ETS1 gene binding.

Taken together, we hypothesize that ETS1-driven regulation of CD74 expression might be the underlying process of the observed rapid CD74 induction after activation, which, together with post-translational chondroitin sulfatinylation of constitutively expressed intracellular CD74, serves to rapidly establish marked CD74 surface expression. Once positioned on the cell surface, CD74, functioning as the cognate MIF receptor, can mediate downstream signaling events [90].

In the absence of an identified classical signaling-competent cytosolic domain in the short cytoplasmic tail of CD74, two alternative distinct tracks of CD74 signaling have been reported. First, CD74 signaling can be mediated by its intracytoplasmic domain (ICD), which is proteolytically cleaved by the intramembrane protease signal peptide peptidase-like (SPPL)2a and subsequently translocates into the nucleus, where it functions as a transcription factor and/or transcriptional coactivator [90–92]. Whether this process occurs in the endolysosomal compartment or on the cell surface and how it is exactly triggered by extracellular MIF has remained partly unclear. A second signaling CD74 pathway involves the association of CD74 with a co-receptor. Depending on the cellular and (patho)physiological context this can be CD44, the initially identified co-receptor of CD74, or one of the MIF chemokine receptors, i.e. CXCR2, CXCR4 or ACKR3/CXCR7 [4, 8, 11, 12]. In our study, we provide evidence for a role of CXCR4, as we obtained evidence from PLA and chemotaxis experiments for CD74/CXCR4 heterocomplex formation to facilitate MIF-elicited chemotaxis of activated T cells. We also obtained evidence for MIF-induced internalization of CD74/CXCR4 heterocomplexes from the surface of T cells.

As mentioned above, CD44 represents another potential co-receptor of CD74 in T cells that is abundantly expressed and is an established activation marker of T cells. Additional studies are necessary to evaluate the functional relevance of CD74/CD44 interactions in T cells [11, 93].

An impaired adaptive immune response linked to sustained T-cell activation and a dysregulated IFN-response is believed to be a significant determinant of COVID-19 progression [30, 32, 94, 95]. Furthermore, accumulating evidence points towards a critical role of MIF as a prognostic marker to predict disease severity and patient outcome in COVID-19 disease. Notably, a recent study by Westmeier et al. investigated MIF receptor expression in CD4$^+$ and CD8$^+$ T cells in COVID-19 patients with mild and severe disease and observed an increased expression of CD74 in CD4$^+$ and CD8$^+$ T cells compared to healthy controls [71]. Interestingly, the authors also observed an inducible expression of CXCR2 and CXCR4 upon SARS-CoV-2 infection pointing towards increased susceptibility to MIF-mediated signaling in the

course of COVID-19 disease. A characterization of T-cell subpopulations in their study revealed a predominant central and effector memory phenotype of the CD74-expressing T cells that further produced higher cytotoxic molecules and expressed enhanced proliferation markers. In accordance, we observed a significant upregulation of CD74 surface expression on CD4$^+$ and CD8$^+$ T cells in the severe disease group, when comparing patient cohorts with mild and severe COVID-19 disease. In contrast, no significant differences between both groups regarding CXCR4 expression was observed. CD74 markedly exceeded HLA-DR expression, which showed no significant changes between both cohorts, again confirming an MHC II–independent regulation of CD74 in T cells. Of note, CXCR4 and CD74 expression was also
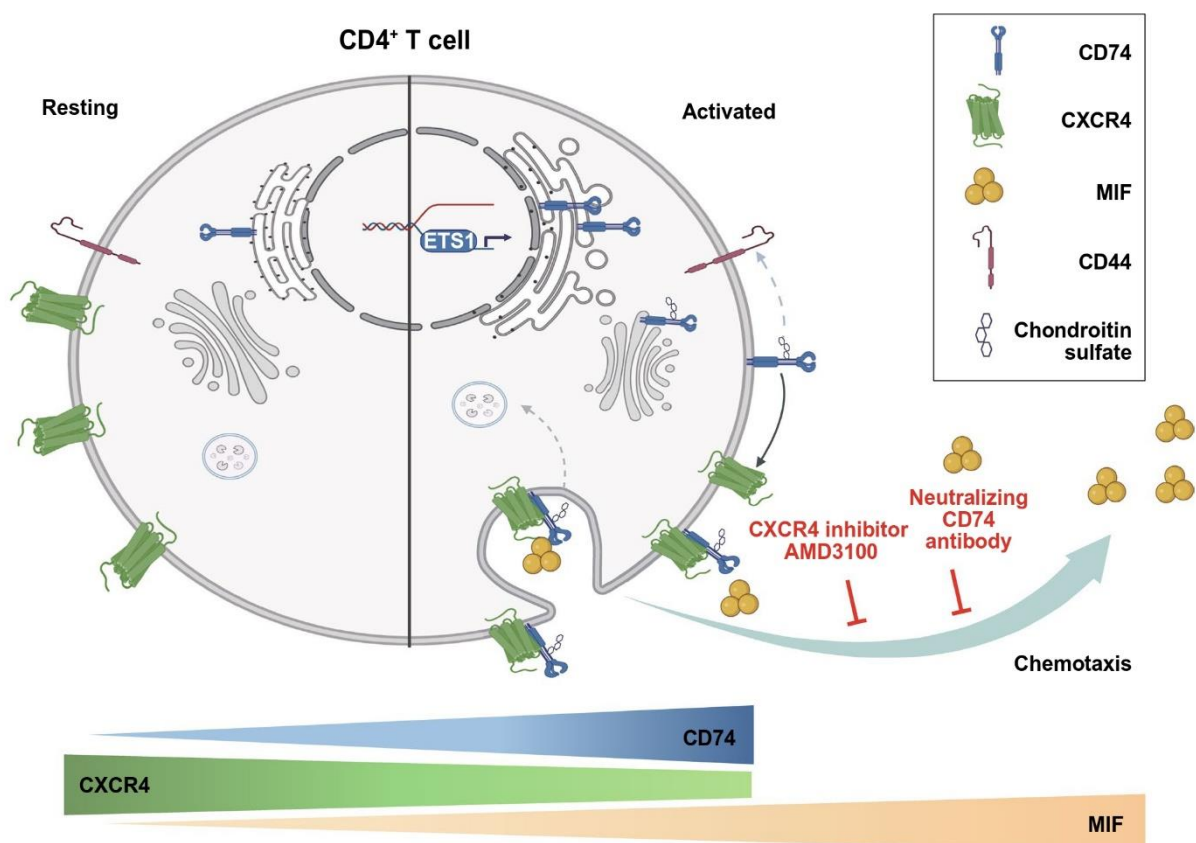
Fig. 7 Scheme of the regulation of the MIF receptors CD74 and CXCR4 in resting and activated CD4$^+$ T-cell state. During resting state, CD4$^+$ T cells express CXCR4 abundantly on the cell surface, while CD74 is constitutively expressed and synthesized intracellularly. Most likely due to its retention signal CD74 resides in the ER with functional circulation in the endolysosomal compartment. Triggered by T-cell activation, CD74 gene expression and protein synthesis is rapidly upregulated in contrast to the initially repressed CXCR4 expression. We speculate, that ETS1 might be involved in the rapid regulation of CD74 in this process. Furthermore, CD74 molecules are post-translationally modified by addition of chondroitin sulfate

moieties. This modification enables rapid transport of CD74 towards the cell surface, where it can act as a functional surface receptor for MIF, a proinflammatory cytokine that is secreted during T-cell activation and exerts additional auto- and paracrine effects. In activated CD4$^+$ T cells, MIF leads to internalization of CD74/CXCR4 receptor complexes. Both receptors are crucial for MIF-induced chemotaxis, as blockade of either CXCR4 or CD74 abrogates CD4$^+$ T-cell migration towards MIF. Scheme was created with BioRender.com (license of the Institute for Stroke and Dementia Research)

monitored in monocyte subpopulations in the same patient cohort revealing enhanced expression of CD74 in classical monocytes again without significant changes in CXCR4 expression. We speculate that the observed upregulation of CD74 reflects increased COVID-19-induced T-cell activation states, which might enhance susceptibility towards MIF [30, 32]. However, suitability of T-cell CD74 as a potential biomarker for disease progression in COVID-19 and its relevance in other inflammatory or malignant diseases accompanied by broad T-cell activation still needs to be evaluated in future prospective trials. Furthermore, due to the small patient cohort and heterogeneity a subgroup-specific analysis based on factors such as age, gender or comorbidities was not feasible in the presented study.

In summary, our data identify CD74 as a functional MIF receptor and MHC II-independent activation marker of activated CD4+ T cells mediating MIF-driven CD4+ T-cell chemotaxis, most likely through complex formation with CXCR4. CD74 and CXCR4 expression levels behave inversely in the course of T-cell activation. Induction of CD74 occurs rapidly upon activation stimulus in naive and memory T cells leading to an activation-induced chondroitin sulfated isoform. We have thus unraveled a previously unrecognized MIF/CD74/CXCR4 signaling pathway in activated human T cells with functional relevance for T-cell motility and potentially other activities of activated T cells (Fig. 7). We confirm high CD74 surface expression in T cells under disease conditions in critically ill COVID-19 patients potentially linking dysregulated CD74 to disease severity. Thus, targeting the dysregulated MIF-CD74 axis might resemble a tractable treatment strategy to interfere with the critical role of MIF in the COVID-19 disease context. To this end, future studies will be needed to clarify whether CD74 could have implications in immunosenescence of T cells with potential relevance for the enhanced susceptibility of the aging population to infections like COVID-19 or reduced responses to vaccinations [96–98].

Author contributions Adrian Hoffmann and Jürgen Bernhagen conceived and designed the study. Lin Zhang, Iris Woltering, Adrian Hoffmann, Mathias Holzner, Markus Brandhofer, Carl-Christian Schaefer, Genta Bushati, Simon Ebert, Bishan Yang performed research and analyzed data. Omar El Bounkari, Patrick Scheiermann, Lin Zhang, Iris Woltering, Adrian Hoffmann, and Jürgen Bernhagen contributed to the interpretation of the data. Maximilian Muenchhoff, Johannes C. Hellmuth, Clemens Scherer, Christian Wichmann, David Effinger and Max Hübner contributed to critical materials. The first draft of the manuscript was written by Adrian Hoffmann, Lin Zhang, and Iris Woltering, with help from Jürgen Bernhagen. All authors revised and commented on the manuscript drafts and approved the final manuscript. Jürgen Bernhagen and Adrian Hoffmann provided funding for the study.

Data availability and material All data and materials as well as software application information are available in the manuscript, the supplementary information, or are available from the corresponding authors upon reasonable request. The dataset published by Szabo et al., which was re-analyzed during the current study is publicly available on the gene expression omnibus (GEO) under accession number GSE126030 [35]. Plots were generated using the Single Cell Expression Atlas of the European Bioinformatics Institute (EBI) of the European Molecular Biology Laboratory (EMBL) (https://www.ebi.ac.uk/gxa/sc/experiments/E-HCAD-8/results/tsne, last visited 20th of December, 2023). Secondly, a bulk-RNAseq data set together with the according proteomic data as recently published by Cano-Gamez et al. was re-analyzed [28]. The RNAseq raw data were accessed via the Open Targets website (https://www.opentargets.org/projects/effectorness) and subsequently re-analyzed as described in the manuscript. The full analysis code is published on GitHub (https://github.com/SimonE1220/CD74Tcelldiff). The available proteomic raw data were accessed via the Proteomics Identifications Database (PRIDE) under the accession number PXD015315. Additionally, a data set published by Wolf et al. was re-analyzed [39]. The data-set is publicly accessible in the GEO with accession number GSE147229 and GSE146787 or via www.immunomics.ch (last visited 7th of December, 2023).

Declarations

Conflict of interest C.S. received speaker honoraria from AstraZeneca on topics outside of the submitted work. J.B. and O.E.B. are inventors on patent applications related to anti-MIF strategies. All other authors declare no competing interests.

Ethics approval and consent to participate Studies abide by the Declaration of Helsinki principles and all patients provided informed con-

sent. Studies were approved by ethics approvals 18-104 and 23-0639 of the Ethics Committee of LMU Munich, which encompasses the use of anonymized tissue and blood specimens for research purposes. The study of patient samples from the COVID-19 Registry of the LMU University Hospital Munich (CORKUM, WHO trial ID DRKS00021225) was approved by the Ethics Committee of LMU Munich (project numbers: 20-245 and 23-0711).

Consent for publication N/A.

References

1. Schröder B (2016) The multifaceted roles of the invariant chain CD74—more than just a chaperone. Biochim Biophys Acta 1863:1269–1281. https://doi.org/10.1016/j.bbamcr.2016.03.026

2. Calandra T, Roger T (2003) Macrophage migration inhibitory factor: a regulator of innate immunity. Nat Rev Immunol 3:791–800. https://doi.org/10.1038/nri1200

3. Kapurniotu A, Gokce O, Bernhagen J (2019) The multitasking potential of alarmins and atypical chemokines. Front Med (Lausanne) 6:3. https://doi.org/10.3389/fmed.2019.00003

4. Bernhagen J, Krohn R, Lue H, Gregory JL, Zernecke A, Koenen RR, Dewor M, Georgiev I, Schober A, Leng L et al (2007) MIF is a noncognate ligand of CXC chemokine receptors in inflammatory and atherogenic cell recruitment. Nat Med 13:587–596. https://doi.org/10.1038/nm1567

5. Leng L, Metz CN, Fang Y, Xu J, Donnelly S, Baugh J, Delohery T, Chen Y, Mitchell RA, Bucala R (2003) MIF signal transduction initiated by binding to CD74. J Exp Med 197:1467–1476. https://doi.org/10.1084/jem.20030286

6. Klasen C, Ohl K, Sternkopf M, Shachar I, Schmitz C, Heussen N, Hobeika E, Levit-Zerdoun E, Tenbrock K, Reth M et al (2014) MIF promotes B cell chemotaxis through the receptors CXCR4 and CD74 and ZAP-70 signaling. J Immunol 192:5273–5284. https://doi.org/10.4049/jimmunol.1302209

7. Schwartz V, Kruttgen A, Weis J, Weber C, Ostendorf T, Lue H, Bernhagen J (2012) Role for CD74 and CXCR4 in clathrin-dependent endocytosis of the cytokine MIF. Eur J Cell Biol 91:435–449. https://doi.org/10.1016/j.ejcb.2011.08.006

8. Schwartz V, Lue H, Kraemer S, Korbiel J, Krohn R, Ohl K, Bucala R, Weber C, Bernhagen J (2009) A functional heteromeric MIF receptor formed by CD74 and CXCR4. FEBS Lett 583:2749–2757. https://doi.org/10.1016/j.febslet.2009.07.058

9. Kontos C, El Bounkari O, Krammer C, Sinitski D, Hille K, Zan C, Yan G, Wang S, Gao Y, Brandhofer M et al (2020) Designed CXCR4 mimic acts as a soluble chemokine receptor that blocks atherogenic inflammation by agonist-specific targeting. Nat Commun 11:5981. https://doi.org/10.1038/s41467-020-19764-z

10. Sinitski D, Kontos C, Krammer C, Asare Y, Kapurniotu A, Bernhagen J (2019) Macrophage migration inhibitory factor (MIF)-based therapeutic concepts in atherosclerosis and inflammation. Thromb Haemost. https://doi.org/10.1055/s-0039-1677803

11. Shi X, Leng L, Wang T, Wang W, Du X, Li J, McDonald C, Chen Z, Murphy JW, Lolis E et al (2006) CD44 is the signaling component of the macrophage migration inhibitory factor-CD74 receptor complex. Immunity 25:595–606. https://doi.org/10.1016/j.immuni.2006.08.020

12. Alampour-Rajabi S, El Bounkari O, Rot A, Muller-Newen G, Bachelerie F, Gawaz M, Weber C, Schober A, Bernhagen J (2015) MIF interacts with CXCR7 to promote receptor internalization, ERK1/2 and ZAP-70 signaling, and lymphocyte chemotaxis. FASEB J 29:4497–4511. https://doi.org/10.1096/fj.15-273904

13. Ma H, Wang J, Thomas DP, Tong C, Leng L, Wang W, Merk M, Zierow S, Bernhagen J, Ren J et al (2010) Impaired macrophage migration inhibitory factor-AMP-activated protein kinase activation and ischemic recovery in the senescent heart. Circulation 122:282–292. https://doi.org/10.1161/circulationaha.110.953208

14. Heinrichs D, Knauel M, Offermanns C, Berres ML, Nellen A, Leng L, Schmitz P, Bucala R, Trautwein C, Weber C et al (2011) Macrophage migration inhibitory factor (MIF) exerts antifibrotic effects in experimental liver fibrosis via CD74. Proc Natl Acad Sci USA 108:17444–17449. https://doi.org/10.1073/pnas.1107023108

15. Qi D, Hu X, Wu X, Merk M, Leng L, Bucala R, Young LH (2009) Cardiac macrophage migration inhibitory factor inhibits JNK pathway activation and injury during ischemia/reperfusion. J Clin Investig 119:3807–3816. https://doi.org/10.1172/jci39738

16. Burton JD, Ely S, Reddy PK, Stein R, Gold DV, Cardillo TM, Goldenberg DM (2004) CD74 is expressed by multiple myeloma and is a promising target for therapy. Clin Cancer Res 10:6606–6611

17. Stein R, Mattes MJ, Cardillo TM, Hansen HJ, Chang CH, Burton J, Govindan S, Goldenberg DM (2007) CD74: a new candidate target for the immunotherapy of B-cell neoplasms. Clin Cancer Res 13:5556s–5563s. https://doi.org/10.1158/1078-0432.CCR-07-1167

18. De la Cruz-Mosso U, Garcia-Iglesias T, Bucala R, Estrada-Garcia I, Gonzalez-Lopez L, Cerpa-Cruz S, Parra-Rojas I, Gamez-Nava JI, Perez-Guerrero EE, Munoz-Valle JF (2018) MIF promotes a differential Th1/Th2/Th17 inflammatory response in human primary cell cultures: Predominance of Th17 cytokine profile in PBMC from healthy subjects and increase of IL-6 and TNF-alpha in PBMC from active SLE patients. Cell Immunol 324:42–49. https://doi.org/10.1016/j.cellimm.2017.12.010

19. Alibashe-Ahmed M, Roger T, Serre-Beinier V, Berishvili E, Reith W, Bosco D, Berney T (2019) Macrophage migration inhibitory factor regulates TLR4 expression and modulates TCR/CD3-mediated activation in CD4+ T lymphocytes. Sci Rep 9:9380. https://doi.org/10.1038/s41598-019-45260-6

20. Hernandez-Palma LA, Garcia-Arellano S, Bucala R, Llamas-Covarrubias MA, De la Cruz-Mosso U, Oregon-Romero E, Cerpa-Cruz S, Parra-Rojas I, Plascencia-Hernandez A, Munoz-Valle JF (2019) Functional MIF promoter haplotypes modulate Th17-related cytokine expression in peripheral blood mononuclear cells from control subjects and rheumatoid arthritis patients. Cytokine 115:89–96. https://doi.org/10.1016/j.cyto.2018.11.014

21. Gaber T, Schellmann S, Erekul KB, Fangradt M, Tykwinska K, Hahne M, Maschmeyer P, Wagegg M, Stahn C, Kolar P et al (2011) Macrophage migration inhibitory factor counterregulates dexamethasone-mediated suppression of hypoxia-inducible factor-1 alpha function and differentially influences human CD4+ T cell proliferation under hypoxia. J Immunol 186:764–774. https://doi.org/10.4049/jimmunol.0903421

22. Bacher M, Metz CN, Calandra T, Mayer K, Chesney J, Lohoff M, Gemsa D, Donnelly T, Bucala R (1996) An essential regulatory

role for macrophage migration inhibitory factor in T-cell activation. Proc Natl Acad Sci USA 93:7849–7854. https://doi.org/10.1073/pnas.93.15.7849

23. Matsumoto K, Kanmatsuse K (2001) Increased production of macrophage migration inhibitory factor by T cells in patients with IgA nephropathy. Am J Nephrol 21:455–464. https://doi.org/10.1159/000046649

24. Kim HK, Garcia AB, Siu E, Tilstam P, Das R, Roberts S, Leng L, Bucala R (2019) Macrophage migration inhibitory factor regulates innate gammadelta T-cell responses via IL-17 expression. FASEB J 33:6919–6932. https://doi.org/10.1096/fj.201802433R

25. David JR (1966) Delayed hypersensitivity in vitro: its mediation by cell-free substances formed by lymphoid cell–antigen interaction. Proc Natl Acad Sci USA 56:72–77. https://doi.org/10.1073/pnas.56.1.72

26. Yang L, Kong Y, Ren H, Li M, Wei CJ, Shi E, Jin WN, Hao J, Vandenbark AA, Offner H (2017) Upregulation of CD74 and its potential association with disease severity in subjects with ischemic stroke. Neurochem Int 107:148–155. https://doi.org/10.1016/j.neuint.2016.11.007

27. Fagone P, Mazzon E, Cavalli E, Bramanti A, Petralia MC, Mangano K, Al-Abed Y, Bramati P, Nicoletti F (2018) Contribution of the macrophage migration inhibitory factor superfamily of cytokines in the pathogenesis of preclinical and human multiple sclerosis: In silico and in vivo evidences. J Neuroimmunol 322:46–56. https://doi.org/10.1016/j.jneuroim.2018.06.009

28. Cano-Gamez E, Soskic B, Roumeliotis TI, So E, Smyth DJ, Baldrighi M, Willé D, Nakic N, Esparza-Gordillo J, Larminie CGC et al (2020) Single-cell transcriptomics identifies an effectorness gradient shaping the response of CD4(+) T cells to cytokines. Nat Commun 11:1801. https://doi.org/10.1038/s41467-020-15543-y

29. Broere F, van Eden W (2019) T cell subsets and T cell-mediated immunity. In: Parnham MJ, Nijkamp FP, Rossi AG (eds) Nijkamp and Parnham's principles of immunopharmacology. Springer International Publishing, Berlin, pp 23–35. https://doi.org/10.1007/978-3-030-10811-3_3

30. Govender M, Hopkins FR, Göransson R, Svanberg C, Shankar EM, Hjorth M, Nilsdotter-Augustinsson Å, Sjöwall J, Nyström S, Larsson M (2022) T cell perturbations persist for at least 6 months following hospitalization for COVID-19. Front Immunol. https://doi.org/10.3389/fimmu.2022.931039

31. Bleilevens C, Soppert J, Hoffmann A, Breuer T, Bernhagen J, Martin L, Stiehler L, Marx G, Dreher M, Stoppe C, Simon TP (2021) Macrophage migration inhibitory factor (MIF) plasma concentration in critically ill COVID-19 patients: a prospective observational study. Diagnostics (Basel). https://doi.org/10.3390/diagnostics11020332

32. Moss P (2022) The T cell immune response against SARS-CoV-2. Nat Immunol 23:186–193. https://doi.org/10.1038/s41590-021-01122-w

33. Bernhagen J, Mitchell RA, Calandra T, Voelter W, Cerami A, Bucala R (1994) Purification, bioactivity, and secondary structure analysis of mouse and human macrophage migration Inhibitory factor (MIF). Biochemistry 33:14144–14155

34. Marimuthu R, Francis H, Dervish S, Li SCH, Medbury H, Williams H (2018) Characterization of human monocyte subsets by whole blood flow cytometry analysis. J Vis Exp. https://doi.org/10.3791/57941

35. Szabo PA, Levitin HM, Miron M, Snyder ME, Senda T, Yuan J, Cheng YL, Bush EC, Dogra P, Thapa P et al (2019) Single-cell transcriptomics of human T cells reveals tissue and activation signatures in health and disease. Nat Commun 10:4706. https://doi.org/10.1038/s41467-019-12464-3

36. Love MI, Huber W, Anders S (2014) Moderated estimation of fold change and dispersion for RNA-seq data with DESeq2. Genome Biol 15:550. https://doi.org/10.1186/s13059-014-0550-8

37. Blighe KRS, Lewis M (2023) EnhancedVolcano: publication-ready volcano plots with enhanced colouring and labeling. R package version Bioconductor version: Release (3.19), Open Source Software for Bioinformatics 1.20.0. https://doi.org/10.18129/B9.bioc.EnhancedVolcano.

38. Wickham H (2016) ggplot2: Elegant graphics for data analysis, 2nd edn. Springer, Cham. https://doi.org/10.1007/978-3-319-24277-4

39. Wolf T, Jin W, Zoppi G, Vogel IA, Akhmedov M, Bleck CKE, Beltraminelli T, Rieckmann JC, Ramirez NJ, Benevento M et al (2020) Dynamics in protein translation sustaining T cell preparedness. Nat Immunol 21:927–937. https://doi.org/10.1038/s41590-020-0714-5

40. Yevshin I, Sharipov R, Kolmykov S, Kondrakhin Y, Kolpakov F (2019) GTRD: a database on gene transcription regulation—2019 update. Nucleic Acids Res 47:D100-d105. https://doi.org/10.1093/nar/gky1128

41. Wong AK, Park CY, Greene CS, Bongo LA, Guan Y, Troyanskaya OG (2012) IMP: a multi-species functional genomics portal for integration, visualization and prediction of protein functions and networks. Nucleic Acids Res 40:W484-490. https://doi.org/10.1093/nar/gks458

42. Szklarczyk D, Gable AL, Nastou KC, Lyon D, Kirsch R, Pyysalo S, Doncheva NT, Legeay M, Fang T, Bork P et al (2021) The STRING database in 2021: customizable protein-protein networks, and functional characterization of user-uploaded gene/measurement sets. Nucleic Acids Res 49:D605-d612. https://doi.org/10.1093/nar/gkaa1074

43. Loetscher M, Geiser T, O'Reilly T, Zwahlen R, Baggiolini M, Moser B (1994) Cloning of a human seven-transmembrane domain receptor, LESTR, that is highly expressed in leukocytes. J Biol Chem 269:232–237

44. Mo H, Monard S, Pollack H, Ip J, Rochford G, Wu L, Hoxie J, Borkowsky W, Ho DD, Moore JP (1998) Expression patterns of the HIV type 1 coreceptors CCR5 and CXCR4 on CD4+ T cells and monocytes from cord and adult blood. AIDS Res Hum Retroviruses 14:607–617. https://doi.org/10.1089/aid.1998.14.607

45. Tian Y, Babor M, Lane J, Schulten V, Patil VS, Seumois G, Rosales SL, Fu Z, Picarda G, Burel J et al (2017) Unique phenotypes and clonal expansions of human CD4 effector memory T cells re-expressing CD45RA. Nat Commun 8:1473. https://doi.org/10.1038/s41467-017-01728-5

46. Clement LT (1992) Isoforms of the CD45 common leukocyte antigen family: markers for human T-cell differentiation. J Clin Immunol 12:1–10. https://doi.org/10.1007/bf00918266

47. Merkenschlager M, Terry L, Edwards R, Beverley PC (1988) Limiting dilution analysis of proliferative responses in human lymphocyte populations defined by the monoclonal antibody UCHL1: implications for differential CD45 expression in T cell memory formation. Eur J Immunol 18:1653–1661. https://doi.org/10.1002/eji.1830181102

48. Akbar AN, Terry L, Timms A, Beverley PC, Janossy G (1988) Loss of CD45R and gain of UCHL1 reactivity is a feature of primed T cells. J Immunol 140:2171–2178

49. Ko HS, Fu SM, Winchester RJ, Yu DT, Kunkel HG (1979) Ia determinants on stimulated human T lymphocytes. Occurrence on mitogen- and antigen-activated T cells. J Exp Med 150:246–255. https://doi.org/10.1084/jem.150.2.246

50. Pieters J, Horstmann H, Bakke O, Griffiths G, Lipp J (1991) Intracellular transport and localization of major histocompatibility complex class II molecules and associated invariant chain. J Cell Biol 115:1213–1223. https://doi.org/10.1083/jcb.115.5.1213

51. Marks MS, Blum JS, Cresswell P (1990) Invariant chain trimers are sequestered in the rough endoplasmic reticulum in the absence of association with HLA class II antigens. J Cell Biol 111:839–855. https://doi.org/10.1083/jcb.111.3.839

52. Strubin M, Berte C, Mach B (1986) Alternative splicing and alternative initiation of translation explain the four forms of the Ia antigen-associated invariant chain. EMBO J 5:3483–3488. https://doi.org/10.1002/j.1460-2075.1986.tb04673.x

53. Abraham RT, Weiss A (2004) Jurkat T cells and development of the T-cell receptor signalling paradigm. Nat Rev Immunol 4:301–308. https://doi.org/10.1038/nri1330

54. Arneson LS, Miller J (2007) The chondroitin sulfate form of invariant chain trimerizes with conventional invariant chain and these complexes are rapidly transported from the trans-Golgi network to the cell surface. Biochem J 406:97–103. https://doi.org/10.1042/bj20070446

55. Miller J, Hatch JA, Simonis S, Cullen SE (1988) Identification of the glycosaminoglycan-attachment site of mouse invariant-chain proteoglycan core protein by site-directed mutagenesis. Proc Natl Acad Sci USA 85:1359–1363. https://doi.org/10.1073/pnas.85.5.1359

56. Sant AJ, Cullen SE, Giacoletto KS, Schwartz BD (1985) Invariant chain is the core protein of the Ia-associated chondroitin sulfate proteoglycan. J Exp Med 162:1916–1934. https://doi.org/10.1084/jem.162.6.1916

57. Koch N, Moldenhauer G, Hofmann WJ, Möller P (1991) Rapid intracellular pathway gives rise to cell surface expression of the MHC class II-associated invariant chain (CD74). J Immunol 147:2643–2651

58. Henne C, Schwenk F, Koch N, Möller P (1995) Surface expression of the invariant chain (CD74) is independent of concomitant expression of major histocompatibility complex class II antigens. Immunology 84:177

59. Ong GL, Goldenberg DM, Hansen HJ, Mattes MJ (1999) Cell surface expression and metabolism of major histocompatibility complex class II invariant chain (CD74) by diverse cell lines. Immunology 98:296–302. https://doi.org/10.1046/j.1365-2567.1999.00868.x

60. Veenstra H, Ferris WF, Bouic PJ (2001) Major histocompatibility complex class II invariant chain expression in non-antigen-presenting cells. Immunology 103:218–225. https://doi.org/10.1046/j.1365-2567.2001.01230.x

61. Klasen C, Ziehm T, Huber M, Asare Y, Kapurniotu A, Shachar I, Bernhagen J, El Bounkari O (2018) LPS-mediated cell surface expression of CD74 promotes the proliferation of B cells in response to MIF. Cell Signal 46:32–42. https://doi.org/10.1016/j.cellsig.2018.02.010

62. Marsh LM, Cakarova L, Kwapiszewska G, von Wulffen W, Herold S, Seeger W, Lohmeyer J (2009) Surface expression of CD74 by type II alveolar epithelial cells: a potential mechanism for macrophage migration inhibitory factor-induced epithelial repair. Am J Physiol Lung Cell Mol Physiol 296:L442-452. https://doi.org/10.1152/ajplung.00525.2007

63. Bories J-C, Willerford DM, Grévin D, Davidson L, Camus A, Martin P, Stéhelin D, Alt FW (1995) Increased T-cell apoptosis and terminal B-cell differentiation induced by inactivation of the Ets-1 proto-oncogene. Nature 377:635–638. https://doi.org/10.1038/377635a0

64. Muthusamy N, Barton K, Leiden JM (1995) Defective activation and survival of T cells lacking the Ets-1 transcription factor. Nature 377:639–642. https://doi.org/10.1038/377639a0

65. Reddy M, Eirikis E, Davis C, Davis HM, Prabhakar U (2004) Comparative analysis of lymphocyte activation marker expression and cytokine secretion profile in stimulated human peripheral blood mononuclear cell cultures: an in vitro model to monitor cellular immune function. J Immunol Methods 293:127–142. https://doi.org/10.1016/j.jim.2004.07.006

66. Poloni C, Schonhofer C, Ivison S, Levings MK, Steiner TS, Cook L (2023) T-cell activation-induced marker assays in health and disease. Immunol Cell Biol 101:491–503. https://doi.org/10.1111/imcb.12636

67. Marić MA, Taylor MD, Blum JS (1994) Endosomal aspartic proteinases are required for invariant-chain processing. Proc Natl Acad Sci USA 91:2171–2175. https://doi.org/10.1073/pnas.91.6.2171

68. Masternak K, Muhlethaler-Mottet A, Villard J, Zufferey M, Steimle V, Reith W (2000) CIITA is a transcriptional coactivator that is recruited to MHC class II promoters by multiple synergistic interactions with an enhanceosome complex. Genes Dev 14:1156–1166

69. Holling TM, Schooten E, van Den Elsen PJ (2004) Function and regulation of MHC class II molecules in T-lymphocytes: of mice and men. Hum Immunol 65:282–290. https://doi.org/10.1016/j.humimm.2004.01.005

70. Brandhofer M, Hoffmann A, Blanchet X, Siminkovitch E, Rohlfing AK, El Bounkari O, Nestele JA, Bild A, Kontos C, Hille K et al (2022) Heterocomplexes between the atypical chemokine MIF and the CXC-motif chemokine CXCL4L1 regulate inflammation and thrombus formation. Cell Mol Life Sci 79:512. https://doi.org/10.1007/s00018-022-04539-0

71. Westmeier J, Brochtrup A, Paniskaki K, Karakoese Z, Werner T, Sutter K, Dolff S, Limmer A, Mittermüller D, Liu J et al (2023) Macrophage migration inhibitory factor receptor CD74 expression is associated with expansion and differentiation of effector T cells in COVID-19 patients. Front Immunol 14:1236374. https://doi.org/10.3389/fimmu.2023.1236374

72. Sánchez-Zuno GA, Bucala R, Hernández-Bello J, Román-Fernández IV, García-Chagollán M, Nicoletti F, Matuz-Flores MG, García-Arellano S, Esparza-Michel JA, Cerpa-Cruz S et al (2021) Canonical (CD74/CD44) and non-canonical (CXCR2, 4 and 7) MIF receptors are differentially expressed in rheumatoid arthritis patients evaluated by DAS28-ESR. J Clin Med. https://doi.org/10.3390/jcm11010120

73. Bermejo M, Martín-Serrano J, Oberlin E, Pedraza MA, Serrano A, Santiago B, Caruz A, Loetscher P, Baggiolini M, Arenzana-Seisdedos F, Alcami J (1998) Activation of blood T lymphocytes down-regulates CXCR4 expression and interferes with propagation of X4 HIV strains. Eur J Immunol 28:3192–3204. https://doi.org/10.1002/(sici)1521-4141(199810)28:10%3c3192::Aid-immu3192%3e3.0.Co;2-e

74. Kumar A, Humphreys TD, Kremer KN, Bramati PS, Bradfield L, Edgar CE, Hedin KE (2006) CXCR4 physically associates with the T cell receptor to signal in T cells. Immunity 25:213–224. https://doi.org/10.1016/j.immuni.2006.06.015

75. Abbal C, Jourdan P, Hori T, Bousquet J, Yssel H, Pène J (1999) TCR-mediated activation of allergen-specific CD45RO(+) memory T lymphocytes results in down-regulation of cell-surface CXCR4 expression and a strongly reduced capacity to migrate in response to stromal cell-derived factor-1. Int Immunol 11:1451–1462. https://doi.org/10.1093/intimm/11.9.1451

76. Zou L, Barnett B, Safah H, Larussa VF, Evdemon-Hogan M, Mottram P, Wei S, David O, Curiel TJ, Zou W (2004) Bone marrow is a reservoir for CD4+CD25+ regulatory T cells that traffic through CXCL12/CXCR4 signals. Cancer Res 64:8451–8455. https://doi.org/10.1158/0008-5472.Can-04-1987

77. Zhang H, Jadhav RR, Cao W, Goronzy IN, Zhao TV, Jin J, Ohtsuki S, Hu Z, Morales J, Greenleaf WJ et al (2023) Aging-associated HELIOS deficiency in naive CD4+ T cells alters chromatin remodeling and promotes effector cell responses. Nat Immunol 24:96–109. https://doi.org/10.1038/s41590-022-01369-x

78. Li M, Yao D, Zeng X, Kasakovski D, Zhang Y, Chen S, Zha X, Li Y, Xu L (2019) Age related human T cell subset evolution and senescence. Immun Ageing 16:24. https://doi.org/10.1186/s12979-019-0165-8

79. Saule P, Trauet J, Dutriez V, Lekeux V, Dessaint J-P, Labalette M (2006) Accumulation of memory T cells from childhood to old age: central and effector memory cells in CD4+ versus effector memory and terminally differentiated memory cells in CD8+ compartment. Mech Ageing Dev 127:274–281. https://doi.org/10.1016/j.mad.2005.11.001

80. Idorn M, Skadborg SK, Kellermann L, Halldórsdóttir HR, Holmen Olofsson G, Met Ö, Thor Straten P (2018) Chemokine receptor engineering of T cells with CXCR2 improves homing towards subcutaneous human melanomas in xenograft mouse model. Oncoimmunology 7:e1450715. https://doi.org/10.1080/2162402x.2018.1450715

81. Balabanian K, Lagane B, Infantino S, Chow KY, Harriague J, Moepps B, Arenzana-Seisdedos F, Thelen M, Bachelerie F (2005) The chemokine SDF-1/CXCL12 binds to and signals through the orphan receptor RDC1 in T lymphocytes. J Biol Chem 280:35760–35766. https://doi.org/10.1074/jbc.M508234200

82. Berahovich RD, Zabel BA, Penfold ME, Lewén S, Wang Y, Miao Z, Gan L, Pereda J, Dias J, Slukvin II et al (2010) CXCR7 protein is not expressed on human or mouse leukocytes. J Immunol 185:5130–5139. https://doi.org/10.4049/jimmunol.1001660

83. Koch N, Lauer W, Habicht J, Dobberstein B (1987) Primary structure of the gene for the murine Ia antigen-associated invariant chains (Ii). An alternatively spliced exon encodes a cysteine-rich domain highly homologous to a repetitive sequence of thyroglobulin. EMBO J 6:1677–1683. https://doi.org/10.1002/j.1460-2075.1987.tb02417.x

84. O'Sullivan DM, Noonan D, Quaranta V (1987) Four Ia invariant chain forms derive from a single gene by alternate splicing and alternate initiation of transcription/translation. J Exp Med 166:444–460. https://doi.org/10.1084/jem.166.2.444

85. Claesson L, Larhammar D, Rask L, Peterson PA (1983) cDNA clone for the human invariant gamma chain of class II histocompatibility antigens and its implications for the protein structure. Proc Natl Acad Sci USA 80:7395–7399. https://doi.org/10.1073/pnas.80.24.7395

86. Koch N, Haemmerling GJ (1985) Ia-associated invariant chain is fatty acylated before addition of sialic acid. Biochemistry 24:6185–6190

87. Kuwana T, Peterson PA, Karlsson L (1998) Exit of major histocompatibility complex class II-invariant chain p35 complexes from the endoplasmic reticulum is modulated by phosphorylation. Proc Natl Acad Sci USA 95:1056–1061. https://doi.org/10.1073/pnas.95.3.1056

88. Buckley CD, Amft N, Bradfield PF, Pilling D, Ross E, Arenzana-Seisdedos F, Amara A, Curnow SJ, Lord JM, Scheel-Toellner D, Salmon M (2000) Persistent induction of the chemokine receptor CXCR4 by TGF-beta 1 on synovial T cells contributes to their accumulation within the rheumatoid synovium. J Immunol 165:3423–3429. https://doi.org/10.4049/jimmunol.165.6.3423

89. Collins T, Korman AJ, Wake CT, Boss JM, Kappes DJ, Fiers W, Ault KA, Gimbrone MA Jr, Strominger JL, Pober JS (1984) Immune interferon activates multiple class II major histocompatibility complex genes and the associated invariant chain gene in human endothelial cells and dermal fibroblasts. Proc Natl Acad Sci USA 81:4917–4921. https://doi.org/10.1073/pnas.81.15.4917

90. Gil-Yarom N, Radomir L, Sever L, Kramer MP, Lewinsky H, Bornstein C, Blecher-Gonen R, Barnett-Itzhaki Z, Mirkin V, Friedlander G et al (2017) CD74 is a novel transcription regulator. Proc Natl Acad Sci USA 114:562–567. https://doi.org/10.1073/pnas.1612195114

91. David K, Friedlander G, Pellegrino B, Radomir L, Lewinsky H, Leng L, Bucala R, Becker-Herman S, Shachar I (2022) CD74 as a regulator of transcription in normal B cells. Cell Rep 41:111572. https://doi.org/10.1016/j.celrep.2022.111572

92. Schneppenheim J, Dressel R, Hüttl S, Lüllmann-Rauch R, Engelke M, Dittmann K, Wienands J, Eskelinen EL, Hermans-Borgmeyer I, Fluhrer R et al (2013) The intramembrane protease SPPL2a promotes B cell development and controls endosomal traffic by cleavage of the invariant chain. J Exp Med 210:41–58. https://doi.org/10.1084/jem.20121069

93. Gore Y, Starlets D, Maharshak N, Becker-Herman S, Kaneyuki U, Leng L, Bucala R, Shachar I (2008) Macrophage migration inhibitory factor induces B cell survival by activation of a CD74-CD44 receptor complex. J Biol Chem 283:2784–2792. https://doi.org/10.1074/jbc.M703265200

94. Karki R, Sharma BR, Tuladhar S, Williams EP, Zalduondo L, Samir P, Zheng M, Sundaram B, Banoth B, Malireddi RKS et al (2021) Synergism of TNF-α and IFN-γ triggers inflammatory cell death, tissue damage, and mortality in SARS-CoV-2 infection and cytokine shock syndromes. Cell 184:149-168.e117. https://doi.org/10.1016/j.cell.2020.11.025

95. Lucas C, Wong P, Klein J, Castro TBR, Silva J, Sundaram M, Ellingson MK, Mao T, Oh JE, Israelow B et al (2020) Longitudinal analyses reveal immunological misfiring in severe COVID-19. Nature 584:463–469. https://doi.org/10.1038/s41586-020-2588-y

96. Mallapaty S (2020) The coronavirus is most deadly if you are older and male—new data reveal the risks. Nature 585:16–17. https://doi.org/10.1038/d41586-020-02483-2

97. Gustafson CE, Kim C, Weyand CM, Goronzy JJ (2020) Influence of immune aging on vaccine responses. J Allergy Clin Immunol 145:1309–1321. https://doi.org/10.1016/j.jaci.2020.03.017

98. Quan X-Q, Ruan L, Zhou H-R, Gao W-L, Zhang Q, Zhang C-T (2023) Age-related changes in peripheral T-cell subpopulations in elderly individuals: an observational study. Open Life Sci. https://doi.org/10.1515/biol-2022-0557

Authors and Affiliations

Lin Zhang[1] · Iris Woltering[1] · Mathias Holzner[1] · Markus Brandhofer[1] · Carl-Christian Schaefer[1] · Genta Bushati[1] · Simon Ebert[1] · Bishan Yang[1] · Maximilian Muenchhoff[2,3,4] · Johannes C. Hellmuth[4,5] · Clemens Scherer[4,6] · Christian Wichmann[7] · David Effinger[8,9] · Max Hübner[8,9] · Omar El Bounkari[1] · Patrick Scheiermann[8] · Jürgen Bernhagen[1,10] · Adrian Hoffmann[1,8,10]

✉ Jürgen Bernhagen
  juergen.bernhagen@med.uni-muenchen.de

✉ Adrian Hoffmann
  adrian.hoffmann@med.uni-muenchen.de

[1] Division of Vascular Biology, Institute for Stroke and Dementia Research (ISD), LMU University Hospital (LMU Klinikum), Ludwig-Maximilians-Universität (LMU) München, Feodor-Lynen-Straße 17, 81377 Munich, Germany

[2] Max von Pettenkofer Institute and Gene Center, Virology, National Reference Center for Retroviruses, Ludwig-Maximilians-Universität (LMU) Munich, Munich, Germany

[3] German Center for Infection Research (DZIF), Partner Site Munich, Munich, Germany

[4] COVID-19 Registry of the LMU Munich (CORKUM), LMU University Hospital, Ludwig-Maximilians-Universität (LMU) Munich, Munich, Germany

[5] Department of Medicine III, LMU University Hospital, Ludwig-Maximilians-Universität (LMU) Munich, Munich, Germany

[6] Department of Medicine I, LMU University Hospital, Ludwig-Maximilians-Universität (LMU) Munich, Munich, Germany

[7] Division of Transfusion Medicine, Cell Therapeutics and Haemostaseology, LMU University Hospital, Ludwig-Maximilians-Universität (LMU) Munich, Munich, Germany

[8] Department of Anaesthesiology, LMU University Hospital, Ludwig-Maximilians-Universität (LMU) Munich, Marchioninistraße 15, 81377 Munich, Germany

[9] Walter Brendel Centre of Experimental Medicine, Ludwig-Maximilians-Universität (LMU) Munich, Munich, Germany

[10] German Centre of Cardiovascular Research (DZHK), Partner Site Munich Heart Alliance, Munich, Germany

6. Publication II: Spiller, L. *et al*., 2023

Plant MDL proteins synergize with the cytokine MIF at CXCR2 and CXCR4 receptors in human cells.

Spiller, L., Manjula, R., Leissing, F., Basquin, J., Bourilhon, P., Sinitski, D., Brandhofer, M., Levecque, S., Gerra, S., Sabelleck, B., **Zhang, L.**, Feederle, R., Flatley, A., Hoffmann, A., Panstruga, R., Bernhagen, J., and Lolis, E. (2023) Plant MDL proteins synergize with the cytokine MIF at CXCR2 and CXCR4 receptors in human cells. *Sci Signal* **16**, eadg2621

DOI: 10.1126/scisignal. adg2621.

SCIENCE SIGNALING | RESEARCH ARTICLE

BIOCHEMISTRY

Plant MDL proteins synergize with the cytokine MIF at CXCR2 and CXCR4 receptors in human cells

Lukas Spiller[1,2]†, Ramu Manjula[1], Franz Leissing[3], Jerome Basquin[4], Priscila Bourilhon[2]‡,
Dzmitry Sinitski[2]§, Markus Brandhofer[2], Sophie Levecque[3], Simona Gerra[2], Björn Sabelleck[3],
Lin Zhang[2,5], Regina Feederle[6,7], Andrew Flatley[6], Adrian Hoffmann[2,5], Ralph Panstruga[3]*,
Jürgen Bernhagen[2,7]*, Elias Lolis[1]*

Mammalian macrophage migration inhibitory factor (MIF) and its paralog, D-dopachrome tautomerase, are multifunctional inflammatory cytokines. Plants have orthologous MIF and D-dopachrome tautomerase–like (MDL) proteins that mimic some of the effects of MIF on immune cells in vitro. We explored the structural and functional similarities between the three *Arabidopsis thaliana* MDLs and MIF. X-ray crystallography of the MDLs revealed high structural similarity between MDL and MIF homotrimers and suggested a potential explanation for the lack of tautomerase activity in the MDLs. MDL1 and MDL2 interacted with each other and with MIF in vitro, in yeast, and in plant leaves and formed hetero-oligomeric complexes with MIF in vitro. The MDLs stimulated signaling through the MIF receptors CXCR2 or CXCR4 and enhanced the responses to MIF in a yeast reporter system, in human neutrophils, and in human lung epithelial cells. Pharmacological inhibitors that disrupted MIF activity or prevented the formation of MIF-MDL hetero-oligomers blocked the observed synergism. These findings demonstrate that MDLs can enhance cellular responses to MIF, which may have functional implications in tissues exposed to MDLs from the diet or environment.

INTRODUCTION

The immune defense system of vertebrates relies on a sophisticated network of innate and adaptive arms and is composed of a remarkable variety of immune cells that communicate and traffic through a circulatory system (1). Cytokines and chemokines are specialized soluble immune mediators and act as coordinators of the human immune response. Accordingly, dysregulated cytokine and chemokine responses are associated with numerous diseases (2). Macrophage migration inhibitory factor (MIF) and its paralog D-dopachrome tautomerase (D-DT; also known as MIF-2) are multifunctional inflammatory cytokines with chemokine-like properties that are key components of the host immune response (3–6). MIF not only signals through its cognate receptor CD74 to control proliferation, survival, and inflammatory responses (7) but also engages in noncognate interactions with the chemokine receptors CXCR2, CXCR4, and CXCR7 to promote immune cell recruitment (8). These activities also causally link MIF to a variety of human diseases, including acute and chronic inflammatory conditions,

atherosclerosis, autoimmune disorders, neurodegenerative diseases, and cancer (4, 8–14).

MIF and D-DT (MIF/D-DT)–like (MDL) proteins have been identified in nearly all kingdoms of life, including uni- and multicellular parasites, fungi, and plants, suggesting that the evolutionary origin of the gene encoding an ancestral form MIF/D-DT dates back more than 900 million years (15–17). Parasite-derived MIF orthologs can mimic mammalian MIF activities to act as virulence factors as a basis for immune evasion and are, in some cases, pharmacological targets (16). Plants have developed effective innate immune mechanisms, such as pattern recognition receptors, to fight microbial attacks but lack an adaptive immune system (18). Moreover, many of the primordial organisms expressing *MIF*-like genes lack a circulation and a cell-based immune system, and in some, even the existence of G protein–coupled receptors (GPCRs), which act as secondary MIF receptors in vertebrates, is controversial. These facts have fueled speculation about MIF as an ancient enzyme that acquired extracellular functions as a cytokine in a process of neofunctionalization (17).

The three-dimensional (3D) structure of human MIF (19) bears notable resemblance to a group of bacterial enzymes consisting of 4-oxalocrotonate tautomerase, 5-(carboxymethyl)-2-hydroxymuconate isomerase, and malonate semialdehyde decarboxylase (20). The MIF monomer has a molecular mass of 12.5 kDa and is composed of two α helices tightly packed against four antiparallel-oriented β strands. However, MIF crystallizes as a homotrimer, in which three monomers interact with each other to form a barrel-shaped structure with a central solvent channel running through the protein assembly (19). Human MIF shares a sequence identity of <20% with the abovementioned microbial enzymes but has a tautomerase catalytic cavity between its subunits and an unusually acidic N-terminal proline residue, exposed after proteolytic removal of the initial methionine residue, with a pK_a of 5.6

[1]Department of Pharmacology, School of Medicine, Yale University, New Haven, CT 06510, USA. [2]Division of Vascular Biology, Institute for Stroke and Dementia Research (ISD), Ludwig-Maximilians-Universität (LMU) München, LMU University Hospital, 81377 Munich, Germany. [3]Unit of Plant Molecular Cell Biology, Institute for Biology I, RWTH Aachen University, 52056 Aachen, Germany. [4]Department of Structural Cell Biology and Crystallization Facility, Max-Planck-Institute for Biochemistry, 82152 Martinsried, Germany. [5]Department of Anesthesiology, LMU University Hospital, 81377 Munich, Germany. [6]Monoclonal Antibody Core Facility, Helmholtz Center Munich, German Research Center for Environmental Health (GmbH), 85764 Neuherberg, Germany. [7]Munich Cluster for Systems Neurology (SyNergy), 81377 Munich, Germany.
*Corresponding author. Email: elias.lolis@yale.edu (E.L.); juergen.bernhagen@med.uni-muenchen.de (J.B.); panstruga@bio1.rwth-aachen.de (R.P.)
†Present address: University of Ulm, Ulm, Germany.
‡Present address: Alytix Biotech, Santa Fe, Argentina.
§Present address: Institute of Microbiology and Laboratory Medicine/WHO–Supranational Reference Laboratory of Tuberculosis, Martinsried, Germany.

(where K_a is the acid dissociation constant), consistent with a function as a catalytic base (21–23). Although MIF can catalyze the tautomerization of the nonphysiological substrate D-dopachrome [or D-dopachrome methyl ester (DME)] and enol-keto forms of the physiological molecule 4-hydroxyphenylpyruvate (HPP) in vitro (21, 22), a bona fide substrate for MIF activity in humans has remained elusive, and a role for the enzymatic activity in human cells has not been clearly demonstrated. However, mutational and inhibitor studies have demonstrated that changes in the catalytic cavity lead to conformational alterations that affect MIF binding to CD74, CXCR2, and CXCR4 (24–28). The tautomerase catalytic site has been used in a variety of methods to identify small-molecule inhibitors that affect several mouse models of disease. Although much less studied, MIF also features redox-regulatory activity related to its redox-sensitive cysteine residues (29) and has been suggested to have nuclease activity owing to a PD-D/E(X)K nuclease motif (30).

Comparison of MIF and MDL proteins across different kingdoms reveals a high degree of sequence conservation, with many sites being under selection in some kingdoms, especially in plants (17, 31). Conservation is high for the tautomerase site, whereas other motifs known to be of functional importance in human MIF (such as the pseudo-ELR motif required for CXCR2 binding) are not well conserved (32). There seems to be a complex interplay between vertebrate MIF and parasite MIF orthologs, with implications for virulence and host defense (33).

Regarding MDLs in the plant kingdom, in silico analysis has demonstrated an extraordinary degree of evolutionary conservation in these proteins and the genes that encode them, and they may have a role in development and defense (17, 34). Multiple MDL genes are typically present per plant species, including model plants such as Arabidopsis thaliana, as well as crops and other food plants. The three Arabidopsis MDLs (herein termed MDLs for simplicity) share a sequence identity of 28 to 33% with human MIF, with higher conservation in the tautomerase cavity (fig. S1) (35). MDL1 and MDL2 localize to the cytoplasm of plant cells, whereas MDL3 resides in peroxisomes (34). In vitro assays indicate that the tautomerase activity of MDLs for the artificial substrates HPP and D-dopachrome is greatly reduced in comparison with human MIF (36). Given the sequence homology between MDLs and human MIF, we previously tested whether MDLs would interact with components of the human MIF signaling network, similar to the virulence paradigm established for parasite MIF orthologs (16, 33, 37). We observed an unexpected degree of cross-kingdom mimicry, with MDLs binding to and activating the human MIF receptors CXCR4 and CD74 and promoting the chemotaxis of human leukocytes (36). This observation expanded the previously established interplay between the plant immune system and MIF-like proteins delivered by the plant-parasitic aphid Acrythosiphon pisum, suggesting the possibility of an unanticipated cross-kingdom interaction between components of the plant and human immune system (38).

In this study, we sought to characterize the structures of MDLs and understand the mechanisms underlying the interplay between plant MDLs, human MIF (hereafter referred to as MIF), and MIF receptors. We determined the crystallographic structures of all three Arabidopsis MDLs, identified structural similarities between MDLs and MIF, and unraveled the presumed basis for the unexpectedly low tautomerase activity of MDLs. We demonstrated by biochemical, cell biological, and biophysical methodologies that MDLs and MIF formed hetero-oligomeric complexes that affected MIF-driven receptor responses by cross-kingdom synergy.

RESULTS

Crystal structures of Arabidopsis MDLs reveal high structural similarity to human MIF and a putative basis for their lack of tautomerase activity

We expressed and purified recombinant C-terminally hexahistidine-tagged MIF orthologs MDL1-6×His, MDL2-6×His, and MDL3-6×His (thereafter referred to as MDL1, MDL2, and MDL3) (fig. S2, A to C). The x-ray structure of these three MDLs was solved and refined to 1.56, 1.40, and 2.00 Å resolutions, respectively (Fig. 1A and table S1). All three MDL proteins crystallized as trimers with a very high overall structural similarity to the human MIF trimer, including three 3_{10} helices (Fig. 1A) with a root mean square deviation (RMSD) ranging from 0.734 Å for MDL1 to 0.906 Å for MDL3 (Fig. 1B). Analysis of a structure-based alignment revealed 27% sequence identity for an all-against-all comparison of all three MDLs and 12% sequence identity for a comparison of the three MDLs with MIF (fig. S1) (35). The 14 invariant residues per monomer in the structural alignment (fig. S1) are localized into separate regions: Region 1 is the catalytic cavity between two subunits and contains Pro^1 and Ser^{63} (all residue numbering refers to that for MIF; fig. S1), whereas region 2 is a discontinuous surface outside the catalytic cavity composed of the six residues Ala^{27}, Gly^{31}, Pro^{33}, Gly^{65}, Ser^{63}, and Asp^{100} (fig. S3, A and B). In region 3, a major portion of the Asp^{100} surface area is outside the solvent channel, adjacent to the MIF allosteric site residue Tyr^{99}, the side chain of which is within the channel serving as a solvent-gating residue (fig. S3C) (26). MDL1 and MDL2 also have a tyrosine residue at the equivalent position, and MDL3 has a phenylalanine residue (fig. S1). There are three residues that belong to multiple regions based on their structural orientation. For example, Ser^{63} is part of both regions 1 and 2 with the hydroxyl group being part of the catalytic cavity and its backbone contributing to the surface area (fig. S3B). Asp^{100} belongs to region 2, where Gly^{65} makes a hydrogen bond between their backbone atoms, but the side chain of Asp^{100} is the only residue in region 3. At region 4, the Arg^{93} side chain makes a hydrogen bond to the backbone of Phe^{49}, which is at the C-terminal end of a β strand involved in subunit-subunit interactions and serves a role in stabilizing this β strand that provides the specificity for MDLs and MIF to form homotrimers (fig. S3D). Regarding the remaining seven invariant residues (Thr^7, Asn^8, Phe^{49}, Gly^{51}, Ala^{57}, Leu^{83}, and Arg^{93}), Ala^{57} and Leu^{83} are buried within the hydrophobic core of the protein, and Thr^7, Asn^8, Phe^{49}, Gly^{51}, and Arg^{93} are localized in loop regions (fig. S3A).

We also examined the tautomerase catalytic cavity in more detail, focusing only on the structures of the MDLs. The electrostatic potential of the catalytic cavity of MDL3 was low, consistent with a lack of catalytic activity for HPP. A view of the electrostatic potential of MDL1 and MDL2 did not explain the large difference in catalytic activity between MIF and MDL1 or MDL2 because each displayed high active site identity and a positive electrostatic potential at the active site (Fig. 1A). We therefore superimposed each MDL on the MIF-HPP enzyme-substrate complex to create a model of HPP interacting with the MDLs' catalytic sites (Fig. 1B) (39). The interactions were analyzed and compared with the respective MIF-HPP

SCIENCE SIGNALING | RESEARCH ARTICLE

complex. The major difference in catalytic residues between human MIF (Pro[1A], Lys[32A], Ser[63A], Ile[64A], Tyr[95C], and Asn[97C], where A, B, and C refer to the trimer subunits) and those of the three MDLs was Lys[98C]. Note that MDL Lys[98] is equivalent to MIF Asn[97] because of an extra residue in the MDLs (fig. S1). Substitution of Asn[97] in MIF by lysine markedly reduces the tautomerase activity for both HPP and DME (36), suggesting that Asn[97] in MIF is important for the tautomerase enzymatic activity of MIF using these artificial substrates, whereas a lysine residue in this position in MIF would not support the enzymatic activity. In turn, this may imply that the lysine residue at that position in the MDLs (Lys[98]) may not support or may even obstruct the enzymatic tautomerase activity. When we inspected the position of this residue in detail, the major structural difference between MDL1 and MIF was the different side-chain orientation of Lys[98], which was oriented away from HPP with a distance of >5.4 Å for all three subunits in MDL1. By contrast, the side-chain amide group of Asn[97] in MIF formed a hydrogen bond with HPP (Fig. 1C). The large distance between Lys[98] of the MDLs and HPP was similar in the analysis for MDL2 and MDL3 with the modeled HPP, resulting in a loss of a hydrogen bond interaction and presumed decreased affinity for HPP (fig. S4, A and B).

An unanticipated difference was observed in MDLs at residue 96, which is the equivalent position of MIF Tyr[95] (fig. S1). The side chain of Tyr[96] for MDL1 had different conformations in the three subunits. In one subunit, it clashed with the modeled HPP, and in the other two subunits, the side chain had no predicted interactions with HPP. The equivalent residues for MDL2 and MDL3 are Phe[96] and Ile[96], respectively. The proteins differed in the position of these residues from Tyr[96] in MDL1, with Phe[96] of MDL2 making van der Waals interactions with HPP (fig. S4A), whereas the Ile[96] of MDL3 was not predicted to interact with HPP at all (fig. S4B). Together, the crystal structures of *Arabidopsis* MDLs revealed a high overall structural similarity to human MIF. This similarity was even more notable at the catalytic cavity with exceptions at residues Lys[98] (which replaces Asn[97] in MIF) and Tyr[96], Phe[96], and Ile[96] (which replace Tyr[95] in MIF). A different orientation and conformation of these residues, respectively, could be the basis of the inactive tautomerase catalytic site in the *Arabidopsis* orthologs.

MIF and MDLs engage in direct protein-protein interactions in vitro, in cells, and in planta

The high degree of structural similarity between MIF and the three MDLs and the capacity of each of these proteins to form homotrimers prompted us to investigate whether these proteins would also physically interact with each other across kingdom boundaries. To test this possibility experimentally, we first performed in vitro coimmunoprecipitation assays with MIF and MDL1 as a representative of the three MDLs. Purified MDL1-6×His and biotinylated MIF-6×His were mixed, complexes pulled down by streptavidin-coated magnetic beads, and the resulting eluate analyzed by blotting and detection with horseradish peroxidase (HRP)–conjugated streptavidin to verify precipitation of biotinylated MIF-6×His and with the custom-made, MDL1-specific monoclonal antibody Atm1 21G9 (fig. S5) to detect coprecipitated MDL1-6×His (Fig. 2A). Complex formation was further confirmed by analyzing immunoblots with an antibody specific for the histidine tag (fig. S6). This revealed an association of the recombinant MIF and MDL1 proteins in vitro.

To determine whether interactions between MIF and MDL also occurred in cells, we tested all pairwise interactions between MIF, MDL1, MDL2, and MDL3 in yeast two-hybrid assays. Similar to our previous report (34), we detected a weak homomeric MDL1-MDL1 interaction and a strong heteromeric MDL1-MDL2 interaction in this system. In accordance with earlier biochemical evidence (19, 40, 41), we also noticed a homomeric MIF-MIF interaction.
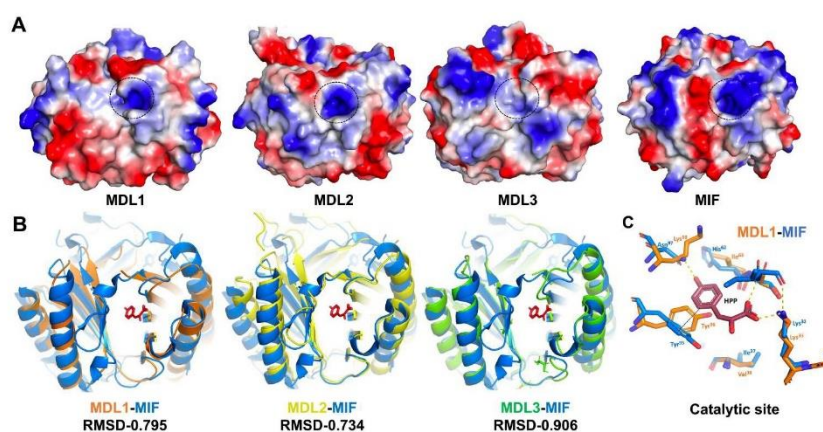
Fig. 1. Structural properties of each MDL protein and comparison to MIF. (**A**) Electrostatic surface potential representation of each *Arabidopsis* MDL (MDL1, MDL2, and MDL3) and human MIF. The tautomerase substrate binding sites are marked with dashed circles. Regions of negative potential are colored red, those of positive potential are colored blue, and neutral regions are shown in white and gray. (**B**) Overlays of MDL structures on the structure of the MIF-HPP complex (PDB 1CA7). The blue cartoon represents the structure of MIF. Orange, yellow, and green cartoons represent MDL1, MDL2, and MDL3, respectively. The RMSD of atomic positions is shown for each complex. The HPP (red) in these overlays is used as the position of the modeled HPP in the MDL-HPP complexes for analysis. (**C**) Residues of MDL1 analogous to the tautomerase catalytic site of human MIF (orange carbon atoms) superimposed on human MIF (blue carbon atoms from PDB 1CA7) with a modeled HPP substrate (red). Hydrogen bonds between MIF and HPP (red carbon atoms) are represented by yellow dashed lines, and the aromatic interaction is shown as a black dashed line.
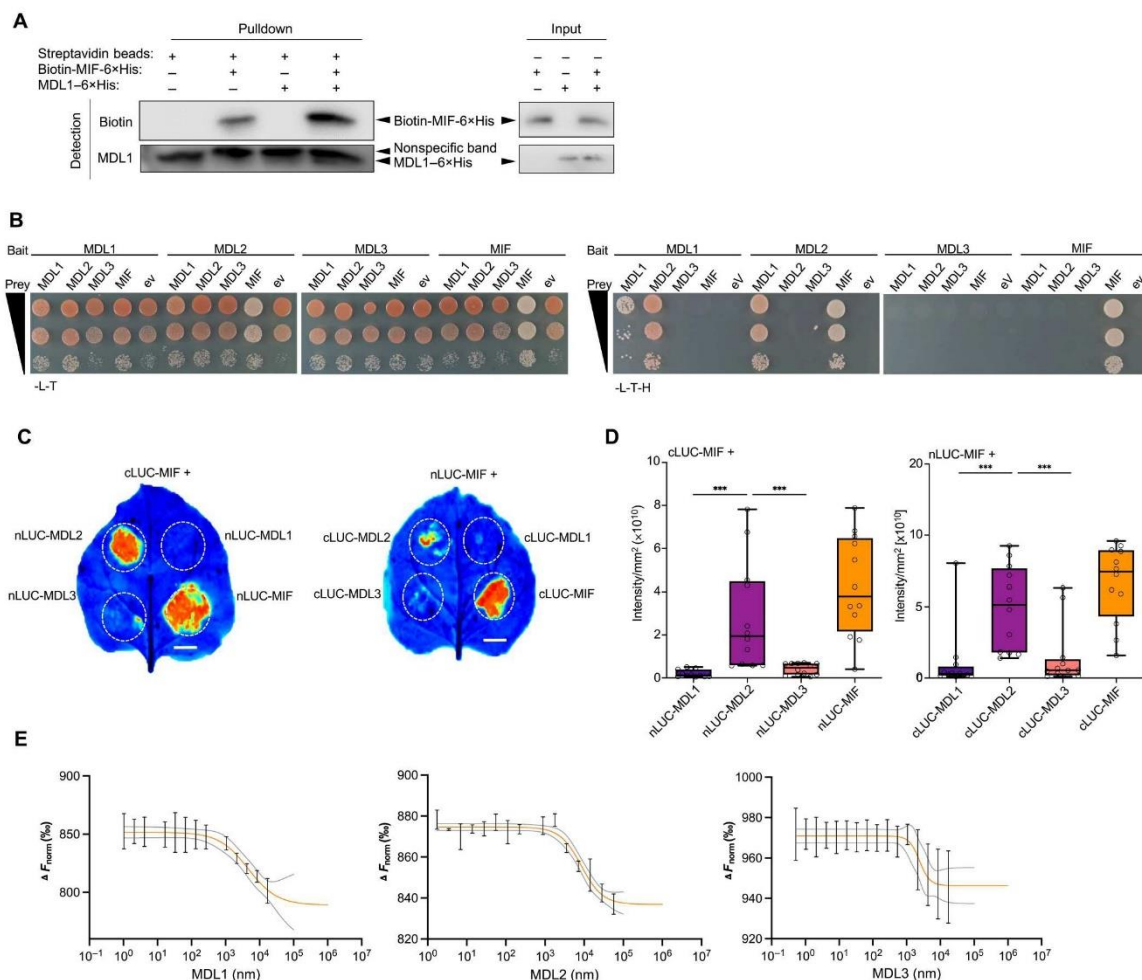
Fig. 2. MIF and MDL proteins interact in vitro, in yeast, and in plant tissues. (**A**) Purified tagged MIF (Biotin-MIF-6×His) and MDL1 (MDL1-6×His) were incubated alone or together, and complexes pulled down by streptavidin-coated beads were blotted after separation by SDS-PAGE. Blots were probed for biotin using a streptavidin-peroxidase conjugate to visualize MIF and for MDL1 using an MDL1-specific antibody. Input sample before pulldown is shown for comparison. The nonspecific band in the pulldown blot probed for MDL1, absent in the input samples, originates from the streptavidin-coated beads used to pull down biotin-tagged MIF and represents streptavidin monomers, which migrate with an apparent molecular mass of 16 kDa in SDS-PAGE. Pulldown and input samples were blotted on separate membranes for technical reasons. The pulldown experiment shown is representative of two independent experiments ($n = 2$). The pulldown blot was also probed with an antibody specific for the hexahistidine tag (fig. S6). (**B**) Interaction between MIF and MDL proteins in a yeast two-hybrid assay. All possible bait-prey combinations were tested as indicated. Control experiments for growth (left) were performed on synthetic complete medium lacking leucine (-L, selection for the bait vector) and tryptophan (-T, selection for the prey vector). Selection for interaction (right) was performed on synthetic complete medium lacking leucine (-L), tryptophan (-T), and histidine (-H, selection for interaction); ev, empty vector. For each condition, a 10× dilution series is shown. Images are representative of three biological replicates ($n = 3$). (**C** and **D**) Interactions between MIF and MDL proteins tested in a luciferase complementation imaging assay in *N. benthamiana* leaves. Representative images (C) show luminescence in representative leaves transfected cLuc-MIF or nLuc-MIF and the indicated nLuc or cLuc MDL fusion constructs, respectively, in discrete areas marked by dashed white circles. Warmer colors indicate a higher amount of luminescence. Scale bars, 1 cm. Luminescence was quantified by measuring the intensity of light emission and calculated per square millimeter (D). The experiment was independently performed three times with four leaves for nLuc-MIF and four leaves for cLuc-MIF in each experiment. Boxplots show the results of the 12 data points per combination ($n = 12$). For statistical analysis, paired t test with post hoc Bonferroni correction was conducted accounting for correlations among intensity measurements on the same leaf (***$P < 0.001$). (**E**) Direct protein-protein interaction studies between fluorescently labeled RED-NHS-MIF and MDL proteins using microscale thermophoresis (MST). For a constant MIF concentration of 100 nM, the difference in normalized fluorescence [per mil (‰)] is plotted against increasing MDL concentrations for analysis of thermophoresis. Values shown represent means ± SD as obtained from at least three biologically independent experiments ($n \geq 3$).

MIF-MDL2 complex formation occurred in yeast, when MDL2 was used as the bait protein (Fig. 2B), but not when MIF was used as bait. To substantiate these findings suggesting direct binding between human MIF and a plant MDL, we performed in planta luciferase complementation imaging (LCI) assays. In this experimental setup, fusion proteins tagged with enzymatically inactive N- and C-terminal segments of firefly luciferase (nLUC and cLUC, respectively) were transiently expressed in *Nicotiana benthamiana* leaves (fig. S7A). Interaction of candidate proteins led to the reconstitution of enzymatically active luciferase, which was detected and quantified upon addition of the substrate luciferin. Coexpression of nLUC-MIF with cLUC-tagged MDL1, MDL2, MDL3, or MIF resulted in strong luciferase activity for the cLUC-MDL2 and nLUC-MIF combination. Similarly, expression of cLUC-MIF yielded strong luciferase activity in the reciprocal combination with nLUC-MDL2 and additionally with nLUC-MIF (Fig. 2, C and D, and fig. S7B). To quantify direct binding between MIF and its MDL homologs, we determined the dissociation constant (K_D) values of MIF-MDL interactions using microscale thermophoresis (MST), a biomolecular interaction methodology suitable to measure protein-protein binding at nano- to micromolar concentrations under solution conditions. We chemically labeled recombinant MIF with the RED-*N*-hydroxysuccinimidyl (NHS) dye to analyze the interaction with unlabeled recombinant MDL1, MDL2, and MDL3, respectively. We observed characteristic sigmoidal binding curves with K_D values less than 5 µM for each MIF-MDL pair (Fig. 2E). Several negative controls, including buffer (fig. S8A), bovine serum albumin (BSA) (fig. S8B), and heat-denatured MDL1 protein (fig. S8C), did not result in sigmoidal binding curves, indicating that the MIF-MDL interactions were due to specific binding. Together, four different types of protein-protein interaction assays (in vitro coimmunoprecipitation, yeast two-hybrid, in planta LCI experiments, and in vitro MST) provided evidence for direct association of MIF and MDL proteins.

MIF and MDLs synergistically activate human chemokine receptors in yeast

We have previously used a genetically modified strain of *Saccharomyces cerevisiae* that expresses functional human chemokine receptors that signal through an altered *S. cerevisiae* Gα (GPA1) protein. In this system, GPA1 activation stimulates the mitogen-activated protein kinase (MAPK) pathway, the transcription factor STE12, and STE12-dependent expression of a β-galactosidase (*lacZ*/β-*gal*) reporter (Fig. 3A) (*25, 42–45*). Capitalizing on this established system for assaying CXCR4 activation (*25*) and an analogous yeast strain expressing CXCR2 generated herein, we tested MIF and the MDLs for activation of intracellular signaling downstream of CXCR4 and CXCR2. Because MDL3 did not exhibit any interactions in the yeast and plant assays, we focused subsequent experiments on MDL1 and MDL2. Both MDL1 and MDL2 activated CXCR4 more potently than did MIF, with each protein used at 20 µM (Fig. 3B). When 10 µM MIF with 10 µM either of MDL1 or MDL2 were tested together, a hyperactivated (synergistic) effect was observed, with the MIF-MDL2 mixture about three times more active than the MIF-MDL1 combination (Fig. 3B). We also verified the specificity of the synergistic effect applying an otherwise isogenic yeast strain lacking CXCR4, which was generated by a plasmid loss approach from the CXCR4-expressing strain (*46*). This experiment confirmed that only negligible reporter activity

was measurable in the absence of CXCR4, thus essentially excluding effects by endogenous yeast factors (fig. S9, A and B). Activation of the chemokine receptor CXCR2 by MIF occurs in mammalian cells (*8, 28, 32*). The MDLs lack the pseudo-ELR motif of two nonadjacent residues present in human MIF (Arg[11] and Asp[44]) that contributes to binding and activation of CXCR2 (*32*). Consequently, MDL1 and MDL2 were not expected to activate CXCR2. However, application of 20 µM MIF, MDL1, and MDL2 revealed that MDL1 and MDL2 activated CXCR2 to a greater extent than did MIF, although the MDL proteins contain uncharged residues in positions 11 and 44 (Fig. 3C and fig. S1). Given the results with CXCR4, we also tested whether the coapplication of MIF and MDLs affected activation in the CXCR2-dependent yeast reporter system. Similar to the effect seen for CXCR4, joint application of MIF with either MDL1 or MDL2 resulted in hyperactivation, indicating a synergistic effect on CXCR2 activation when MIF was mixed with either MDL1 or MDL2 (Fig. 3C).

We used pharmacological probes to support these results. The MIF small-molecule inhibitor 4,5-dihydro-3-(4-hydroxyphenyl)-5-isoxazoleacetic acid methyl ester (ISO-1) binds to the tautomerase pocket of MIF, thereby inhibiting its catalytic activity as well as its CD74-mediated induction of MAPK activation, p53-dependent apoptosis, and cell proliferation (*47–49*). ISO-1 was previously also shown to partially block MIF-CXCR4 reporter activation (*42*) and MDL1-induced monocyte chemotaxis (*36*), indicating that this inhibitor might likewise affect CXCR4 activation by MDL1. In the yeast-based CXCR4 reporter system, coapplication of ISO-1 (100 µM) with MIF, MDL1, or MDL2 strongly reduced the activating capacity of these proteins (Fig. 3D). We also noticed a marked reduction of the synergistic effect triggered by the joint application of MIF with MDL1 or MDL2 by ISO-1. The US Food and Drug Administration–approved drug AMD3100 is a CXCR4 receptor antagonist that prevents the binding of CXCR4 ligands, such as CXCL12, and partially inhibits MIF, thus constraining CXCR4 signaling (*25*). Using AMD3100 in the yeast reporter assay at a 10-fold molar excess over the concentration of the tested ligands, we observed significantly reduced CXCR4 activation by MIF and MDL2, both in single application and in combination of the two proteins (Fig. 3E). For MDL1 alone, there was no inhibition by AMD3100 and only a mild reduction in signaling when coapplied with MIF. The CXCR2 antagonist SB225002 (*50*) (used at 20-fold molar excess over the ligands) reduced activation by MIF, MDL1, and MDL2 to similar degrees (Fig. 3F).

To further explore the observed synergistic effect between MIF and the MDLs, we performed concentration-response experiments using the synergism between MIF and MDL1 on CXCR4 (Fig. 3B) as an example. We initially coincubated the previously applied concentration of 20 µM MIF with 1 to 4 µM MDL1. Synergy occurred at 1 µM MDL1 and further increased at higher concentrations, with a fivefold enhancement of reporter activity at 4 µM MDL1 (Fig. 3G). To study synergy in greater detail, we next used a subthreshold concentration of 1 µM MIF while varying MDL1 from 0.01 to 10 µM. A significant synergistic effect was already noted at 1 µM MDL1 and continuously increased at higher concentrations (Fig. 3H and fig. S10, A and B). The apparent half maximal effective concentration (EC_{50}) for a synergistic effect of MDL1 under 1 µM MIF for this assay was determined to be 2.5 to 3 µM (Fig. 3I and fig. S10, C and D). A similar value was determined when the luminescence response of the MDL1-alone treatment was subtracted (fig. S11, A to

SCIENCE SIGNALING | RESEARCH ARTICLE
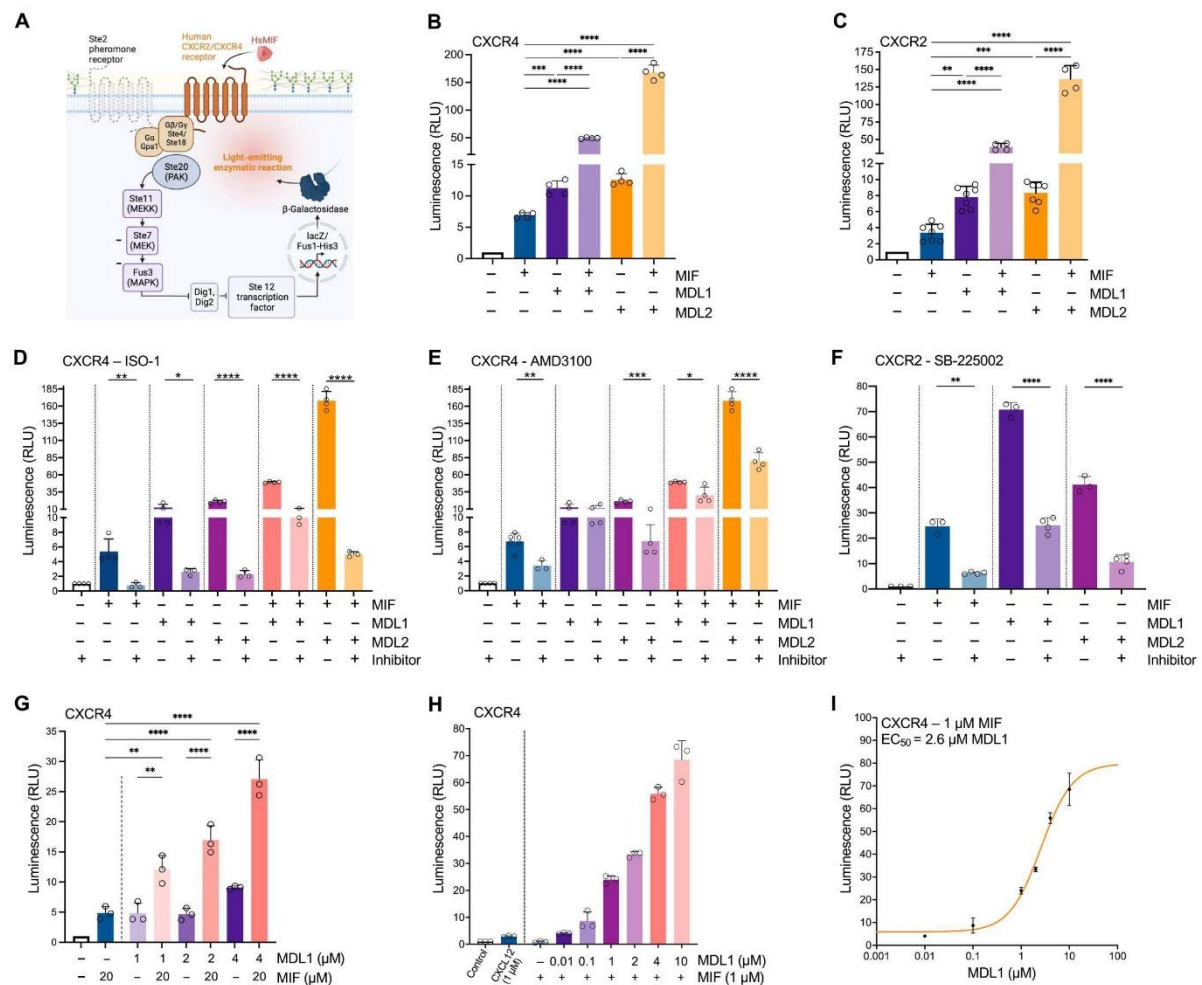
Fig. 3. MDL1 and MDL2 activate CXCR2 and CXCR4 in yeast and synergize with MIF. We measured the activation of CXCR2 and CXCR4 by recombinant MIF, MDL1, and MDL2, alone or in combination, and in the absence or presence of specific inhibitors, in a yeast-based reporter system. (**A**) Schematic illustration of the modified pheromone signaling pathway in *S. cerevisiae*. The endogenous GPCR Ste2 has been replaced by the human chemokine receptor CXCR2 or CXCR4 and linked to the Ste2 downstream signaling cascade. Ligand binding results in activation of the MAPK pathway and eventually triggers expression of the *lacZ* reporter gene. The resulting β-galactosidase activity was measured using a luminescence assay. PAK, p21-activated protein kinase; MEK, MAPK kinase; MEKK, MEK kinase. (**B** and **C**) Quantification of luminescence [in relative light units (RLUs)] 30 min after the addition of recombinant proteins to the CXCR4 (B) or CXCR2 (C) yeast reporter system. MIF and MDLs were used either individually or mixed 1:1 for a final total concentration of 20 μM protein per treatment. (**D** to **F**) Quantification of luminescence in CXCR4 or CXCR2 reporter cells stimulated with MIF, MDL1, and MDL2 as indicated in the absence or presence of 100 μM ISO-1 (D), 100 μM AMD3100 (E), or 200 μM SB225002 (F). (**G**) Titration experiment in the yeast CXCR4 reporter system. Luminescence was measured in response to increasing concentrations (0, 1, 2, and 4 μM) of MDL1 alone or in combination with 20 μM MIF. For comparison, the effect of MIF alone at a concentration of 20 μM is shown. Values shown in (B) to (G) represent means ± SD as obtained from at least three biologically independent experiments ($n \geq 3$) with RLUs of each experiment assessed in technical duplicates and normalized to untreated controls. Individual data points are indicated by white circles. (**H**) Representative concentration-response experiment in the CXCR4 reporter system depicted as bar graph. The graph shows luminescence (in RLU) due to *lacZ* reporter gene activation upon the addition of subthreshold amounts of MIF (1 μM) and MDL (increasing concentrations 0 to 10 μM). The response to the endogenous CXCR4 ligand CXCL12 (1 μM) is shown for comparison. (**I**) Concentration-response curve for MIF-MDL1 interaction in the CXCR4 reporter system. The curve was modeled on the basis of (H) assuming a nonlinear fit and shows a half maximal effective concentration (EC_{50}) of 2.6 μM MDL1 for the synergistic effect. In (H) and (I), technical triplicates from one experiment are shown. Two additional biologically independent experiments, each performed with technical triplicates, are presented in the Supplementary Materials (fig. S10, A to D) for $n = 3$ independent experiments. Statistical analysis was performed using one-way ANOVA with Tukey's multiple comparison ($*P < 0.05$, $**P < 0.01$, $***P < 0.001$, and $****P < 0.0001$).

SCIENCE SIGNALING | RESEARCH ARTICLE

D) (51). Together, the results of these experiments showed that MDL1 and MDL2 were better agonists than MIF when used alone. When used in combination with MIF, MDL1 or MDL2 induced receptor hyperactivation, which was largely blocked by MIF-, CXCR2-, or CXCR4-specific small-molecule inhibitors.

MIF-MDL hetero-oligomers are responsible for synergism
MIF can form various stable types of trimers or homo-oligomers, whereas monomers and dimers are less stable (24, 40, 52–54). This prompted us to investigate whether MIF and MDLs can also form hetero-oligomers, which could be the basis of the observed synergistic effect on CXCR2 and CXCR4 receptor activation. MIF and MDL1 each eluted as trimers when individually subjected to size exclusion chromatography (SEC) (Fig. 4A), but a mixture of MIF and MDL1 showed formation of potential hexamers in addition to trimers (Fig. 4B). Elution volumes and protein markers were used to obtain a calibration curve (fig. S12, A and B) and to derive a standard equation (fig. S12C) to accurately calculate molecular masses from observed elution volumes (fig. S12D). This allowed estimations for the molecular masses of MIF (43.8 ± 0.7 kDa) and MDL1 (38.0 ± 0.3 kDa), as well as MDL2 (35.9 ± 0.6 kDa), when the proteins were applied individually (Table 1). These masses are well in line with the expected masses of the respective trimers. The estimated molecular masses obtained for SEC analysis of the MIF and MDL1 mixture were determined to be 38.5 ± 0.7 and 82.5 ± 0.6 kDa (Table 1), values that are in good agreement with the molecular masses of a (homomeric or heteromeric) trimer and a hetero-oligomeric hexamer, respectively.

We noticed that only about one-third of the MIF and MDL1 mixture formed hetero-hexamers (Fig. 4B). To establish whether this proportion of the hetero-hexamer had any functional role, we used the molecule p425, a sulfonated azo compound and allosteric MIF inhibitor proposed to bind at the interface of two adjacent MIF trimers (Fig. 4C) and to inhibit MIF tautomerase and CD74 activities (52, 53). We tested whether p425 affected hetero-hexamer formation between MIF and MDLs using SEC and MST assays. In the presence of 100 μM p425, binding of MIF to MDL1 was disrupted, as indicated by a disappearance of the putative hexamer peak in the SEC chromatogram (Fig. 4D). Furthermore, no direct binding was observed in the MST experiment with the MIF-p425-MDL1 mixture (Fig. 4E) or for the MIF-p425-MDL2 and MIF-p425-MDL3 mixtures (fig. S13, A and B).
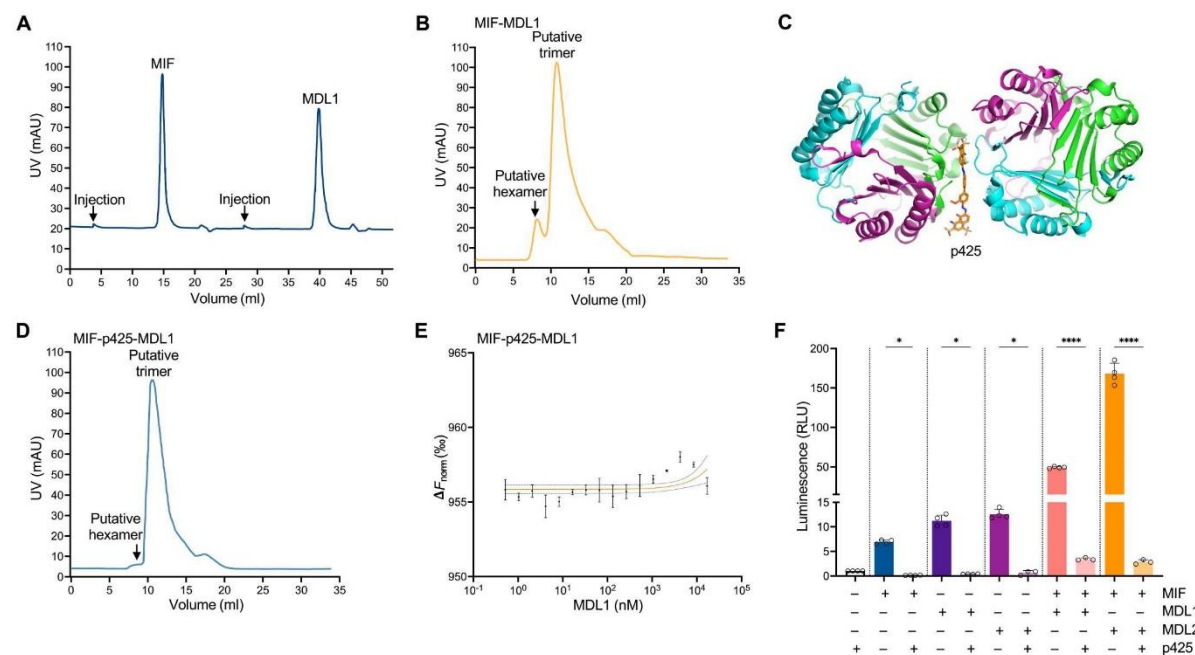
Fig. 4. MIF and MDL1 form hetero-oligomeric complexes in vitro. (**A** and **B**) Representative result from size exclusion chromatography (SEC) of MIF-6×His and MDL1-6×His applied to the column individually (A) or as a 1:1 mixture (B) in 20 mM sodium phosphate (pH 7.4) at a constant flow rate of 0.5 ml/min. Depicted is the UV absorbance in milliarbitrary units (mAU) over the flow in milliliters. (**C**) The crystal structure of MIF and p425 showing interactions between two trimers. (**D**) Representative SEC of an MIF, MDL1, and p425 mixture. The positions of the putative hexamer and the trimer are shown. (**E**) Direct protein-protein interaction studies between fluorescently labeled RED-NHS-MIF and MDL1 using MST. Inhibitor p425 was used at a 10-fold excess to MIF. For a constant MIF concentration of 100 nM, the difference in normalized fluorescence (given in ‰) is plotted against increasing MDL1 concentrations for analysis of thermophoresis. Values shown represent means ± SD as obtained from at least three biological replicates. (**F**) Quantification of luminescence (in RLUs) in CXCR4-*lacZ* reporter yeast stimulated with MIF, MDL1, and MDL2 recombinant proteins, alone or in 1:1 combination, at a final total protein concentration of 20 μM, in the absence or presence of 100 μM p425. Values shown represent means ± SD as obtained from at least three independent experiments ($n \geq 3$) with RLUs of each experiment assessed in technical duplicates and normalized to untreated controls. Individual data points are indicated by white circles. Statistical analysis was performed using one-way ANOVA with Tukey's post hoc multiple comparisons test (*$P < 0.05$ and ****$P < 0.0001$).

Spiller *et al., Sci. Signal.* **16**, eadg2621 (2023)   21 November 2023

Table 1. Chromatography statistics for SEC of recombinant MIF-6xHis and MDL-6xHis proteins.

Protein	MIF- 6×His	MDL1- 6×His	MDL2- 6×His	MDL1-6×His + MIF-6×His*	
Elution volume V_e (ml)†	11.71 ± 0.08	12.39 ± 0.04	12.67 ± 0.08	8.673 ± 0.36	12.33 ± 0.09
Calculated molecular massaccording to V_e (Da)†	43,831± 731	38,039± 317	35,883± 598	82,543± 6,194	38,518± −723
Predicted monomericmolecular mass (Da)‡	13,410	13,258	13,045	—	—
Ratio calculated/predicted molecular mass	3.27	2.87	2.75	—	—

*Note that the two subcolumns represent the two peaks obtained for this protein combination. †Values shown represent means ± SD as obtained from at least three independent experiments. ‡On the basis of the corresponding amino acid sequence.

To investigate whether the trimer or hexamer contributed to the observed activation and synergism in the yeast-based assay, we used p425 (100 μM) in the CXCR4 signaling assay with application of the individual agonists MIF, MDL1, or MDL2 alone or with coapplication of MIF with MDL1 or MDL2. Signaling activity was completely abolished by p425 with the individual proteins (Fig. 4F), suggesting that activation of CXCR4 requires access to the tautomerase site, in agreement with our findings with the MIF small-molecule inhibitor ISO-1 in the yeast-based CXCR4 reporter system (Fig. 3D) and in mammalian cells (25). Coadministration of p425 with MIF and either MDL1 or MDL2 also significantly reduced CXCR4 synergistic activity to slightly above basal amounts (Fig. 4E). This result, together with the SEC and MST data, strongly suggested that the observed synergism was due to a hexamer formed by trimeric MIF and a trimeric MDL.

MIF and MDL1 synergistically promote chemotactic migration of human neutrophils

To determine whether synergism occurs in human cells, we tested the effect of MIF and MDL1 on primary human neutrophil chemotaxis because neutrophils abundantly produce CXCR2 and CXCR4 (but not CD74) and have been shown to migrate upon stimulation with MIF (50). Neutrophil chemotaxis was first examined in a Transwell migration device (fig. S14A). MDL1 was added to the lower chamber as a chemoattractant, and its chemotactic activity toward neutrophils in the upper chamber was compared with MIF and CXCL8 (10 ng/ml) as a bona fide CXCR2 agonist and positive control. MDL1 increased neutrophil chemotaxis in a concentration-dependent manner, with a typical bell-shaped curve and a maximal chemotactic index of about 2 observed at 500 ng/ml. This effect was significantly higher than that of MIF (500 ng/ml) (Fig. 5A). Experiments comparing chemotaxis of a mixture of MIF (250 ng/ml) and MDL1 (250 ng/ml) versus chemotaxis by an individual regimen of MIF (500 ng/ml) or MDL1 (500 ng/ml) demonstrated synergism (Fig. 5B).

We next studied 3D chemotaxis of primary human neutrophils as assessed by single-cell migration tracks in the *x-y* direction using live-cell microscopy (fig. S14B). As expected, compared with the negative control (buffer), the positive controls CXCL8 (500 ng/ml) and MIF (500 ng/ml) led to a significant shift in migration tracks from a random distribution to chemotaxis toward the chemokines (Fig. 5, C to E, and fig. S15, A to C and F). MDL1 had a similar promigratory effect as MIF (Fig. 5F and fig. S15, D and F). Again, addition of an MIF and MDL1 mixture produced a synergistic effect (Fig. 5, G and H, and fig. S15, E and F).

We next tested the effect of the CXCR2 and CXCR4 inhibitors SB-225002 and AMD3100, respectively, on MIF- or MDL1-induced neutrophil chemotaxis in both Transwell and 3D live imaging chemotaxis assays. When assessed by Transwell assay, MIF-induced neutrophil chemotaxis was inhibited by both the CXCR2 and CXCR4 antagonists, but MDL1-induced chemotaxis was only inhibited by SB-225002 across the entire concentration range from 100 to 1000 ng/ml (Fig. 6A). The difference in inhibitor effects between MIF and MDL1 might be explained by only partially overlapping receptor binding sites. Similar results were observed with 3D chemotaxis viewed by live-cell microscopy. The CXCR4 antagonist AMD3100 only inhibited MIF-induced chemotaxis but not that elicited by MDL1 (Fig. 6B and fig. S16, A and C), whereas the CXCR2 antagonist SB-225002 inhibited chemotaxis induced by both proteins (Fig. 6C and fig. S16, B and C). In summary, these results were quantitated (Fig. 6D) and were similar to those obtained with the *S. cerevisiae* signaling system (Fig. 3, E and F), overall indicating that MDLs can elicit MIF chemokine receptor–mediated responses and interact synergistically with MIF in human cells.

MIF and MDL1 synergistically promote AKT signaling downstream of CXCR4 and inflammatory gene expression in human lung epithelial cells

To test MIF receptor activation by MDLs and their synergistic effects with MIF on another human cell type, we assessed the effects of MDLs individually and in combination with MIF on the A549 human lung epithelial cell line. This cell line is a well-established model for human type II pneumocytes that has been used for a variety of studies on lung inflammation and infection (55), and MIF is known to promote inflammatory effects in pneumocytes (12). Flow cytometric analysis of known MIF receptors showed this cell line to produce substantial amounts of CXCR4, whereas CXCR2, CXCR7, and CD74 were not detected in our analysis (fig. S17). MIF can bind and activate CXCR4 to elicit downstream activation of phosphoinositide 3-kinase (PI3K) and the kinase AKT that is relevant in both physiology and pathophysiology (56). In line with previous studies, we observed an increase in phosphorylated AKT (pAKT) abundance up to three- to fourfold within 15 min of MIF stimulation (Fig. 7, A and B) (57, 58). We also confirmed the previously described capacity of MDL1 to activate AKT signaling (Fig. 7, A and B) (36). An equimolar coapplication of MIF and MDL1 resulted in a markedly stronger effect with an increase in pAKT concentrations of eight- to ninefold (Fig. 7B).
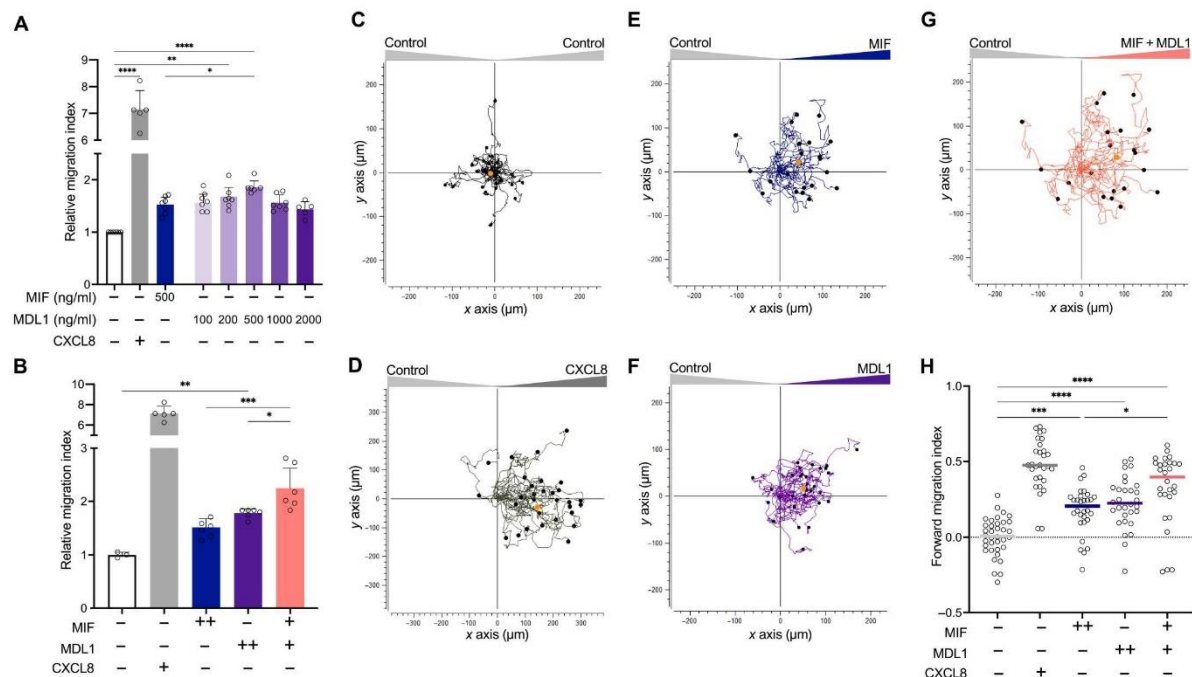
Fig. 5. MDLs promote human neutrophil chemotaxis and augment the chemotactic effect of human MIF. (**A**) Quantification of chemotactic migration of primary human neutrophils in Transwell chemotaxis assays, presented as the relative migration index, toward different concentrations of MDL1 in the lower chamber. Chemotaxis toward MIF (500 ng/ml) and that toward the cognate CXCR2 agonist CXCL8 (10 ng/ml) were included for comparison. Addition of 20 mM sodium phosphate buffer (pH 7.2) to the lower chamber served as negative control to normalize treatments to spontaneous (random) migration. The bars represent means ± SD of five to seven biological replicates (white circles indicate individual data points). (**B**) Comparison of chemotaxis in response to MIF (500 ng/ml), MDL1 (500 ng/ml), or a 1:1 combination of MIF and MDL1 (250 ng/ml each). CXCL8 (10 ng/ml) served as a positive control, and buffer was the negative control. Bars represent means ± SD of three to seven biological replicates (white circles indicate individual data points). (**C** to **G**) Representative experiments showing 3D chemotaxis of primary human neutrophils as assessed by live-cell microscopy of single-cell migration tracks in the *x/y* direction in micrometers. Cells were placed in collagen matrices containing buffer only (control) to track random motility (C) or between a matrix containing buffer and one containing CXCL8 (10 ng/ml) (D), MIF (500 ng/ml) (E), MDL1 (500 ng/ml) (F), or a 1:1 mixture of MIF and MDL1 (250 ng/ml each) (G). Orange dots represent the center of mass in each experiment. (**H**) Quantification of results shown in (C) to (G). The migration tracks of 30 randomly selected cells per treatment group were recorded, and the forward migration index plotted (*n* = 30). Statistical analysis was performed using one-way ANOVA with Tukey's post hoc multiple comparison between the buffer control and the treatment groups (*$P < 0.05$, **$P < 0.01$, ***$P < 0.001$, and ****$P < 0.0001$).

Together, these data supported a synergistic mechanism for AKT signaling promoted by MIF and MDL1 in A549 lung epithelial cells.

Lung macrophages and lung epithelial cells are important sources of inflammatory mediators after the inhalation of potentially harmful material. We therefore also used reverse transcription quantitative polymerase chain reaction (RT-qPCR) to measure the expression of major proinflammatory mediator genes *TNF-α*, *IFN-γ*, *CCL2*, *IL-1β*, *IL-6*, and *CXCL8* in A549 cells after stimulation with bacterial lipopolysaccharide (LPS), MIF, MDL1, or a combination of MIF and MDL1 (Fig. 7, C to H). LPS stimulation resulted in a very strong (10- to 120-fold) increase in inflammatory gene expression in A549 cells for all cytokine genes examined, with the strongest effects observed for *IFN-γ* and *TNF-α*. MIF increased the expression of all tested proinflammatory genes although to a lesser degree than did LPS. The strongest MIF effects were seen for *TNF-α* and *IL-6*, which increased over baseline by about sixfold (Fig. 7, C to H). Stimulation by MDL1 activated proinflammatory cytokine gene expression in a range similar to that observed for MIF, with slightly stronger increases for all transcripts (Fig. 7, C to H). When A549 cells were

stimulated with a combination of MDL1 and MIF, inflammatory cytokine gene induction was significantly stronger than for treatment with either alone, showing an observed rate of increase of 5- to 40-fold. This synergistic effect was most pronounced for *IFN-γ*, *TNF-α*, and *IL-6* (Fig. 7, C to H). Together, these data demonstrated that MDL1 stimulated AKT activation in CXCR4-expressing human lung epithelial cells and induced proinflammatory cytokine responses. They also showed a marked synergistic effect for the combination of the human MIF and plant MDL1 proteins that was particularly pronounced for the cytokine gene expression response. These results are consistent with MDL1 promoting intracellular signaling and proinflammatory gene expression in lung epithelial cells by binding to CXCR4 and show that MDL1 can enhance the responses of lung epithelial cells to MIF.

Overall, our findings demonstrate that MDLs bound and activated CXCR4, stimulated CXCR4-dependent migration of primary human neutrophils, and elicited cellular proinflammatory responses in cultured human lung epithelial cells similarly to MIF. MDLs
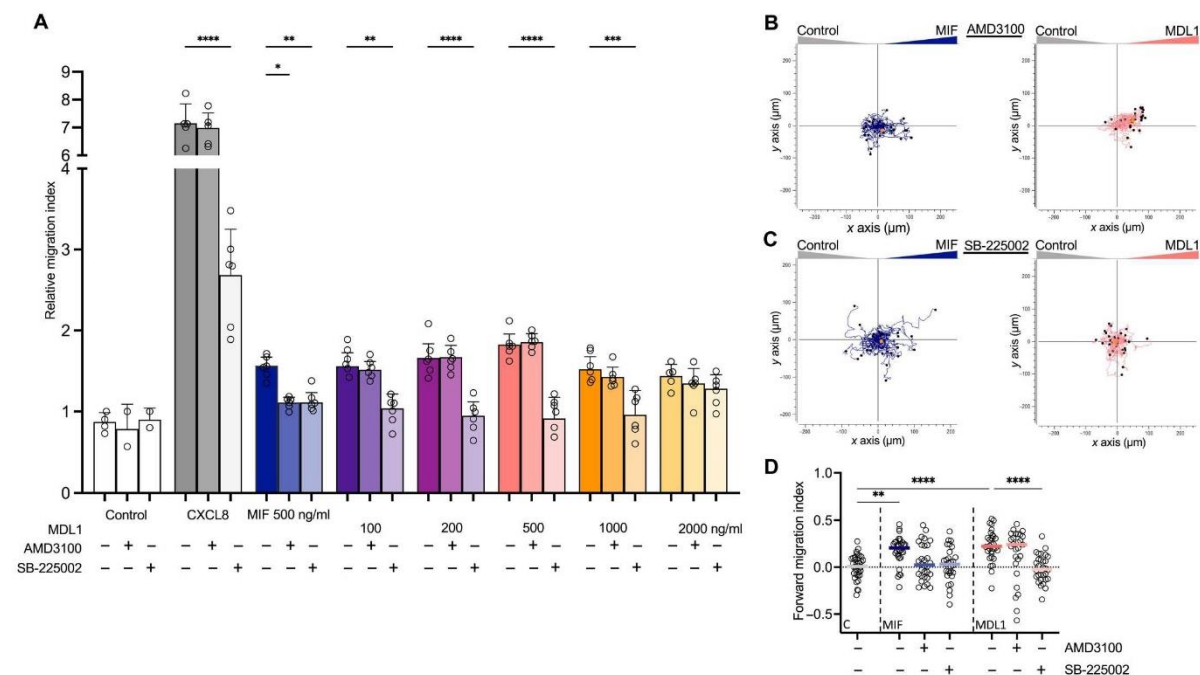
Fig. 6. MDL1-mediated neutrophil chemotaxis is inhibited by a CXCR2 inhibitor but not by a CXCR4 inhibitor. (**A**) Quantification of chemotaxis toward various concentrations of MDL1 (100 to 2000 ng/ml) in Transwell assays in the absence or presence of the CXCR4 inhibitor AMD3100 or the CXCR2 inhibitor SB-225002 as indicated. Migration toward CXCL8 (10 ng/ml) or MIF (500 ng/ml) is shown for comparison, and migration toward 20 mM sodium phosphate buffer (pH 7.2) was used to normalize treatments to random migration (control). The bars represent means ± SD of three to six biological replicates ($n = 3$ to 6), except for the AMD3100 and SB225002 control incubations in the buffer control setting, which are arithmetic means of two independent experiments ($n = 2$). White circles indicate individual data points. (**B** and **C**) Representative experiments showing 3D chemotaxis of primary human neutrophils as assessed by live-cell microscopy of single-cell migration tracks in the x/y direction in micrometer. The cells were placed between a matrix containing buffer only (control) and a matrix containing MIF (500 ng/ml) or MDL1 (500 ng/ml) in the presence of either AMD3100 (B) or SB-225002 (C). Orange dots represent the center of mass for each experiment. (**D**) Quantification of the results in (B) and (C) plus experiments in the absence of the inhibitors. The migration tracks of 30 randomly selected cells per treatment group were recorded, and the forward migration index plotted ($n = 30$). Statistical analysis was performed using one-way ANOVA with Tukey's post hoc multiple comparison (*$P < 0.05$, **$P < 0.01$, ***$P < 0.001$, and ****$P < 0.0001$).

formed hetero-oligomeric complexes with MIF in vitro and synergistically promoted MIF responses in cells.

DISCUSSION

We investigated structural, biochemical, and functional properties of MDLs, plant orthologs of the atypical human cytokine MIF. Analysis of the structural data obtained for all three *Arabidopsis* MDLs showed an extraordinary degree of structural conservation with the overall architecture of mammalian MIF proteins, including the enzymatic site, thereby confirming previous sequence-based in silico modeling (31). Despite the high degree of conservation at the tautomerase active site, a notable difference in enzymatic catalysis was previously observed for all three MDLs in comparison with MIF (36). The crystal structures in our present study may offer a structural explanation for this observation. Lys[98], which is present in all three MDLs and replaces Asn[97] in MIF, has no stabilizing interaction with the modeled substrate, HPP. In addition, there are other residues that differ between the MDLs and MIF, such as Tyr[96] of MDL1, which has a different conformation than the corresponding

tyrosine in MIF (Tyr[95]), and the existence of Phe[96] and Ile[96] at this position in MDL2 and MDL3, respectively. A different orientation or conformation of these residues in the 3D context of the cavity could be the structural basis of the inactive tautomerase catalytic site in the *Arabidopsis* orthologs (36). However, we cannot eliminate the possibility that binding of HPP to the MDL1 or MDL2 enzymatic site occurs in a nonproductive manner for catalysis because the MIF inhibitor ISO-1 was designed on the basis of the MIF-HPP structure (39) and inhibits MDL-mediated activities.

We present evidence for direct protein-protein interaction and cooperative signaling of MIF with MDLs tested in a variety of systems, including yeast two-hybrid assays, in planta experiments, MST, CXCR2, and CXCR4 signaling assays, and inhibition of signaling by pharmacological agents affecting MIF, CXCR2, and CXCR4 as well as MIF-MDL oligomerization. Furthermore, we obtained evidence for synergistic effects of MDL1 and MIF on inflammatory responses of human cells that can also be explained by protein-protein interactions or cooperative signaling. We acknowledge that in some assays in which an MIF-MDL2 interaction was detected, none was seen for MIF-MDL1. For example, in the yeast

SCIENCE SIGNALING | RESEARCH ARTICLE

Fig. 7. MIF and MDL1 synergistically stimulate inflammatory gene expression in A549 lung epithelial cells. (**A**) Analysis of the AKT signaling pathway in A549 lung epithelial cells using immunoblotting for total AKT and phosphorylated (activated) AKT [pAKT(Ser^{473})] after short-term stimulation with MIF (200 ng/ml) or MDL1 (200 ng/ml) or a 1:1 mixture of the two (100 ng/ml each). Untreated control samples were used as negative control. β-Actin is a loading control. (**B**) Densitometric quantification of pAKT band intensities in (A) relative to AKT and normalized to β-actin. Bars represent means ± SD of five biologically independent experiments (white circles indicate individual data points). Statistical analysis was performed using one-way ANOVA with Tukey's post hoc multiple comparison between the untreated control and the treatments. (**C** to **H**) RT-qPCR analysis of *TNF-α* (C), *IFN-γ* (D), *CCL2* (**E**), *IL-1β* (F), *IL-6* (G), and *CXCL8* (H) expression in A549 lung epithelial cells after 4 hours of stimulation with either MIF (100 ng/ml) or MDL 1 (100 ng/ml) or a 1:1 mixrture of MIF and MDL1 (100 ng/ml each). For comparison, stimulation with MIF (200 ng/ml) is shown as well as stimulation with LPS (10 ng/ml, positive control) and 20 mM sodium phosphate buffer (pH 7.2) (buffer control). Transcript abundance is shown as fold change relative to untreated controls and the housekeeping gene *RPLP0*. Values shown represent means ± SD as obtained from four to six biological replicates (black dots indicate individual data points). Statistical analysis was performed using one-way ANOVA with multiple comparison (*$P <$ 0.05, **$P <$ 0.01, ***$P <$ 0.001, and ****$P <$ 0.0001). (**I**) Schematic illustration of the CXCR4 receptor, a typical GPCR, which activates the PI3K-AKT pathway as one of its downstream signaling cascades known to be involved in cell proliferation and migration. MIF or MDL1 binding to CXCR4 results in activation of the pathway.
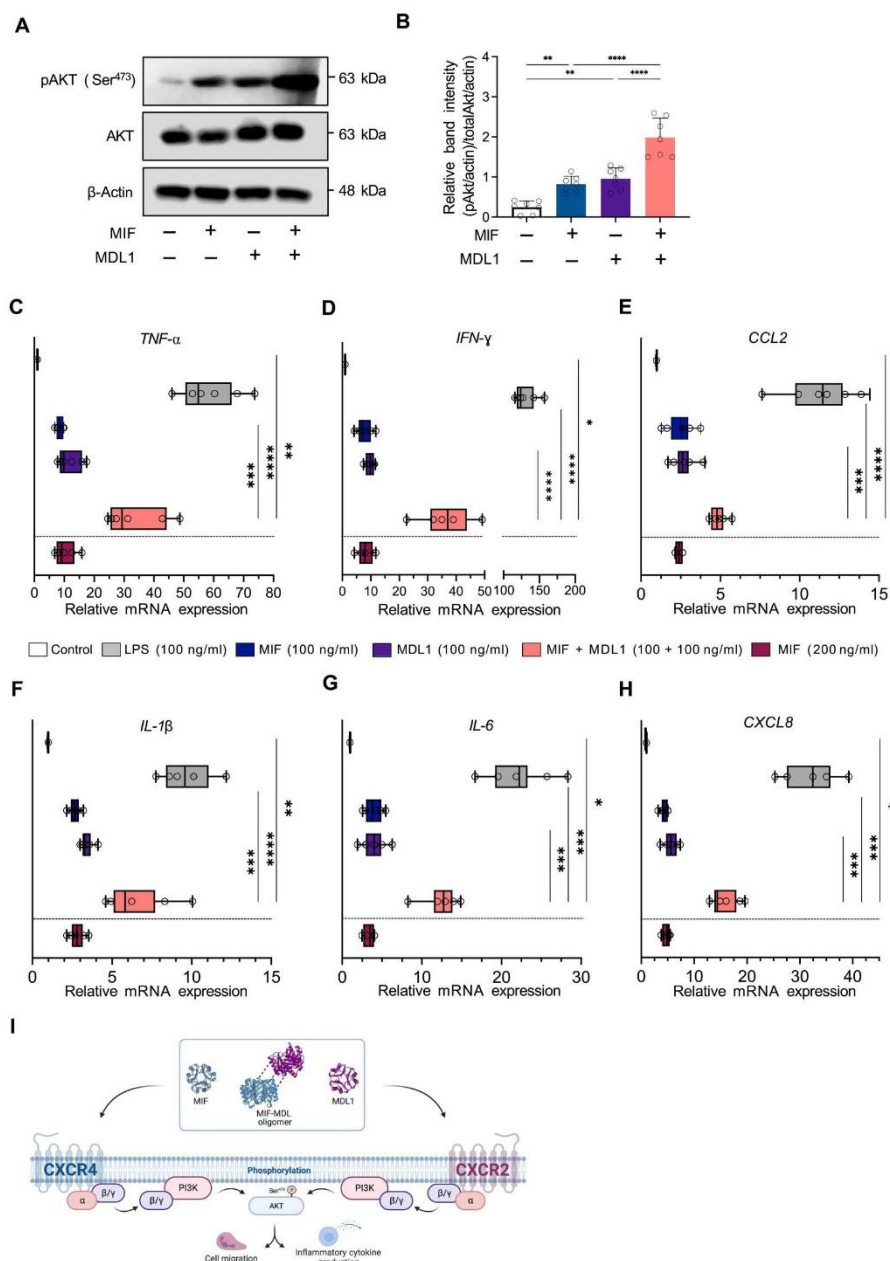
two-hybrid and in planta luciferase complementation assays, we found that only MDL2 interacted with MIF. By contrast, both MDL1 and MDL2 interacted with CXCR2 and CXCR4 in the yeast signaling system, and SEC showed interactions between MIF and MDL1 that were abrogated by the inhibitor p425. Further studies are necessary to provide an explanation for the observed MDL paralog–specific differences depending on the assay.

Moreover, we detected homomeric MDL1-MDL1 and heteromeric MDL1-MDL2 interactions in the yeast two-hybrid assay, confirming a previous in planta analysis (*34*). The assay does not provide any information as to whether these represented interactions of MDL subunits within a trimer or allosteric interactions between MDL trimers. To this end, future studies will be needed to clarify

SCIENCE SIGNALING | RESEARCH ARTICLE

whether and to what extent homomeric MDL or MIF oligomerization competes with MDL-MIF hetero-oligomerization.

Plant cells do secrete proteins, but there is no evidence that MDLs are exported outside the cell (*34*). Furthermore, there are no proteins resembling the MIF receptors for MDLs to activate these types of receptors in plants. Although the absence of proteins resembling known receptors does not exclude the possibility that MDLs activate other receptors or intracellular proteins, evidence points to MDLs functioning as intracellular cytoplasmic (MDL1 and MDL2) or peroxisomal (MDL3) enzymes. To understand the role of MDLs in plant life, the respective physiological substrate needs to be identified for each MDL.

Whereas the yeast, in planta, and MST assays did not yield stoichiometric information, the SEC experiment suggested that a dimer of two different MIF-MDL homotrimers was formed and was functionally active. This conclusion was supported by experiments using the inhibitor p425, which prevented or disrupted oligomerization as analyzed by SEC, blocked MIF-MDL1 binding in the MST assay, and attenuated hetero-oligomer–mediated synergism in the CXCR2- or CXCR4-engineered strains of *S. cerevisiae*. Its mode of action involves intercalation between the interface region of two MIF trimers, thereby inhibiting MIF-mediated inflammatory responses (*52, 53, 59*). We would eliminate the possibility that there is a mixture of MIF and MDL within a trimer due to the dissociation rate of 7.7×10^{-16} M^2 for MIF as determined by sedimentation velocity and equilibrium experiments (*54*). Although the dissociation rates of the MDLs have not been measured, we assume, in analogy to MIF, that they function as tight trimers and that the MDL1-MDL2 association observed in the two-hybrid assay was also based on an oligomer of homotrimers, which also might be important information for determining the functional role of MDL1-MDL2 complexes in plants.

Given the results of the protein-protein interaction experiments, we probed whether there was signaling activity in a genetically modified strain of *S. cerevisiae* expressing functionally active CXCR4 (*25, 42–45*). In addition to CXCR4, in the present study, CXCR2 was also used for analogous experiments. Both MDL1 and MDL2 induced signaling through CXCR2 and CXCR4. The MIF inhibitor ISO-1 inhibited CXCR4 signaling by both MDLs, but antagonists of CXCR2 (SB-225002) and CXCR4 (AMD3100) had different effects on MDL1- and MDL2-mediated signaling. Whereas SB-225002 and AMD3100 inhibited MDL2-mediated activation of CXCR2 and CXCR4, respectively, there was significantly reduced or no effect of AMD3100 on CXCR4 activation by MDL1, suggesting an allosteric mechanism of MDL1 activation that bypasses the CXCR4 transmembrane cavity that is necessary for orthosteric activation (*60*). This finding thus also illustrated the plasticity of CXCR4 activation and might play a role in the synergy that occurred when MDL1 or MDL2 were mixed with MIF to costimulate either CXCR2 or CXCR4. The inhibitors (ISO-1, SB-225002, and AMD3100) decreased activation of the receptors. To assess how these two MIF-MDL complexes synergized, the inhibitor p425, which greatly reduced synergism to almost basal amounts, provided initial insight. To gain greater mechanistic insight as to whether MIF and MDL1 and MDL2 associated or acted independently to achieve signaling synergy, we used SEC to show that MIF and MDLs combined to form a putative trimer-trimer (hexameric) complex.

The synergism between MIF and *Arabidopsis* MDLs that occurred in vitro and in *S. cerevisiae* genetically modified to express functional chemokine receptors is not physiological. To investigate whether these interactions have biological relevance, we considered mammalian tissues and organs that could potentially interact with plants or plant cells, with the most obvious being the integumentary, digestive, and pulmonary systems. We chose to examine synergism between human MIF and plant MDLs using primary human neutrophils and the human lung epithelial cell line A549. We studied neutrophil chemotaxis, AKT activation, and proinflammatory gene expression as functional readouts of the host immune and inflammatory response. We found that synergistic MIF-MDL1 effects shaped both neutrophil migration and the inflammatory response of A549 cells. The receptor antagonist and receptor expression profiles suggested that synergism in neutrophils involved both CXCR2 and CXCR4, whereas the synergistic effects in A549 cells were likely mediated by CXCR4.

Despite the synergism we observed, we realize that the cross-kingdom interactions between human MIF and *Arabidopsis* MDLs, which share high-sequence identity with MDLs from other plants, are unexpected. We speculate that mammalian MIF activity might be affected by direct association with plant-derived MDL proteins after contact with the skin, inhalation of plant particles, or upon ingestion in the pharyngeal tract or gut. For example, interactions might occur with immune cells within pharyngeal secondary lymphoid organs or with intestinal MIF by MDL fractions that have escaped digestion (*61*). It could be further speculated that synergism with host proteins could potentially be involved in hyperactivation responses of the integumentary or digestive system, but this aspect has not been explored. In addition, other plants are identified as "medicinal plants" with immunomodulatory activities on mammals through mechanisms that remain poorly understood. Plant-derived peptides (*62*) and proteins (*63*) have been likewise proposed to affect mammalian immune status and may be involved in enhancing allergic or inflammatory mechanisms. Although *Arabidopsis* is neither a medicinal nor an edible plant, the highly sequence-related MDL orthologs are omnipresent in other species of the plant kingdom (*31*). Additional in vitro and in vivo studies are necessary to test the hypothesis that the activity of MIF proteins as components of the human system might be altered when exposed to plant MDL proteins. Such studies involving MIF and MDLs are needed to broaden our understanding of these proteins in potential cross-kingdom interactions.

MATERIALS AND METHODS
Expression and purification of recombinant proteins
Clones of MIF and the three *A. thaliana* MIF ortholog genes, *MDL1*, *MDL2*, and *MDL3*, in pET21a were previously generated (*64*) and used in this work. Briefly, classical cloning strategies were applied, and all genes were C-terminally fused to a hexahistidine tag included in the pET21a vector using the restriction endonucleases Nde I and Xho I. Plasmids were transformed into competent *Escherichia coli* Rosetta (DE3) cells to express the pET21-derived genes and to yield MIF-6×His, MDL1-6×His, MDL2-6×His, and MDL3-6×His fusion proteins. Protein expression was induced by isopropyl-β-D-thiogalactopyranoside (Sigma-Aldrich, Deisenhofen, Germany) as previously described (*36*).

To release intracellular protein, a high-pressure cell homogenizer (French press, Avestin EmulsiFlex C5 by Avestin Europe GmbH, Mannheim, Germany) was used to lyse cells at about 75 MPa. Homogenization and all following purification steps were carried out on ice and under constant cooling. For homogenization, fresh or frozen bacterial pellets gently thawed on ice were resuspended in 1 ml of ice-cold immobilized metal affinity chromatography (IMAC) binding buffer [20 mM sodium phosphate, 0.5 M NaCl, and 20 mM imidazole (pH 7.2)]. Lysates were then centrifuged at 18,000g for 30 min at 4°C to remove cell debris. The protein-containing supernatants were collected and filtered before usage in fast protein liquid chromatography (FPLC; ÄKTA Pure, GE Healthcare/Cytiva, Freiburg, Germany).

For purification, IMAC and subsequent SEC were performed on an FPLC. Nickel-loaded IMAC columns (HisTrap, GE Healthcare/Cytiva) equilibrated with at least five column volumes of IMAC binding buffer were loaded with protein lysates under a flow rate of 1 ml/min. His-tagged protein was then eluted by a gradient over 30 min and a flow rate of 0.5 ml/min from 0 to 100% IMAC elution buffer [20 mM sodium phosphate, 0.5 M NaCl, and 0.5 M imidazole (pH 7.2)]. During elution, samples were collected in fractions of 0.5 ml, and protein content was monitored via an ultraviolet (UV) detector at 280 nm. Protein-containing fractions were combined and purified further via SEC on a Superdex 75 10/300 GL column (GE Healthcare/Cytiva) using 20 mM sodium phosphate buffer (pH 7.2), a buffer condition previously reported to preserve MIF bioactivity (64). Protein-containing and imidazole-free fractions were collected and sterile-filtered over a 0.2-µm filter before further use. Protein purity was assessed by SDS–polyacrylamide gel electrophoresis (PAGE) with Coomassie and silver staining as well as anti-6×His immunoblot (see below). Endotoxin content of every batch of protein was measured photometrically in sterile-filtered protein solution using the Pierce LAL Chromogenic Endotoxin Quantitation Kit (Thermo Fisher Scientific, Dreieich, Germany) essentially following the manufacturer's instructions. Purified protein was stored at 4°C and used within a maximum of 4 weeks.

Protein crystallization and structure determination
For crystallization, buffers of all MDL proteins were exchanged for 20 mM Hepes and 250 mM NaCl (pH 7.5) immediately after purification, and the protein was then concentrated (MDL1, 12.3 mg/ml; MDL2, 11.1 mg/ml; MDL3, 9.8 mg/ml). For all MDL proteins, crystallization experiments were carried out using sitting drop/vapor diffusion crystallization in a 200 + 200–nl format using a Phoenix crystallization robot in MRC-2 crystallization plates. Individual crystallization conditions for MDL1 consisted of 50 mM tris (pH 8.0), 0.2 M calcium acetate, and 26% PEG 8000. For MDL2, the crystallization conditions were 50 mM tris (pH 8.0) and 2.25 M ammonium sulfate; for MDL3, they were 50 mM MES (pH 6.0), 4% 2-methyl-2,4-pentanediol (MPD), 0.2 M ammonium acetate, and 30% PEG 3350. All crystals were grown at 292.15 K. For cryoprotection, individual crystals were transferred to a new drop containing the mother liquor enriched with 30% ethylene glycol for MDL1, 30% glycerol for MDL2, and 30% ethylene glycol for MDL3 and flash-frozen in liquid nitrogen. X-ray data were collected at 100 K at the Paul Scherrer Institute synchrotron using a Dectris Eiger2 16 M Detector (wavelength, 0.9999 Å).

Diffraction data reduction was done using the XDS program (65). The observed reflections were scaled and merged using Aimless (66) provided in the CCP4 software. The crystal structures were solved with human MIF monomer by molecular replacement using Phaser (67). The structure solution yielded a trimer in the asymmetric unit for MDL1 and MDL2 and a monomer for MDL3. The refinement of the structures was performed using the module Phenix.refine (68) of the PHENIX package. Cycles of refinement and model building were performed using Phenix.refine and Coot (69). The stereochemistry of these crystal structures was assessed using MOLPROBITY (70). Individual refinement statistics for each protein are listed in table S1. Structural data for MDL1, MDL2, and MDL3 were collected at 1.56, 1.40, and 2.0 Å resolutions, respectively. The crystal structures were compared with each other and with the previously published MIF structure [Protein Data Bank (PDB) 3DJH; (71)] using PyMOL and Chimera software for visualization and analysis (72).

Generation of monoclonal antibodies recognizing MDL1
Lou/c rats were immunized with 60 µg of purified full-length MDL1-6×His protein, 5 nmol of CpG (TIB MOLBIOL, Berlin, Germany), and an equal volume of incomplete Freund's adjuvant (Sigma-Aldrich, St. Louis, USA). Hybridoma supernatants were generated and screened as described previously (34). Selected supernatants were validated by slot blot immunoassay on recombinant purified human MIF, human MIF-2/D-DT, and the three MDL proteins for specificity and sensitivity (fig. S5). Hybridoma cells from clone ATM1 21G9 immunoglobulin G2b/ĸ (IgG2b/ĸ) were subcloned twice by limiting dilution to obtain a stable monoclonal antibody–producing cell line.

SDS-PAGE and immunoblot analysis of recombinant MDL-6×His proteins
After purification, protein purity was assessed via SDS-PAGE and Coomassie staining or silver staining, and immunoblotting was performed with an antibody recognizing hexahistidine tags. Electrophoresis was performed in 15% acrylamide gels under reducing conditions as described before (36). For immunoblot analysis, electrophoresed proteins were transferred to nitrocellulose membranes using tris-glycine transfer buffer (Thermo Fisher Scientific), followed by blocking (1% BSA) and staining in TBST [tris-buffered saline, 150 mM NaCl, 20 mM tris, and 0.01% Tween-20 (pH 7.3)] supplemented with 1% BSA (Sigma-Aldrich). Hexahistidine-tagged proteins were then detected using a murine monoclonal antibody specific for 6×His tag (Ma1-135, Invitrogen, Karlsruhe, Germany) as primary antibody and revealed by HRP-conjugated goat anti-mouse IgG (ab6789, Abcam, Cambridge, UK). Imaging was performed upon addition of SuperSignal West Dura Extended Duration Substrate (Thermo Fisher Scientific) on an Odyssey Fc Imaging System using ImageStudioTM software (LICOR Biosciences, Bad Homburg, Germany).

Coimmunoprecipitation
Before immunoprecipitation, MIF-6×His was biotinylated using a commercial biotin labeling kit (Roche Diagnostics GmbH, Mannheim, Germany), performed essentially as per the manufacturer's instructions. For biotinylation, 1 mg of recombinant MIF-6×His at a concentration of 1 mg/ml in 20 mM sodium phosphate buffer (pH 7.2) was used. Coimmunoprecipitation experiments were then carried out using Dynabeads M-280 streptavidin (Thermo Fisher Scientific). To this end, 800 µg of recombinant

proteins (biotin-MIF-6×His and/or MDL1-6×His) were mixed in a total volume of 100 µl of phosphate-buffered saline (PBS; pH 7.4) and incubated overnight at 4°C to allow time for interaction. The beads were resuspended thoroughly, and 20 µl of beads was washed with 0.5 ml of washing buffer [PBS and 0. 1% Tween 20 (pH 7.4)]. After magnetic isolation, the beads were resuspended in the protein mixture and incubated with slight agitation for 2 hours at room temperature. Thereafter, the beads and all protein bound to them were magnetically isolated for 3 min, with the supernatant then removed. The beads were washed three times with 0.5 ml of washing buffer, resuspended in 40 µl of denaturing SDS-PAGE sample buffer containing dithiothreitol as reducing agent, and boiled for 5 min at 95°C. Protein samples were magnetically separated from the beads before analysis by SDS-PAGE.

After blotting, biotin-MIF-6×His was revealed via its biotin tag using streptavidin-peroxidase conjugate (Roche Diagnostics GmbH, Mannheim, Germany; 1:1000 dilution), whereas MDL1-6×His was revealed either via its hexahistidine tag using an HRP-conjugated antibody specific for the 6×His tag (GeneTex Inc., USA; 1:1000 dilution) or by a custom-made antibody specific for MDL1 (clone ATM1 21G9; see above). This custom-made antibody was used in the form of a 1:10 dilution of hybridoma supernatant as a primary antibody, in combination with a mouse-derived, HRP-conjugated secondary antibody specific for rat IgG2b immunoglobulins (1:1000 dilution). Where necessary, antibodies were removed from membranes by a 10-min incubation in Restore PLUS Western blot stripping buffer (Invitrogen), and membranes were again blocked with 1% BSA in TBST, followed by incubation with the respective antibodies. Imaging was performed on an Odyssey Fc Imaging System using ImageStudio software (LICOR Biosciences, Bad Homburg, Germany) and SuperSignal West Femto Maximum Sensitivity Substrate (Thermo Fisher Scientific).

Yeast two-hybrid binding assay
For yeast two-hybrid assay, Gateway cloning-compatible vectors pDEST32 and pDEST22 (Invitrogen ProQuest yeast two-hybrid system) were used, which enable N-terminal fusions of bait and prey proteins with the Gal4 activation and DNA binding domains, respectively. MIF and MDL coding sequences were mobilized from pDONR207 entry clones via Gateway recombination into pDEST32 and pDEST22. The resulting plasmids were transformed into S. cerevisiae strain PJ69-4A (73). Yeast transformants were dropped on appropriate synthetic complete medium lacking selective amino acids for growth control and detecting putative interactions. For drop tests, yeast cultures were grown overnight, washed with sterile water, and adjusted to an optical density at 600 nm (OD$_{600}$) of 1; 10-fold dilution series were established; and 4 µl per strain and dilution was dropped onto the corresponding medium. Photographs were taken after 3 days of yeast growth. Bait and prey protein expression was validated by immunoblot analysis using the GAL4 (DBD) (SC-510) and GAL4 (AD) (SC-1663) monoclonal antibodies (Santa Cruz Biotechnology, Dallas, TX, USA).

Chemokine receptor signaling assay in yeast
For receptor signaling experiments, we used the functional CXCR4- or CXCR2-expressing transformants of S. cerevisiae strain CY12946 that has been previously described (25, 42–44). Briefly, the endogenous yeast pheromone receptor was replaced by human CXCR4 or CXCR2, respectively, with the activated human chemokine receptor

being functionally linked to the downstream MAPK-type signaling pathway, ultimately resulting in expression of the lacZ/β-gal reporter gene upon receptor binding. The β-galactosidase enzymatic activity (assessed photometrically) was therefore used as a surrogate parameter for chemokine receptor activation.

An S. cerevisiae CY12946 strain lacking CXCR4 was used as a negative control to account for potential background signaling mediated by endogenous yeast proteins or for off-target effects of MIF, MDL1, or CXCL12 not mediated via CXCR4. This strain was generated from the CXCR4-expressing clone by a plasmid loss assay [https://openwetware.org/wiki/McClean:_Plasmid_Loss_Assay; modified from (46)]. A single yeast colony of CY12946-hCXCR4 was grown overnight to saturation in nonselective yeast extract, peptone, and dextrose (YPD) liquid medium. A subculture was grown in liquid medium to mid-log phase (OD$_{600}$ ~ 0.5) and diluted by 100,000. Of these diluted cells, 200 µl was plated on a YPD agar plate. The culture plate was grown for 3 to 4 days at 30°C until the colonies had an appreciable size. A replica of this plate was then made on a selective agar plate in complete minimal dropout medium (synthetic medium–Leu). The replica plate was placed in an incubator at 30°C for 3 days and compared with the parent to select clones lacking CXCR4 (i.e., clones that lost the ability to grow on the selective medium).

To test for activation of the signaling reporter pathway, yeast cells were grown in a 24-well plate until reaching an OD$_{600}$ of 0.3 to 0.8 and then incubated with the respective protein samples (MDL1-6×His, MDL2-6×His, and MDL3-6×His) or the known agonist MIF-6×His, either individually or as combinations, either with or without inhibitors added, or with controls as indicated (buffer, CXCL12). A concentration of 10 to 20 µM protein has previously been shown to create stable responses and was used as a reference point for the inhibitor studies. Because of the barrier function of the yeast cell wall, high ligand concentrations are needed for stable receptor activation, for example, 1 to 2 µM in the case of CXCL12 (43). Activation of chemokine receptors was detected by measuring β-galactosidase activity using the commercially available Beta-Glo assay system (Promega Corp, Madison, WI, USA), and the luminescence signal was recorded on a multimodal plate reader (Enspire 2300, PerkinElmer Life Sciences, Rodgau, Germany). The kit was used per the manufacturer's instructions and is based on coupling β-galactosidase enzymatic activity to a luciferase reaction. After mixing assay buffer and assay substrate in a 1:1 ratio, a volume of this mixture equal to the medium volume was added to each well. After mixing and incubation at room temperature for 30 min, luminescence of each sample was measured.

LCI assays
For LCI assays, Gateway cloning–compatible vectors pAMPAT-nLUC-GWY and pAMPAT-cLUC-GWY (34) were used, which enable N-terminal fusions of bait and prey proteins with the nLUC and cLUC, respectively. MIF and MDL coding sequences were mobilized from pDONR207 entry clones via Gateway recombination into pAMPAT-nLUC-GWY and pAMPAT-cLUC-GWY. The resulting plasmids were transformed into Agrobacterium tumefaciens strain GVG3101 (pMP90RK). Bacterial cultures were grown overnight, resuspended in infiltration medium [10 mM MES (pH 5.6), 10 mM MgCl$_2$, and 200 µM acetosyringone] to an OD$_{600}$ of 0.5, and incubated at room temperature for 2 hours. For coinfiltration, equal volumes of each A. tumefaciens transformant were mixed

SCIENCE SIGNALING | RESEARCH ARTICLE

and infiltrated with a needleless syringe from the abaxial side into fully expanded leaves of 4- to 6-week-old *N. benthamiana* plants. The leaves were sprayed with 1 mM D-luciferin (PerkinElmer) dissolved in water supplemented with 0.01% (v/v) Tween 20 at 3 days after infiltration. Leaves were kept in the dark for 10 min before luminescence was detected with a ChemiDoc XRS+ imagine system (Bio-Rad, Feldkirchen, Germany). Luminescence intensities per square millimeter–infiltrated leaf area of different combinations were evaluated using the Image Lab software (Bio-Rad, version 6.1). For each combination of interaction partners, three independent experiments consisting of two different plants and two leaves per plant were evaluated. *Agrobacterium*-mediated transient expression of LCI constructs in *N. benthamiana* was validated by immunoblot analysis using a polyclonal primary antibody specific for luciferase (Merck; diluted 1:1000).

Primary human neutrophils and chemotaxis
Blood was obtained from healthy human volunteers [ethics approval, Ludwig-Maximilians-Universität (LMU), Munich, Germany; AZ 18-104]. After red blood cell lysis and removal of the supernatant, the neutrophil pellet was gently resuspended in RPMI 1640 medium (Invitrogen/Gibco, Karlsruhe, Germany) supplemented with 10% heat-inactivated fetal bovine serum (FBS) and 1% penicillin-streptomycin. Flow cytometric analysis of neutrophils using characteristic forward/side scatter verified a purity of 98 to 99%. Isolated primary human neutrophils were kept at room temperature and were used immediately after isolation.

For Transwell migration, freshly isolated neutrophils in RPMI 1640 without supplements were set up to migrate for 4 hours over a membrane with a pore size of 5 μm (Corning Inc. New York, USA). Lower chambers were filled with 600 μl of RPMI 1640 containing chemokines/treatments and inhibitors according to the respective experimental design. Transwell plates were incubated at 37°C for 30 min to allow prewarming of medium and plate. Then, 100 μl of cell suspension containing 1×10^6 cells in RPMI 1640 was carefully added to the upper chambers of a Transwell insert after placing the filters onto the lower chambers.

The 3D gel matrix chemotaxis assay was performed using commercially available Ibidi μ-slides (Ibidi GmbH, Gräfelfing, Germany) with a tissue-like collagen matrix, allowing the study of cell migration under native-like conditions. Live-cell imaging, time-lapse microscopy, and single-cell tracking allow for measuring a variety of chemotactic parameters, complementing the end-point results obtained in Transwell migration experiments. To this end, 8×10^6 cells/100 μl in RPMI 1640 without supplements were prepared and used immediately. The collagen gel matrix was prepared at a final collagen concentration of 1 mg/ml, with all components handled on ice to ensure slow gel polymerization. Then, 6.3 μl of collagen-cell suspension was added to the appropriate filling ports. Afterward, all filling ports were closed with dedicated plugs, and gels were incubated at 37°C and 5% CO_2 for 30 min to allow solidification of the collagen matrix. Channels were checked microscopically, and only perfectly filled channels were used in the experiment. After matrix preparation, 65 μl of chemoattractant-free RPMI 1640 was added to the chamber on one side of the matrix, and 65 μl of chemoattractant-containing RPMI 1640 medium was added to the other side. This created a native chemoattractant gradient over the cell-containing gel matrix. Immediately after adding treatments, slides were installed on a motorized and preheated

microscopy stage. Automated time-lapse microscopy was performed for 2 hours at a time interval of 1 min on a Leica inverted DMi8-Life Cell Imaging System equipped with a DMC2900 Digital Microscope Camera with complementary metal-oxide semiconductor sensor and live cell–imaging software (Leica Microsystems, Wetzlar, Germany). Images were imported as stacks to ImageJ software and analyzed with the manual tracking extension and the chemotaxis/migration tools from Ibidi GmbH.

AKT signaling pathway analysis
The MIF-CXCR4-PI3K-AKT axis is a well-studied MIF response pathway, implicated among others in cell survival, migration, and cancer development (*57, 74*). A549 cells were obtained from the German Collection of Microorganisms and Cell Cultures GmbH (DSMZ) and maintained in Ham's F-12K medium (Invitrogen/Gibco) supplemented with 10% FBS and 1% penicillin-streptomycin (Sigma-Aldrich, Deisenhofen, Germany). The cells were plated in 150-cm^2 cell culture flasks and cultured at 37°C in a humidified atmosphere containing 5% CO_2. Culture medium was changed every 2 days. The cells were subcultured before reaching confluency using a 0.1% trypsin solution in EDTA (Sigma-Aldrich). The cells were split 1:10 during each passage, with passages used in this study ranging from 3 to 10. The cells were treated with MIF, MDL1, or the combination of the two (1:1 ratio), each at a final concentration of 16 nM. After 10 min of incubation, treated cells were lysed in NuPAGE lithium dodecyl sulfate/dithiothreitol lysis buffer including PhosphoSTOP reagent (Roche Applied Science, Mannheim, Germany). Lysates were run in 11% SDS-PAGE gels and blotted onto nitrocellulose membrane. Immunoblots were developed with antibodies specific for phosphorylated (pAKT; ab81283, Abcam, Cambridge, UK) and total (ab8805, Abcam) AKT, as well as an antibody directed against β-actin (ab8227, Abcam) as an internal reference. Respective HRP-conjugated secondary antibodies (211-032-171, Jackson ImmunoResearch, Ely, UK) were used for detection. Imaging and densitometric band quantification were performed upon addition of SuperSignal West Dura Extended Duration Substrate (Thermo Fisher Scientific) on an Odyssey Fc Imaging System using ImageStudio software (LICOR Biosciences, Bad Homburg, Germany). Densitometric quantification was done by normalizing both total AKT and pAKT to β-actin and then comparing the amount of normalized pAKT with normalized AKT.

Isolation of mRNA and RT-qPCR in A549 cells
For RT-qPCR, 1×10^6 A549 cells were seeded in six-well plates and grown as described above until they reached confluency. Cells were treated with recombinant proteins for 4 hours at the indicated concentrations. mRNA was extracted using TRIzol reagent (Invitrogen, Karlsruhe, Germany) per the manufacturer's instructions. mRNA was reverse-transcribed into cDNA using the First Strand cDNA Synthesis Kit (Thermo Fisher Scientific) following the manufacturer's instructions. RT-qPCR was carried out using the SYBR Green PCR Master Mix (Thermo Fisher Scientific) on a RotorGene 6000 (QIAGEN, Hilden, Germany). The thermal cycling conditions were as follows: initial denaturation at 95°C for 3 min, followed by 40 cycles of 95°C for 10 s and 55°C for 30 s and then followed by 95°C for 1 min and 55°C for 1 min. The fold change was derived by calculating the ratio between each experimental group and control. Ribosomal protein, large, P0 (RPLP0) was used as housekeeping gene for normalization. The relative expression levels were

normalized to endogenous control and were expressed as $2^{-\Delta\Delta Ct}$. Primers used for the RT-qPCR experiments are listed in table S2.

Microscale thermophoresis

All MST experiments were performed on a Monolith NT.115 instrument with green/red filters (NanoTemper Technologies, Munich, Germany). MST and light-emitting diode power were set at 40 and 60%, respectively, for MDL1 and MDL2 or 40 and 90% for MDL3 measurements to obtain stable fluorescent signals around 1000 fluorescent counts. All measurements were performed at 37° C with MST traces tracked for 40 s (laser-off, 5 s; laser-on, 30 s; laser-off, 5 s). A stock solution of 200 nM RED-NHS-MIF-6×His was prepared in 20 mM sodium phosphate buffer (pH 7.4), containing 0.2% BSA, according to the manufacturer's protocol.

For titration of each plant ortholog, each protein substock solution was prepared by serial 1:1 dilution, starting from a 20 μM stock solution in 20 mM sodium phosphate buffer (pH 7.4) and 0.1% BSA. RED-NHS-MIF-6×His and each MDL substock were mixed at a 1:1 ratio resulting in a final MIF concentration of 100 nM and incubated for 10 min in the dark at room temperature. Premium-coated capillaries we used as initial screening had shown slight sticking of protein to standard capillary walls. Incubated mixtures were loaded into capillaries, and MST measurements started immediately. Obtained MST traces were analyzed at an MST-on time of 1.5 s using the MO.Affinity Analysis version 2.2.4 (NanoTemper Technologies) for each of the three potential interaction pairs. Apparent K_D values were calculated using the same software. Visualization was done using Prism GraphPad (Version 9.4.1) assuming a one-on-one binding model with sigmoidal curve fitting models for each set up.

Size exclusion chromatography

SEC experiments were performed on an FPLC system (ÄKTA Pure, GE Healthcare/Cytiva, Freiburg, Germany) with a Superdex 75 10/300 GL column (GE Healthcare/Cytiva) using 20 mM sodium phosphate buffer (pH 7.4) and a constant flow of 0.5 ml/min. Proteins were used for SEC 1 day after purification, either individually or in a 1:1 mixture of MIF-6×His and MDL1-6×His, incubated at 4°C overnight. Proteins were loaded individually, one after another, and peaks observed by UV absorbance (280 nm) in milliarbitrary units over the elution volume in milliliter. Unicorn 7.0 software (GE Healthcare/Cytiva, Freiburg, Germany) was used to analyze chromatograms for individual elution volumes. Experiments were performed in triplicates.

For the described SEC setup, a standard curve and standard equation were generated using the GE gel filtration calibration kit, low molecular weight, as per the manufacturer's instructions (GE Healthcare/Cytiva). From observed elution volumes and known molecular mass of sample proteins, a standard curve and standard equation were calculated and visualized using Prism GraphPad (version 9.4.1).

Statistics

Statistical analyses were performed with GraphPad Prism 9 (Graph-Pad Prism Software Inc., San Diego, CA). After testing for normality by Shapiro-Wilk test, data were analyzed by one-way analysis of variance (ANOVA) followed by post hoc comparison with Tukey's test with multiple comparisons, paired t test with post hoc Bonferroni correction, or unpaired t test, as appropriate. To account for small sample size and potential error in normality tests, appropriate non-parametric tests (Kruskal-Wallis test, Wilcoxon signed rank test, and Mann-Whitney test, respectively) were performed for comparison and showed similar results. Data are presented as means ± SD. $P < 0.05$ is considered as significant. Asterisks indicate statistically significant differences as follows: $*P < 0.05$; $**P < 0.01$; $***P < 0.005$; $****P < 0.0001$.

Supplementary Materials

This PDF file includes:
Figs. S1 to S17
Tables S1 and S2

Other Supplementary Material for this manuscript includes the following:
MDAR Reproducibility Checklist

REFERENCES AND NOTES

1. C. A. Janeway Jr., R. Medzhitov, Innate immune recognition. *Ann. Rev. Immunol.* **20**, 197–216 (2002).
2. A. W. Thomson, *The Cytokine Handbook*. (Academic Press, 4th edition, 2003).
3. T. Calandra, T. Roger, Macrophage migration inhibitory factor: A regulator of innate immunity. *Nat. Rev. Immunol.* **3**, 791–800 (2003).
4. I. Kang, R. Bucala, The immunobiology of MIF: Function, genetics and prospects for precision medicine. *Nat. Rev. Rheumatol.* **15**, 427–437 (2019).
5. A. Kapurniotu, O. Gokce, J. Bernhagen, The multitasking potential of alarmins and atypical chemokines. *Front. Med. (Lausanne)* **6**, 3 (2019).
6. M. Merk, S. Zierow, L. Leng, R. Das, X. Du, W. Schulte, J. Fan, H. Lue, Y. Chen, H. Xiong, F. Chagnon, J. Bernhagen, E. Lolis, G. Mor, O. Lesur, R. Bucala, The D-dopachrome tautomerase (DDT) gene product is a cytokine and functional homolog of macrophage migration inhibitory factor (MIF). *Proc. Natl. Acad. Sci. USA* **108**, E577–E585 (2011).
7. L. Leng, C. N. Metz, Y. Fang, J. Xu, S. Donnelly, J. Baugh, T. Delohery, Y. Chen, R. A. Mitchell, R. Bucala, MIF signal transduction initiated by binding to CD74. *J. Exp. Med.* **197**, 1467–1476 (2003).
8. J. Bernhagen, R. Krohn, H. Lue, J. L. Gregory, A. Zernecke, R. R. Koenen, M. Dewor, I. Georgiev, A. Schober, L. Leng, T. Kooistra, G. Fingerle-Rowson, P. Ghezzi, R. Kleemann, S. R. McColl, R. Bucala, M. J. Hickey, C. Weber, MIF is a noncognate ligand of CXC chemokine receptors in inflammatory and atherogenic cell recruitment. *Nat. Med.* **13**, 587–596 (2007).
9. E. F. Morand, M. Leech, J. Bernhagen, MIF: A new cytokine link between rheumatoid arthritis and atherosclerosis. *Nat. Rev. Drug Discov.* **5**, 399–411 (2006).
10. A. Zernecke, J. r. Bernhagen, C. Weber, Macrophage migration inhibitory factor in cardiovascular disease. *Circulation* **117**, 1594–1602 (2008).
11. H. Conroy, L. Mawhinney, S. C. Donnelly, Inflammation and cancer: Macrophage migration inhibitory factor (MIF)--The potential missing link. *QJM* **103**, 831–836 (2010).
12. M. Sauler, R. Bucala, P. J. Lee, Role of macrophage migration inhibitory factor in age-related lung disease. *Am. J. Physiol. Lung. Cell Mol. Physiol.* **309**, L1–L10 (2015).
13. P. V. Tilstam, D. Qi, L. Leng, L. Young, R. Bucala, MIF family cytokines in cardiovascular diseases and prospects for precision-based therapeutics. *Expert Opin. Ther. Targets* **21**, 671–683 (2017).
14. M. F. Leyton-Jaimes, J. Kahn, A. Israelson, Macrophage migration inhibitory factor: A multifaceted cytokine implicated in multiple neurological diseases. *Exp. Neurol.* **301**, 83–91 (2018).
15. R. Panstruga, S. C. Donnelly, J. Bernhagen, A cross-kingdom view on the immunomodulatory role of MIF/D-DT proteins in mammalian and plant Pseudomonas infections. *Immunology* **166**, 287–298 (2022).
16. A. Sparkes, P. De Baetselier, K. Roelants, C. De Trez, S. Magez, J. A. Van Ginderachter, G. Raes, R. Bucala, B. Stijlemans, Reprint of: The non-mammalian MIF superfamily. *Immunobiology* **222**, 858–867 (2017).
17. C. Michelet, E. G. J. Danchin, M. Jaouannet, J. Bernhagen, R. Panstruga, K. H. Kogel, H. Keller, C. Coustau, Cross-kingdom analysis of diversity, evolutionary history, and site selection within the eukaryotic macrophage migration inhibitory factor superfamily. *Genes (Basel)* **10**, 740 (2019).
18. S. H. Spoel, X. Dong, How do plants achieve immunity? Defence without specialized immune cells. *Nat. Rev. Immunol.* **12**, 89–100 (2012).

SCIENCE SIGNALING | RESEARCH ARTICLE

19. H. W. Sun, J. Bernhagen, R. Bucala, E. Lolis, Crystal structure at 2.6-A resolution of human macrophage migration inhibitory factor. *Proc. Natl. Acad. Sci. U.S.A.* **93**, 5191–5196 (1996).

20. G. Poelarends, V. Veetil, C. Whitman, The chemical versatility of the β–α–β fold: Catalytic promiscuity and divergent evolution in the tautomerase superfamily. *Cell Mol. Life Sci.* **65**, 3606–3618 (2008).

21. E. Rosengren, P. Aman, S. Thelin, C. Hansson, S. Ahlfors, P. Bjork, L. Jacobsson, H. Rorsman, The macrophage migration inhibitory factor MIF is a phenylpyruvate tautomerase. *FEBS Lett.* **417**, 85–88 (1997).

22. E. Rosengren, R. Bucala, P. Aman, L. Jacobsson, G. Odh, C. N. Metz, H. Rorsman, The immunoregulatory mediator macrophage migration inhibitory factor (MIF) catalyzes a tautomerization reaction. *Molecul. Med. (Cambridge, Mass.)* **2**, 143–149 (1996).

23. M. Swope, H. W. Sun, P. R. Blake, E. Lolis, Direct link between cytokine activity and a catalytic site for macrophage migration inhibitory factor. *EMBO J.* **17**, 3534–3541 (1998).

24. C. Fan, D. Rajasekaran, M. A. Syed, L. Leng, J. P. Loria, V. Bhandari, R. Bucala, E. J. Lolis, MIF intersubunit disulfide mutant antagonist supports activation of CD74 by endogenous MIF trimer at physiologic concentrations. *Proc. Natl. Acad. Sci. U.S.A.* **110**, 10994–10999 (2013).

25. D. Rajasekaran, S. Groning, C. Schmitz, S. Zierow, N. Drucker, M. Bakou, K. Kohl, A. Mertens, H. Lue, C. Weber, A. Xiao, G. Luker, A. Kapurniotu, E. J. Lolis, J. Bernhagen, Macrophage migration inhibitory factor-CXCR4 receptor interactions. *J. Biol. Chem.* **291**, 15881–15895 (2016).

26. G. Pantouris, J. Ho, D. Shah, M. A. Syed, L. Leng, V. Bhandari, R. Bucala, V. S. Batista, J. P. Loria, E. J. Lolis, Nanosecond dynamics regulate the MIF-induced activity of CD74. *Angew. Chem. Int. Ed. Engl.* **57**, 7116–7119 (2018).

27. G. Pantouris, M. A. Syed, C. Fan, D. Rajasekaran, T. Y. Cho, E. M. Rosenberg Jr., R. Bucala, V. Bhandari, E. J. Lolis, An analysis of MIF structural features that control functional activation of CD74. *Chem. Biol.* **22**, 1197–1205 (2015).

28. Y. Cho, G. V. Crichlow, J. J. Vermeire, L. Leng, X. Du, M. E. Hodsdon, R. Bucala, M. Cappello, M. Gross, F. Gaeta, K. Johnson, E. J. Lolis, Allosteric inhibition of macrophage migration inhibitory factor revealed by ibudilast. *Proc. Natl. Acad. Sci. U.S.A.* **107**, 11313–11318 (2010).

29. M. Brandhofer, J. Bernhagen, Cytokine aerobics: Oxidation controls cytokine dynamics and function. *Structure* **30**, 787–790 (2022).

30. Y. Wang, R. An, G. K. Umanah, H. Park, K. Nambiar, S. M. Eacker, B. Kim, L. Bao, M. M. Harraz, C. Chang, R. Chen, J. E. Wang, T.-I. Kam, J. S. Jeong, Z. Xie, S. Neifert, J. Qian, S. A. Andrabi, S. Blackshaw, H. Zhu, H. Song, G.-l. Ming, V. L. Dawson, T. M. Dawson, A nuclease that mediates cell death induced by DNA damage and poly(ADP-ribose) polymerase-1. *Science* **354**, 1 (2016).

31. R. Panstruga, K. Baumgarten, J. Bernhagen, Phylogeny and evolution of plant macrophage migration inhibitory factor/D-dopachrome tautomerase-like proteins. *BMC Evol. Biol.* **15**, 64 (2015).

32. C. Weber, S. Kraemer, M. Drechsler, H. Lue, R. R. Koenen, A. Kapurniotu, A. Zernecke, J. Bernhagen, Structural determinants of MIF functions in CXCR2-mediated inflammatory and atherogenic leukocyte recruitment. *Proc. Natl. Acad. Sci. U.S.A.* **105**, 16278–16283 (2008).

33. Y. Cho, B. F. Jones, J. J. Vermeire, L. Leng, L. DiFedele, L. M. Harrison, H. Xiong, Y. K. Kwong, Y. Chen, R. Bucala, E. Lolis, M. Cappello, Structural and functional characterization of a secreted hookworm macrophage migration inhibitory factor (MIF) that interacts with the human MIF receptor CD74. *J. Biol. Chem.* **282**, 23447–23456 (2007).

34. K. Gruner, F. Leissing, D. Sinitski, H. Thieron, C. Axstmann, K. Baumgarten, A. Reinstadler, P. Winkler, M. Altmann, A. Flatley, M. Jaouannet, K. Zienkiewicz, I. Feussner, H. Keller, C. Coustau, P. Falter-Braun, R. Feederle, J. Bernhagen, R. Panstruga, Chemokine-like MDL proteins modulate flowering time and innate immunity in plants. *J. Biol. Chem.* **296**, 100611 (2021).

35. X. Robert, P. Gouet, Deciphering key features in protein structures with the new ENDscript server. *Nucleic Acids Res.* **42**, W320–W324 (2014).

36. D. Sinitski, K. Gruner, M. Brandhofer, C. Kontos, P. Winkler, A. Reinstadler, P. Bourilhon, Z. Xiao, R. Cool, A. Kapurniotu, F. J. Dekker, R. Panstruga, J. Bernhagen, Cross-kingdom mimicry of the receptor signaling and leukocyte recruitment activity of a human cytokine by its plant orthologs. *J. Biol. Chem.* **295**, 850–867 (2020).

37. Y. Cho, J. J. Vermeire, J. S. Merkel, L. Leng, X. Du, R. Bucala, M. Cappello, E. Lolis, Drug repositioning and pharmacophore identification in the discovery of hookworm MIF inhibitors. *Chem. Biol.* **18**, 1089–1101 (2011).

38. E. Naessens, G. Dubreuil, P. Giordanengo, O. L. Baron, N. Minet-Kebdani, H. Keller, C. Coustau, A secreted MIF cytokine enables aphid feeding and represses plant immune responses. *Curr. Biol.* **25**, 1898–1903 (2015).

39. J. B. Lubetsky, A. Dios, J. Han, B. Aljabari, B. Ruzsicska, R. Mitchell, E. Lolis, Y. Al-Abed, The tautomerase active site of macrophage migration inhibitory factor is a potential target for discovery of novel anti-inflammatory agents. *J. Biol. Chem.* **277**, 24976–24982 (2002).

40. R. Mischke, R. Kleemann, H. Brunner, J. Bernhagen, Cross-linking and mutational analysis of the oligomerization state of the cytokine macrophage migration inhibitory factor (MIF). *FEBS Lett.* **427**, 85–90 (1998).

41. R. Kleemann, A. Hausser, G. Geiger, R. Mischke, A. Burger-Kentischer, O. Flieger, F. J. Johannes, T. Roger, T. Calandra, A. Kapurniotu, M. Grell, D. Finkelmeier, H. Brunner, J. Bernhagen, Intracellular action of the cytokine MIF to modulate AP-1 activity and the cell cycle through Jab1. *Nature* **408**, 211–216 (2000).

42. A. Sachpatzidis, B. K. Benton, J. P. Manfredi, H. Wang, A. Hamilton, H. G. Dohlman, E. Lolis, Identification of allosteric peptide agonists of CXCR4. *J. Biol. Chem.* **278**, 896–907 (2003).

43. J. W. Murphy, D. Rajasekaran, J. Merkel, E. Skeens, C. Keeler, M. E. Hodsdon, G. P. Lisi, E. Lolis, High-throughput screening of a functional human CXCL12-CXCR4 signaling axis in a genetically modified *S. cerevisiae*: Discovery of a novel up-regulator of CXCR4 activity. *Front. Mol. Biosci.* **7**, 164 (2020).

44. E. M. Rosenberg Jr., R. E. D. Harrison, L. K. Tsou, N. Drucker, B. Humphries, D. Rajasekaran, K. E. Luker, C.-H. Wu, J.-S. Song, C.-J. Wang, J. W. Murray, Y.-C. Cheng, K.-S. Shia, G. D. Luker, D. Morikis, E. J. Lolis, Functional characterization, dynamics, and mechanism of CXCR4 antagonists on a constitutively active mutant. *Cell. Chem. Biol.* **26**, 662–673 (2019).

45. M. Lacy, C. Kontos, M. Brandhofer, K. Hille, S. Groning, D. Sinitski, P. Bourilhon, E. Rosenberg, C. Krammer, T. Thavayogarajah, G. Pantouris, M. Bakou, C. Weber, E. Lolis, J. Bernhagen, A. Kapurniotu, Identification of an Arg-Leu-Arg tripeptide that contributes to the binding interface between the cytokine MIF and the chemokine receptor CXCR4. *Sci. Rep.* **8**, 5171 (2018).

46. V. Lundblad, H. Zhou, Manipulation of plasmids from yeast cells. *Curr. Protoc. Mol. Biol.* **Chapter 13**, Unit13.19 (2001).

47. C. Piette, M. Deprez, T. Roger, A. Noel, J. M. Foidart, C. Munaut, The dexamethasone-induced inhibition of proliferation, migration, and invasion in glioma cell lines is antagonized by macrophage migration inhibitory factor (MIF) and can be enhanced by specific MIF inhibitors. *J. Biol. Chem.* **284**, 32483–32492 (2009).

48. J. L. Liang, D. Z. Xiao, X. Y. Liu, Q. X. Lin, Z. X. Shan, J. N. Zhu, S. G. Lin, X. Y. Yu, High glucose induces apoptosis in AC16 human cardiomyocytes via macrophage migration inhibitory factor and c-Jun N-terminal kinase. *Clin. Exp. Pharmacol. Physiol.* **37**, 969–973 (2010).

49. H. Song, Q. Shen, S. Hu, J. Jin, The role of macrophage migration inhibitory factor in promoting benign prostatic hyperplasia epithelial cell growth by modulating COX-2 and P53 signaling. *Biol. Open.* **9**, (2020).

50. L. Schindler, L. Zwissler, C. Krammer, U. Hendgen-Cotta, T. Rassaf, M. B. Hampton, N. Dickerhof, J. Bernhagen, Macrophage migration inhibitory factor inhibits neutrophil apoptosis by inducing cytokine release from mononuclear cells. *J. Leukoc. Biol.* **110**, 893–905 (2021).

51. R. J. Tallarida, Quantitative methods for assessing drug synergism. *Cancer* **2**, 1003–1008 (2011).

52. F. Bai, O. A. Asojo, P. Cirillo, M. Ciustea, M. Ledizet, P. A. Aristoff, L. Leng, R. A. Koski, T. J. Powell, R. Bucala, K. G. Anthony, A novel allosteric inhibitor of macrophage migration inhibitory factor (MIF). *J. Biol. Chem.* **287**, 30653–30663 (2012).

53. P. F. Cirillo, O. A. Asojo, U. Khire, Y. Lee, S. Mootien, P. Hegan, A. G. Sutherland, E. Peterson-Roth, M. Ledizet, R. A. Koski, K. G. Anthony, Inhibition of macrophage migration inhibitory factor by a chimera of two allosteric binders. *ACS Med. Chem. Lett.* **11**, 1843–1847 (2020).

54. J. S. Philo, T. H. Yang, M. LaBarre, Re-examining the oligomerization state of macrophage migration inhibitory factor (MIF) in solution. *Biophys. Chem.* **108**, 77–87 (2004).

55. L. Cao, X. Wang, X. Liu, W. Meng, W. Guo, C. Duan, X. Liang, L. Kang, P. Lv, Q. Lin, R. Zhang, X. Zhang, H. Shen, Tumor necrosis factor α–dependent lung inflammation promotes the progression of lung adenocarcinoma originating from alveolar type II cells by upregulating MIF-CD74. *Lab. Invest.* **103**, 100034 (2023).

56. M. Osaki, M. Oshimura, H. Ito, PI3K-Akt pathway: Its functions and alterations in human cancer. *Apoptosis* **9**, 667–676 (2004).

57. H. Lue, M. Thiele, J. Franz, E. Dahl, S. Speckgens, L. Leng, G. Fingerle-Rowson, R. Bucala, B. Luscher, J. Bernhagen, Macrophage migration inhibitory factor (MIF) promotes cell survival by activation of the Akt pathway and role for CSN5//JAB1 in the control of autocrine MIF activity. *Oncogene* **26**, 5046–5059 (2007).

58. C. Emontzpohl, C. Stoppe, A. Theissen, C. Beckers, U. P. Neumann, G. Lurje, C. Ju, J. Bernhagen, R. H. Tolba, Z. Czigany, The role of macrophage migration inhibitory factor in remote ischemic conditioning induced hepatoprotection in a rodent model of liver transplantation. *Shock* **52**, e124–e134 (2019).

59. J. Khalilpour, S. Roshan-Milani, F. H. Gharalari, A. A. Fard, Macrophage migration inhibitory factor antagonist (p425) ameliorates kidney histopathological and functional changes in diabetic rats. *J. Bras. Nefrol.* **41**, 315–322 (2019).

60. L. Qin, I. Kufareva, L. G. Holden, C. Wang, Y. Zheng, C. Zhao, G. Fenalti, H. Wu, G. W. Han, V. Cherezov, R. Abagyan, R. C. Stevens, T. M. Handel, Crystal structure of the chemokine receptor CXCR4 in complex with a viral chemokine. *Science* **347**, 1117–1122 (2015).

61. C. Maaser, L. Eckmann, G. Paesold, H. S. Kim, M. F. Kagnoff, Ubiquitous production of macrophage migration inhibitory factor by human gastric and intestinal epithelium. *Gastroenterology* **122**, 667–680 (2002).

62. M. Pavlicevic, N. Marmiroli, E. Maestri, Immunomodulatory peptides-A promising source for novel functional food production and drug discovery. *Peptides* **148**, 170696 (2022).

63. F. Clement, S. N. Pramod, Y. P. Venkatesh, Identity of the immunomodulatory proteins from garlic (Allium sativum) with the major garlic lectins or agglutinins. *Int. Immunopharmacol.* **10**, 316–324 (2010).

64. J. Bernhagen, R. A. Mitchell, T. Calandra, W. Voelter, A. Cerami, R. Bucala, Purification, bioactivity, and secondary structure analysis of mouse and human macrophage migration inhibitory factor (MIF). *Biochemistry* **33**, 14144–14155 (1994).

65. W. Kabsch, XDS. *Acta Crystallogr. D Biol. Crystallogr.* **66**, 125–132 (2010).

66. P. R. Evans, G. N. Murshudov, How good are my data and what is the resolution? *Acta Crystallogr. D Biol. Crystallogr.* **69**, 1204–1214 (2013).

67. A. J. McCoy, R. W. Grosse-Kunstleve, P. D. Adams, M. D. Winn, L. C. Storoni, R. J. Read, Phaser crystallographic software. *J. Appl. Crystallogr.* **40**, 658–674 (2007).

68. P. V. Afonine, R. W. Grosse-Kunstleve, N. Echols, J. J. Headd, N. W. Moriarty, M. Mustyakimov, T. C. Terwilliger, A. Urzhumtsev, P. H. Zwart, P. D. Adams, Towards automated crystallographic structure refinement with phenix.refine. *Acta Crystallogr. D Biol. Crystallogr.* **68**, 352–367 (2012).

69. P. Emsley, K. Cowtan, Coot: Model-building tools for molecular graphics. *Acta Crystallogr. D Biol. Crystallogr.* **60**, 2126–2132 (2004).

70. V. B. Chen, W. B. Arendall 3rd, J. J. Headd, D. A. Keedy, R. M. Immormino, G. J. Kapral, L. W. Murray, J. S. Richardson, D. C. Richardson, MolProbity: All-atom structure validation for macromolecular crystallography. *Acta Crystallogr. D Biol. Crystallogr.* **66**, 12–21 (2010).

71. E. F. Pettersen, T. D. Goddard, C. C. Huang, G. S. Couch, D. M. Greenblatt, E. C. Meng, T. E. Ferrin, UCSF Chimera—A visualization system for exploratory research and analysis. *J. Comput. Chem.* **25**, 1605–1612 (2004).

72. G. V. Crichlow, J. B. Lubetsky, L. Leng, R. Bucala, E. J. Lolis, Structural and kinetic analyses of macrophage migration inhibitory factor active site interactions. *Biochemistry* **48**, 132–139 (2009).

73. P. James, J. Halladay, E. A. Craig, Genomic libraries and a host strain designed for highly efficient two-hybrid selection in yeast. *Genetics* **144**, 1425–1436 (1996).

74. L. Garcia-Gerique, M. García, A. Garrido-Garcia, S. Gómez-González, M. Torrebadell, E. Prada, G. Pascual-Pasto, O. Muñoz, S. Perez-Jaume, I. Lemos, N. Salvador, M. Vila-Ubach, A. Doncel-Requena, M. Suñol, A. M. Carcaboso, J. Mora, C. Lavarino, MIF/CXCR4 signaling axis contributes to survival, invasion, and drug resistance of metastatic neuroblastoma cells in the bone marrow microenvironment. *BMC Cancer* **22**, 669 (2022).

Science Signaling

Plant MDL proteins synergize with the cytokine MIF at CXCR2 and CXCR4 receptors in human cells

Lukas Spiller, Ramu Manjula, Franz Leissing, Jerome Basquin, Priscila Bourilhon, Dzmitry Sinitski, Markus Brandhofer, Sophie Levecque, Simona Gerra, Björn Sabelleck, Lin Zhang, Regina Feederle, Andrew Flatley, Adrian Hoffmann, Ralph Panstruga, Jürgen Bernhagen, and Elias Lolis

View the article online
https://www.science.org/doi/10.1126/scisignal.adg2621
Permissions
https://www.science.org/help/reprints-and-permissions

Use of this article is subject to the Terms of service

7. Appendix

This section contains supplementary data files from chapters 5 and 6.

7.1 Supplementary data for Zhang, L. *et al*,2024

<u>Supplementary File</u>

CD74 is a functional MIF receptor on activated CD4^{+} T cells

Lin Zhang[1, *], Iris Woltering[1, *], Mathias Holzner[1], Markus Brandhofer[1], Carl-Christian Schaefer[1], Genta Bushati[1], Simon Ebert[1], Bishan Yang[1], Maximilian Muenchhoff[2,3,4], Johannes C. Hellmuth[4,5], Clemens Scherer[4,6], Christian Wichmann[7], David Effinger[8,9], Max Hübner[8,9], Omar El Bounkari[1], Patrick Scheiermann[8], Jürgen Bernhagen[1,10, #], Adrian Hoffmann[1,8,10, #]

[1]Division of Vascular Biology, Institute for Stroke and Dementia Research (ISD), LMU University Hospital (LMU Klinikum), Ludwig-Maximilians-Universität (LMU) München, Feodor-Lynen-Straße 17, 81377 Munich, Germany; [2]Max-von-Pettenkofer Institute and Gene Center, Virology, National Reference Center for Retroviruses, Ludwig-Maximilians-Universität (LMU) München, Munich, Germany; [3]German Center for Infection Research (DZIF), Partner Site Munich, Munich, Germany; [4]COVID-19 Registry of the LMU Munich (CORKUM), LMU University Hospital, Ludwig-Maximilians-Universität (LMU) München, Munich, Germany; [5]Department of Medicine III, LMU University Hospital, Ludwig-Maximilians-Universität (LMU) München, Munich, Germany; [6]Department of Medicine I, LMU University Hospital, Ludwig-Maximilians-Universität (LMU) München, Munich, Germany; [7]Division of Transfusion Medicine Cell Therapeutics and Haemostaseology, LMU University Hospital, Ludwig-Maximilians-Universität (LMU) München, Munich, Germany; [8]Department of Anaesthesiology, LMU University Hospital, Ludwig-Maximilians-Universität (LMU) München, Marchioninistraße 15, 81377 Munich, Germany; [9]Walter Brendel Centre of Experimental Medicine, Ludwig-Maximilians-Universität (LMU) München, Munich, Germany; [10]German Centre of Cardiovascular Research (DZHK), Partner Site Munich Heart Alliance, Munich, Germany.

*Lin Zhang and Iris Woltering are equally contributing first authors.

#Correspondence:

Professor Jürgen Bernhagen, PhD
Chair of Vascular Biology, Institute for Stroke and Dementia Research (ISD)
LMU University Hospital (LMU Klinikum), Ludwig-Maximilians-Universität (LMU) München
Feodor-Lynen-Straße 17, 81377 Munich, Germany
Tel.: 0049-89-4400-46151
E-Mail: juergen.bernhagen@med.uni-muenchen.de

Adrian Hoffmann, MD
Department of Anaesthesiology, LMU University Hospital
Ludwig-Maximilians-Universität (LMU) München
Marchioninistraße 15, 81377 Munich, Germany
Tel.: 0049-894400-16-81177
E-Mail: adrian.hoffmann@med.uni-muenchen.de

Table of Contents
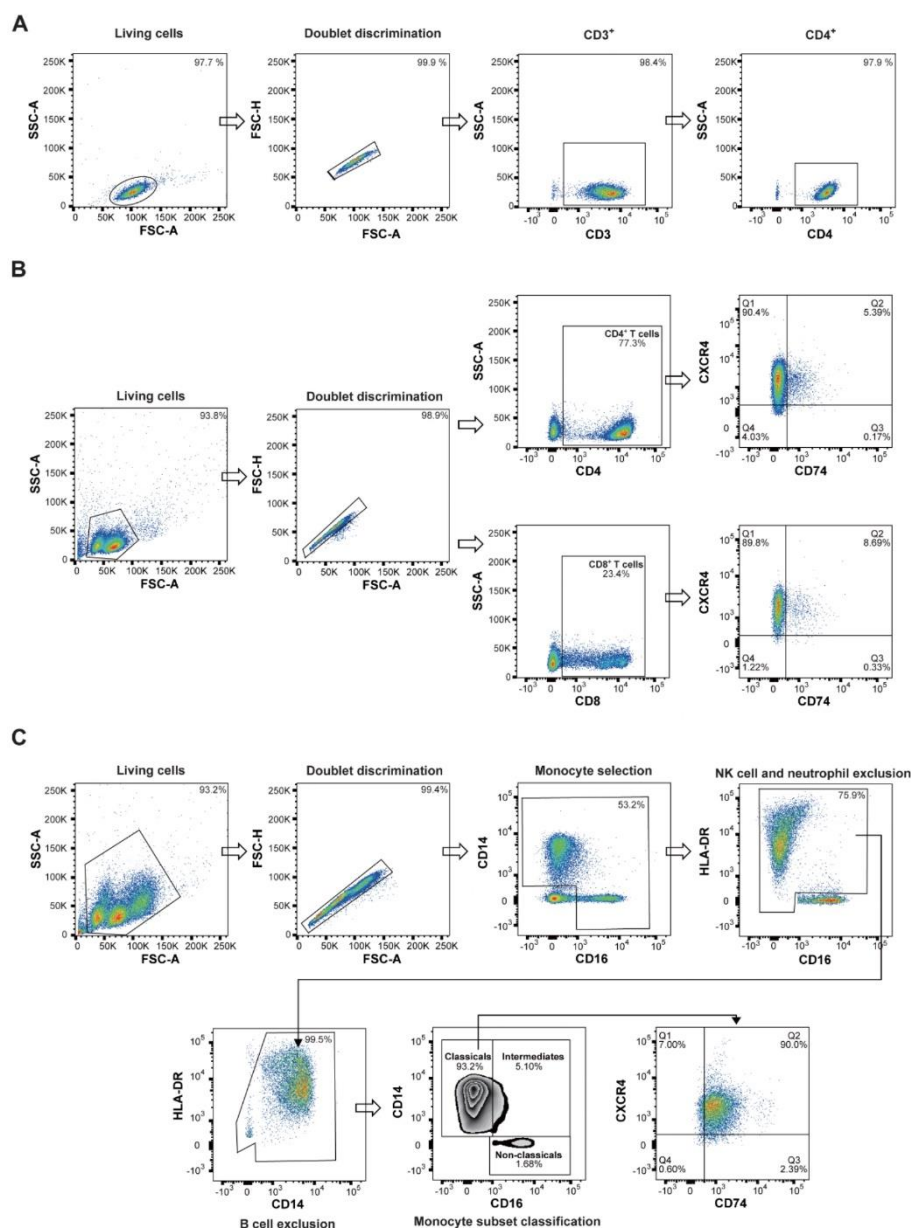
Supplementary Figure 1. Flow cytometry gating strategies. **A** Gating strategy and cell purity after CD4⁺ T-cell isolation. Visualization of a representative flow cytometry gating consisting of exclusion of debris, dead cells and doublets and verification of CD3⁺ CD4⁺ T-cell purity after CD4⁺ T-cell isolation from PBMCs of healthy donors. **B** Gating strategy to characterize T-cell subpopulations from COVID-19 patients after CD3⁺ T-cell isolation. Visualization of a representative flow cytometry gating consisting of exclusion of debris, dead cells and doublets and validation of CXCR4 and CD74 receptor expression after CD3⁺ T-cell isolation from PBMCs. **C** Gating strategy to characterize monocyte subpopulations from COVID-19 patients.

Visualization of a representative flow cytometry gating of monocyte subpopulations according to Marimuthu et al with determination of CD74 and CXCR4 expression on classical and non-classical monocytes in PBMC fraction of CD3⁺-negative cells after CD3⁺-positive selection. Steps include exclusion of debris, dead cells and doublets, and selecting monocyte subsets by CD16 vs. CD14 plot after exclusion of HLA-DR⁻ natural killer (NK) cells and HLA-DR^high CD14^low B cells [1].
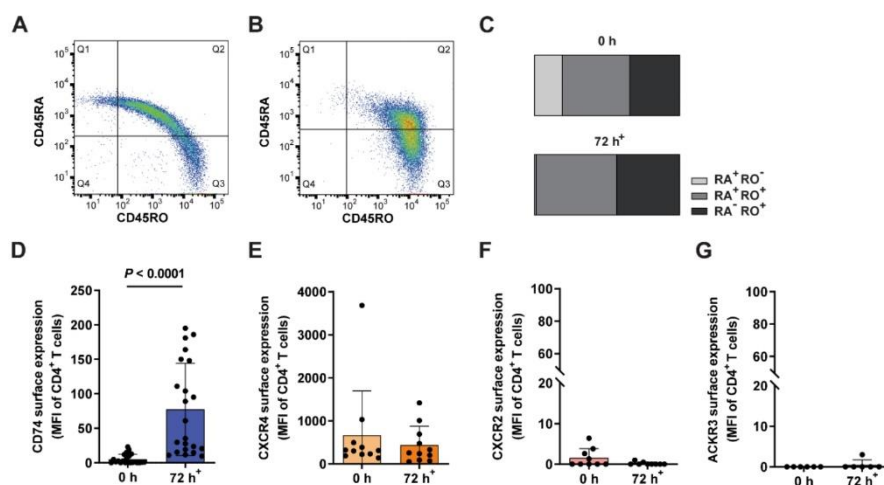
Supplementary Figure 2. Characterization of CD4$^+$ T cells. **A**-**C** Validation of *in vitro* T-cell activation. Surface expression of the naive cell marker CD45RA and CD45RO, as a marker of activated or effector/memory T cells, was measured **A** directly after isolation or **B** after 72 h of *in vitro* activation using anti-CD3$^+$/anti-CD28$^+$ coated beads. **C** Quantification of RA$^+$RO$^-$ (light gray), RA$^+$RO$^+$ (dark gray) and RA$^-$RO$^+$ (black) CD4$^+$ T cells of nine independent experiments (n = 9) is provided as fraction of a whole in the bottom row. **D**-**G** Alternative quantification of MIF receptor profiling on primary human CD4$^+$ T cells upon activation as shown in Fig. 2. Flow cytometry-based cell surface receptor profiling of the four MIF receptors CD74, CXCR4, CXCR2, and ACKR3, as indicated, on purified human CD4$^+$ T cells before (0 h) and after 72 h of *in vitro* T-cell activation. Comparison and quantification of the cell surface median fluorescence intensity (MFI) for each of the four receptors (**E**, n=22; **F**, n=11; **G**, n=9; **H**, n=6). Statistical differences were analyzed by Wilcoxon matched-pairs signed-rank test and indicated by actual *P* values.
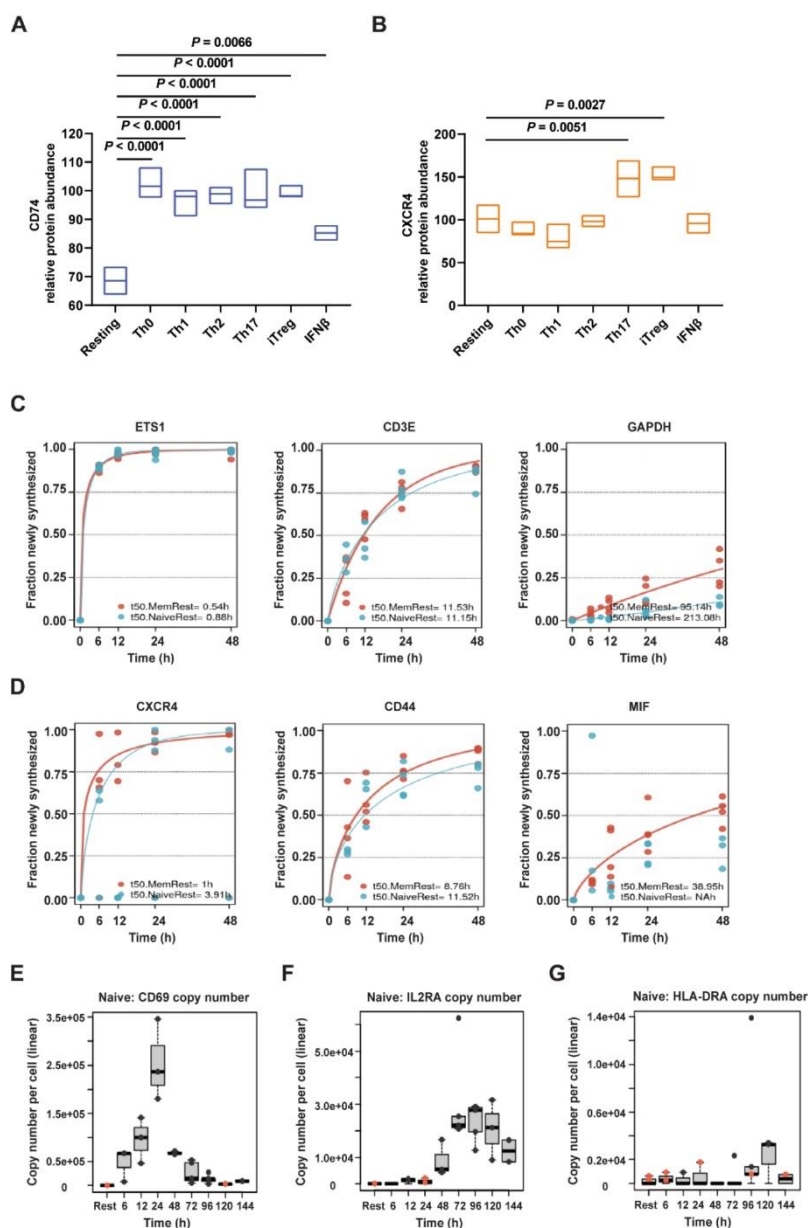
Supplementary Figure 3. Renewal rates and protein dynamics of selected proteins. **A-B** Re-analysis of publicly available proteomic data of memory CD4$^+$ T cells after 5 d of different activation and cytokine polarization conditions (resting: no activation, no added cytokines; Th0: control with no added cytokines; Th1: IL-12, anti-human IL-4 antibody; TH2: IL-4, anti-human IFN-γ antibody, Th17: IL-6, IL-23, IL-1β, TGF-β1, anti-human IL-4 antibody, anti-human IFN-γ antibody; iTreg: TGF-β1, IL-2; IFN-β-stimulated group) according to Cano-Gamez et al. regarding protein abundance of **A** CD74 and **B** CXCR4 [2]. Statistical differences were analyzed by one-way ANOVA with post-hoc multiple comparisons test. **C-D** Comparison of protein

renewal rates in resting naive (blue) vs. resting memory (orange) CD4$^+$ T cells. Fraction of newly synthesized protein calculated from LC-MS/MS analysis of pulsed SILAC of CD4$^+$ T cells. Cells were analyzed after 0 h, 6 h, 12 h, 24 h and 48 h in culture. **C** Exemplary representation of fast (ETS1), intermediate (CD3E) and slow (GAPDH) renewal rate. **D** Renewal rates of CXCR4 (left), CD44 (middle) and MIF (right). **E**-**G** Time course of protein expression per cell upon activation of naive CD4$^+$ T cells. Label-free quantification of proteins via the MaxQuant algorithm without and after 6 h, 12 h, 24 h, 48 h, 72 h, 96 h, 120 h and 144 h of *in vitro* activation. Proteins identified by MS/MS (black) or matching (orange). Estimation of copy number per cell based on protein mass of cell. **E-G** Comparative presentation of established **E** fast (CD69), **F** intermediate (IL2Rα/CD25) and **G** late (HLA-DRA) T-cell activation markers. Data in **C-G** retrieved and re-analyzed from Wolf et al [3].
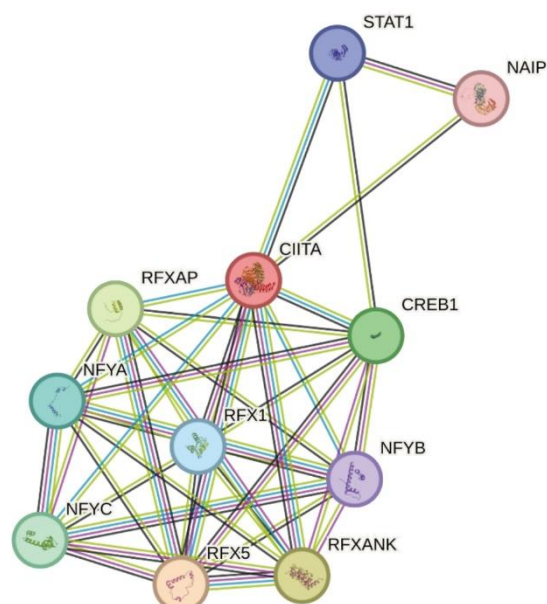
Supplementary Figure 4. CIITA interaction network. Visualization of the ten proteins most strongly associated with functional CIITA interaction as predicted by the STRING database [4].
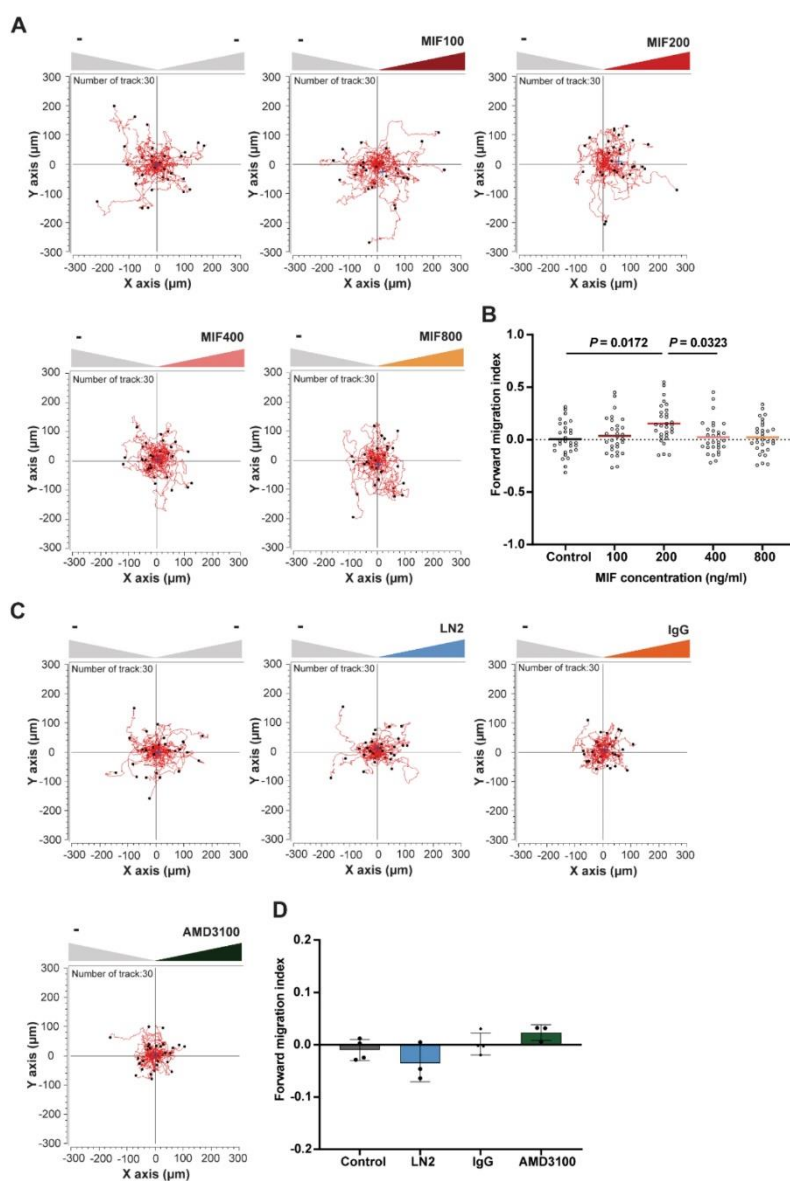
Supplementary Figure 5. Dose curves and controls of the 3D chemotaxis experiments. **A-B** MIF dose-dependently induces chemotaxis of activated CD4+ T cells. Trajectory plots (x, y = 0 at time 0 h) and corresponding quantification of migrated activated CD4+ T cells in a three-dimensional (3D) aqueous collagen-gel matrix towards MIF chemoattractant gradients (MIF concentrations: 100 ng/ml – 800 ng/ml as indicated, -: control medium). Plotted is the calculated forward migration index (FMI, mean ± SD) based on manual tracking of at least 30 individual cells per treatment (n=1). Statistical differences were analyzed by Kruskal-Wallis test with Dunn post-hoc test. **C-D** Inhibitor-only controls of the presented chemotaxis experiment in Fig. 5. Representative trajectory plots and quantification of migrated activated CD4+ T cells in the

presence of a CD74 neutralizing antibody, a corresponding isotype control (IgG) or the CXCR4 receptor inhibitor AMD3100. Cell motility in **A**-**D** was monitored by time-lapse microscopy for 2 h at 37°C, images were obtained every minute using the Leica DMi8 microscope. Single cell tracking was performed of 30 cells per experimental group. The blue crosshair indicates the cell population's center of mass after migration. Quantification of the 3D chemotaxis experiment in **C**-**D** showing no chemotactic effects of the inhibitors alone. Plotted is the calculated forward migration index (FMI, mean ± SD) based on manual tracking of at least 30 individual cells per treatment (n=3-4). Statistical differences were analyzed by Kruskal-Wallis test with Dunn's post-hoc test.
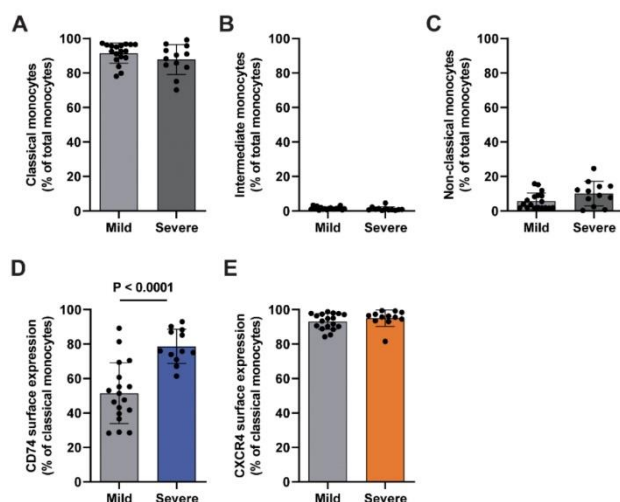
Supplementary Figure 6. Characterization of monocyte subpopulations from COVID-19 patients. **A-C** Comparison of monocyte subpopulations in patients with mild and severe COVID-19 disease. Percentages of monocyte subpopulations in patients with mild (WHO 1-3, 18 patients) vs. severe (WHO ≥ 5, 12 patients) COVID-19 disease determined via flow cytometry as described in Supp. Fig. 1C. **D-E** Upregulation of CD74 surface expression in classical monocytes of critically ill COVID-19 patients. CD74 and CXCR4 surface expression in classical monocyte subpopulation in mild vs. severe COVID-19 disease patients. Bar charts in **A-E** show means ± SD with individual datapoints representing independent patients. Statistical differences were analyzed by unpaired t test for **A**, **C**, **D** and Mann-Whitney U test for **B** and **F** and indicated by actual *P* values.

Supplementary Table 1. List of antibodies used for flow cytometry experiments with additional information.

Antibody	Dilution	Cat Nummber	Company
Anti- hCD14- Pacific Blue	1:100	301828	BioLegend (San Diego, USA)
Anti- hCD16- PerCP	1:100	360720	BioLegend (San Diego, USA)
Anti- hCD3- APC	1:100	300412	BioLegend (San Diego, USA)
Anti- hCD4- PE	1:100	130-113-214	Miltenyi Biotec (Bergisch Gladbach, Germany)
Anti- hCD45 RA- PerCP	1:100	304156	BioLegend (San Diego, USA)
Anti- hCD45 RO- APC	1:100	304210	BioLegend (San Diego, USA)
Anti- hCD74- FITC	1:100	555540	BD Biosciences (Franklin Lakes, USA)
Anti- hCD8- Pacific Blue	1:100	344718	BioLegend (San Diego, USA)
Anti- hCXCR2- FITC	1:100	FAB331F	R&D Systems (Minneapolis, USA)
Anti- hCXCR4- APC	1:100	305510	BioLegend (San Diego, USA)
Anti- hCXCR4- APC/Cy 7	1:100	306528	BioLegend (San Diego, USA)
Anti- hCXCR7- PE	1:100	FAB4227P	R&D Systems (Minneapolis, USA)
Anti- hHLA-DR- PE	1:100	307606	BioLegend (San Diego, USA)
Anti- hHLA-DR- PerCP	1:100	307628	BioLegend (San Diego, USA)

Supplementary Table 2. List of potential transcription factor binding sites upstream from the *CD74* gene locus. Potential transcription factor binding sites at a maximum distance of 500 bp from the *CD74* gene locus were identified in the Gene Transcription Regulation Database (GTRD) [5]. See accompanying excel file for detailed list.

Supplementary Table 3. List of predicted transcription factors involved in CD74 gene expression. Potential transcription factors involved in the transcriptional regulation of CD74 identified using the PathwayNet database [6]. Shown are genes with a relationship confidence of more than 0.1. Yellow marked are CIITA-associated transcription factors that were identified in Supp. Fig. 4. Orange marked are genes with no binding site within 500 bp of the CD74 gene as identified in Supp. Table 2. See accompanying excel file.

Supplementary Table 2

Chromosome	From	To	Type	ID	TF Count
chr5	150399783	150399869	IKZF3	ms.IKZF3_HUMAN.43303.v1	1
chr5	150409943	150410017	IKZF3	ms.IKZF3_HUMAN.43304.v1	
chr5	150409909	150409961	CEBPB	ms.CEBPB_HUMAN.991826.v1	2
chr5	150410634	150410692	CEBPB	ms.CEBPB_HUMAN.991827.v1	
chr5	150411383	150411473	CEBPB	ms.CEBPB_HUMAN.991828.v1	
chr5	150412020	150412048	CEBPB	ms.CEBPB_HUMAN.991829.v1	
chr5	150412196	150412286	CEBPB	ms.CEBPB_HUMAN.991830.v1	
chr5	150412372	150412405	CEBPB	ms.CEBPB_HUMAN.991831.v1	
chr5	150412675	150412735	CEBPB	ms.CEBPB_HUMAN.991832.v1	
chr5	150412945	150413005	CEBPB	ms.CEBPB_HUMAN.991833.v1	
chr5	150400929	150401011	SMAD3	ms.SMAD3_HUMAN.205993.v1	3
chr5	150410326	150410426	MSC	ms.MUSC_HUMAN.38879.v1	4
chr5	150412400	150412458	STAG2	ms.STAG2_HUMAN.64359.v1	5
chr5	150410264	150410340	ME1	ms.MAOX_HUMAN.216167.v1	6
chr5	150410605	150410689	ME1	ms.MAOX_HUMAN.216168.v1	
chr5	150410912	150410955	ME1	ms.MAOX_HUMAN.216169.v1	
chr5	150411264	150411348	ME1	ms.MAOX_HUMAN.216170.v1	
chr5	150407963	150408061	FOSB	ms.FOSB_HUMAN.27181.v1	7
chr5	150409779	150409833	PRDM10	ms.PRD10_HUMAN.35972.v1	8
chr5	150410155	150410209	PRDM10	ms.PRD10_HUMAN.35973.v1	
chr5	150410568	150410616	PRDM10	ms.PRD10_HUMAN.35974.v1	
chr5	150400629	150400729	RAD21	ms.RAD21_HUMAN.833725.v1	9
chr5	150401680	150401780	RAD21	ms.RAD21_HUMAN.833726.v1	
chr5	150403064	150403164	RAD21	ms.RAD21_HUMAN.833727.v1	
chr5	150407401	150407501	RAD21	ms.RAD21_HUMAN.833728.v1	
chr5	150408369	150408469	RAD21	ms.RAD21_HUMAN.833729.v1	
chr5	150409772	150409872	RAD21	ms.RAD21_HUMAN.833730.v1	
chr5	150410590	150410653	RAD21	ms.RAD21_HUMAN.833731.v1	
chr5	150412372	150412416	RAD21	ms.RAD21_HUMAN.833732.v1	
chr5	150412448	150412532	RAD21	ms.RAD21_HUMAN.833733.v1	
chr5	150412563	150412647	RAD21	ms.RAD21_HUMAN.833734.v1	
chr5	150412634	150412734	RAD21	ms.RAD21_HUMAN.833735.v1	
chr5	150412859	150412959	RAD21	ms.RAD21_HUMAN.833736.v1	
chr5	150399965	150400055	ZEB1	ms.ZEB1_HUMAN.146750.v1	10
chr5	150402737	150402810	ZEB1	ms.ZEB1_HUMAN.146751.v1	
chr5	150405488	150405513	ZEB1	ms.ZEB1_HUMAN.146752.v1	
chr5	150405873	150405957	ZEB1	ms.ZEB1_HUMAN.146753.v1	
chr5	150406225	150406259	ZEB1	ms.ZEB1_HUMAN.146754.v1	
chr5	150408653	150408743	ZEB1	ms.ZEB1_HUMAN.146755.v1	
chr5	150409122	150409206	ZEB1	ms.ZEB1_HUMAN.146756.v1	
chr5	150409290	150409380	ZEB1	ms.ZEB1_HUMAN.146757.v1	
chr5	150412883	150412968	ZEB1	ms.ZEB1_HUMAN.146758.v1	
chr5	150408810	150408898	TRIM22	ms.TRI22_HUMAN.29192.v1	11
chr5	150400879	150400973	PEX2	ms.PEX2_HUMAN.114565.v1	12
chr5	150401771	150401865	PEX2	ms.PEX2_HUMAN.114566.v1	
chr5	150401936	150402030	PEX2	ms.PEX2_HUMAN.114567.v1	
chr5	150402617	150402711	PEX2	ms.PEX2_HUMAN.114568.v1	
chr5	150404631	150404725	PEX2	ms.PEX2_HUMAN.114569.v1	

chr5	150412457	150412515	PEX2	ms.PEX2_HUMAN.114570.v1	
chr5	150399741	150399827	SIRT1	ms.SIR1_HUMAN.107590.v1	13
chr5	150402179	150402265	SIRT1	ms.SIR1_HUMAN.107591.v1	
chr5	150402290	150402376	SIRT1	ms.SIR1_HUMAN.107592.v1	
chr5	150407011	150407097	SIRT1	ms.SIR1_HUMAN.107593.v1	
chr5	150408292	150408360	SIRT1	ms.SIR1_HUMAN.107594.v1	
chr5	150410155	150410219	SIRT1	ms.SIR1_HUMAN.107595.v1	
chr5	150400567	150400603	AGO2	ms.AGO2_HUMAN.86756.v1	14
chr5	150400894	150400914	AGO2	ms.AGO2_HUMAN.86757.v1	
chr5	150401607	150401645	AGO2	ms.AGO2_HUMAN.86758.v1	
chr5	150402534	150402554	AGO2	ms.AGO2_HUMAN.86759.v1	
chr5	150403149	150403169	AGO2	ms.AGO2_HUMAN.86760.v1	
chr5	150404695	150404715	AGO2	ms.AGO2_HUMAN.86761.v1	
chr5	150406212	150406250	AGO2	ms.AGO2_HUMAN.86762.v1	
chr5	150406991	150407011	AGO2	ms.AGO2_HUMAN.86763.v1	
chr5	150407616	150407640	AGO2	ms.AGO2_HUMAN.86764.v1	
chr5	150412674	150412697	AGO2	ms.AGO2_HUMAN.86765.v1	
chr5	150402016	150402080	TBX5	ms.TBX5_HUMAN.38757.v1	15
chr5	150412626	150412666	TEAD3	ms.TEAD3_HUMAN.25817.v1	16
chr5	150400251	150400317	PBX3	ms.PBX3_HUMAN.106534.v1	17
chr5	150401462	150401528	PBX3	ms.PBX3_HUMAN.106535.v1	
chr5	150402237	150402297	PBX3	ms.PBX3_HUMAN.106536.v1	
chr5	150404760	150404852	PBX3	ms.PBX3_HUMAN.106537.v1	
chr5	150405523	150405589	PBX3	ms.PBX3_HUMAN.106538.v1	
chr5	150408209	150408275	PBX3	ms.PBX3_HUMAN.106539.v1	
chr5	150408354	150408414	PBX3	ms.PBX3_HUMAN.106540.v1	
chr5	150409964	150410001	PBX3	ms.PBX3_HUMAN.106541.v1	
chr5	150410176	150410236	PBX3	ms.PBX3_HUMAN.106542.v1	
chr5	150410809	150410875	PBX3	ms.PBX3_HUMAN.106543.v1	
chr5	150411744	150411804	PBX3	ms.PBX3_HUMAN.106544.v1	
chr5	150412688	150412732	PBX3	ms.PBX3_HUMAN.106545.v1	
chr5	150410012	150410052	PBX1	ms.PBX1_HUMAN.43238.v1	18
chr5	150410561	150410609	PBX1	ms.PBX1_HUMAN.43239.v1	
chr5	150412853	150412901	PBX1	ms.PBX1_HUMAN.43240.v1	
chr5	150402521	150402593	DNMT1	ms.DNMT1_HUMAN.1567.v1	19
chr5	150409883	150409935	MBD1	ms.MBD1_HUMAN.5577.v1	20
chr5	150409933	150409964	RFX5	ms.RFX5_HUMAN.23734.v1	21
chr5	150410312	150410374	RFX5	ms.RFX5_HUMAN.23735.v1	
chr5	150410406	150410494	RFX5	ms.RFX5_HUMAN.23736.v1	
chr5	150410727	150410753	RFX5	ms.RFX5_HUMAN.23737.v1	
chr5	150411085	150411173	RFX5	ms.RFX5_HUMAN.23738.v1	
chr5	150411470	150411497	RFX5	ms.RFX5_HUMAN.23739.v1	
chr5	150411711	150411799	RFX5	ms.RFX5_HUMAN.23740.v1	
chr5	150412965	150412994	RFX5	ms.RFX5_HUMAN.23741.v1	
chr5	150406178	150406252	MNT	ms.MNT_HUMAN.57695.v1	22
chr5	150410603	150410659	NFIA	ms.NFIA_HUMAN.35058.v1	23
chr5	150411410	150411474	MAFK	ms.MAFK_HUMAN.98627.v1	24
chr5	150407526	150407606	NFKB1	ms.NFKB1_HUMAN.413716.v1	25
chr5	150412609	150412700	NFKB1	ms.NFKB1_HUMAN.413717.v1	
chr5	150412719	150412799	NFKB1	ms.NFKB1_HUMAN.413718.v1	

chr5	150412838	150412951	NFKB1	ms.NFKB1_HUMAN.413719.v1	
chr5	150401765	150401865	DTL	ms.DTL_HUMAN.138368.v1	26
chr5	150402238	150402338	DTL	ms.DTL_HUMAN.138369.v1	
chr5	150402806	150402906	DTL	ms.DTL_HUMAN.138370.v1	
chr5	150407060	150407160	DTL	ms.DTL_HUMAN.138371.v1	
chr5	150410191	150410291	DTL	ms.DTL_HUMAN.138372.v1	
chr5	150400002	150400078	STAT2	ms.STAT2_HUMAN.147962.v1	27
chr5	150400145	150400233	STAT2	ms.STAT2_HUMAN.147963.v1	
chr5	150401341	150401417	STAT2	ms.STAT2_HUMAN.147964.v1	
chr5	150412671	150412723	STAT2	ms.STAT2_HUMAN.147965.v1	
chr5	150409922	150410002	NFYC	ms.NFYC_HUMAN.14855.v1	28
chr5	150410695	150410775	NFYC	ms.NFYC_HUMAN.14856.v1	
chr5	150412924	150413004	NFYC	ms.NFYC_HUMAN.14857.v1	
chr5	150406301	150406363	CBFB	ms.PEBB_HUMAN.9276.v1	29
chr5	150410000	150410062	CBFB	ms.PEBB_HUMAN.9277.v1	
chr5	150412678	150412756	CBFB	ms.PEBB_HUMAN.9278.v1	
chr5	150399565	150399633	RUNX2	ms.RUNX2_HUMAN.145223.v1	30
chr5	150412857	150412925	RUNX2	ms.RUNX2_HUMAN.145224.v1	
chr5	150404572	150404618	AGO1	ms.AGO1_HUMAN.87684.v1	31
chr5	150406819	150406879	AGO1	ms.AGO1_HUMAN.87685.v1	
chr5	150406875	150406957	AGO1	ms.AGO1_HUMAN.87686.v1	
chr5	150400688	150400790	LEO1	ms.LEO1_HUMAN.59120.v1	32
chr5	150401882	150401974	LEO1	ms.LEO1_HUMAN.59121.v1	
chr5	150402641	150402733	LEO1	ms.LEO1_HUMAN.59122.v1	
chr5	150407103	150407206	LEO1	ms.LEO1_HUMAN.59123.v1	
chr5	150400190	150400272	TBX21	ms.TBX21_HUMAN.76406.v1	33
chr5	150412879	150412911	TBX21	ms.TBX21_HUMAN.76407.v1	
chr5	150403150	150403238	RING1	ms.RING1_HUMAN.286620.v1	34
chr5	150411600	150411688	RING1	ms.RING1_HUMAN.286621.v1	
chr5	150412604	150412674	RING1	ms.RING1_HUMAN.286622.v1	
chr5	150412687	150412775	RING1	ms.RING1_HUMAN.286623.v1	
chr5	150399545	150399653	BRD4	ms.BRD4_HUMAN.2097140.v1	35
chr5	150399717	150399821	BRD4	ms.BRD4_HUMAN.2097141.v1	
chr5	150399987	150400019	BRD4	ms.BRD4_HUMAN.2097142.v1	
chr5	150401782	150401890	BRD4	ms.BRD4_HUMAN.2097143.v1	
chr5	150401930	150402038	BRD4	ms.BRD4_HUMAN.2097144.v1	
chr5	150402068	150402176	BRD4	ms.BRD4_HUMAN.2097145.v1	
chr5	150402940	150403044	BRD4	ms.BRD4_HUMAN.2097146.v1	
chr5	150403014	150403129	BRD4	ms.BRD4_HUMAN.2097147.v1	
chr5	150403133	150403237	BRD4	ms.BRD4_HUMAN.2097148.v1	
chr5	150403388	150403492	BRD4	ms.BRD4_HUMAN.2097149.v1	
chr5	150404208	150404312	BRD4	ms.BRD4_HUMAN.2097150.v1	
chr5	150404665	150404769	BRD4	ms.BRD4_HUMAN.2097151.v1	
chr5	150405111	150405157	BRD4	ms.BRD4_HUMAN.2097152.v1	
chr5	150406568	150406672	BRD4	ms.BRD4_HUMAN.2097153.v1	
chr5	150406747	150406851	BRD4	ms.BRD4_HUMAN.2097154.v1	
chr5	150407236	150407268	BRD4	ms.BRD4_HUMAN.2097155.v1	
chr5	150407341	150407380	BRD4	ms.BRD4_HUMAN.2097156.v1	
chr5	150408465	150408512	BRD4	ms.BRD4_HUMAN.2097157.v1	
chr5	150409888	150409957	BRD4	ms.BRD4_HUMAN.2097158.v1	

chr5	150409963	150410071 BRD4	ms.BRD4_HUMAN.2097159.v1	
chr5	150410097	150410197 BRD4	ms.BRD4_HUMAN.2097160.v1	
chr5	150410195	150410251 BRD4	ms.BRD4_HUMAN.2097161.v1	
chr5	150410319	150410406 BRD4	ms.BRD4_HUMAN.2097162.v1	
chr5	150410569	150410589 BRD4	ms.BRD4_HUMAN.2097163.v1	
chr5	150410609	150410705 BRD4	ms.BRD4_HUMAN.2097164.v1	
chr5	150410855	150410942 BRD4	ms.BRD4_HUMAN.2097165.v1	
chr5	150410970	150411045 BRD4	ms.BRD4_HUMAN.2097166.v1	
chr5	150411333	150411437 BRD4	ms.BRD4_HUMAN.2097167.v1	
chr5	150411395	150411499 BRD4	ms.BRD4_HUMAN.2097168.v1	
chr5	150411607	150411713 BRD4	ms.BRD4_HUMAN.2097169.v1	
chr5	150412162	150412232 BRD4	ms.BRD4_HUMAN.2097170.v1	
chr5	150412367	150412415 BRD4	ms.BRD4_HUMAN.2097171.v1	
chr5	150412467	150412498 BRD4	ms.BRD4_HUMAN.2097172.v1	
chr5	150412633	150412730 BRD4	ms.BRD4_HUMAN.2097173.v1	
chr5	150412877	150412925 BRD4	ms.BRD4_HUMAN.2097174.v1	
chr5	150413079	150413143 BRD4	ms.BRD4_HUMAN.2097175.v1	
chr5	150399690	150399744 BHLHE40	ms.BHE40_HUMAN.88925.v1	36
chr5	150407881	150407951 BHLHE40	ms.BHE40_HUMAN.88926.v1	
chr5	150409920	150409998 BHLHE40	ms.BHE40_HUMAN.88927.v1	
chr5	150410718	150410755 BHLHE40	ms.BHE40_HUMAN.88928.v1	
chr5	150411377	150411447 BHLHE40	ms.BHE40_HUMAN.88929.v1	
chr5	150412536	150412610 BHLHE40	ms.BHE40_HUMAN.88930.v1	
chr5	150412957	150413011 BHLHE40	ms.BHE40_HUMAN.88931.v1	
chr5	150409942	150409960 CREM	ms.CREM_HUMAN.58783.v1	37
chr5	150410730	150410762 CREM	ms.CREM_HUMAN.58784.v1	
chr5	150411478	150411502 CREM	ms.CREM_HUMAN.58785.v1	
chr5	150412965	150412991 CREM	ms.CREM_HUMAN.58786.v1	
chr5	150402649	150402743 HDAC2	ms.HDAC2_HUMAN.389330.v1	38
chr5	150403081	150403169 HDAC2	ms.HDAC2_HUMAN.389331.v1	
chr5	150410388	150410482 HDAC2	ms.HDAC2_HUMAN.389332.v1	
chr5	150410679	150410783 HDAC2	ms.HDAC2_HUMAN.389333.v1	
chr5	150412620	150412708 HDAC2	ms.HDAC2_HUMAN.389334.v1	
chr5	150412786	150412874 HDAC2	ms.HDAC2_HUMAN.389335.v1	
chr5	150410616	150410680 EHF	ms.EHF_HUMAN.27914.v1	39
chr5	150400903	150400981 ZBTB7A	ms.ZBT7A_HUMAN.236127.v1	40
chr5	150403154	150403232 ZBTB7A	ms.ZBT7A_HUMAN.236128.v1	
chr5	150406920	150406998 ZBTB7A	ms.ZBT7A_HUMAN.236129.v1	
chr5	150410054	150410140 ZBTB7A	ms.ZBT7A_HUMAN.236130.v1	
chr5	150410806	150410884 ZBTB7A	ms.ZBT7A_HUMAN.236131.v1	
chr5	150410858	150410944 ZBTB7A	ms.ZBT7A_HUMAN.236132.v1	
chr5	150412749	150412835 ZBTB7A	ms.ZBT7A_HUMAN.236133.v1	
chr5	150412542	150412649 UBTF	ms.UBF1_HUMAN.32333.v1	41
chr5	150412655	150412713 SOX13	ms.SOX13_HUMAN.47512.v1	42
chr5	150412630	150412714 TP53BP1	ms.TP53B_HUMAN.32306.v1	43
chr5	150401816	150401894 ZFHX3	ms.ZFHX3_HUMAN.9145.v1	44
chr5	150402138	150402216 ZFHX3	ms.ZFHX3_HUMAN.9146.v1	
chr5	150404682	150404760 ZFHX3	ms.ZFHX3_HUMAN.9147.v1	
chr5	150405095	150405173 ZFHX3	ms.ZFHX3_HUMAN.9148.v1	
chr5	150406880	150406958 ZFHX3	ms.ZFHX3_HUMAN.9149.v1	

chr5	150407161	150407239	ZFHX3	ms.ZFHX3_HUMAN.9150.v1	
chr5	150407239	150407317	ZFHX3	ms.ZFHX3_HUMAN.9151.v1	
chr5	150401285	150401349	MEIS2	ms.MEIS2_HUMAN.24513.v1	45
chr5	150400895	150400941	ZBTB6	ms.ZBTB6_HUMAN.18115.v1	46
chr5	150403850	150403914	ZBTB6	ms.ZBTB6_HUMAN.18116.v1	
chr5	150410299	150410345	ZBTB6	ms.ZBTB6_HUMAN.18117.v1	
chr5	150412789	150412883	ETS2	ms.ETS2_HUMAN.4864.v1	47
chr5	150409914	150409988	BRCA1	ms.BRCA1_HUMAN.46969.v1	48
chr5	150410691	150410765	BRCA1	ms.BRCA1_HUMAN.46970.v1	
chr5	150402633	150402723	TFAP2C	ms.AP2C_HUMAN.240960.v1	49
chr5	150406859	150406888	TFAP2C	ms.AP2C_HUMAN.240961.v1	
chr5	150412642	150412700	IKZF2	ms.IKZF2_HUMAN.16072.v1	50
chr5	150410502	150410588	CHD4	ms.CHD4_HUMAN.63648.v1	51
chr5	150404312	150404390	CHD8	ms.CHD8_HUMAN.93641.v1	52
chr5	150412641	150412719	CHD8	ms.CHD8_HUMAN.93642.v1	
chr5	150412395	150412445	GABPA	ms.GABPA_HUMAN.134508.v1	53
chr5	150412617	150412705	GABPA	ms.GABPA_HUMAN.134509.v1	
chr5	150412821	150412889	GABPA	ms.GABPA_HUMAN.134510.v1	
chr5	150413099	150413197	GABPA	ms.GABPA_HUMAN.134511.v1	
chr5	150412603	150412681	GABPB1	ms.GABP1_HUMAN.29848.v1	54
chr5	150399930	150400022	FOXA2	ms.FOXA2_HUMAN.1397586.v1	55
chr5	150401958	150402017	FOXA2	ms.FOXA2_HUMAN.1397587.v1	
chr5	150409835	150409927	FOXA2	ms.FOXA2_HUMAN.1397588.v1	
chr5	150409952	150410054	FOXA2	ms.FOXA2_HUMAN.1397589.v1	
chr5	150410073	150410144	FOXA2	ms.FOXA2_HUMAN.1397590.v1	
chr5	150410173	150410265	FOXA2	ms.FOXA2_HUMAN.1397591.v1	
chr5	150410421	150410523	FOXA2	ms.FOXA2_HUMAN.1397592.v1	
chr5	150410659	150410753	FOXA2	ms.FOXA2_HUMAN.1397593.v1	
chr5	150412219	150412311	FOXA2	ms.FOXA2_HUMAN.1397594.v1	
chr5	150412581	150412683	FOXA2	ms.FOXA2_HUMAN.1397595.v1	
chr5	150412657	150412749	FOXA2	ms.FOXA2_HUMAN.1397596.v1	
chr5	150412900	150412967	FOXA2	ms.FOXA2_HUMAN.1397597.v1	
chr5	150412995	150413097	FOXA2	ms.FOXA2_HUMAN.1397598.v1	
chr5	150399595	150399689	NR3C1	ms.GCR_HUMAN.656067.v1	56
chr5	150402099	150402197	NR3C1	ms.GCR_HUMAN.656068.v1	
chr5	150410544	150410638	NR3C1	ms.GCR_HUMAN.656069.v1	
chr5	150410857	150410955	NR3C1	ms.GCR_HUMAN.656070.v1	
chr5	150412723	150412821	NR3C1	ms.GCR_HUMAN.656071.v1	
chr5	150407467	150407537	KDM5B	ms.KDM5B_HUMAN.152181.v1	57
chr5	150412601	150412657	KDM5B	ms.KDM5B_HUMAN.152182.v1	
chr5	150412696	150412776	TEAD1	ms.TEAD1_HUMAN.193277.v1	58
chr5	150401787	150401826	BRD9	ms.BRD9_HUMAN.220449.v1	59
chr5	150402100	150402143	BRD9	ms.BRD9_HUMAN.220450.v1	
chr5	150402570	150402674	BRD9	ms.BRD9_HUMAN.220451.v1	
chr5	150405127	150405159	BRD9	ms.BRD9_HUMAN.220452.v1	
chr5	150407232	150407308	BRD9	ms.BRD9_HUMAN.220453.v1	
chr5	150410566	150410670	BRD9	ms.BRD9_HUMAN.220454.v1	
chr5	150412694	150412798	BRD9	ms.BRD9_HUMAN.220455.v1	
chr5	150412855	150412943	BRD9	ms.BRD9_HUMAN.220456.v1	
chr5	150413351	150413433	RCOR1	ms.RCOR1_HUMAN.99450.v1	60

chr5	150402347	150402431	ZBED1	ms.ZBED1_HUMAN.4221.v1	61
chr5	150407581	150407665	ZBED1	ms.ZBED1_HUMAN.4222.v1	
chr5	150412656	150412722	ZBED1	ms.ZBED1_HUMAN.4223.v1	
chr5	150406957	150407057	LARP7	ms.LARP7_HUMAN.38095.v1	62
chr5	150407981	150408067	FOSL2	ms.FOSL2_HUMAN.161813.v1	63
chr5	150412603	150412689	FOSL2	ms.FOSL2_HUMAN.161814.v1	
chr5	150400442	150400522	TSC22D4	ms.T22D4_HUMAN.11474.v1	64
chr5	150402676	150402756	TSC22D4	ms.T22D4_HUMAN.11475.v1	
chr5	150405225	150405305	TSC22D4	ms.T22D4_HUMAN.11476.v1	
chr5	150406872	150406952	TSC22D4	ms.T22D4_HUMAN.11477.v1	
chr5	150407040	150407120	TSC22D4	ms.T22D4_HUMAN.11478.v1	
chr5	150408440	150408520	TSC22D4	ms.T22D4_HUMAN.11479.v1	
chr5	150405379	150405429	TCF4	ms.ITF2_HUMAN.187726.v1	65
chr5	150412692	150412733	TCF4	ms.ITF2_HUMAN.187727.v1	
chr5	150407284	150407378	SUZ12	ms.SUZ12_HUMAN.409285.v1	66
chr5	150408570	150408664	SUZ12	ms.SUZ12_HUMAN.409286.v1	
chr5	150412725	150412823	SUZ12	ms.SUZ12_HUMAN.409287.v1	
chr5	150409899	150410021	NFYB	ms.NFYB_HUMAN.7550.v1	67
chr5	150410670	150410792	NFYB	ms.NFYB_HUMAN.7551.v1	
chr5	150412849	150412971	NFYB	ms.NFYB_HUMAN.7552.v1	
chr5	150409916	150409974	CIITA	ms.C2TA_HUMAN.1518.v1	68
chr5	150410710	150410776	CIITA	ms.C2TA_HUMAN.1519.v1	
chr5	150411454	150411518	CIITA	ms.C2TA_HUMAN.1520.v1	
chr5	150412967	150413019	CIITA	ms.C2TA_HUMAN.1521.v1	
chr5	150399895	150399987	ZBTB33	ms.KAISO_HUMAN.96406.v1	69
chr5	150400042	150400134	ZBTB33	ms.KAISO_HUMAN.96407.v1	
chr5	150400535	150400615	ZBTB33	ms.KAISO_HUMAN.96408.v1	
chr5	150400723	150400807	ZBTB33	ms.KAISO_HUMAN.96409.v1	
chr5	150401042	150401134	ZBTB33	ms.KAISO_HUMAN.96410.v1	
chr5	150401820	150401912	ZBTB33	ms.KAISO_HUMAN.96411.v1	
chr5	150402313	150402341	ZBTB33	ms.KAISO_HUMAN.96412.v1	
chr5	150403312	150403404	ZBTB33	ms.KAISO_HUMAN.96413.v1	
chr5	150404263	150404355	ZBTB33	ms.KAISO_HUMAN.96414.v1	
chr5	150405029	150405113	ZBTB33	ms.KAISO_HUMAN.96415.v1	
chr5	150407160	150407252	ZBTB33	ms.KAISO_HUMAN.96416.v1	
chr5	150407598	150407690	ZBTB33	ms.KAISO_HUMAN.96417.v1	
chr5	150408255	150408367	ZBTB33	ms.KAISO_HUMAN.96418.v1	
chr5	150408643	150408735	ZBTB33	ms.KAISO_HUMAN.96419.v1	
chr5	150409890	150409982	ZBTB33	ms.KAISO_HUMAN.96420.v1	
chr5	150410157	150410241	ZBTB33	ms.KAISO_HUMAN.96421.v1	
chr5	150410230	150410278	ZBTB33	ms.KAISO_HUMAN.96422.v1	
chr5	150410883	150410975	ZBTB33	ms.KAISO_HUMAN.96423.v1	
chr5	150412664	150412736	ZBTB33	ms.KAISO_HUMAN.96424.v1	
chr5	150406883	150406957	ARNTL	ms.BMAL1_HUMAN.62768.v1	70
chr5	150402738	150402782	NSD2	ms.NSD2_HUMAN.14300.v1	71
chr5	150409905	150409949	NSD2	ms.NSD2_HUMAN.14301.v1	
chr5	150411388	150411432	NSD2	ms.NSD2_HUMAN.14302.v1	
chr5	150412229	150412273	NSD2	ms.NSD2_HUMAN.14303.v1	
chr5	150399648	150399746	EP300	ms.EP300_HUMAN.1195129.v1	72
chr5	150399984	150400084	EP300	ms.EP300_HUMAN.1195130.v1	

chr5	150400108	150400208	EP300	ms.EP300_HUMAN.1195131.v1	
chr5	150401243	150401341	EP300	ms.EP300_HUMAN.1195132.v1	
chr5	150401659	150401759	EP300	ms.EP300_HUMAN.1195133.v1	
chr5	150401785	150401885	EP300	ms.EP300_HUMAN.1195134.v1	
chr5	150402662	150402762	EP300	ms.EP300_HUMAN.1195135.v1	
chr5	150403112	150403212	EP300	ms.EP300_HUMAN.1195136.v1	
chr5	150409882	150409980	EP300	ms.EP300_HUMAN.1195137.v1	
chr5	150409969	150410069	EP300	ms.EP300_HUMAN.1195138.v1	
chr5	150410162	150410262	EP300	ms.EP300_HUMAN.1195139.v1	
chr5	150410360	150410408	EP300	ms.EP300_HUMAN.1195140.v1	
chr5	150410500	150410598	EP300	ms.EP300_HUMAN.1195141.v1	
chr5	150410644	150410744	EP300	ms.EP300_HUMAN.1195142.v1	
chr5	150411032	150411132	EP300	ms.EP300_HUMAN.1195143.v1	
chr5	150411379	150411479	EP300	ms.EP300_HUMAN.1195144.v1	
chr5	150412286	150412386	EP300	ms.EP300_HUMAN.1195145.v1	
chr5	150412434	150412517	EP300	ms.EP300_HUMAN.1195146.v1	
chr5	150412593	150412703	EP300	ms.EP300_HUMAN.1195147.v1	
chr5	150412682	150412758	EP300	ms.EP300_HUMAN.1195148.v1	
chr5	150412862	150412911	EP300	ms.EP300_HUMAN.1195149.v1	
chr5	150413129	150413200	EP300	ms.EP300_HUMAN.1195150.v1	
chr5	150413192	150413290	EP300	ms.EP300_HUMAN.1195151.v1	
chr5	150406865	150406937	RBFOX2	ms.RFOX2_HUMAN.69845.v1	73
chr5	150412638	150412710	RBFOX2	ms.RFOX2_HUMAN.69846.v1	
chr5	150411341	150411413	NFKB2	ms.NFKB2_HUMAN.80500.v1	74
chr5	150412832	150412932	NFKB2	ms.NFKB2_HUMAN.80501.v1	
chr5	150409548	150409636	SOX8	ms.SOX8_HUMAN.219397.v1	75
chr5	150412841	150412935	SETDB1	ms.SETB1_HUMAN.78503.v1	76
chr5	150400210	150400302	SFPQ	ms.SFPQ_HUMAN.229998.v1	77
chr5	150401147	150401167	BRD2	ms.BRD2_HUMAN.317422.v1	78
chr5	150407622	150407728	BRD2	ms.BRD2_HUMAN.317423.v1	
chr5	150408264	150408310	BRD2	ms.BRD2_HUMAN.317424.v1	
chr5	150410086	150410192	BRD2	ms.BRD2_HUMAN.317425.v1	
chr5	150410323	150410429	BRD2	ms.BRD2_HUMAN.317426.v1	
chr5	150410839	150410945	BRD2	ms.BRD2_HUMAN.317427.v1	
chr5	150412551	150412612	BRD2	ms.BRD2_HUMAN.317428.v1	
chr5	150412653	150412759	BRD2	ms.BRD2_HUMAN.317429.v1	
chr5	150412927	150412973	BRD2	ms.BRD2_HUMAN.317430.v1	
chr5	150413135	150413241	BRD2	ms.BRD2_HUMAN.317431.v1	
chr5	150401213	150401311	E2F8	ms.E2F8_HUMAN.227540.v1	79
chr5	150403311	150403405	E2F8	ms.E2F8_HUMAN.227541.v1	
chr5	150406749	150406843	E2F8	ms.E2F8_HUMAN.227542.v1	
chr5	150410258	150410332	E2F8	ms.E2F8_HUMAN.227543.v1	
chr5	150410583	150410613	E2F8	ms.E2F8_HUMAN.227544.v1	
chr5	150411718	150411816	E2F8	ms.E2F8_HUMAN.227545.v1	
chr5	150412418	150412516	E2F8	ms.E2F8_HUMAN.227546.v1	
chr5	150412581	150412655	E2F8	ms.E2F8_HUMAN.227547.v1	
chr5	150412737	150412820	E2F8	ms.E2F8_HUMAN.227548.v1	
chr5	150412796	150412884	E2F8	ms.E2F8_HUMAN.227549.v1	
chr5	150404577	150404641	CRTC2	ms.CRTC2_HUMAN.46415.v1	80
chr5	150412405	150412491	CTCFL	ms.CTCFL_HUMAN.83954.v1	81

chr5	150404243	150404347 SMARCA4	ms.SMCA4_HUMAN.853083.v1	82
chr5	150407299	150407374 SMARCA4	ms.SMCA4_HUMAN.853084.v1	
chr5	150409856	150409915 SMARCA4	ms.SMCA4_HUMAN.853085.v1	
chr5	150410379	150410483 SMARCA4	ms.SMCA4_HUMAN.853086.v1	
chr5	150410572	150410630 SMARCA4	ms.SMCA4_HUMAN.853087.v1	
chr5	150412354	150412390 SMARCA4	ms.SMCA4_HUMAN.853088.v1	
chr5	150412525	150412573 SMARCA4	ms.SMCA4_HUMAN.853089.v1	
chr5	150412836	150412904 SMARCA4	ms.SMCA4_HUMAN.853090.v1	
chr5	150412891	150413013 SMARCA4	ms.SMCA4_HUMAN.853091.v1	
chr5	150413077	150413181 SMARCA4	ms.SMCA4_HUMAN.853092.v1	
chr5	150399886	150399970 BMI1	ms.BMI1_HUMAN.439018.v1	83
chr5	150401041	150401127 BMI1	ms.BMI1_HUMAN.439019.v1	
chr5	150405505	150405589 BMI1	ms.BMI1_HUMAN.439020.v1	
chr5	150411609	150411693 BMI1	ms.BMI1_HUMAN.439021.v1	
chr5	150408759	150408785 ZNF263	ms.ZN263_HUMAN.156292.v1	84
chr5	150400327	150400409 CBFA2T3	ms.MTG16_HUMAN.67842.v1	85
chr5	150401151	150401215 CBFA2T3	ms.MTG16_HUMAN.67843.v1	
chr5	150406058	150406122 CBFA2T3	ms.MTG16_HUMAN.67844.v1	
chr5	150404625	150404711 PTEN	ms.PTEN_HUMAN.46889.v1	86
chr5	150410156	150410248 RBBP5	ms.RBBP5_HUMAN.94723.v1	87
chr5	150410774	150410866 RBBP5	ms.RBBP5_HUMAN.94724.v1	
chr5	150412785	150412877 RBBP5	ms.RBBP5_HUMAN.94725.v1	
chr5	150410194	150410282 BRD3	ms.BRD3_HUMAN.126303.v1	88
chr5	150410886	150410974 BRD3	ms.BRD3_HUMAN.126304.v1	
chr5	150412560	150412594 BRD3	ms.BRD3_HUMAN.126305.v1	
chr5	150399654	150399744 YY1	ms.TYY1_HUMAN.336583.v1	89
chr5	150399801	150399891 YY1	ms.TYY1_HUMAN.336584.v1	
chr5	150400252	150400342 YY1	ms.TYY1_HUMAN.336585.v1	
chr5	150400678	150400768 YY1	ms.TYY1_HUMAN.336586.v1	
chr5	150400921	150401021 YY1	ms.TYY1_HUMAN.336587.v1	
chr5	150401456	150401556 YY1	ms.TYY1_HUMAN.336588.v1	
chr5	150401948	150401975 YY1	ms.TYY1_HUMAN.336589.v1	
chr5	150402375	150402427 YY1	ms.TYY1_HUMAN.336590.v1	
chr5	150403166	150403256 YY1	ms.TYY1_HUMAN.336591.v1	
chr5	150403388	150403488 YY1	ms.TYY1_HUMAN.336592.v1	
chr5	150405070	150405160 YY1	ms.TYY1_HUMAN.336593.v1	
chr5	150405261	150405328 YY1	ms.TYY1_HUMAN.336594.v1	
chr5	150406302	150406392 YY1	ms.TYY1_HUMAN.336595.v1	
chr5	150406853	150406933 YY1	ms.TYY1_HUMAN.336596.v1	
chr5	150407231	150407288 YY1	ms.TYY1_HUMAN.336597.v1	
chr5	150407384	150407474 YY1	ms.TYY1_HUMAN.336598.v1	
chr5	150407479	150407569 YY1	ms.TYY1_HUMAN.336599.v1	
chr5	150408256	150408356 YY1	ms.TYY1_HUMAN.336600.v1	
chr5	150410054	150410161 YY1	ms.TYY1_HUMAN.336601.v1	
chr5	150412241	150412331 YY1	ms.TYY1_HUMAN.336602.v1	
chr5	150412682	150412708 YY1	ms.TYY1_HUMAN.336603.v1	
chr5	150413124	150413194 YY1	ms.TYY1_HUMAN.336604.v1	
chr5	150410601	150410693 CDK7	ms.CDK7_HUMAN.35271.v1	90
chr5	150412777	150412865 CDK7	ms.CDK7_HUMAN.35272.v1	
chr5	150400603	150400691 JUN	ms.JUN_HUMAN.521173.v1	91

chr5	150401348	150401436 JUN	ms.JUN_HUMAN.521174.v1	
chr5	150401829	150401909 JUN	ms.JUN_HUMAN.521175.v1	
chr5	150402564	150402665 JUN	ms.JUN_HUMAN.521176.v1	
chr5	150402659	150402747 JUN	ms.JUN_HUMAN.521177.v1	
chr5	150403155	150403243 JUN	ms.JUN_HUMAN.521178.v1	
chr5	150404941	150405029 JUN	ms.JUN_HUMAN.521179.v1	
chr5	150405495	150405583 JUN	ms.JUN_HUMAN.521180.v1	
chr5	150405718	150405806 JUN	ms.JUN_HUMAN.521181.v1	
chr5	150407929	150408034 JUN	ms.JUN_HUMAN.521182.v1	
chr5	150409903	150409983 JUN	ms.JUN_HUMAN.521183.v1	
chr5	150409977	150410057 JUN	ms.JUN_HUMAN.521184.v1	
chr5	150410127	150410191 JUN	ms.JUN_HUMAN.521185.v1	
chr5	150410478	150410535 JUN	ms.JUN_HUMAN.521186.v1	
chr5	150411502	150411608 JUN	ms.JUN_HUMAN.521187.v1	
chr5	150412206	150412286 JUN	ms.JUN_HUMAN.521188.v1	
chr5	150412631	150412695 JUN	ms.JUN_HUMAN.521189.v1	
chr5	150412725	150412777 JUN	ms.JUN_HUMAN.521190.v1	
chr5	150412926	150412960 JUN	ms.JUN_HUMAN.521191.v1	
chr5	150409888	150409934 CENPA	ms.CENPA_HUMAN.109500.v1	92
chr5	150410544	150410636 CENPA	ms.CENPA_HUMAN.109501.v1	
chr5	150399659	150399757 PPARG	ms.PPARG_HUMAN.700328.v1	93
chr5	150400754	150400852 PPARG	ms.PPARG_HUMAN.700329.v1	
chr5	150400988	150401086 PPARG	ms.PPARG_HUMAN.700330.v1	
chr5	150403109	150403207 PPARG	ms.PPARG_HUMAN.700331.v1	
chr5	150404939	150405037 PPARG	ms.PPARG_HUMAN.700332.v1	
chr5	150405458	150405556 PPARG	ms.PPARG_HUMAN.700333.v1	
chr5	150406591	150406689 PPARG	ms.PPARG_HUMAN.700334.v1	
chr5	150407237	150407335 PPARG	ms.PPARG_HUMAN.700335.v1	
chr5	150407800	150407898 PPARG	ms.PPARG_HUMAN.700336.v1	
chr5	150408478	150408576 PPARG	ms.PPARG_HUMAN.700337.v1	
chr5	150409020	150409118 PPARG	ms.PPARG_HUMAN.700338.v1	
chr5	150410065	150410163 PPARG	ms.PPARG_HUMAN.700339.v1	
chr5	150410214	150410312 PPARG	ms.PPARG_HUMAN.700340.v1	
chr5	150410573	150410672 PPARG	ms.PPARG_HUMAN.700341.v1	
chr5	150412287	150412385 PPARG	ms.PPARG_HUMAN.700342.v1	
chr5	150412359	150412463 PPARG	ms.PPARG_HUMAN.700343.v1	
chr5	150412672	150412754 PPARG	ms.PPARG_HUMAN.700344.v1	
chr5	150412814	150412864 PPARG	ms.PPARG_HUMAN.700345.v1	
chr5	150413104	150413202 PPARG	ms.PPARG_HUMAN.700346.v1	
chr5	150413212	150413310 PPARG	ms.PPARG_HUMAN.700347.v1	
chr5	150408009	150408107 SMARCC1	ms.SMRC1_HUMAN.486549.v1	94
chr5	150410229	150410300 SMARCC1	ms.SMRC1_HUMAN.486550.v1	
chr5	150410478	150410576 SMARCC1	ms.SMRC1_HUMAN.486551.v1	
chr5	150410549	150410647 SMARCC1	ms.SMRC1_HUMAN.486552.v1	
chr5	150412650	150412748 SMARCC1	ms.SMRC1_HUMAN.486553.v1	
chr5	150400906	150400985 ZNF366	ms.ZN366_HUMAN.46326.v1	95
chr5	150401847	150401941 ZNF366	ms.ZN366_HUMAN.46327.v1	
chr5	150404201	150404307 ZNF366	ms.ZN366_HUMAN.46328.v1	
chr5	150405445	150405539 ZNF366	ms.ZN366_HUMAN.46329.v1	
chr5	150407180	150407292 ZNF366	ms.ZN366_HUMAN.46330.v1	

chr5	150410047	150410100	ZNF366	ms.ZN366_HUMAN.46331.v1	
chr5	150410719	150410747	ZNF366	ms.ZN366_HUMAN.46332.v1	
chr5	150411409	150411501	ZNF366	ms.ZN366_HUMAN.46333.v1	
chr5	150411510	150411577	ZNF366	ms.ZN366_HUMAN.46334.v1	
chr5	150412425	150412494	ZNF366	ms.ZN366_HUMAN.46335.v1	
chr5	150412518	150412637	ZNF366	ms.ZN366_HUMAN.46336.v1	
chr5	150412600	150412706	ZNF366	ms.ZN366_HUMAN.46337.v1	
chr5	150403738	150403806	ZNF770	ms.ZN770_HUMAN.61568.v1	96
chr5	150410760	150410834	ZNF770	ms.ZN770_HUMAN.61569.v1	
chr5	150409912	150410010	KMT2B	ms.KMT2B_HUMAN.199160.v1	97
chr5	150410692	150410790	KMT2B	ms.KMT2B_HUMAN.199161.v1	
chr5	150412539	150412637	KMT2B	ms.KMT2B_HUMAN.199162.v1	
chr5	150412731	150412829	KMT2B	ms.KMT2B_HUMAN.199163.v1	
chr5	150412855	150412953	KMT2B	ms.KMT2B_HUMAN.199164.v1	
chr5	150409927	150409963	XRCC5	ms.XRCC5_HUMAN.152756.v1	98
chr5	150412760	150412784	XRCC5	ms.XRCC5_HUMAN.152757.v1	
chr5	150406936	150407024	HSF1	ms.HSF1_HUMAN.76733.v1	99
chr5	150412676	150412772	GATA6	ms.GATA6_HUMAN.194627.v1	100
chr5	150412643	150412737	MEIS3P1	ms.ME3L1_HUMAN.51233.v1	1
chr5	150402537	150402560	GTF2F1	ms.T2FA_HUMAN.58190.v1	2
chr5	150409886	150409972	GTF2F1	ms.T2FA_HUMAN.58191.v1	
chr5	150410700	150410786	GTF2F1	ms.T2FA_HUMAN.58192.v1	
chr5	150412820	150412872	GTF2F1	ms.T2FA_HUMAN.58193.v1	
chr5	150407943	150408005	MITF	ms.MITF_HUMAN.194620.v1	3
chr5	150412127	150412209	MITF	ms.MITF_HUMAN.194621.v1	
chr5	150412456	150412538	MITF	ms.MITF_HUMAN.194622.v1	
chr5	150401138	150401232	NEUROG2	ms.NGN2_HUMAN.80160.v1	4
chr5	150411874	150411974	UPF1	ms.RENT1_HUMAN.52600.v1	5
chr5	150401045	150401119	BCL11A	ms.BC11A_HUMAN.53499.v1	6
chr5	150406434	150406508	BCL11A	ms.BC11A_HUMAN.53500.v1	
chr5	150406998	150407060	BCL11A	ms.BC11A_HUMAN.53501.v1	
chr5	150408511	150408589	BCL11A	ms.BC11A_HUMAN.53502.v1	
chr5	150409859	150409933	BCL11A	ms.BC11A_HUMAN.53503.v1	
chr5	150410852	150410926	BCL11A	ms.BC11A_HUMAN.53504.v1	
chr5	150411511	150411613	BCL11A	ms.BC11A_HUMAN.53505.v1	
chr5	150412681	150412741	BCL11A	ms.BC11A_HUMAN.53506.v1	
chr5	150413092	150413166	BCL11A	ms.BC11A_HUMAN.53507.v1	
chr5	150406812	150406921	SP1	ms.SP1_HUMAN.284658.v1	7
chr5	150407181	150407281	SP1	ms.SP1_HUMAN.284659.v1	
chr5	150409939	150409987	SP1	ms.SP1_HUMAN.284660.v1	
chr5	150410083	150410169	SP1	ms.SP1_HUMAN.284661.v1	
chr5	150410159	150410245	SP1	ms.SP1_HUMAN.284662.v1	
chr5	150410713	150410746	SP1	ms.SP1_HUMAN.284663.v1	
chr5	150412508	150412594	SP1	ms.SP1_HUMAN.284664.v1	
chr5	150412618	150412731	SP1	ms.SP1_HUMAN.284665.v1	
chr5	150412777	150412863	SP1	ms.SP1_HUMAN.284666.v1	
chr5	150412920	150412984	SP1	ms.SP1_HUMAN.284667.v1	
chr5	150400718	150400798	MYNN	ms.MYNN_HUMAN.15306.v1	8
chr5	150408580	150408686	REST	ms.REST_HUMAN.203736.v1	9
chr5	150410230	150410336	REST	ms.REST_HUMAN.203737.v1	

chr5	150411811	150411917	REST	ms.REST_HUMAN.203738.v1	
chr5	150412555	150412651	REST	ms.REST_HUMAN.203739.v1	
chr5	150412692	150412740	REST	ms.REST_HUMAN.203740.v1	
chr5	150412771	150412877	REST	ms.REST_HUMAN.203741.v1	
chr5	150406158	150406242	NCOA1	ms.NCOA1_HUMAN.164190.v1	10
chr5	150409885	150409949	NCOA1	ms.NCOA1_HUMAN.164191.v1	
chr5	150400373	150400475	IRF4	ms.IRF4_HUMAN.145223.v1	11
chr5	150400634	150400726	IRF4	ms.IRF4_HUMAN.145224.v1	
chr5	150400995	150401087	IRF4	ms.IRF4_HUMAN.145225.v1	
chr5	150401295	150401387	IRF4	ms.IRF4_HUMAN.145226.v1	
chr5	150401846	150401948	IRF4	ms.IRF4_HUMAN.145227.v1	
chr5	150405322	150405424	IRF4	ms.IRF4_HUMAN.145228.v1	
chr5	150406732	150406834	IRF4	ms.IRF4_HUMAN.145229.v1	
chr5	150409868	150409960	IRF4	ms.IRF4_HUMAN.145230.v1	
chr5	150409969	150410061	IRF4	ms.IRF4_HUMAN.145231.v1	
chr5	150410183	150410275	IRF4	ms.IRF4_HUMAN.145232.v1	
chr5	150411436	150411540	IRF4	ms.IRF4_HUMAN.145233.v1	
chr5	150411764	150411858	IRF4	ms.IRF4_HUMAN.145234.v1	
chr5	150412416	150412518	IRF4	ms.IRF4_HUMAN.145235.v1	
chr5	150412790	150412854	IRF4	ms.IRF4_HUMAN.145236.v1	
chr5	150412885	150412969	IRF4	ms.IRF4_HUMAN.145237.v1	
chr5	150402585	150402697	INO80	ms.INO80_HUMAN.81912.v1	12
chr5	150407173	150407261	NCOR1	ms.NCOR1_HUMAN.167926.v1	13
chr5	150410523	150410581	NCOR1	ms.NCOR1_HUMAN.167927.v1	
chr5	150403942	150404028	RARG	ms.RARG_HUMAN.22622.v1	14
chr5	150404320	150404406	RARG	ms.RARG_HUMAN.22623.v1	
chr5	150399817	150399907	REL	ms.REL_HUMAN.31534.v1	15
chr5	150400549	150400639	REL	ms.REL_HUMAN.31535.v1	
chr5	150403788	150403878	REL	ms.REL_HUMAN.31536.v1	
chr5	150406431	150406521	REL	ms.REL_HUMAN.31537.v1	
chr5	150407263	150407353	REL	ms.REL_HUMAN.31538.v1	
chr5	150408272	150408362	REL	ms.REL_HUMAN.31539.v1	
chr5	150410296	150410386	REL	ms.REL_HUMAN.31540.v1	
chr5	150411746	150411836	REL	ms.REL_HUMAN.31541.v1	
chr5	150412645	150412745	REL	ms.REL_HUMAN.31542.v1	
chr5	150412765	150412865	REL	ms.REL_HUMAN.31543.v1	
chr5	150406830	150406908	SP4	ms.SP4_HUMAN.28592.v1	16
chr5	150412560	150412644	SMAD2	ms.SMAD2_HUMAN.139287.v1	17
chr5	150401910	150401970	NR1H3	ms.NR1H3_HUMAN.38319.v1	18
chr5	150402159	150402219	NR1H3	ms.NR1H3_HUMAN.38320.v1	
chr5	150407224	150407300	NR1H3	ms.NR1H3_HUMAN.38321.v1	
chr5	150410653	150410741	HES1	ms.HES1_HUMAN.71659.v1	19
chr5	150410503	150410591	SMAD1	ms.SMAD1_HUMAN.123423.v1	20
chr5	150412649	150412723	SMAD1	ms.SMAD1_HUMAN.123424.v1	
chr5	150412614	150412716	PHF8	ms.PHF8_HUMAN.57277.v1	21
chr5	150400611	150400699	CDKN1B	ms.CDN1B_HUMAN.77751.v1	22
chr5	150410113	150410203	CDKN1B	ms.CDN1B_HUMAN.77752.v1	
chr5	150412626	150412689	CDKN1B	ms.CDN1B_HUMAN.77753.v1	
chr5	150412762	150412832	CDKN1B	ms.CDN1B_HUMAN.77754.v1	
chr5	150411584	150411676	CHD7	ms.CHD7_HUMAN.160552.v1	23

chr5	150410062	150410136 TEAD4	ms.TEAD4_HUMAN.239204.v1	24
chr5	150410169	150410207 TEAD4	ms.TEAD4_HUMAN.239205.v1	
chr5	150410774	150410864 TEAD4	ms.TEAD4_HUMAN.239206.v1	
chr5	150410866	150410904 TEAD4	ms.TEAD4_HUMAN.239207.v1	
chr5	150412574	150412664 TEAD4	ms.TEAD4_HUMAN.239208.v1	
chr5	150412670	150412744 TEAD4	ms.TEAD4_HUMAN.239209.v1	
chr5	150412830	150412872 TEAD4	ms.TEAD4_HUMAN.239210.v1	
chr5	150406179	150406263 USP7	ms.UBP7_HUMAN.31278.v1	25
chr5	150412433	150412537 WDR5	ms.WDR5_HUMAN.41217.v1	26
chr5	150410148	150410280 ZFHX2	ms.ZFHX2_HUMAN.31202.v1	27
chr5	150400544	150400608 TARDBP	ms.TADBP_HUMAN.45603.v1	28
chr5	150412685	150412755 TARDBP	ms.TADBP_HUMAN.45604.v1	
chr5	150400195	150400271 AHR	ms.AHR_HUMAN.129113.v1	29
chr5	150412656	150412756 AHR	ms.AHR_HUMAN.129114.v1	
chr5	150412897	150412979 AHR	ms.AHR_HUMAN.129115.v1	
chr5	150409860	150409940 NRF1	ms.NRF1_HUMAN.46771.v1	30
chr5	150412561	150412585 NRF1	ms.NRF1_HUMAN.46772.v1	
chr5	150412648	150412759 NR2F6	ms.NR2F6_HUMAN.62227.v1	31
chr5	150399813	150399835 NR2F1	ms.COT1_HUMAN.71271.v1	
chr5	150403625	150403711 NR2F1	ms.COT1_HUMAN.71272.v1	
chr5	150412629	150412681 NR2F1	ms.COT1_HUMAN.71273.v1	
chr5	150412673	150412755 NR2F1	ms.COT1_HUMAN.71274.v1	
chr5	150403242	150403312 PADI2	ms.PADI2_HUMAN.219372.v1	32
chr5	150410616	150410716 HOXA6	ms.HXA6_HUMAN.8338.v1	33
chr5	150409918	150409990 HIF1A	ms.HIF1A_HUMAN.289740.v1	34
chr5	150410753	150410825 HIF1A	ms.HIF1A_HUMAN.289741.v1	
chr5	150402627	150402675 RBM39	ms.RBM39_HUMAN.63603.v1	35
chr5	150412730	150412794 RBM39	ms.RBM39_HUMAN.63604.v1	
chr5	150403293	150403357 SCRT1	ms.SCRT1_HUMAN.70016.v1	36
chr5	150410383	150410483 ZNF35	ms.ZNF35_HUMAN.44147.v1	37
chr5	150400524	150400553 FLI1	ms.FLI1_HUMAN.522532.v1	38
chr5	150400827	150400927 FLI1	ms.FLI1_HUMAN.522533.v1	
chr5	150400895	150400985 FLI1	ms.FLI1_HUMAN.522534.v1	
chr5	150401269	150401297 FLI1	ms.FLI1_HUMAN.522535.v1	
chr5	150402191	150402291 FLI1	ms.FLI1_HUMAN.522536.v1	
chr5	150402538	150402638 FLI1	ms.FLI1_HUMAN.522537.v1	
chr5	150410086	150410116 FLI1	ms.FLI1_HUMAN.522538.v1	
chr5	150410550	150410659 FLI1	ms.FLI1_HUMAN.522539.v1	
chr5	150411457	150411557 FLI1	ms.FLI1_HUMAN.522540.v1	
chr5	150412321	150412421 FLI1	ms.FLI1_HUMAN.522541.v1	
chr5	150412480	150412580 FLI1	ms.FLI1_HUMAN.522542.v1	
chr5	150412621	150412711 FLI1	ms.FLI1_HUMAN.522543.v1	
chr5	150412836	150412908 FLI1	ms.FLI1_HUMAN.522544.v1	
chr5	150404129	150404213 HNF1B	ms.HNF1B_HUMAN.49637.v1	39
chr5	150409922	150410006 HNF1B	ms.HNF1B_HUMAN.49638.v1	
chr5	150410693	150410777 HNF1B	ms.HNF1B_HUMAN.49639.v1	
chr5	150412924	150413008 HNF1B	ms.HNF1B_HUMAN.49640.v1	
chr5	150410392	150410484 CBX3	ms.CBX3_HUMAN.165650.v1	40
chr5	150406168	150406260 LMNA	ms.LMNA_HUMAN.345943.v1	41
chr5	150412925	150412995 INTS13	ms.INT13_HUMAN.48102.v1	42

chr5	150410290	150410338 ZFP64	ms.ZF64A_HUMAN.80626.v1	43
chr5	150410582	150410621 ZFP64	ms.ZF64A_HUMAN.80627.v1	
chr5	150412551	150412647 ZFP64	ms.ZF64A_HUMAN.80628.v1	
chr5	150412650	150412757 ZFP64	ms.ZF64A_HUMAN.80629.v1	
chr5	150406904	150406924 PCBP1	ms.PCBP1_HUMAN.39972.v1	44
chr5	150404127	150404221 ESRRA	ms.ERR1_HUMAN.57991.v1	45
chr5	150404249	150404307 ESRRA	ms.ERR1_HUMAN.57992.v1	
chr5	150400770	150400854 VDR	ms.VDR_HUMAN.130279.v1	46
chr5	150401060	150401134 VDR	ms.VDR_HUMAN.130280.v1	
chr5	150401164	150401248 VDR	ms.VDR_HUMAN.130281.v1	
chr5	150401696	150401790 VDR	ms.VDR_HUMAN.130282.v1	
chr5	150401895	150401979 VDR	ms.VDR_HUMAN.130283.v1	
chr5	150402323	150402417 VDR	ms.VDR_HUMAN.130284.v1	
chr5	150403455	150403549 VDR	ms.VDR_HUMAN.130285.v1	
chr5	150404111	150404205 VDR	ms.VDR_HUMAN.130286.v1	
chr5	150404203	150404287 VDR	ms.VDR_HUMAN.130287.v1	
chr5	150405591	150405685 VDR	ms.VDR_HUMAN.130288.v1	
chr5	150406162	150406256 VDR	ms.VDR_HUMAN.130289.v1	
chr5	150406347	150406441 VDR	ms.VDR_HUMAN.130290.v1	
chr5	150406834	150406918 VDR	ms.VDR_HUMAN.130291.v1	
chr5	150408151	150408209 VDR	ms.VDR_HUMAN.130292.v1	
chr5	150410566	150410660 VDR	ms.VDR_HUMAN.130293.v1	
chr5	150411576	150411670 VDR	ms.VDR_HUMAN.130294.v1	
chr5	150411739	150411833 VDR	ms.VDR_HUMAN.130295.v1	
chr5	150412544	150412628 VDR	ms.VDR_HUMAN.130296.v1	
chr5	150412690	150412764 VDR	ms.VDR_HUMAN.130297.v1	
chr5	150412786	150412890 VDR	ms.VDR_HUMAN.130298.v1	
chr5	150401731	150401831 RUNX1	ms.X5C3Z9_HUMAN.56425.v1	47
chr5	150412606	150412706 SLC30A9	ms.ZNT9_HUMAN.17947.v1	48
chr5	150401098	150401182 ELF3	ms.ELF3_HUMAN.142900.v1	49
chr5	150410072	150410150 ELF3	ms.ELF3_HUMAN.142901.v1	
chr5	150410136	150410214 ELF3	ms.ELF3_HUMAN.142902.v1	
chr5	150410580	150410641 ELF3	ms.ELF3_HUMAN.142903.v1	
chr5	150413165	150413199 ELF3	ms.ELF3_HUMAN.142904.v1	
chr5	150410452	150410567 EP400	ms.EP400_HUMAN.51377.v1	50
chr5	150410556	150410619 EP400	ms.EP400_HUMAN.51378.v1	
chr5	150411411	150411497 KDM5A	ms.KDM5A_HUMAN.39728.v1	51
chr5	150409886	150409978 SRC	ms.SRC_HUMAN.25684.v1	52
chr5	150410613	150410705 SRC	ms.SRC_HUMAN.25685.v1	
chr5	150410693	150410785 SRC	ms.SRC_HUMAN.25686.v1	
chr5	150412642	150412734 ARID4B	ms.ARI4B_HUMAN.41500.v1	53
chr5	150412643	150412761 RUNX3	ms.RUNX3_HUMAN.49536.v1	54
chr5	150412829	150412947 RUNX3	ms.RUNX3_HUMAN.49537.v1	
chr5	150400777	150400863 EED	ms.EED_HUMAN.128434.v1	55
chr5	150410224	150410310 EED	ms.EED_HUMAN.128435.v1	
chr5	150412694	150412774 EED	ms.EED_HUMAN.128436.v1	
chr5	150410092	150410172 GRHL2	ms.GRHL2_HUMAN.104121.v1	56
chr5	150407231	150407328 ZNF341	ms.ZN341_HUMAN.50528.v1	57
chr5	150410690	150410766 ZNF341	ms.ZN341_HUMAN.50529.v1	
chr5	150412868	150412944 ZNF341	ms.ZN341_HUMAN.50530.v1	

chr5	150399762	150399826	EBF1	ms.COE1_HUMAN.99201.v1	58
chr5	150406865	150406947	EBF1	ms.COE1_HUMAN.99202.v1	
chr5	150408382	150408464	EBF1	ms.COE1_HUMAN.99203.v1	
chr5	150409913	150409979	EBF1	ms.COE1_HUMAN.99204.v1	
chr5	150410531	150410563	EBF1	ms.COE1_HUMAN.99205.v1	
chr5	150411305	150411406	EBF1	ms.COE1_HUMAN.99206.v1	
chr5	150412772	150412836	EBF1	ms.COE1_HUMAN.99207.v1	
chr5	150407221	150407321	EGR3	ms.EGR3_HUMAN.118363.v1	59
chr5	150407916	150408042	EGR3	ms.EGR3_HUMAN.118364.v1	
chr5	150408258	150408384	EGR3	ms.EGR3_HUMAN.118365.v1	
chr5	150410161	150410287	EGR3	ms.EGR3_HUMAN.118366.v1	
chr5	150412692	150412776	CBX1	ms.CBX1_HUMAN.19827.v1	60
chr5	150399835	150399929	RXRA	ms.RXRA_HUMAN.238622.v1	61
chr5	150400573	150400667	RXRA	ms.RXRA_HUMAN.238623.v1	
chr5	150401343	150401415	RXRA	ms.RXRA_HUMAN.238624.v1	
chr5	150401816	150401910	RXRA	ms.RXRA_HUMAN.238625.v1	
chr5	150402121	150402215	RXRA	ms.RXRA_HUMAN.238626.v1	
chr5	150406819	150406913	RXRA	ms.RXRA_HUMAN.238627.v1	
chr5	150407163	150407257	RXRA	ms.RXRA_HUMAN.238628.v1	
chr5	150407568	150407662	RXRA	ms.RXRA_HUMAN.238629.v1	
chr5	150408417	150408511	RXRA	ms.RXRA_HUMAN.238630.v1	
chr5	150408625	150408713	RXRA	ms.RXRA_HUMAN.238631.v1	
chr5	150409899	150409987	RXRA	ms.RXRA_HUMAN.238632.v1	
chr5	150411286	150411374	RXRA	ms.RXRA_HUMAN.238633.v1	
chr5	150412549	150412643	RXRA	ms.RXRA_HUMAN.238634.v1	
chr5	150412794	150412866	RXRA	ms.RXRA_HUMAN.238635.v1	
chr5	150412652	150412710	PML	ms.PML_HUMAN.14584.v1	62
chr5	150413141	150413199	PML	ms.PML_HUMAN.14585.v1	
chr5	150413032	150413124	GATAD2B	ms.P66B_HUMAN.178921.v1	63
chr5	150400360	150400454	RUNX1	ms.RUNX1_HUMAN.823083.v1	64
chr5	150401086	150401180	RUNX1	ms.RUNX1_HUMAN.823084.v1	
chr5	150401246	150401258	RUNX1	ms.RUNX1_HUMAN.823085.v1	
chr5	150401774	150401868	RUNX1	ms.RUNX1_HUMAN.823086.v1	
chr5	150406277	150406371	RUNX1	ms.RUNX1_HUMAN.823087.v1	
chr5	150406859	150406945	RUNX1	ms.RUNX1_HUMAN.823088.v1	
chr5	150408113	150408207	RUNX1	ms.RUNX1_HUMAN.823089.v1	
chr5	150409893	150409979	RUNX1	ms.RUNX1_HUMAN.823090.v1	
chr5	150410025	150410066	RUNX1	ms.RUNX1_HUMAN.823091.v1	
chr5	150410091	150410184	RUNX1	ms.RUNX1_HUMAN.823092.v1	
chr5	150410218	150410312	RUNX1	ms.RUNX1_HUMAN.823093.v1	
chr5	150410404	150410498	RUNX1	ms.RUNX1_HUMAN.823094.v1	
chr5	150410561	150410629	RUNX1	ms.RUNX1_HUMAN.823095.v1	
chr5	150410675	150410761	RUNX1	ms.RUNX1_HUMAN.823096.v1	
chr5	150411057	150411151	RUNX1	ms.RUNX1_HUMAN.823097.v1	
chr5	150411185	150411279	RUNX1	ms.RUNX1_HUMAN.823098.v1	
chr5	150411395	150411423	RUNX1	ms.RUNX1_HUMAN.823099.v1	
chr5	150412328	150412422	RUNX1	ms.RUNX1_HUMAN.823100.v1	
chr5	150412441	150412546	RUNX1	ms.RUNX1_HUMAN.823101.v1	
chr5	150412622	150412656	RUNX1	ms.RUNX1_HUMAN.823102.v1	
chr5	150412683	150412749	RUNX1	ms.RUNX1_HUMAN.823103.v1	

chr5	150412867	150412917 RUNX1	ms.RUNX1_HUMAN.823104.v1	
chr5	150413105	150413191 RUNX1	ms.RUNX1_HUMAN.823105.v1	
chr5	150413295	150413389 RUNX1	ms.RUNX1_HUMAN.823106.v1	
chr5	150412681	150412731 HNF4A	ms.HNF4A_HUMAN.241492.v1	65
chr5	150410847	150410939 MLLT3	ms.AF9_HUMAN.16589.v1	66
chr5	150412500	150412592 MLLT3	ms.AF9_HUMAN.16590.v1	
chr5	150401056	150401144 CREBBP	ms.CBP_HUMAN.92095.v1	67
chr5	150406854	150406934 CREBBP	ms.CBP_HUMAN.92096.v1	
chr5	150410664	150410748 CREBBP	ms.CBP_HUMAN.92097.v1	
chr5	150410965	150411057 CREBBP	ms.CBP_HUMAN.92098.v1	
chr5	150412723	150412746 CREBBP	ms.CBP_HUMAN.92099.v1	
chr5	150412813	150412924 CREBBP	ms.CBP_HUMAN.92100.v1	
chr5	150409887	150409959 SETX	ms.SETX_HUMAN.7425.v1	68
chr5	150413351	150413417 SMARCA5	ms.SMCA5_HUMAN.25782.v1	69
chr5	150409848	150409936 FIP1L1	ms.FIP1_HUMAN.39717.v1	70
chr5	150412563	150412647 FIP1L1	ms.FIP1_HUMAN.39718.v1	
chr5	150405367	150405459 HDAC1	ms.HDAC1_HUMAN.222606.v1	71
chr5	150410203	150410295 HDAC1	ms.HDAC1_HUMAN.222607.v1	
chr5	150412818	150412910 HDAC1	ms.HDAC1_HUMAN.222608.v1	
chr5	150399895	150399971 ELF1	ms.ELF1_HUMAN.192282.v1	72
chr5	150401228	150401304 ELF1	ms.ELF1_HUMAN.192283.v1	
chr5	150402474	150402562 ELF1	ms.ELF1_HUMAN.192284.v1	
chr5	150407178	150407264 ELF1	ms.ELF1_HUMAN.192285.v1	
chr5	150408548	150408636 ELF1	ms.ELF1_HUMAN.192286.v1	
chr5	150410041	150410117 ELF1	ms.ELF1_HUMAN.192287.v1	
chr5	150410583	150410659 ELF1	ms.ELF1_HUMAN.192288.v1	
chr5	150412700	150412789 ELF1	ms.ELF1_HUMAN.192289.v1	
chr5	150412886	150412962 ELF1	ms.ELF1_HUMAN.192290.v1	
chr5	150409916	150410002 CBX6	ms.CBX6_HUMAN.9830.v1	73
chr5	150412676	150412734 SRF	ms.SRF_HUMAN.99987.v1	74
chr5	150412850	150412908 SRF	ms.SRF_HUMAN.99988.v1	
chr5	150400392	150400418 RELA	ms.TF65_HUMAN.1074099.v1	75
chr5	150400461	150400553 RELA	ms.TF65_HUMAN.1074100.v1	
chr5	150401353	150401445 RELA	ms.TF65_HUMAN.1074101.v1	
chr5	150403137	150403229 RELA	ms.TF65_HUMAN.1074102.v1	
chr5	150403429	150403521 RELA	ms.TF65_HUMAN.1074103.v1	
chr5	150404172	150404194 RELA	ms.TF65_HUMAN.1074104.v1	
chr5	150405530	150405622 RELA	ms.TF65_HUMAN.1074105.v1	
chr5	150405771	150405863 RELA	ms.TF65_HUMAN.1074106.v1	
chr5	150406924	150407016 RELA	ms.TF65_HUMAN.1074107.v1	
chr5	150407014	150407106 RELA	ms.TF65_HUMAN.1074108.v1	
chr5	150407550	150407642 RELA	ms.TF65_HUMAN.1074109.v1	
chr5	150407992	150408092 RELA	ms.TF65_HUMAN.1074110.v1	
chr5	150408068	150408160 RELA	ms.TF65_HUMAN.1074111.v1	
chr5	150409303	150409395 RELA	ms.TF65_HUMAN.1074112.v1	
chr5	150409933	150410013 RELA	ms.TF65_HUMAN.1074113.v1	
chr5	150410535	150410627 RELA	ms.TF65_HUMAN.1074114.v1	
chr5	150410650	150410750 RELA	ms.TF65_HUMAN.1074115.v1	
chr5	150411363	150411455 RELA	ms.TF65_HUMAN.1074116.v1	
chr5	150412382	150412474 RELA	ms.TF65_HUMAN.1074117.v1	

chr5	150412525	150412617	RELA	ms.TF65_HUMAN.1074118.v1	
chr5	150412668	150412760	RELA	ms.TF65_HUMAN.1074119.v1	
chr5	150412828	150412888	RELA	ms.TF65_HUMAN.1074120.v1	
chr5	150412929	150413021	RELA	ms.TF65_HUMAN.1074121.v1	
chr5	150413108	150413125	RELA	ms.TF65_HUMAN.1074122.v1	
chr5	150412738	150412824	SRSF1	ms.SRSF1_HUMAN.29760.v1	76
chr5	150400453	150400541	DPF2	ms.REQU_HUMAN.182026.v1	77
chr5	150407948	150408036	DPF2	ms.REQU_HUMAN.182027.v1	
chr5	150410078	150410178	DPF2	ms.REQU_HUMAN.182028.v1	
chr5	150410531	150410615	DPF2	ms.REQU_HUMAN.182029.v1	
chr5	150411043	150411131	DPF2	ms.REQU_HUMAN.182030.v1	
chr5	150412155	150412255	DPF2	ms.REQU_HUMAN.182031.v1	
chr5	150412827	150412927	DPF2	ms.REQU_HUMAN.182032.v1	
chr5	150410200	150410300	APOBEC3B	ms.ABC3B_HUMAN.22363.v1	78
chr5	150409939	150409965	RFXANK	ms.RFXK_HUMAN.10629.v1	79
chr5	150410733	150410759	RFXANK	ms.RFXK_HUMAN.10630.v1	
chr5	150411474	150411500	RFXANK	ms.RFXK_HUMAN.10631.v1	
chr5	150412967	150412993	RFXANK	ms.RFXK_HUMAN.10632.v1	
chr5	150403937	150404005	ZIM3	ms.ZIM3_HUMAN.16505.v1	80
chr5	150412186	150412248	MLLT1	ms.ENL_HUMAN.55493.v1	81
chr5	150412528	150412590	MLLT1	ms.ENL_HUMAN.55494.v1	
chr5	150410290	150410378	MECOM	ms.EVI1_HUMAN.90952.v1	82
chr5	150410529	150410601	MECOM	ms.EVI1_HUMAN.90953.v1	
chr5	150412634	150412722	MECOM	ms.EVI1_HUMAN.90954.v1	
chr5	150412732	150412820	MECOM	ms.EVI1_HUMAN.90955.v1	
chr5	150413095	150413173	MECOM	ms.EVI1_HUMAN.90956.v1	
chr5	150412680	150412758	HMG20A	ms.HM20A_HUMAN.31465.v1	83
chr5	150400655	150400743	NEUROD1	ms.NDF1_HUMAN.227655.v1	84
chr5	150401556	150401644	NEUROD1	ms.NDF1_HUMAN.227656.v1	
chr5	150410381	150410455	NEUROD1	ms.NDF1_HUMAN.227657.v1	
chr5	150410485	150410551	NEUROD1	ms.NDF1_HUMAN.227658.v1	
chr5	150412608	150412696	NEUROD1	ms.NDF1_HUMAN.227659.v1	
chr5	150409924	150409975	IRF3	ms.IRF3_HUMAN.10924.v1	85
chr5	150410716	150410743	IRF3	ms.IRF3_HUMAN.10925.v1	
chr5	150412605	150412705	SSU72	ms.SSU72_HUMAN.39736.v1	86
chr5	150400336	150400394	ETS1	ms.ETS1_HUMAN.481777.v1	87
chr5	150400624	150400638	ETS1	ms.ETS1_HUMAN.481778.v1	
chr5	150401069	150401083	ETS1	ms.ETS1_HUMAN.481779.v1	
chr5	150410173	150410233	ETS1	ms.ETS1_HUMAN.481780.v1	
chr5	150410589	150410649	ETS1	ms.ETS1_HUMAN.481781.v1	
chr5	150412550	150412610	ETS1	ms.ETS1_HUMAN.481782.v1	
chr5	150412789	150412849	ETS1	ms.ETS1_HUMAN.481783.v1	
chr5	150412910	150412948	ETS1	ms.ETS1_HUMAN.481784.v1	
chr5	150401187	150401261	LYL1	ms.LYL1_HUMAN.97249.v1	88
chr5	150410241	150410323	LYL1	ms.LYL1_HUMAN.97250.v1	
chr5	150410607	150410667	ZBTB16	ms.ZBT16_HUMAN.30953.v1	89
chr5	150409917	150409997	TET2	ms.TET2_HUMAN.32129.v1	90
chr5	150410709	150410789	TET2	ms.TET2_HUMAN.32130.v1	
chr5	150410386	150410464	EBF3	ms.COE3_HUMAN.62287.v1	91
chr5	150410513	150410577	EBF3	ms.COE3_HUMAN.62288.v1	

chr5	150409902	150409976	HINFP	ms.HINFP_HUMAN.7326.v1	92
chr5	150407795	150407819	ZNF600	ms.ZN600_HUMAN.13925.v1	93
chr5	150412618	150412664	GATA4	ms.GATA4_HUMAN.320632.v1	94
chr5	150412860	150412934	BICRA	ms.BICRA_HUMAN.36609.v1	95
chr5	150402608	150402694	SP140	ms.SP140_HUMAN.109827.v1	96
chr5	150404599	150404685	SP140	ms.SP140_HUMAN.109828.v1	
chr5	150412626	150412766	RAG2	ms.RAG2_HUMAN.41192.v1	97
chr5	150399884	150399944	FOXP1	ms.FOXP1_HUMAN.202257.v1	98
chr5	150401080	150401160	FOXP1	ms.FOXP1_HUMAN.202258.v1	
chr5	150401784	150401844	FOXP1	ms.FOXP1_HUMAN.202259.v1	
chr5	150401946	150402006	FOXP1	ms.FOXP1_HUMAN.202260.v1	
chr5	150402072	150402132	FOXP1	ms.FOXP1_HUMAN.202261.v1	
chr5	150402819	150402879	FOXP1	ms.FOXP1_HUMAN.202262.v1	
chr5	150404669	150404729	FOXP1	ms.FOXP1_HUMAN.202263.v1	
chr5	150405091	150405151	FOXP1	ms.FOXP1_HUMAN.202264.v1	
chr5	150406242	150406302	FOXP1	ms.FOXP1_HUMAN.202265.v1	
chr5	150409862	150409922	FOXP1	ms.FOXP1_HUMAN.202266.v1	
chr5	150410191	150410251	FOXP1	ms.FOXP1_HUMAN.202267.v1	
chr5	150410534	150410594	FOXP1	ms.FOXP1_HUMAN.202268.v1	
chr5	150410661	150410741	FOXP1	ms.FOXP1_HUMAN.202269.v1	
chr5	150411357	150411437	FOXP1	ms.FOXP1_HUMAN.202270.v1	
chr5	150412667	150412733	FOXP1	ms.FOXP1_HUMAN.202271.v1	
chr5	150412838	150412913	FOXP1	ms.FOXP1_HUMAN.202272.v1	
chr5	150409938	150409958	NFE2	ms.NFE2_HUMAN.250722.v1	99
chr5	150410736	150410774	NFE2	ms.NFE2_HUMAN.250723.v1	
chr5	150411472	150411488	NFE2	ms.NFE2_HUMAN.250724.v1	
chr5	150412957	150412997	NFE2	ms.NFE2_HUMAN.250725.v1	
chr5	150410483	150410567	MAML1	ms.MAML1_HUMAN.2482.v1	200
chr5	150400849	150400943	TAF1	ms.TAF1_HUMAN.131530.v1	1
chr5	150408367	150408469	TAF1	ms.TAF1_HUMAN.131531.v1	
chr5	150412692	150412745	TAF1	ms.TAF1_HUMAN.131532.v1	
chr5	150412857	150412892	TAF1	ms.TAF1_HUMAN.131533.v1	
chr5	150413110	150413162	TAF1	ms.TAF1_HUMAN.131534.v1	
chr5	150412674	150412784	SMC1A	ms.SMC1A_HUMAN.136044.v1	2
chr5	150410366	150410460	IRF1	ms.IRF1_HUMAN.85531.v1	3
chr5	150412752	150412830	IRF1	ms.IRF1_HUMAN.85532.v1	
chr5	150412863	150412923	IRF1	ms.IRF1_HUMAN.85533.v1	
chr5	150410260	150410336	ATOH1	ms.ATOH1_HUMAN.15799.v1	4
chr5	150401049	150401143	SUPT5H	ms.SPT5H_HUMAN.135678.v1	5
chr5	150401432	150401536	SUPT5H	ms.SPT5H_HUMAN.135679.v1	
chr5	150401654	150401761	SUPT5H	ms.SPT5H_HUMAN.135680.v1	
chr5	150401823	150401929	SUPT5H	ms.SPT5H_HUMAN.135681.v1	
chr5	150401908	150402012	SUPT5H	ms.SPT5H_HUMAN.135682.v1	
chr5	150402446	150402550	SUPT5H	ms.SPT5H_HUMAN.135683.v1	
chr5	150402997	150403091	SUPT5H	ms.SPT5H_HUMAN.135684.v1	
chr5	150403430	150403524	SUPT5H	ms.SPT5H_HUMAN.135685.v1	
chr5	150404216	150404320	SUPT5H	ms.SPT5H_HUMAN.135686.v1	
chr5	150410608	150410712	SUPT5H	ms.SPT5H_HUMAN.135687.v1	
chr5	150412670	150412776	SUPT5H	ms.SPT5H_HUMAN.135688.v1	
chr5	150399947	150400037	CREB1	ms.CREB1_HUMAN.306754.v1	6

chr5	150401273	150401363	CREB1	ms.CREB1_HUMAN.306755.v1	
chr5	150402650	150402732	CREB1	ms.CREB1_HUMAN.306756.v1	
chr5	150409941	150409967	CREB1	ms.CREB1_HUMAN.306757.v1	
chr5	150410004	150410086	CREB1	ms.CREB1_HUMAN.306758.v1	
chr5	150410731	150410748	CREB1	ms.CREB1_HUMAN.306759.v1	
chr5	150411478	150411498	CREB1	ms.CREB1_HUMAN.306760.v1	
chr5	150412330	150412420	CREB1	ms.CREB1_HUMAN.306761.v1	
chr5	150412538	150412628	CREB1	ms.CREB1_HUMAN.306762.v1	
chr5	150412677	150412702	CREB1	ms.CREB1_HUMAN.306763.v1	
chr5	150412967	150412986	CREB1	ms.CREB1_HUMAN.306764.v1	
chr5	150413184	150413197	CREB1	ms.CREB1_HUMAN.306765.v1	
chr5	150406158	150406250	CLOCK	ms.CLOCK_HUMAN.109907.v1	7
chr5	150406883	150406975	CLOCK	ms.CLOCK_HUMAN.109908.v1	
chr5	150408810	150408902	CLOCK	ms.CLOCK_HUMAN.109909.v1	
chr5	150400539	150400633	DNMT3B	ms.DNM3B_HUMAN.76070.v1	8
chr5	150406791	150406877	OGG1	ms.OGG1_HUMAN.85827.v1	9
chr5	150409113	150409199	OGG1	ms.OGG1_HUMAN.85828.v1	
chr5	150399749	150399821	TFAP2A	ms.AP2A_HUMAN.138385.v1	10
chr5	150402671	150402743	TFAP2A	ms.AP2A_HUMAN.138386.v1	
chr5	150404221	150404293	TFAP2A	ms.AP2A_HUMAN.138387.v1	
chr5	150410282	150410362	BCLAF1	ms.BCLF1_HUMAN.9342.v1	11
chr5	150411744	150411824	BCLAF1	ms.BCLF1_HUMAN.9343.v1	
chr5	150405490	150405568	NFATC3	ms.NFAC3_HUMAN.16425.v1	12
chr5	150409402	150409480	NFATC3	ms.NFAC3_HUMAN.16426.v1	
chr5	150402081	150402177	NELFE	ms.NELFE_HUMAN.86186.v1	13
chr5	150404549	150404645	NELFE	ms.NELFE_HUMAN.86187.v1	
chr5	150412908	150413004	NELFE	ms.NELFE_HUMAN.86188.v1	
chr5	150409923	150410003	LEF1	ms.LEF1_HUMAN.18618.v1	14
chr5	150399817	150399849	ESR1	ms.ESR1_HUMAN.3198315.v1	15
chr5	150400196	150400224	ESR1	ms.ESR1_HUMAN.3198316.v1	
chr5	150400964	150400988	ESR1	ms.ESR1_HUMAN.3198317.v1	
chr5	150401068	150401172	ESR1	ms.ESR1_HUMAN.3198318.v1	
chr5	150401391	150401495	ESR1	ms.ESR1_HUMAN.3198319.v1	
chr5	150401599	150401628	ESR1	ms.ESR1_HUMAN.3198320.v1	
chr5	150401668	150401772	ESR1	ms.ESR1_HUMAN.3198321.v1	
chr5	150401973	150402011	ESR1	ms.ESR1_HUMAN.3198322.v1	
chr5	150402513	150402591	ESR1	ms.ESR1_HUMAN.3198323.v1	
chr5	150402610	150402694	ESR1	ms.ESR1_HUMAN.3198324.v1	
chr5	150402695	150402799	ESR1	ms.ESR1_HUMAN.3198325.v1	
chr5	150402867	150402971	ESR1	ms.ESR1_HUMAN.3198326.v1	
chr5	150403155	150403187	ESR1	ms.ESR1_HUMAN.3198327.v1	
chr5	150403271	150403375	ESR1	ms.ESR1_HUMAN.3198328.v1	
chr5	150403893	150403997	ESR1	ms.ESR1_HUMAN.3198329.v1	
chr5	150404298	150404338	ESR1	ms.ESR1_HUMAN.3198330.v1	
chr5	150404439	150404543	ESR1	ms.ESR1_HUMAN.3198331.v1	
chr5	150404631	150404707	ESR1	ms.ESR1_HUMAN.3198332.v1	
chr5	150404784	150404852	ESR1	ms.ESR1_HUMAN.3198333.v1	
chr5	150405409	150405457	ESR1	ms.ESR1_HUMAN.3198334.v1	
chr5	150405550	150405636	ESR1	ms.ESR1_HUMAN.3198335.v1	
chr5	150405832	150405881	ESR1	ms.ESR1_HUMAN.3198336.v1	

chr5	150406126	150406230 ESR1	ms.ESR1_HUMAN.3198337.v1	
chr5	150406261	150406333 ESR1	ms.ESR1_HUMAN.3198338.v1	
chr5	150406823	150406930 ESR1	ms.ESR1_HUMAN.3198339.v1	
chr5	150406932	150407044 ESR1	ms.ESR1_HUMAN.3198340.v1	
chr5	150407006	150407105 ESR1	ms.ESR1_HUMAN.3198341.v1	
chr5	150407238	150407288 ESR1	ms.ESR1_HUMAN.3198342.v1	
chr5	150407643	150407679 ESR1	ms.ESR1_HUMAN.3198343.v1	
chr5	150408270	150408287 ESR1	ms.ESR1_HUMAN.3198344.v1	
chr5	150408531	150408643 ESR1	ms.ESR1_HUMAN.3198345.v1	
chr5	150409186	150409267 ESR1	ms.ESR1_HUMAN.3198346.v1	
chr5	150409740	150409844 ESR1	ms.ESR1_HUMAN.3198347.v1	
chr5	150409876	150409969 ESR1	ms.ESR1_HUMAN.3198348.v1	
chr5	150409997	150410101 ESR1	ms.ESR1_HUMAN.3198349.v1	
chr5	150410209	150410301 ESR1	ms.ESR1_HUMAN.3198350.v1	
chr5	150410680	150410725 ESR1	ms.ESR1_HUMAN.3198351.v1	
chr5	150410863	150410903 ESR1	ms.ESR1_HUMAN.3198352.v1	
chr5	150411115	150411219 ESR1	ms.ESR1_HUMAN.3198353.v1	
chr5	150411318	150411422 ESR1	ms.ESR1_HUMAN.3198354.v1	
chr5	150411585	150411650 ESR1	ms.ESR1_HUMAN.3198355.v1	
chr5	150412146	150412250 ESR1	ms.ESR1_HUMAN.3198356.v1	
chr5	150412400	150412525 ESR1	ms.ESR1_HUMAN.3198357.v1	
chr5	150412565	150412663 ESR1	ms.ESR1_HUMAN.3198358.v1	
chr5	150412667	150412691 ESR1	ms.ESR1_HUMAN.3198359.v1	
chr5	150412845	150412943 ESR1	ms.ESR1_HUMAN.3198360.v1	
chr5	150413353	150413457 ESR1	ms.ESR1_HUMAN.3198361.v1	
chr5	150400089	150400185 PGR	ms.PRGR_HUMAN.896471.v1	16
chr5	150400267	150400375 PGR	ms.PRGR_HUMAN.896472.v1	
chr5	150402095	150402191 PGR	ms.PRGR_HUMAN.896473.v1	
chr5	150403125	150403221 PGR	ms.PRGR_HUMAN.896474.v1	
chr5	150404580	150404644 PGR	ms.PRGR_HUMAN.896475.v1	
chr5	150405444	150405540 PGR	ms.PRGR_HUMAN.896476.v1	
chr5	150406148	150406244 PGR	ms.PRGR_HUMAN.896477.v1	
chr5	150406889	150406909 PGR	ms.PRGR_HUMAN.896478.v1	
chr5	150407561	150407669 PGR	ms.PRGR_HUMAN.896479.v1	
chr5	150409923	150409977 PGR	ms.PRGR_HUMAN.896480.v1	
chr5	150410080	150410188 PGR	ms.PRGR_HUMAN.896481.v1	
chr5	150410246	150410274 PGR	ms.PRGR_HUMAN.896482.v1	
chr5	150410569	150410665 PGR	ms.PRGR_HUMAN.896483.v1	
chr5	150410745	150410769 PGR	ms.PRGR_HUMAN.896484.v1	
chr5	150410804	150410912 PGR	ms.PRGR_HUMAN.896485.v1	
chr5	150410866	150410962 PGR	ms.PRGR_HUMAN.896486.v1	
chr5	150411627	150411735 PGR	ms.PRGR_HUMAN.896487.v1	
chr5	150412292	150412388 PGR	ms.PRGR_HUMAN.896488.v1	
chr5	150412554	150412650 PGR	ms.PRGR_HUMAN.896489.v1	
chr5	150412917	150413007 PGR	ms.PRGR_HUMAN.896490.v1	
chr5	150410665	150410705 HOXB13	ms.HXB13_HUMAN.214115.v1	17
chr5	150409918	150409986 KDM6A	ms.KDM6A_HUMAN.75999.v1	18
chr5	150410692	150410770 KDM6A	ms.KDM6A_HUMAN.76000.v1	
chr5	150412608	150412695 KDM6A	ms.KDM6A_HUMAN.76001.v1	
chr5	150412988	150413080 KDM6A	ms.KDM6A_HUMAN.76002.v1	

chr5	150403331	150403405 JUND	ms.JUND_HUMAN.214253.v1	19
chr5	150408923	150408983 JUND	ms.JUND_HUMAN.214254.v1	
chr5	150412531	150412591 JUND	ms.JUND_HUMAN.214255.v1	
chr5	150412739	150412875 DRAP1	ms.NC2A_HUMAN.19322.v1	20
chr5	150409848	150409963 ATF7	ms.ATF7_HUMAN.67242.v1	21
chr5	150413114	150413172 ATF7	ms.ATF7_HUMAN.67243.v1	
chr5	150399990	150400010 TAL1	ms.TAL1_HUMAN.415267.v1	22
chr5	150401172	150401238 TAL1	ms.TAL1_HUMAN.415268.v1	
chr5	150402321	150402341 TAL1	ms.TAL1_HUMAN.415269.v1	
chr5	150402597	150402617 TAL1	ms.TAL1_HUMAN.415270.v1	
chr5	150406025	150406091 TAL1	ms.TAL1_HUMAN.415271.v1	
chr5	150406105	150406125 TAL1	ms.TAL1_HUMAN.415272.v1	
chr5	150406997	150407089 LMNB1	ms.LMNB1_HUMAN.306740.v1	23
chr5	150409995	150410079 ETV6	ms.ETV6_HUMAN.36956.v1	24
chr5	150413139	150413215 ETV6	ms.ETV6_HUMAN.36957.v1	
chr5	150410971	150411053 MYOG	ms.MYOG_HUMAN.140062.v1	25
chr5	150409903	150409977 MYOD1	ms.MYOD1_HUMAN.266593.v1	26
chr5	150410156	150410230 MYOD1	ms.MYOD1_HUMAN.266594.v1	
chr5	150410747	150410795 MYOD1	ms.MYOD1_HUMAN.266595.v1	
chr5	150405601	150405659 SRSF3	ms.SRSF3_HUMAN.103530.v1	27
chr5	150412544	150412608 SRSF3	ms.SRSF3_HUMAN.103531.v1	
chr5	150401087	150401167 BACH1	ms.BACH1_HUMAN.13259.v1	28
chr5	150408673	150408753 BACH1	ms.BACH1_HUMAN.13260.v1	
chr5	150399613	150399707 RUNX1T1	ms.MTG8_HUMAN.134372.v1	29
chr5	150406944	150407038 RUNX1T1	ms.MTG8_HUMAN.134373.v1	
chr5	150410121	150410213 RUNX1T1	ms.MTG8_HUMAN.134374.v1	
chr5	150412563	150412657 RUNX1T1	ms.MTG8_HUMAN.134375.v1	
chr5	150412715	150412807 RUNX1T1	ms.MTG8_HUMAN.134376.v1	
chr5	150400974	150401086 MBD4	ms.MBD4_HUMAN.823648.v1	30
chr5	150407385	150407483 MBD4	ms.MBD4_HUMAN.823649.v1	
chr5	150410249	150410361 MBD4	ms.MBD4_HUMAN.823650.v1	
chr5	150410528	150410632 MBD4	ms.MBD4_HUMAN.823651.v1	
chr5	150410694	150410738 MBD4	ms.MBD4_HUMAN.823652.v1	
chr5	150412531	150412629 MBD4	ms.MBD4_HUMAN.823653.v1	
chr5	150412616	150412720 MBD4	ms.MBD4_HUMAN.823654.v1	
chr5	150412717	150412791 MBD4	ms.MBD4_HUMAN.823655.v1	
chr5	150412870	150412940 MBD4	ms.MBD4_HUMAN.823656.v1	
chr5	150412420	150412548 ZFP91	ms.ZFP91_HUMAN.4238.v1	31
chr5	150404268	150404320 NR5A2	ms.NR5A2_HUMAN.54245.v1	32
chr5	150410570	150410684 NFIC	ms.NFIC_HUMAN.94434.v1	33
chr5	150412653	150412739 NFIC	ms.NFIC_HUMAN.94435.v1	
chr5	150410547	150410583 MEF2B	ms.MEF2B_HUMAN.62630.v1	34
chr5	150411023	150411115 MEF2B	ms.MEF2B_HUMAN.62631.v1	
chr5	150411562	150411672 MEF2B	ms.MEF2B_HUMAN.62632.v1	
chr5	150412852	150412916 MEF2B	ms.MEF2B_HUMAN.62633.v1	
chr5	150412930	150413004 MEF2B	ms.MEF2B_HUMAN.62634.v1	
chr5	150402812	150402890 CUL4A	ms.CUL4A_HUMAN.109436.v1	34
chr5	150407050	150407128 CUL4A	ms.CUL4A_HUMAN.109437.v1	
chr5	150408513	150408613 CUL4A	ms.CUL4A_HUMAN.109438.v1	
chr5	150410192	150410270 CUL4A	ms.CUL4A_HUMAN.109439.v1	

chr5	150406832	150406908	SP2	ms.SP2_HUMAN.40160.v1	35
chr5	150408295	150408365	SP2	ms.SP2_HUMAN.40161.v1	
chr5	150410005	150410034	SP2	ms.SP2_HUMAN.40162.v1	
chr5	150400821	150400897	MAX	ms.MAX_HUMAN.360619.v1	36
chr5	150401414	150401508	MAX	ms.MAX_HUMAN.360620.v1	
chr5	150406168	150406244	MAX	ms.MAX_HUMAN.360621.v1	
chr5	150409856	150409930	MAX	ms.MAX_HUMAN.360622.v1	
chr5	150410275	150410357	MAX	ms.MAX_HUMAN.360623.v1	
chr5	150410504	150410521	MAX	ms.MAX_HUMAN.360624.v1	
chr5	150410791	150410801	MAX	ms.MAX_HUMAN.360625.v1	
chr5	150412564	150412657	MAX	ms.MAX_HUMAN.360626.v1	
chr5	150412664	150412762	MAX	ms.MAX_HUMAN.360627.v1	
chr5	150412780	150412793	MAX	ms.MAX_HUMAN.360628.v1	
chr5	150408415	150408501	TBL1XR1	ms.TBL1R_HUMAN.27016.v1	37
chr5	150409925	150409988	CHD2	ms.CHD2_HUMAN.48563.v1	38
chr5	150410714	150410750	CHD2	ms.CHD2_HUMAN.48564.v1	
chr5	150412947	150412994	CHD2	ms.CHD2_HUMAN.48565.v1	
chr5	150400013	150400117	CHD1	ms.CHD1_HUMAN.95816.v1	39
chr5	150400101	150400192	CHD1	ms.CHD1_HUMAN.95817.v1	
chr5	150400343	150400431	CHD1	ms.CHD1_HUMAN.95818.v1	
chr5	150401786	150401886	CHD1	ms.CHD1_HUMAN.95819.v1	
chr5	150407171	150407275	CHD1	ms.CHD1_HUMAN.95820.v1	
chr5	150408207	150408295	CHD1	ms.CHD1_HUMAN.95821.v1	
chr5	150411187	150411291	CHD1	ms.CHD1_HUMAN.95822.v1	
chr5	150412095	150412183	CHD1	ms.CHD1_HUMAN.95823.v1	
chr5	150412536	150412614	CHD1	ms.CHD1_HUMAN.95824.v1	
chr5	150413336	150413424	CHD1	ms.CHD1_HUMAN.95825.v1	
chr5	150406928	150406992	SREBF2	ms.SRBP2_HUMAN.97054.v1	40
chr5	150412773	150412853	SREBF2	ms.SRBP2_HUMAN.97055.v1	
chr5	150410241	150410321	FOXO1	ms.FOXO1_HUMAN.124928.v1	41
chr5	150410506	150410578	FOXO1	ms.FOXO1_HUMAN.124929.v1	
chr5	150401475	150401565	STAT5B	ms.STA5B_HUMAN.268646.v1	42
chr5	150401897	150401987	STAT5B	ms.STA5B_HUMAN.268647.v1	
chr5	150404759	150404849	STAT5B	ms.STA5B_HUMAN.268648.v1	
chr5	150407323	150407358	STAT5B	ms.STA5B_HUMAN.268649.v1	
chr5	150408314	150408404	STAT5B	ms.STA5B_HUMAN.268650.v1	
chr5	150410885	150410975	STAT5B	ms.STA5B_HUMAN.268651.v1	
chr5	150412459	150412549	STAT5B	ms.STA5B_HUMAN.268652.v1	
chr5	150412559	150412649	STAT5B	ms.STA5B_HUMAN.268653.v1	
chr5	150412713	150412803	STAT5B	ms.STA5B_HUMAN.268654.v1	
chr5	150412861	150412957	STAT5B	ms.STA5B_HUMAN.268655.v1	
chr5	150413108	150413195	STAT5B	ms.STA5B_HUMAN.268656.v1	
chr5	150401339	150401433	NIPBL	ms.NIPBL_HUMAN.149798.v1	43
chr5	150409882	150409968	NIPBL	ms.NIPBL_HUMAN.149799.v1	
chr5	150410063	150410097	NIPBL	ms.NIPBL_HUMAN.149800.v1	
chr5	150410157	150410251	NIPBL	ms.NIPBL_HUMAN.149801.v1	
chr5	150411090	150411184	NIPBL	ms.NIPBL_HUMAN.149802.v1	
chr5	150411595	150411689	NIPBL	ms.NIPBL_HUMAN.149803.v1	
chr5	150412528	150412622	NIPBL	ms.NIPBL_HUMAN.149804.v1	
chr5	150412668	150412779	NIPBL	ms.NIPBL_HUMAN.149805.v1	

chr5	150400889	150400960 KMT2A	ms.KMT2A_HUMAN.520121.v1	44
chr5	150400979	150401077 KMT2A	ms.KMT2A_HUMAN.520122.v1	
chr5	150402022	150402141 KMT2A	ms.KMT2A_HUMAN.520123.v1	
chr5	150402904	150403010 KMT2A	ms.KMT2A_HUMAN.520124.v1	
chr5	150403145	150403245 KMT2A	ms.KMT2A_HUMAN.520125.v1	
chr5	150403235	150403282 KMT2A	ms.KMT2A_HUMAN.520126.v1	
chr5	150404033	150404131 KMT2A	ms.KMT2A_HUMAN.520127.v1	
chr5	150406805	150406905 KMT2A	ms.KMT2A_HUMAN.520128.v1	
chr5	150406866	150406966 KMT2A	ms.KMT2A_HUMAN.520129.v1	
chr5	150407228	150407264 KMT2A	ms.KMT2A_HUMAN.520130.v1	
chr5	150407722	150407820 KMT2A	ms.KMT2A_HUMAN.520131.v1	
chr5	150409045	150409145 KMT2A	ms.KMT2A_HUMAN.520132.v1	
chr5	150409861	150409959 KMT2A	ms.KMT2A_HUMAN.520133.v1	
chr5	150410124	150410222 KMT2A	ms.KMT2A_HUMAN.520134.v1	
chr5	150410568	150410668 KMT2A	ms.KMT2A_HUMAN.520135.v1	
chr5	150410650	150410748 KMT2A	ms.KMT2A_HUMAN.520136.v1	
chr5	150410872	150410970 KMT2A	ms.KMT2A_HUMAN.520137.v1	
chr5	150411583	150411683 KMT2A	ms.KMT2A_HUMAN.520138.v1	
chr5	150412440	150412538 KMT2A	ms.KMT2A_HUMAN.520139.v1	
chr5	150412633	150412660 KMT2A	ms.KMT2A_HUMAN.520140.v1	
chr5	150412720	150412780 KMT2A	ms.KMT2A_HUMAN.520141.v1	
chr5	150412924	150413018 KMT2A	ms.KMT2A_HUMAN.520142.v1	
chr5	150400397	150400485 ARID2	ms.ARID2_HUMAN.109649.v1	45
chr5	150405027	150405119 BCL3	ms.BCL3_HUMAN.70102.v1	46
chr5	150406901	150406993 BCL3	ms.BCL3_HUMAN.70103.v1	
chr5	150412630	150412726 BCL3	ms.BCL3_HUMAN.70104.v1	
chr5	150404617	150404688 INTS11	ms.INT11_HUMAN.287416.v1	47
chr5	150406813	150406899 INTS11	ms.INT11_HUMAN.287417.v1	
chr5	150406902	150406988 INTS11	ms.INT11_HUMAN.287418.v1	
chr5	150407227	150407313 INTS11	ms.INT11_HUMAN.287419.v1	
chr5	150408160	150408246 INTS11	ms.INT11_HUMAN.287420.v1	
chr5	150412540	150412626 INTS11	ms.INT11_HUMAN.287421.v1	
chr5	150412722	150412848 ZNF580	ms.ZN580_HUMAN.30465.v1	48
chr5	150402908	150402960 TP53	ms.P53_HUMAN.565672.v1	49
chr5	150407165	150407275 TP53	ms.P53_HUMAN.565673.v1	
chr5	150409928	150410018 TP53	ms.P53_HUMAN.565674.v1	
chr5	150410154	150410252 TP53	ms.P53_HUMAN.565675.v1	
chr5	150410816	150410839 TP53	ms.P53_HUMAN.565676.v1	
chr5	150412692	150412790 TP53	ms.P53_HUMAN.565677.v1	
chr5	150412898	150412996 TP53	ms.P53_HUMAN.565678.v1	
chr5	150403158	150403222 SPIB	ms.SPIB_HUMAN.33675.v1	50
chr5	150412831	150412863 SPIB	ms.SPIB_HUMAN.33676.v1	
chr5	150402114	150402214 TRPS1	ms.TRPS1_HUMAN.868977.v1	51
chr5	150402559	150402611 TRPS1	ms.TRPS1_HUMAN.868978.v1	
chr5	150403174	150403274 TRPS1	ms.TRPS1_HUMAN.868979.v1	
chr5	150406829	150406929 TRPS1	ms.TRPS1_HUMAN.868980.v1	
chr5	150406886	150406986 TRPS1	ms.TRPS1_HUMAN.868981.v1	
chr5	150407167	150407267 TRPS1	ms.TRPS1_HUMAN.868982.v1	
chr5	150407844	150407944 TRPS1	ms.TRPS1_HUMAN.868983.v1	
chr5	150408270	150408370 TRPS1	ms.TRPS1_HUMAN.868984.v1	

chr5	150409060	150409134	TRPS1	ms.TRPS1_HUMAN.868985.v1	
chr5	150409147	150409247	TRPS1	ms.TRPS1_HUMAN.868986.v1	
chr5	150409303	150409403	TRPS1	ms.TRPS1_HUMAN.868987.v1	
chr5	150410211	150410311	TRPS1	ms.TRPS1_HUMAN.868988.v1	
chr5	150411640	150411740	TRPS1	ms.TRPS1_HUMAN.868989.v1	
chr5	150412593	150412683	TRPS1	ms.TRPS1_HUMAN.868990.v1	
chr5	150412689	150412786	TRPS1	ms.TRPS1_HUMAN.868991.v1	
chr5	150399748	150399808	SPI1	ms.SPI1_HUMAN.1291404.v1	52
chr5	150400116	150400188	SPI1	ms.SPI1_HUMAN.1291405.v1	
chr5	150400396	150400508	SPI1	ms.SPI1_HUMAN.1291406.v1	
chr5	150400656	150400734	SPI1	ms.SPI1_HUMAN.1291407.v1	
chr5	150400724	150400836	SPI1	ms.SPI1_HUMAN.1291408.v1	
chr5	150401019	150401131	SPI1	ms.SPI1_HUMAN.1291409.v1	
chr5	150401223	150401277	SPI1	ms.SPI1_HUMAN.1291410.v1	
chr5	150401854	150401877	SPI1	ms.SPI1_HUMAN.1291411.v1	
chr5	150401952	150402030	SPI1	ms.SPI1_HUMAN.1291412.v1	
chr5	150403450	150403509	SPI1	ms.SPI1_HUMAN.1291413.v1	
chr5	150403918	150404030	SPI1	ms.SPI1_HUMAN.1291414.v1	
chr5	150404267	150404379	SPI1	ms.SPI1_HUMAN.1291415.v1	
chr5	150404586	150404698	SPI1	ms.SPI1_HUMAN.1291416.v1	
chr5	150406312	150406346	SPI1	ms.SPI1_HUMAN.1291417.v1	
chr5	150406595	150406707	SPI1	ms.SPI1_HUMAN.1291418.v1	
chr5	150406965	150407077	SPI1	ms.SPI1_HUMAN.1291419.v1	
chr5	150407235	150407347	SPI1	ms.SPI1_HUMAN.1291420.v1	
chr5	150407388	150407466	SPI1	ms.SPI1_HUMAN.1291421.v1	
chr5	150408200	150408236	SPI1	ms.SPI1_HUMAN.1291422.v1	
chr5	150409836	150409948	SPI1	ms.SPI1_HUMAN.1291423.v1	
chr5	150410080	150410114	SPI1	ms.SPI1_HUMAN.1291424.v1	
chr5	150410249	150410289	SPI1	ms.SPI1_HUMAN.1291425.v1	
chr5	150410610	150410653	SPI1	ms.SPI1_HUMAN.1291426.v1	
chr5	150411031	150411097	SPI1	ms.SPI1_HUMAN.1291427.v1	
chr5	150411341	150411416	SPI1	ms.SPI1_HUMAN.1291428.v1	
chr5	150411410	150411522	SPI1	ms.SPI1_HUMAN.1291429.v1	
chr5	150411660	150411772	SPI1	ms.SPI1_HUMAN.1291430.v1	
chr5	150411785	150411897	SPI1	ms.SPI1_HUMAN.1291431.v1	
chr5	150412355	150412381	SPI1	ms.SPI1_HUMAN.1291432.v1	
chr5	150412586	150412640	SPI1	ms.SPI1_HUMAN.1291433.v1	
chr5	150412831	150412856	SPI1	ms.SPI1_HUMAN.1291434.v1	
chr5	150412956	150413068	SPI1	ms.SPI1_HUMAN.1291435.v1	
chr5	150413186	150413216	SPI1	ms.SPI1_HUMAN.1291436.v1	
chr5	150401143	150401217	LDB1	ms.LDB1_HUMAN.115579.v1	53
chr5	150406203	150406277	LDB1	ms.LDB1_HUMAN.115580.v1	
chr5	150409936	150410022	LDB1	ms.LDB1_HUMAN.115581.v1	
chr5	150410416	150410490	LDB1	ms.LDB1_HUMAN.115582.v1	
chr5	150410606	150410692	LDB1	ms.LDB1_HUMAN.115583.v1	
chr5	150412453	150412539	LDB1	ms.LDB1_HUMAN.115584.v1	
chr5	150412798	150412884	LDB1	ms.LDB1_HUMAN.115585.v1	
chr5	150408782	150408882	WRNIP1	ms.WRIP1_HUMAN.2678.v1	54
chr5	150406901	150406959	PAX2	ms.PAX2_HUMAN.73810.v1	55
chr5	150399937	150400019	MYC	ms.MYC_HUMAN.872711.v1	56

chr5	150400133	150400221	MYC	ms.MYC_HUMAN.872712.v1
chr5	150400203	150400291	MYC	ms.MYC_HUMAN.872713.v1
chr5	150400500	150400589	MYC	ms.MYC_HUMAN.872714.v1
chr5	150400707	150400795	MYC	ms.MYC_HUMAN.872715.v1
chr5	150400823	150400905	MYC	ms.MYC_HUMAN.872716.v1
chr5	150400991	150401016	MYC	ms.MYC_HUMAN.872717.v1
chr5	150401067	150401149	MYC	ms.MYC_HUMAN.872718.v1
chr5	150401229	150401311	MYC	ms.MYC_HUMAN.872719.v1
chr5	150401404	150401492	MYC	ms.MYC_HUMAN.872720.v1
chr5	150401745	150401817	MYC	ms.MYC_HUMAN.872721.v1
chr5	150401896	150401968	MYC	ms.MYC_HUMAN.872722.v1
chr5	150402236	150402318	MYC	ms.MYC_HUMAN.872723.v1
chr5	150402714	150402802	MYC	ms.MYC_HUMAN.872724.v1
chr5	150402836	150402924	MYC	ms.MYC_HUMAN.872725.v1
chr5	150403047	150403129	MYC	ms.MYC_HUMAN.872726.v1
chr5	150404041	150404129	MYC	ms.MYC_HUMAN.872727.v1
chr5	150404155	150404237	MYC	ms.MYC_HUMAN.872728.v1
chr5	150404886	150404974	MYC	ms.MYC_HUMAN.872729.v1
chr5	150405034	150405116	MYC	ms.MYC_HUMAN.872730.v1
chr5	150405390	150405450	MYC	ms.MYC_HUMAN.872731.v1
chr5	150405579	150405651	MYC	ms.MYC_HUMAN.872732.v1
chr5	150406180	150406221	MYC	ms.MYC_HUMAN.872733.v1
chr5	150406329	150406433	MYC	ms.MYC_HUMAN.872734.v1
chr5	150406611	150406693	MYC	ms.MYC_HUMAN.872735.v1
chr5	150406924	150406960	MYC	ms.MYC_HUMAN.872736.v1
chr5	150407167	150407268	MYC	ms.MYC_HUMAN.872737.v1
chr5	150407515	150407551	MYC	ms.MYC_HUMAN.872738.v1
chr5	150408556	150408644	MYC	ms.MYC_HUMAN.872739.v1
chr5	150408642	150408724	MYC	ms.MYC_HUMAN.872740.v1
chr5	150409248	150409330	MYC	ms.MYC_HUMAN.872741.v1
chr5	150409493	150409581	MYC	ms.MYC_HUMAN.872742.v1
chr5	150409861	150409933	MYC	ms.MYC_HUMAN.872743.v1
chr5	150410062	150410134	MYC	ms.MYC_HUMAN.872744.v1
chr5	150410166	150410248	MYC	ms.MYC_HUMAN.872745.v1
chr5	150410316	150410398	MYC	ms.MYC_HUMAN.872746.v1
chr5	150410390	150410459	MYC	ms.MYC_HUMAN.872747.v1
chr5	150410525	150410619	MYC	ms.MYC_HUMAN.872748.v1
chr5	150410751	150410833	MYC	ms.MYC_HUMAN.872749.v1
chr5	150411487	150411575	MYC	ms.MYC_HUMAN.872750.v1
chr5	150411592	150411674	MYC	ms.MYC_HUMAN.872751.v1
chr5	150412274	150412338	MYC	ms.MYC_HUMAN.872752.v1
chr5	150412642	150412696	MYC	ms.MYC_HUMAN.872753.v1
chr5	150412801	150412883	MYC	ms.MYC_HUMAN.872754.v1
chr5	150413110	150413182	MYC	ms.MYC_HUMAN.872755.v1
chr5	150406895	150406965	FOS	ms.FOS_HUMAN.331525.v1
chr5	150408026	150408036	FOS	ms.FOS_HUMAN.331526.v1
chr5	150409941	150409981	FOS	ms.FOS_HUMAN.331527.v1
chr5	150410714	150410724	FOS	ms.FOS_HUMAN.331528.v1
chr5	150410788	150410864	FOS	ms.FOS_HUMAN.331529.v1
chr5	150412669	150412739	FOS	ms.FOS_HUMAN.331530.v1

chr5	150412794	150412864	FOS	ms.FOS_HUMAN.331531.v1	
chr5	150412942	150412976	FOS	ms.FOS_HUMAN.331532.v1	
chr5	150412598	150412662	HNRNPLL	ms.HNRLL_HUMAN.75847.v1	58
chr5	150412733	150412757	HNRNPLL	ms.HNRLL_HUMAN.75848.v1	
chr5	150412919	150412939	HNRNPLL	ms.HNRLL_HUMAN.75849.v1	
chr5	150406831	150406933	ZNF467	ms.ZN467_HUMAN.28410.v1	59
chr5	150403296	150403386	POU5F1	ms.PO5F1_HUMAN.371520.v1	60
chr5	150407208	150407298	POU5F1	ms.PO5F1_HUMAN.371521.v1	
chr5	150412446	150412536	POU5F1	ms.PO5F1_HUMAN.371522.v1	
chr5	150409957	150410045	RBM25	ms.RBM25_HUMAN.143000.v1	61
chr5	150410701	150410741	RBM25	ms.RBM25_HUMAN.143001.v1	
chr5	150412933	150413005	RBM25	ms.RBM25_HUMAN.143002.v1	
chr5	150411470	150411554	CDX2	ms.CDX2_HUMAN.220746.v1	62
chr5	150400409	150400503	ZNF143	ms.ZN143_HUMAN.281652.v1	63
chr5	150401876	150401970	ZNF143	ms.ZN143_HUMAN.281653.v1	
chr5	150403217	150403295	ZNF143	ms.ZN143_HUMAN.281654.v1	
chr5	150406329	150406423	ZNF143	ms.ZN143_HUMAN.281655.v1	
chr5	150408518	150408612	ZNF143	ms.ZN143_HUMAN.281656.v1	
chr5	150409928	150409989	ZNF143	ms.ZN143_HUMAN.281657.v1	
chr5	150410717	150410783	ZNF143	ms.ZN143_HUMAN.281658.v1	
chr5	150411206	150411299	ZNF143	ms.ZN143_HUMAN.281659.v1	
chr5	150412947	150413013	ZNF143	ms.ZN143_HUMAN.281660.v1	
chr5	150412555	150412645	KLF6	ms.KLF6_HUMAN.47847.v1	64
chr5	150412863	150412955	MED12	ms.MED12_HUMAN.156441.v1	65
chr5	150407950	150408014	EGR2	ms.EGR2_HUMAN.94917.v1	66
chr5	150408273	150408349	EGR2	ms.EGR2_HUMAN.94918.v1	
chr5	150410181	150410245	EGR2	ms.EGR2_HUMAN.94919.v1	
chr5	150410176	150410272	ZSCAN22	ms.ZSC22_HUMAN.23624.v1	67
chr5	150401744	150401806	ZBTB48	ms.TZAP_HUMAN.138523.v1	68
chr5	150407530	150407616	ZBTB48	ms.TZAP_HUMAN.138524.v1	
chr5	150409895	150409979	ZBTB48	ms.TZAP_HUMAN.138525.v1	
chr5	150410325	150410409	ZBTB48	ms.TZAP_HUMAN.138526.v1	
chr5	150413159	150413221	ZBTB48	ms.TZAP_HUMAN.138527.v1	
chr5	150399951	150400011	POU2F2	ms.PO2F2_HUMAN.38812.v1	69
chr5	150400088	150400162	POU2F2	ms.PO2F2_HUMAN.38813.v1	
chr5	150400821	150400881	POU2F2	ms.PO2F2_HUMAN.38814.v1	
chr5	150400942	150401031	POU2F2	ms.PO2F2_HUMAN.38815.v1	
chr5	150405411	150405471	POU2F2	ms.PO2F2_HUMAN.38816.v1	
chr5	150407124	150407184	POU2F2	ms.PO2F2_HUMAN.38817.v1	
chr5	150407512	150407590	POU2F2	ms.PO2F2_HUMAN.38818.v1	
chr5	150408319	150408379	POU2F2	ms.PO2F2_HUMAN.38819.v1	
chr5	150408589	150408670	POU2F2	ms.PO2F2_HUMAN.38820.v1	
chr5	150410180	150410254	POU2F2	ms.PO2F2_HUMAN.38821.v1	
chr5	150410904	150410964	POU2F2	ms.PO2F2_HUMAN.38822.v1	
chr5	150411391	150411424	POU2F2	ms.PO2F2_HUMAN.38823.v1	
chr5	150412011	150412085	POU2F2	ms.PO2F2_HUMAN.38824.v1	
chr5	150412669	150412715	POU2F2	ms.PO2F2_HUMAN.38825.v1	
chr5	150399919	150399997	NR2F2	ms.COT2_HUMAN.260448.v1	70
chr5	150401883	150401961	NR2F2	ms.COT2_HUMAN.260449.v1	
chr5	150403102	150403180	NR2F2	ms.COT2_HUMAN.260450.v1	

chr5	150404252	150404330 NR2F2	ms.COT2_HUMAN.260451.v1	
chr5	150407202	150407270 NR2F2	ms.COT2_HUMAN.260452.v1	
chr5	150407803	150407881 NR2F2	ms.COT2_HUMAN.260453.v1	
chr5	150410917	150411009 ARID3A	ms.ARI3A_HUMAN.13893.v1	71
chr5	150410609	150410717 NANOG	ms.NANOG_HUMAN.143195.v1	72
chr5	150412693	150412801 NANOG	ms.NANOG_HUMAN.143196.v1	
chr5	150411294	150411362 GFI1	ms.GFI1_HUMAN.107524.v1	73
chr5	150410565	150410625 CDK8	ms.CDK8_HUMAN.183096.v1	74
chr5	150410724	150410758 CDK8	ms.CDK8_HUMAN.183097.v1	
chr5	150412560	150412648 CDK8	ms.CDK8_HUMAN.183098.v1	
chr5	150412721	150412809 CDK8	ms.CDK8_HUMAN.183099.v1	
chr5	150412772	150412860 CDK8	ms.CDK8_HUMAN.183100.v1	
chr5	150412885	150412932 CDK8	ms.CDK8_HUMAN.183101.v1	
chr5	150412956	150413008 CDK8	ms.CDK8_HUMAN.183102.v1	
chr5	150402711	150402811 PALB2	ms.PALB2_HUMAN.21060.v1	75
chr5	150403102	150403202 PALB2	ms.PALB2_HUMAN.21061.v1	
chr5	150400053	150400149 STAT3	ms.STAT3_HUMAN.282182.v1	76
chr5	150400316	150400396 STAT3	ms.STAT3_HUMAN.282183.v1	
chr5	150400397	150400493 STAT3	ms.STAT3_HUMAN.282184.v1	
chr5	150401883	150401979 STAT3	ms.STAT3_HUMAN.282185.v1	
chr5	150402659	150402739 STAT3	ms.STAT3_HUMAN.282186.v1	
chr5	150403055	150403135 STAT3	ms.STAT3_HUMAN.282187.v1	
chr5	150409949	150409972 STAT3	ms.STAT3_HUMAN.282188.v1	
chr5	150410008	150410104 STAT3	ms.STAT3_HUMAN.282189.v1	
chr5	150410113	150410183 STAT3	ms.STAT3_HUMAN.282190.v1	
chr5	150410556	150410626 STAT3	ms.STAT3_HUMAN.282191.v1	
chr5	150410667	150410737 STAT3	ms.STAT3_HUMAN.282192.v1	
chr5	150410849	150410945 STAT3	ms.STAT3_HUMAN.282193.v1	
chr5	150411317	150411413 STAT3	ms.STAT3_HUMAN.282194.v1	
chr5	150411440	150411510 STAT3	ms.STAT3_HUMAN.282195.v1	
chr5	150412355	150412451 STAT3	ms.STAT3_HUMAN.282196.v1	
chr5	150412719	150412759 STAT3	ms.STAT3_HUMAN.282197.v1	
chr5	150412904	150412927 STAT3	ms.STAT3_HUMAN.282198.v1	
chr5	150413358	150413438 STAT3	ms.STAT3_HUMAN.282199.v1	
chr5	150400654	150400681 TAF15	ms.RBP56_HUMAN.69432.v1	77
chr5	150412586	150412616 TAF15	ms.RBP56_HUMAN.69433.v1	
chr5	150406864	150406950 CNOT3	ms.CNOT3_HUMAN.101720.v1	78
chr5	150401289	150401361 ATF2	ms.ATF2_HUMAN.97245.v1	79
chr5	150409946	150409960 ATF2	ms.ATF2_HUMAN.97246.v1	
chr5	150412670	150412708 ATF2	ms.ATF2_HUMAN.97247.v1	
chr5	150409926	150409980 ATF1	ms.ATF1_HUMAN.62761.v1	80
chr5	150410731	150410751 ATF1	ms.ATF1_HUMAN.62762.v1	
chr5	150411458	150411502 ATF1	ms.ATF1_HUMAN.62763.v1	
chr5	150412967	150412985 ATF1	ms.ATF1_HUMAN.62764.v1	
chr5	150407921	150407983 ATF3	ms.ATF3_HUMAN.164693.v1	81
chr5	150409922	150410000 ATF3	ms.ATF3_HUMAN.164694.v1	
chr5	150401124	150401222 CDK9	ms.CDK9_HUMAN.280527.v1	82
chr5	150404497	150404595 CDK9	ms.CDK9_HUMAN.280528.v1	
chr5	150411239	150411337 CDK9	ms.CDK9_HUMAN.280529.v1	
chr5	150411415	150411513 CDK9	ms.CDK9_HUMAN.280530.v1	

chr5	150412376	150412412	CDK9	ms.CDK9_HUMAN.280531.v1	
chr5	150412441	150412539	CDK9	ms.CDK9_HUMAN.280532.v1	
chr5	150412548	150412632	CDK9	ms.CDK9_HUMAN.280533.v1	
chr5	150412645	150412695	CDK9	ms.CDK9_HUMAN.280534.v1	
chr5	150412798	150412896	CDK9	ms.CDK9_HUMAN.280535.v1	
chr5	150413128	150413228	CDK9	ms.CDK9_HUMAN.280536.v1	
chr5	150410166	150410266	KDM4A	ms.KDM4A_HUMAN.53697.v1	83
chr5	150412711	150412735	KDM4A	ms.KDM4A_HUMAN.53698.v1	
chr5	150413191	150413215	KDM4A	ms.KDM4A_HUMAN.53699.v1	
chr5	150402514	150402546	RBM22	ms.RBM22_HUMAN.119248.v1	
chr5	150406988	150407020	RBM22	ms.RBM22_HUMAN.119249.v1	84
chr5	150412834	150412866	RBM22	ms.RBM22_HUMAN.119250.v1	
chr5	150401419	150401507	DCP1A	ms.DCP1A_HUMAN.21481.v1	85
chr5	150402199	150402287	DCP1A	ms.DCP1A_HUMAN.21482.v1	
chr5	150405531	150405623	TP63	ms.P63_HUMAN.421422.v1	86
chr5	150406202	150406304	TP63	ms.P63_HUMAN.421423.v1	
chr5	150406835	150406927	TP63	ms.P63_HUMAN.421424.v1	
chr5	150401965	150402047	ARNT	ms.ARNT_HUMAN.188892.v1	87
chr5	150403162	150403254	SIRT6	ms.SIR6_HUMAN.120972.v1	88
chr5	150406187	150406257	PDX1	ms.PDX1_HUMAN.118716.v1	89
chr5	150413002	150413072	PDX1	ms.PDX1_HUMAN.118717.v1	
chr5	150409882	150409982	HIF3A	ms.HIF3A_HUMAN.34503.v1	90
chr5	150412740	150412840	PHF5A	ms.PHF5A_HUMAN.31555.v1	91
chr5	150400115	150400199	TCF3	ms.TFE2_HUMAN.107080.v1	92
chr5	150400781	150400865	TCF3	ms.TFE2_HUMAN.107081.v1	
chr5	150400944	150401028	TCF3	ms.TFE2_HUMAN.107082.v1	
chr5	150401208	150401282	TCF3	ms.TFE2_HUMAN.107083.v1	
chr5	150405331	150405415	TCF3	ms.TFE2_HUMAN.107084.v1	
chr5	150406216	150406300	TCF3	ms.TFE2_HUMAN.107085.v1	
chr5	150406952	150407036	TCF3	ms.TFE2_HUMAN.107086.v1	
chr5	150407561	150407645	TCF3	ms.TFE2_HUMAN.107087.v1	
chr5	150408493	150408575	TCF3	ms.TFE2_HUMAN.107088.v1	
chr5	150410123	150410207	TCF3	ms.TFE2_HUMAN.107089.v1	
chr5	150410480	150410554	TCF3	ms.TFE2_HUMAN.107090.v1	
chr5	150410533	150410607	TCF3	ms.TFE2_HUMAN.107091.v1	
chr5	150410860	150410944	TCF3	ms.TFE2_HUMAN.107092.v1	
chr5	150411356	150411440	TCF3	ms.TFE2_HUMAN.107093.v1	
chr5	150412706	150412722	TCF3	ms.TFE2_HUMAN.107094.v1	
chr5	150413118	150413202	TCF3	ms.TFE2_HUMAN.107095.v1	
chr5	150412649	150412733	SMAD4	ms.SMAD4_HUMAN.99181.v1	93
chr5	150401151	150401227	MYB	ms.MYB_HUMAN.159512.v1	94
chr5	150407560	150407640	MYB	ms.MYB_HUMAN.159513.v1	
chr5	150410223	150410323	MYB	ms.MYB_HUMAN.159514.v1	
chr5	150410445	150410525	MYB	ms.MYB_HUMAN.159515.v1	
chr5	150412839	150412915	MYB	ms.MYB_HUMAN.159516.v1	
chr5	150412675	150412725	BATF	ms.BATF_HUMAN.62545.v1	95
chr5	150400073	150400167	ERG	ms.ERG_HUMAN.675567.v1	96
chr5	150400543	150400637	ERG	ms.ERG_HUMAN.675568.v1	
chr5	150401016	150401110	ERG	ms.ERG_HUMAN.675569.v1	
chr5	150401188	150401272	ERG	ms.ERG_HUMAN.675570.v1	

chr5	150403084	150403178	ERG	ms.ERG_HUMAN.675571.v1	
chr5	150406904	150406988	ERG	ms.ERG_HUMAN.675572.v1	
chr5	150407030	150407116	ERG	ms.ERG_HUMAN.675573.v1	
chr5	150407218	150407233	ERG	ms.ERG_HUMAN.675574.v1	
chr5	150410058	150410081	ERG	ms.ERG_HUMAN.675575.v1	
chr5	150410599	150410693	ERG	ms.ERG_HUMAN.675576.v1	
chr5	150412552	150412626	ERG	ms.ERG_HUMAN.675577.v1	
chr5	150412614	150412673	ERG	ms.ERG_HUMAN.675578.v1	
chr5	150412739	150412833	ERG	ms.ERG_HUMAN.675579.v1	
chr5	150412831	150412927	ERG	ms.ERG_HUMAN.675580.v1	
chr5	150412905	150412956	ERG	ms.ERG_HUMAN.675581.v1	
chr5	150413030	150413109	ERG	ms.ERG_HUMAN.675582.v1	
chr5	150412165	150412257	MXD3	ms.MAD3_HUMAN.16073.v1	97
chr5	150405222	150405322	CRY1	ms.CRY1_HUMAN.50211.v1	98
chr5	150406264	150406364	CRY1	ms.CRY1_HUMAN.50212.v1	
chr5	150406768	150406868	CRY1	ms.CRY1_HUMAN.50213.v1	
chr5	150409922	150409998	OTX2	ms.OTX2_HUMAN.322862.v1	99
chr5	150410470	150410494	OTX2	ms.OTX2_HUMAN.322863.v1	
chr5	150410589	150410689	OTX2	ms.OTX2_HUMAN.322864.v1	
chr5	150410674	150410750	OTX2	ms.OTX2_HUMAN.322865.v1	
chr5	150410747	150410835	OTX2	ms.OTX2_HUMAN.322866.v1	
chr5	150400217	150400289	ZNF384	ms.ZN384_HUMAN.162533.v1	300
chr5	150408050	150408120	ZNF384	ms.ZN384_HUMAN.162534.v1	
chr5	150409697	150409769	ZNF384	ms.ZN384_HUMAN.162535.v1	
chr5	150410686	150410726	ZNF384	ms.ZN384_HUMAN.162536.v1	
chr5	150405295	150405355	RBAK	ms.RBAK_HUMAN.44506.v1	1
chr5	150401156	150401218	GATA2	ms.GATA2_HUMAN.899699.v1	2
chr5	150406874	150406946	GATA2	ms.GATA2_HUMAN.899700.v1	
chr5	150410218	150410306	GATA2	ms.GATA2_HUMAN.899701.v1	
chr5	150410404	150410492	GATA2	ms.GATA2_HUMAN.899702.v1	
chr5	150410901	150410965	GATA2	ms.GATA2_HUMAN.899703.v1	
chr5	150412608	150412664	GATA2	ms.GATA2_HUMAN.899704.v1	
chr5	150413044	150413132	GATA2	ms.GATA2_HUMAN.899705.v1	
chr5	150400751	150400843	TRIM28	ms.TIF1B_HUMAN.279133.v1	3
chr5	150409855	150409929	TRIM28	ms.TIF1B_HUMAN.279134.v1	
chr5	150410560	150410634	TRIM28	ms.TIF1B_HUMAN.279135.v1	
chr5	150412030	150412130	TRIM28	ms.TIF1B_HUMAN.279136.v1	
chr5	150412847	150412906	TRIM28	ms.TIF1B_HUMAN.279137.v1	
chr5	150409329	150409379	MAPK14	ms.MK14_HUMAN.38511.v1	4
chr5	150410617	150410651	VEZF1	ms.VEZF1_HUMAN.61926.v1	5
chr5	150412880	150412918	VEZF1	ms.VEZF1_HUMAN.61927.v1	
chr5	150410076	150410150	H2AFZ	ms.H2AZ_HUMAN.198106.v1	
chr5	150410268	150410314	H2AFZ	ms.H2AZ_HUMAN.198107.v1	
chr5	150410851	150410923	H2AFZ	ms.H2AZ_HUMAN.198108.v1	
chr5	150412531	150412603	H2AFZ	ms.H2AZ_HUMAN.198109.v1	
chr5	150405075	150405155	NCOR2	ms.NCOR2_HUMAN.79013.v1	6
chr5	150410537	150410603	NCOR2	ms.NCOR2_HUMAN.79014.v1	
chr5	150412804	150412896	SP5	ms.SP5_HUMAN.147507.v1	7
chr5	150399557	150399635	PAX5	ms.PAX5_HUMAN.113064.v1	8
chr5	150399894	150399936	PAX5	ms.PAX5_HUMAN.113065.v1	

chr5	150400379	150400467	PAX5	ms.PAX5_HUMAN.113066.v1	
chr5	150400484	150400592	PAX5	ms.PAX5_HUMAN.113067.v1	
chr5	150400855	150400951	PAX5	ms.PAX5_HUMAN.113068.v1	
chr5	150401264	150401318	PAX5	ms.PAX5_HUMAN.113069.v1	
chr5	150401857	150401963	PAX5	ms.PAX5_HUMAN.113070.v1	
chr5	150402264	150402370	PAX5	ms.PAX5_HUMAN.113071.v1	
chr5	150403003	150403109	PAX5	ms.PAX5_HUMAN.113072.v1	
chr5	150404822	150404865	PAX5	ms.PAX5_HUMAN.113073.v1	
chr5	150405375	150405471	PAX5	ms.PAX5_HUMAN.113074.v1	
chr5	150406997	150407103	PAX5	ms.PAX5_HUMAN.113075.v1	
chr5	150407383	150407505	PAX5	ms.PAX5_HUMAN.113076.v1	
chr5	150408585	150408681	PAX5	ms.PAX5_HUMAN.113077.v1	
chr5	150409910	150409949	PAX5	ms.PAX5_HUMAN.113078.v1	
chr5	150410833	150410920	PAX5	ms.PAX5_HUMAN.113079.v1	
chr5	150411730	150411826	PAX5	ms.PAX5_HUMAN.113080.v1	
chr5	150412264	150412360	PAX5	ms.PAX5_HUMAN.113081.v1	
chr5	150412667	150412732	PAX5	ms.PAX5_HUMAN.113082.v1	
chr5	150413124	150413151	PAX5	ms.PAX5_HUMAN.113083.v1	
chr5	150405497	150405589	GATA3	ms.GATA3_HUMAN.396899.v1	9
chr5	150409754	150409846	GATA3	ms.GATA3_HUMAN.396900.v1	
chr5	150412637	150412701	GATA3	ms.GATA3_HUMAN.396901.v1	
chr5	150410111	150410201	MAZ	ms.MAZ_HUMAN.179831.v1	10
chr5	150408358	150408404	PKNOX1	ms.PKNX1_HUMAN.62800.v1	11
chr5	150409954	150409986	PKNOX1	ms.PKNX1_HUMAN.62801.v1	
chr5	150401946	150402010	HDGFL3	ms.HDGR3_HUMAN.80973.v1	12
chr5	150402129	150402187	HDGFL3	ms.HDGR3_HUMAN.80974.v1	
chr5	150407991	150408055	HDGFL3	ms.HDGR3_HUMAN.80975.v1	
chr5	150401738	150401828	AR	ms.ANDR_HUMAN.2136818.v1	13
chr5	150402722	150402804	AR	ms.ANDR_HUMAN.2136819.v1	
chr5	150403429	150403475	AR	ms.ANDR_HUMAN.2136820.v1	
chr5	150404218	150404322	AR	ms.ANDR_HUMAN.2136821.v1	
chr5	150404545	150404607	AR	ms.ANDR_HUMAN.2136822.v1	
chr5	150406172	150406288	AR	ms.ANDR_HUMAN.2136823.v1	
chr5	150407038	150407131	AR	ms.ANDR_HUMAN.2136824.v1	
chr5	150407206	150407296	AR	ms.ANDR_HUMAN.2136825.v1	
chr5	150409184	150409300	AR	ms.ANDR_HUMAN.2136826.v1	
chr5	150409899	150410003	AR	ms.ANDR_HUMAN.2136827.v1	
chr5	150410160	150410264	AR	ms.ANDR_HUMAN.2136828.v1	
chr5	150410255	150410359	AR	ms.ANDR_HUMAN.2136829.v1	
chr5	150410374	150410464	AR	ms.ANDR_HUMAN.2136830.v1	
chr5	150410555	150410675	AR	ms.ANDR_HUMAN.2136831.v1	
chr5	150411670	150411774	AR	ms.ANDR_HUMAN.2136832.v1	
chr5	150412641	150412733	AR	ms.ANDR_HUMAN.2136833.v1	
chr5	150412835	150412865	AR	ms.ANDR_HUMAN.2136834.v1	
chr5	150412368	150412474	RARA	ms.RARA_HUMAN.174938.v1	14
chr5	150412717	150412811	RARA	ms.RARA_HUMAN.174939.v1	
chr5	150412809	150412915	RARA	ms.RARA_HUMAN.174940.v1	
chr5	150405963	150406043	RELB	ms.RELB_HUMAN.97590.v1	15
chr5	150410688	150410766	RELB	ms.RELB_HUMAN.97591.v1	
chr5	150412598	150412678	RELB	ms.RELB_HUMAN.97592.v1	

chr5	150412852	150412872	RELB	ms.RELB_HUMAN.97593.v1	
chr5	150406861	150406892	GLIS1	ms.GLIS1_HUMAN.90820.v1	16
chr5	150409935	150409974	GLIS1	ms.GLIS1_HUMAN.90821.v1	
chr5	150410228	150410294	GLIS1	ms.GLIS1_HUMAN.90822.v1	
chr5	150412690	150412740	HEY1	ms.HEY1_HUMAN.61256.v1	17
chr5	150401133	150401193	GATA1	ms.GATA1_HUMAN.249719.v1	18
chr5	150412579	150412639	GATA1	ms.GATA1_HUMAN.249720.v1	
chr5	150409835	150409919	TCF7L2	ms.TF7L2_HUMAN.155691.v1	19
chr5	150412614	150412698	TCF7L2	ms.TF7L2_HUMAN.155692.v1	
chr5	150401275	150401327	SMAD5	ms.SMAD5_HUMAN.19753.v1	20
chr5	150404242	150404328	SMAD5	ms.SMAD5_HUMAN.19754.v1	
chr5	150405291	150405377	SMAD5	ms.SMAD5_HUMAN.19755.v1	
chr5	150412686	150412738	SMAD5	ms.SMAD5_HUMAN.19756.v1	
chr5	150412622	150412706	NONO	ms.NONO_HUMAN.35259.v1	21
chr5	150413130	150413170	TERF1	ms.TERF1_HUMAN.3016.v1	22
chr5	150410674	150410742	POU2F1	ms.PO2F1_HUMAN.41224.v1	23
chr5	150412663	150412733	TCF7	ms.TCF7_HUMAN.22014.v1	24
chr5	150412685	150412765	MAF	ms.MAF_HUMAN.78932.v1	25
chr5	150404247	150404325	TFAP4	ms.TFAP4_HUMAN.168048.v1	26
chr5	150410008	150410078	TFAP4	ms.TFAP4_HUMAN.168049.v1	
chr5	150411464	150411528	TFAP4	ms.TFAP4_HUMAN.168050.v1	
chr5	150399600	150399712	CTCF	ms.CTCF_HUMAN.1840028.v1	27
chr5	150399690	150399792	CTCF	ms.CTCF_HUMAN.1840029.v1	
chr5	150399835	150399937	CTCF	ms.CTCF_HUMAN.1840030.v1	
chr5	150400286	150400398	CTCF	ms.CTCF_HUMAN.1840031.v1	
chr5	150400868	150400953	CTCF	ms.CTCF_HUMAN.1840032.v1	
chr5	150401226	150401338	CTCF	ms.CTCF_HUMAN.1840033.v1	
chr5	150401665	150401767	CTCF	ms.CTCF_HUMAN.1840034.v1	
chr5	150401850	150401952	CTCF	ms.CTCF_HUMAN.1840035.v1	
chr5	150402392	150402494	CTCF	ms.CTCF_HUMAN.1840036.v1	
chr5	150402708	150402810	CTCF	ms.CTCF_HUMAN.1840037.v1	
chr5	150402807	150402927	CTCF	ms.CTCF_HUMAN.1840038.v1	
chr5	150404126	150404228	CTCF	ms.CTCF_HUMAN.1840039.v1	
chr5	150404365	150404399	CTCF	ms.CTCF_HUMAN.1840040.v1	
chr5	150405414	150405532	CTCF	ms.CTCF_HUMAN.1840041.v1	
chr5	150406803	150406905	CTCF	ms.CTCF_HUMAN.1840042.v1	
chr5	150407452	150407538	CTCF	ms.CTCF_HUMAN.1840043.v1	
chr5	150408015	150408071	CTCF	ms.CTCF_HUMAN.1840044.v1	
chr5	150408507	150408548	CTCF	ms.CTCF_HUMAN.1840045.v1	
chr5	150409311	150409413	CTCF	ms.CTCF_HUMAN.1840046.v1	
chr5	150409896	150409980	CTCF	ms.CTCF_HUMAN.1840047.v1	
chr5	150410192	150410212	CTCF	ms.CTCF_HUMAN.1840048.v1	
chr5	150410241	150410319	CTCF	ms.CTCF_HUMAN.1840049.v1	
chr5	150410349	150410451	CTCF	ms.CTCF_HUMAN.1840050.v1	
chr5	150410748	150410850	CTCF	ms.CTCF_HUMAN.1840051.v1	
chr5	150410859	150410961	CTCF	ms.CTCF_HUMAN.1840052.v1	
chr5	150411155	150411257	CTCF	ms.CTCF_HUMAN.1840053.v1	
chr5	150411316	150411418	CTCF	ms.CTCF_HUMAN.1840054.v1	
chr5	150411463	150411565	CTCF	ms.CTCF_HUMAN.1840055.v1	
chr5	150411836	150411938	CTCF	ms.CTCF_HUMAN.1840056.v1	

chr5	150412138	150412240 CTCF	ms.CTCF_HUMAN.1840057.v1	
chr5	150412367	150412401 CTCF	ms.CTCF_HUMAN.1840058.v1	
chr5	150412677	150412699 CTCF	ms.CTCF_HUMAN.1840059.v1	
chr5	150412796	150412821 CTCF	ms.CTCF_HUMAN.1840060.v1	
chr5	150412920	150413024 CTCF	ms.CTCF_HUMAN.1840061.v1	
chr5	150413159	150413200 CTCF	ms.CTCF_HUMAN.1840062.v1	
chr5	150400398	150400486 FANCD2	ms.FACD2_HUMAN.143422.v1	28
chr5	150412722	150412766 CEBPD	ms.CEBPD_HUMAN.41875.v1	29
chr5	150409875	150409963 ZIC5	ms.ZIC5_HUMAN.33704.v1	30
chr5	150402565	150402659 CEBPA	ms.CEBPA_HUMAN.397582.v1	31
chr5	150410146	150410240 CEBPA	ms.CEBPA_HUMAN.397583.v1	
chr5	150410609	150410680 CEBPA	ms.CEBPA_HUMAN.397584.v1	
chr5	150410741	150410835 CEBPA	ms.CEBPA_HUMAN.397585.v1	
chr5	150412019	150412045 CEBPA	ms.CEBPA_HUMAN.397586.v1	
chr5	150412204	150412302 CEBPA	ms.CEBPA_HUMAN.397587.v1	
chr5	150412383	150412421 CEBPA	ms.CEBPA_HUMAN.397588.v1	
chr5	150412489	150412583 CEBPA	ms.CEBPA_HUMAN.397589.v1	
chr5	150412667	150412737 CEBPA	ms.CEBPA_HUMAN.397590.v1	
chr5	150410631	150410731 ZNF362	ms.ZN362_HUMAN.3751.v1	32
chr5	150407343	150407429 FOXM1	ms.FOXM1_HUMAN.157639.v1	33
chr5	150409866	150409944 FOXM1	ms.FOXM1_HUMAN.157640.v1	
chr5	150410389	150410485 FOXM1	ms.FOXM1_HUMAN.157641.v1	
chr5	150412693	150412771 FOXM1	ms.FOXM1_HUMAN.157642.v1	
chr5	150412864	150412950 FOXM1	ms.FOXM1_HUMAN.157643.v1	
chr5	150413044	150413111 FOXM1	ms.FOXM1_HUMAN.157644.v1	
chr5	150402949	150403023 SNAI2	ms.SNAI2_HUMAN.271102.v1	34
chr5	150406264	150406314 SNAI2	ms.SNAI2_HUMAN.271103.v1	
chr5	150410168	150410222 SNAI2	ms.SNAI2_HUMAN.271104.v1	
chr5	150412902	150412952 SNAI2	ms.SNAI2_HUMAN.271105.v1	
chr5	150403123	150403143 HNRNPL	ms.HNRPL_HUMAN.46855.v1	35
chr5	150406909	150406929 HNRNPL	ms.HNRPL_HUMAN.46856.v1	
chr5	150409884	150409968 HNRNPL	ms.HNRPL_HUMAN.46857.v1	
chr5	150410709	150410740 HNRNPL	ms.HNRPL_HUMAN.46858.v1	
chr5	150412593	150412677 HNRNPL	ms.HNRPL_HUMAN.46859.v1	
chr5	150412884	150412968 HNRNPL	ms.HNRPL_HUMAN.46860.v1	
chr5	150410181	150410255 MCM7	ms.MCM7_HUMAN.160777.v1	36
chr5	150401948	150402042 E2F1	ms.E2F1_HUMAN.252034.v1	37
chr5	150409910	150410010 E2F1	ms.E2F1_HUMAN.252035.v1	
chr5	150410682	150410782 E2F1	ms.E2F1_HUMAN.252036.v1	
chr5	150411436	150411536 E2F1	ms.E2F1_HUMAN.252037.v1	
chr5	150412919	150413019 E2F1	ms.E2F1_HUMAN.252038.v1	
chr5	150410070	150410146 STAT1	ms.STAT1_HUMAN.336757.v1	38
chr5	150410669	150410745 STAT1	ms.STAT1_HUMAN.336758.v1	
chr5	150412467	150412531 STAT1	ms.STAT1_HUMAN.336759.v1	
chr5	150412641	150412750 STAT1	ms.STAT1_HUMAN.336760.v1	
chr5	150412841	150412897 STAT1	ms.STAT1_HUMAN.336761.v1	
chr5	150412903	150412979 STAT1	ms.STAT1_HUMAN.336762.v1	
chr5	150407980	150408050 JUNB	ms.JUNB_HUMAN.194984.v1	39
chr5	150413076	150413158 JUNB	ms.JUNB_HUMAN.194985.v1	
chr5	150413232	150413314 JUNB	ms.JUNB_HUMAN.194986.v1	

chr5	150401475	150401553	STAT5A	ms.STA5A_HUMAN.234445.v1	40
chr5	150406436	150406514	STAT5A	ms.STA5A_HUMAN.234446.v1	
chr5	150407140	150407218	STAT5A	ms.STA5A_HUMAN.234447.v1	
chr5	150407471	150407545	STAT5A	ms.STA5A_HUMAN.234448.v1	
chr5	150410386	150410464	STAT5A	ms.STA5A_HUMAN.234449.v1	
chr5	150411220	150411298	STAT5A	ms.STA5A_HUMAN.234450.v1	
chr5	150412654	150412702	STAT5A	ms.STA5A_HUMAN.234451.v1	
chr5	150403262	150403326	CBX5	ms.CBX5_HUMAN.12085.v1	41
chr5	150412670	150412710	CBX5	ms.CBX5_HUMAN.12086.v1	
chr5	150407003	150407023	HEXIM1	ms.HEXI1_HUMAN.81904.v1	42
chr5	150412612	150412632	HEXIM1	ms.HEXI1_HUMAN.81905.v1	
chr5	150412657	150412677	U2AF1	ms.U2AF1_HUMAN.34658.v1	43
chr5	150400797	150400885	KLF5	ms.KLF5_HUMAN.106898.v1	44
chr5	150401987	150402034	FOXA1	ms.FOXA1_HUMAN.1807254.v1	45
chr5	150404570	150404672	FOXA1	ms.FOXA1_HUMAN.1807255.v1	
chr5	150406857	150406959	FOXA1	ms.FOXA1_HUMAN.1807256.v1	
chr5	150407278	150407349	FOXA1	ms.FOXA1_HUMAN.1807257.v1	
chr5	150407648	150407758	FOXA1	ms.FOXA1_HUMAN.1807258.v1	
chr5	150408993	150409095	FOXA1	ms.FOXA1_HUMAN.1807259.v1	
chr5	150409921	150409951	FOXA1	ms.FOXA1_HUMAN.1807260.v1	
chr5	150410332	150410382	FOXA1	ms.FOXA1_HUMAN.1807261.v1	
chr5	150410471	150410514	FOXA1	ms.FOXA1_HUMAN.1807262.v1	
chr5	150410661	150410734	FOXA1	ms.FOXA1_HUMAN.1807263.v1	
chr5	150411023	150411133	FOXA1	ms.FOXA1_HUMAN.1807264.v1	
chr5	150411142	150411244	FOXA1	ms.FOXA1_HUMAN.1807265.v1	
chr5	150411190	150411300	FOXA1	ms.FOXA1_HUMAN.1807266.v1	
chr5	150411357	150411467	FOXA1	ms.FOXA1_HUMAN.1807267.v1	
chr5	150412522	150412602	FOXA1	ms.FOXA1_HUMAN.1807268.v1	
chr5	150413063	150413142	FOXA1	ms.FOXA1_HUMAN.1807269.v1	
chr5	150413209	150413321	FOXA1	ms.FOXA1_HUMAN.1807270.v1	
chr5	150401227	150401309	TCF12	ms.HTF4_HUMAN.238915.v1	46
chr5	150401739	150401821	TCF12	ms.HTF4_HUMAN.238916.v1	
chr5	150401977	150402059	TCF12	ms.HTF4_HUMAN.238917.v1	
chr5	150405382	150405460	TCF12	ms.HTF4_HUMAN.238918.v1	
chr5	150406694	150406776	TCF12	ms.HTF4_HUMAN.238919.v1	
chr5	150407570	150407652	TCF12	ms.HTF4_HUMAN.238920.v1	
chr5	150408575	150408653	TCF12	ms.HTF4_HUMAN.238921.v1	
chr5	150410143	150410221	TCF12	ms.HTF4_HUMAN.238922.v1	
chr5	150410486	150410564	TCF12	ms.HTF4_HUMAN.238923.v1	
chr5	150410560	150410638	TCF12	ms.HTF4_HUMAN.238924.v1	
chr5	150411182	150411260	TCF12	ms.HTF4_HUMAN.238925.v1	
chr5	150412707	150412733	TCF12	ms.HTF4_HUMAN.238926.v1	
chr5	150412744	150412822	TCF12	ms.HTF4_HUMAN.238927.v1	
chr5	150412859	150412957	TCF12	ms.HTF4_HUMAN.238928.v1	
chr5	150403088	150403176	SSRP1	ms.SSRP1_HUMAN.410411.v1	47
chr5	150404660	150404748	SSRP1	ms.SSRP1_HUMAN.410412.v1	
chr5	150406214	150406302	SSRP1	ms.SSRP1_HUMAN.410413.v1	
chr5	150410205	150410293	SSRP1	ms.SSRP1_HUMAN.410414.v1	
chr5	150400856	150400948	MTA3	ms.MTA3_HUMAN.12197.v1	48
chr5	150401187	150401265	MTA3	ms.MTA3_HUMAN.12198.v1	

chr5	150410830	150410922	MTA3	ms.MTA3_HUMAN.12199.v1	
chr5	150412605	150412683	MTA3	ms.MTA3_HUMAN.12200.v1	
chr5	150410222	150410242	CCAR2	ms.CCAR2_HUMAN.30077.v1	49
chr5	150412620	150412640	CCAR2	ms.CCAR2_HUMAN.30078.v1	
chr5	150412854	150412874	CCAR2	ms.CCAR2_HUMAN.30079.v1	
chr5	150401832	150401896	PARP1	ms.PARP1_HUMAN.144307.v1	50
chr5	150409822	150409914	PARP1	ms.PARP1_HUMAN.144308.v1	
chr5	150412572	150412664	PARP1	ms.PARP1_HUMAN.144309.v1	
chr5	150413123	150413215	PARP1	ms.PARP1_HUMAN.144310.v1	
chr5	150399818	150399906	IKZF1	ms.IKZF1_HUMAN.196600.v1	51
chr5	150401793	150401863	IKZF1	ms.IKZF1_HUMAN.196601.v1	
chr5	150409980	150410050	IKZF1	ms.IKZF1_HUMAN.196602.v1	
chr5	150410031	150410101	IKZF1	ms.IKZF1_HUMAN.196603.v1	
chr5	150410266	150410338	IKZF1	ms.IKZF1_HUMAN.196604.v1	
chr5	150410424	150410494	IKZF1	ms.IKZF1_HUMAN.196605.v1	
chr5	150411363	150411435	IKZF1	ms.IKZF1_HUMAN.196606.v1	
chr5	150412557	150412633	IKZF1	ms.IKZF1_HUMAN.196607.v1	
chr5	150412711	150412800	IKZF1	ms.IKZF1_HUMAN.196608.v1	
chr5	150412587	150412661	ZBTB11	ms.ZBT11_HUMAN.15390.v1	52
chr5	150409698	150409824	ZNF22	ms.ZNF22_HUMAN.18973.v1	53
chr5	150410626	150410726	ZNF22	ms.ZNF22_HUMAN.18974.v1	
chr5	150403047	150403137	MYCN	ms.MYCN_HUMAN.537836.v1	54
chr5	150404251	150404341	MYCN	ms.MYCN_HUMAN.537837.v1	
chr5	150406158	150406248	MYCN	ms.MYCN_HUMAN.537838.v1	
chr5	150406774	150406868	MYCN	ms.MYCN_HUMAN.537839.v1	
chr5	150406922	150407024	MYCN	ms.MYCN_HUMAN.537840.v1	
chr5	150409865	150409973	MYCN	ms.MYCN_HUMAN.537841.v1	
chr5	150410189	150410279	MYCN	ms.MYCN_HUMAN.537842.v1	
chr5	150410644	150410734	MYCN	ms.MYCN_HUMAN.537843.v1	
chr5	150412140	150412230	MYCN	ms.MYCN_HUMAN.537844.v1	
chr5	150412546	150412668	MYCN	ms.MYCN_HUMAN.537845.v1	
chr5	150400842	150400934	HDAC6	ms.HDAC6_HUMAN.18345.v1	55
chr5	150401896	150401988	HDAC6	ms.HDAC6_HUMAN.18346.v1	
chr5	150408062	150408150	HDAC6	ms.HDAC6_HUMAN.18347.v1	
chr5	150412323	150412359	HDAC6	ms.HDAC6_HUMAN.18348.v1	
chr5	150412591	150412627	HDAC6	ms.HDAC6_HUMAN.18349.v1	
chr5	150412450	150412516	STAT4	ms.STAT4_HUMAN.38676.v1	56
chr5	150409931	150409952	USF2	ms.USF2_HUMAN.91545.v1	57
chr5	150410718	150410763	USF2	ms.USF2_HUMAN.91546.v1	
chr5	150412750	150412804	USF2	ms.USF2_HUMAN.91547.v1	
chr5	150409902	150409972	JMJD6	ms.JMJD6_HUMAN.44214.v1	58
chr5	150410700	150410770	JMJD6	ms.JMJD6_HUMAN.44215.v1	
chr5	150411462	150411532	JMJD6	ms.JMJD6_HUMAN.44216.v1	
chr5	150399680	150399776	BCL6	ms.BCL6_HUMAN.128037.v1	59
chr5	150400621	150400660	BCL6	ms.BCL6_HUMAN.128038.v1	
chr5	150409921	150410017	BCL6	ms.BCL6_HUMAN.128039.v1	
chr5	150410209	150410287	BCL6	ms.BCL6_HUMAN.128040.v1	
chr5	150410263	150410359	BCL6	ms.BCL6_HUMAN.128041.v1	
chr5	150410384	150410480	BCL6	ms.BCL6_HUMAN.128042.v1	
chr5	150410549	150410591	BCL6	ms.BCL6_HUMAN.128043.v1	

chr5	150411498	150411580 BCL6	ms.BCL6_HUMAN.128044.v1	
chr5	150412596	150412692 BCL6	ms.BCL6_HUMAN.128045.v1	
chr5	150412668	150412764 BCL6	ms.BCL6_HUMAN.128046.v1	
chr5	150412850	150412932 BCL6	ms.BCL6_HUMAN.128047.v1	
chr5	150412023	150412067 CEBPG	ms.CEBPG_HUMAN.74054.v1	60
chr5	150402210	150402266 USF1	ms.USF1_HUMAN.110413.v1	61
chr5	150406264	150406320 USF1	ms.USF1_HUMAN.110414.v1	
chr5	150409895	150409945 USF1	ms.USF1_HUMAN.110415.v1	
chr5	150400676	150400760 NFATC1	ms.NFAC1_HUMAN.62287.v1	62
chr5	150407424	150407508 NFATC1	ms.NFAC1_HUMAN.62288.v1	
chr5	150408574	150408658 NFATC1	ms.NFAC1_HUMAN.62289.v1	
chr5	150411390	150411474 NFATC1	ms.NFAC1_HUMAN.62290.v1	
chr5	150412711	150412797 CCND2	ms.CCND2_HUMAN.8687.v1	63
chr5	150399586	150399674 SMC3	ms.SMC3_HUMAN.310692.v1	64
chr5	150407044	150407112 SMC3	ms.SMC3_HUMAN.310693.v1	
chr5	150407432	150407520 SMC3	ms.SMC3_HUMAN.310694.v1	
chr5	150409833	150409921 SMC3	ms.SMC3_HUMAN.310695.v1	
chr5	150410376	150410464 SMC3	ms.SMC3_HUMAN.310696.v1	
chr5	150410741	150410829 SMC3	ms.SMC3_HUMAN.310697.v1	
chr5	150399732	150399810 NFYA	ms.NFYA_HUMAN.196203.v1	65
chr5	150409942	150409975 NFYA	ms.NFYA_HUMAN.196204.v1	
chr5	150410701	150410742 NFYA	ms.NFYA_HUMAN.196205.v1	
chr5	150412642	150412660 NFYA	ms.NFYA_HUMAN.196206.v1	
chr5	150412702	150412788 NFYA	ms.NFYA_HUMAN.196207.v1	
chr5	150412872	150412950 NFYA	ms.NFYA_HUMAN.196208.v1	
chr5	150400656	150400734 ZIC2	ms.ZIC2_HUMAN.34771.v1	66
chr5	150406867	150406945 ZIC2	ms.ZIC2_HUMAN.34772.v1	
chr5	150409908	150409984 ZIC2	ms.ZIC2_HUMAN.34773.v1	
chr5	150410667	150410739 ZIC2	ms.ZIC2_HUMAN.34774.v1	
chr5	150410503	150410603 GCM2	ms.GCM2_HUMAN.26516.v1	67
chr5	150412836	150412922 ETV5	ms.ETV5_HUMAN.57324.v1	68
chr5	150406738	150406834 EGR1	ms.EGR1_HUMAN.84371.v1	69
chr5	150407940	150408038 EGR1	ms.EGR1_HUMAN.84372.v1	
chr5	150408571	150408667 EGR1	ms.EGR1_HUMAN.84373.v1	
chr5	150412638	150412729 EGR1	ms.EGR1_HUMAN.84374.v1	
chr5	150413106	150413178 EGR1	ms.EGR1_HUMAN.84375.v1	
chr5	150409753	150409853 ATF7IP	ms.MCAF1_HUMAN.31049.v1	70
chr5	150401006	150401100 KDM1A	ms.KDM1A_HUMAN.383122.v1	71
chr5	150403340	150403368 KDM1A	ms.KDM1A_HUMAN.383123.v1	
chr5	150410398	150410492 KDM1A	ms.KDM1A_HUMAN.383124.v1	
chr5	150411037	150411131 KDM1A	ms.KDM1A_HUMAN.383125.v1	
chr5	150411248	150411342 KDM1A	ms.KDM1A_HUMAN.383126.v1	
chr5	150411851	150411951 KDM1A	ms.KDM1A_HUMAN.383127.v1	
chr5	150413258	150413352 KDM1A	ms.KDM1A_HUMAN.383128.v1	
chr5	150413393	150413445 KDM1A	ms.KDM1A_HUMAN.383129.v1	
chr5	150412476	150412564 CXXC1	ms.CXXC1_HUMAN.14668.v1	72
chr5	150412653	150412741 GATAD2A	ms.P66A_HUMAN.225472.v1	73
chr5	150409903	150409987 TBP	ms.TBP_HUMAN.213957.v1	74
chr5	150410205	150410315 TBP	ms.TBP_HUMAN.213958.v1	
chr5	150410741	150410825 TBP	ms.TBP_HUMAN.213959.v1	

chr5	150412747	150412785 TBP	ms.TBP_HUMAN.213960.v1	
chr5	150403904	150403970 SIX5	ms.SIX5_HUMAN.17330.v1	75
chr5	150412950	150413016 SIX5	ms.SIX5_HUMAN.17331.v1	
				375

Supplementary Table 3

Gene	Description	Confidence
RFX5	regulatory factor X, 5 (influences HLA class II expression)	0.9999
NFYC	nuclear transcription factor Y, gamma	0.9981
CREB1	cAMP responsive element binding protein 1	0.9893
NFYA	nuclear transcription factor Y, alpha	0.9832
RFXANK	regulatory factor X-associated ankyrin-containing protein	0.9061
NFYB	nuclear transcription factor Y, beta	0.8608
STAT1	signal transducer and activator of transcription 1, 91kDa	0.5640
SP1	Sp1 transcription factor	0.3411
TP53	tumor protein p53	0.2508
ETS2	v-ets erythroblastosis virus E26 oncogene homolog 2 (avian)	0.1587
IRF1	interferon regulatory factor 1	0.1502
ETS1	v-ets erythroblastosis virus E26 oncogene homolog 1 (avian)	0.1366
RELA	v-rel reticuloendotheliosis viral oncogene homolog A (avian)	0.1359
IRF8	interferon regulatory factor 8	0.1097
NR1H3	nuclear receptor subfamily 1, group H, member 3	0.1074
GATA3	GATA binding protein 3	0.1055
HOXB3	homeobox B3	0.1022
ZFP36L1	zinc finger protein 36, C3H type-like 1	0.1013
CEBPB	CCAAT/enhancer binding protein (C/EBP), beta	0.1010

Color code explanation:

CIITA associated

no binding site within 500bp of CD74 gene

CD74 transcriptional regulation

https://pathwaynet.princeton.edu/predictions/gene/?network=human-transcriptional-regulation&gene

1/11/2024

References cited in Supplementary file.

1. Marimuthu R, Francis H, Dervish S, Li SCH, Medbury H, and Williams H (2018) Characterization of human monocyte subsets by whole blood flow cytometry analysis. *J Vis Exp.* https://doi.org/10.3791/57941.

2. Cano-Gamez E, Soskic B, Roumeliotis TI, So E, Smyth DJ, Baldrighi M, Willé D, Nakic N, Esparza-Gordillo J, Larminie CGC, Bronson PG, Tough DF, Rowan WC, Choudhary JS, and Trynka G (2020) Single-cell transcriptomics identifies an effectorness gradient shaping the response of CD4(+) T cells to cytokines. *Nat Commun* 11, 1801. https://doi.org/10.1038/s41467-020-15543-y.

3. Wolf T, Jin W, Zoppi G, Vogel IA, Akhmedov M, Bleck CKE, Beltraminelli T, Rieckmann JC, Ramirez NJ, Benevento M et al (2020) Dynamics in protein translation sustaining T cell preparedness. *Nat Immunol* 21:927–937. https://doi.org/10.1038/s41590- 020- 0714-5.

4. Szklarczyk D, Gable AL, Nastou KC, Lyon D, Kirsch R, Pyysalo S, Doncheva NT, Legeay M, Fang T, Bork P, Jensen LJ, and von Mering C (2021) The STRING database in 2021: customizable protein-protein networks, and functional characterization of user-uploaded gene/measurement sets. *Nucleic Acids Res* 49, D605-d612. https://doi.org/-10.1093/nar/gkaa1074.

5. Yevshin I, Sharipov R, Kolmykov S, Kondrakhin Y, and Kolpakov F (2019) GTRD: a database on gene transcription regulation-2019 update. *Nucleic Acids Res* 47, D100-d105. https://doi. org/10.1093/nar/gky1128.

6. Wong AK, Park CY, Greene CS, Bongo LA, Guan Y, and Troyanskaya OG (2012) IMP: a multi-species functional genomics portal for integration, visualization and prediction of protein functions and networks. *Nucleic Acids Res* 40, W484-490. https://doi.org/10.1093/nar/gks458.

7.2 Supplementary data for Spiller, L. *et al*, 2023

Supplementary Materials for

Plant MDL proteins synergize with the cytokine MIF at CXCR2 and CXCR4 receptors in human cells

Lukas Spiller *et al.*

Corresponding author: Elias Lolis, elias.lolis@yale.edu; Jürgen Bernhagen,
juergen.bernhagen@med.uni-muenchen.de; Ralph Panstruga, panstruga@bio1.rwth-aachen.de

The PDF file includes:

Figs. S1 to S17
Tables S1 and S2

Other Supplementary Material for this manuscript includes the following:

MDAR Reproducibility Checklist
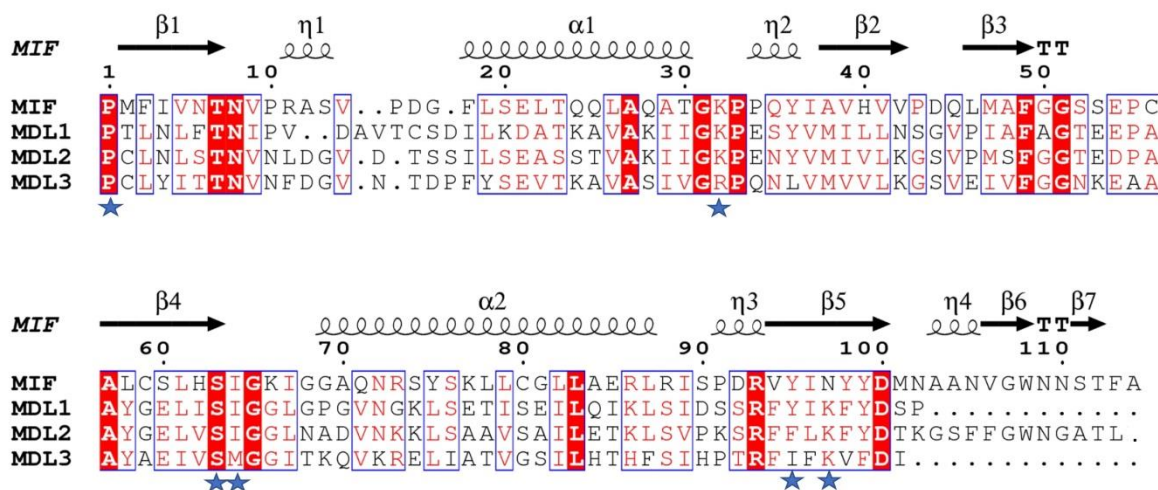
Fig. S1. Structure-based sequence alignment of the *Arabidopsis* MDLs and human MIF. The ESpript application (35) was used to align the structures. The red boxes highlight the invariant residues among the three MDLs and MIF. Similar residues and regions are surrounded by blue boxes. The secondary structure elements are noted above the sequences, with the 3_{10}-helix represented by the η symbol, helices with squiggles, β-strands with arrows, and β-turns with TT letters. Blue stars below the aligned sequences indicate the position of residues in the tautomerase catalytic site of MIF. The last 12 and 9 residues of MDL1 and MDL3, respectively, are not aligned due to the lack of electron density. Some MIF studies refer to the initiating Met[1], which is later posttranslationally cleaved, as the first residue, but in this and some other studies, Pro[1] is used as the first residue. After residue 17, there is one extra amino acid in a loop for all three MDLs relative to MIF, resulting in residue numbers for MDLs that are greater than those for the corresponding residues in MIF.

Protein	LPS concentration in EU/ml	LPS concentration in ng/ml
MIF-6xHIS	1.36 +/- 0.16	0.136 +/- 0.016
MDL1-6xHIS	1.43 +/- 0.15	0.143 +/- 0.015
MDL2-6xHIS	1.45 +/- 0.23	0.145 +/- 0.023
MDL3-6xHIS	1.38 +/- 0.11	0.138 +/- 0.011
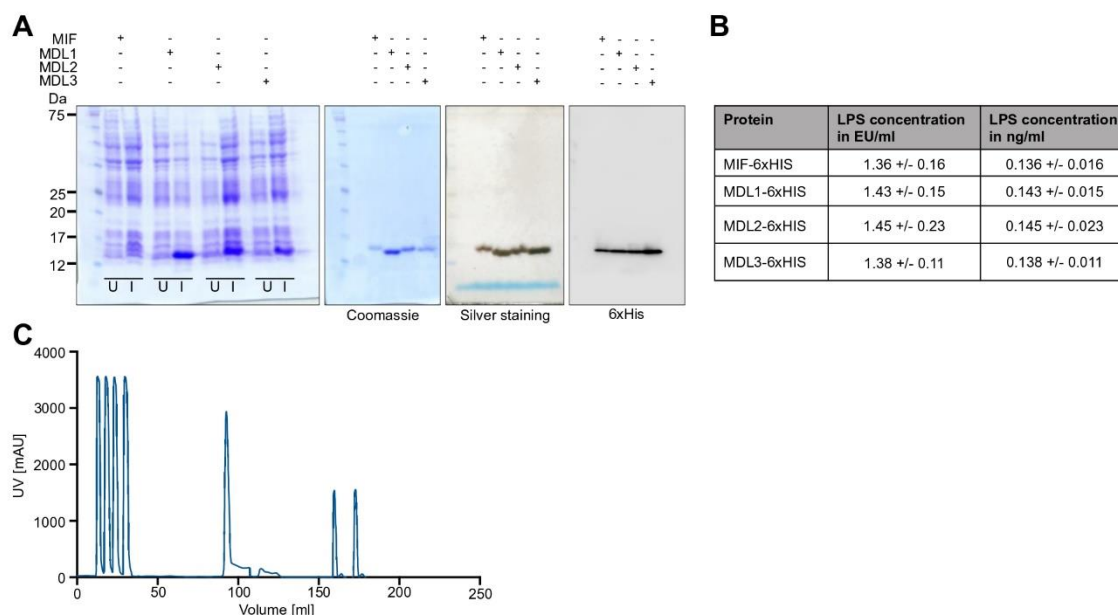
Fig. S2. Expression and purification of recombinant MIF and MDL proteins. (**A**) Electro-phoretic analysis of crude protein lysates before (uninduced, [U]) and after induction [I] with isopropyl-β-D-thiogalactopyranoside (IPTG). Cell lysates are shown with Coomassie staining. Purified proteins after immobilized metal affinity chromatography (IMAC) and subsequent size exclusion chromatography (SEC) are also shown using Coomassie staining, silver staining, and immunoblotting with an antibody directed against the hexahistidine tag. The blots shown are representative of at least n = 3 independent experiments. (**B**) Quantification of lipopolysaccharide (LPS) content in purified recombinant proteins using a chromogenic endotoxin detection assay. LPS concentrations are given in endotoxin units (EU)/mL and ng/mL. Values are from three biological replicates (n=3). (**C**) Chromatogram of IMAC and subsequent SEC purification shown for MDL1 as an example. Injections of the bacterial lysate (up to 50 mL) are followed in the course of the elution of the hexahistidine-tagged protein by an imidazole gradient (around 100 mL). For further purification and buffer exchange, this step was followed by two runs of SEC (from 150 mL onward). The chromatogram is representative of at least n = 3 independent experiments.
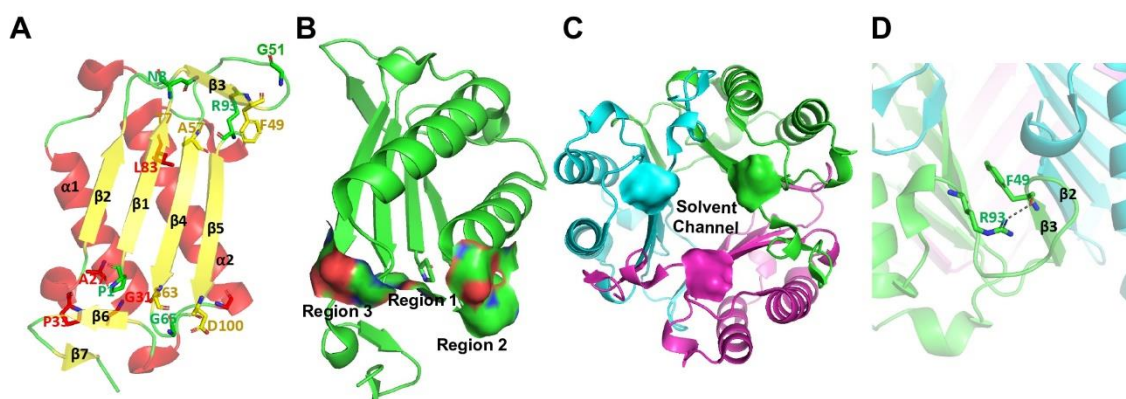
Fig. S3. Structural views and regions of the invariant residues in MIF and MDL proteins.
(**A**) All 14 invariant residues among the three MDLs and MIF are shown in a MIF monomer. (**B**) Surface areas of regions 1, 2, and 3. Region 1 contains the Pro^1 and Ser^{63} of the tautomerase enzymatic site. Region 2 consists of Ala^{27}, Gly^{31}, Pro^{33}, Gly^{65}, Ser^{63}, and Asp^{100}. For Ser^{63}, the backbone atoms are in region 2, whereas the side chain is part of region 1. (**C**) The human MIF trimer creates a solvent channel (water molecules not shown) along the 3-fold axis of the trimeric structure. The solvent channel is surrounded by three surface areas (shown as a smooth surfaces) of Asp^{100} side chains from each subunit (shown in different colors) at one end of the channel, which makes up region 3. (**D**) In region 4, a hydrogen bond between the side chain of Arg^{93} and the backbone of Phe^{49} stabilizes the β-strand important for subunit-subunit interactions (cartoons in blue and green represent two different subunits).
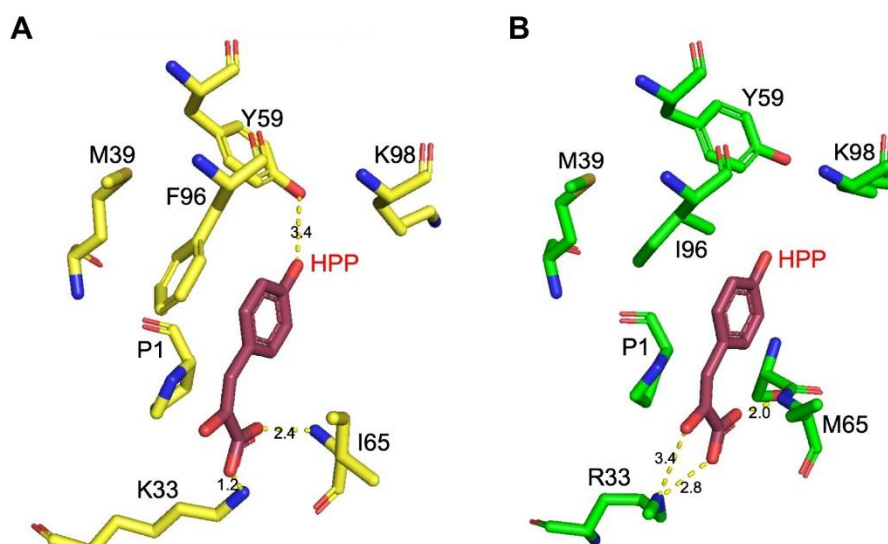
Fig. S4. Interactions of MDL2 and MDL3 tautomerase enzymatic site residues interacting with a modelled HPP substrate molecule. Residues of **(A)** MDL2 and **(B)** MDL3 analogous to the tautomerase catalytic site in human MIF, shown in yellow and green, respectively, were superimposed on the MIF-HPP complex to examine putative interactions between ligand and protein. Potential hydrogen bonds are shown between the MDLs and HPP represented by yellow lines.
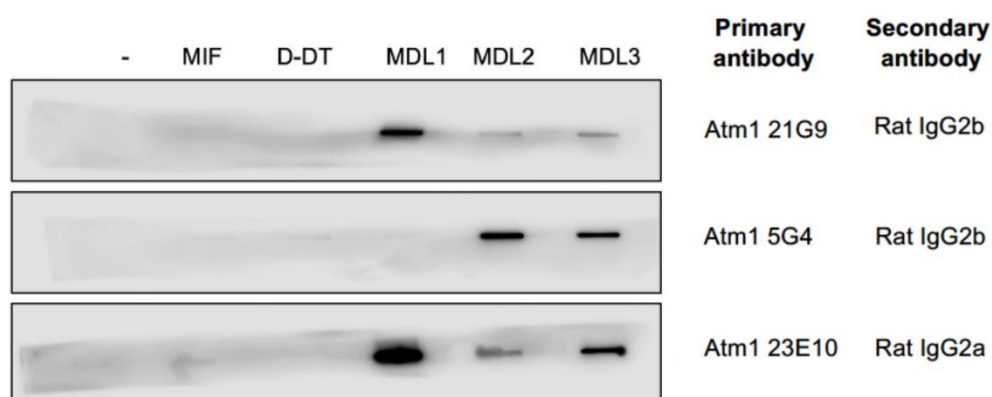
Fig. S5. Slot blot screening for sensitivity and specificity of custom-made monoclonal antibodies directed against MDL1 and MDL2. Custom-made monoclonal antibodies generated against MDL1 and MDL2 were screened by slot blotting. Promising monoclonal antibodies directed against MDL1 and MDL2 were probed against purified recombinant human MIF (MIF), human MIF-2/D-DT, and the three *Arabidopsis* MDL proteins as indicated. The far left-hand lane (-) was a negative control without protein. HRP-coupled immunoglobulin subclass-specific secondary antibodies were used as indicated for detection. Antibody clones directed against MDL2 were previously established (*34*). Clone Atm-5G4, generated against MDL2, was used in this study also recognizes MDL3. Two candidate antibodies directed against MDL1 (Atm1_21G9 and Atm1_23E10) distinguished between MIF or D-DT and the MDLs, but Atm_21G9 showed greater specificity for MDL1. Screening was performed with the primary hybridoma supernatant (shown here) and then validated with the established clone, which was used for subsequent experiments. The blot is representative of n = 3 independent experiments.
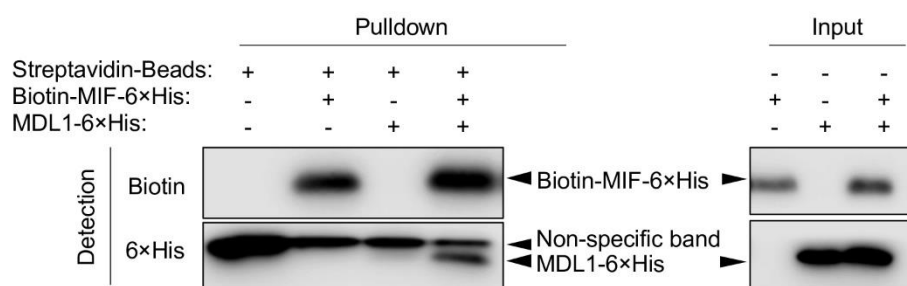
Fig. S6. MIF and MDL proteins bind to each other in vitro. (A) Purified tagged MIF (biotin-MIF-6×His) and MDL1 (MDL1-6×His) were incubated alone or together, and complexes pulled down by streptavidin-coated beads were immunoblotted after separation by SDS-PAGE. Blots were developed for His-tagged proteins by using a hexahistidine tag–specific antibody to visualize MIF and MDL1. The upper band in the bottom panel of the pulldown, absent in the input samples, originates from the streptavidin-coated beads used to pull down biotin-tagged MIF and is non-specific. Blots are representative of n = 3 independent experiments.
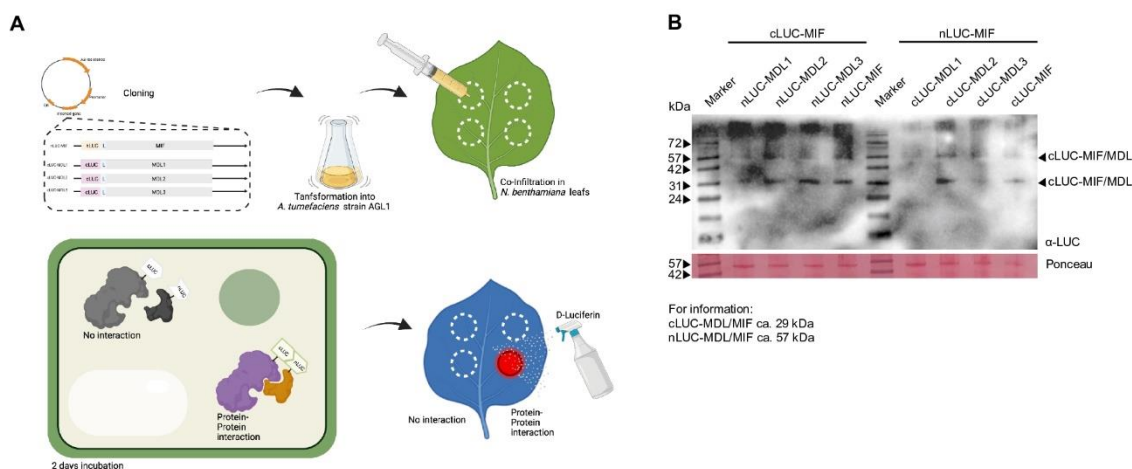
Fig. S7. Luciferase complementation imaging assay. (**A**) Schematic illustration of luciferase complementation imaging assay upon transient expression of test genes in *N. benthamiana* leaves. Constructs of *MIF* and three *MDL* genes were N-terminally fused to N- and C-terminal segments of firefly luciferase. These plasmids were transferred into *A. tumefaciens* strain GV3101 (pmP90RK) for subsequent transformation into plant cells. For co-infiltration, equal volumes of each *A. tumefaciens* transformant culture were mixed and infiltrated with a syringe lacking a cannula from the lower (abaxial) side into fully expanded leaves of four- to six-week-old *N. benthamiana* plants. Imaging was done after three days of incubation following spraying the leaves with the lucifase substrate D-luciferin. (**B**) Immunoblot analysis of transient expression of luciferase complementation fusion proteins. Protein extracts of *A. tumefaciens* infiltrated *N. benthamiana* leaves were separated by SDS-PAGE, blotted onto a nitrocellulose membrane, and probed with a luciferase-specific primary antibody and a secondary antibody coupled to horseradish peroxidase (HRP). Chemiluminescence detection of antigen-antibody complexes was performed with SuperSignal™ West Femto Western substrate. As a loading control, membranes were stained in Ponceau S solution, showing primarily the large subunit of ribulose-1,5-bisphophate carboxylase/oxygenase, a prominent protein of ~56 kDa in plant protein extracts. Expected molecular masses are ~57 kDa for the nLUC-MIF/MDL fusion proteins and ~29 kDa for the cLUC-MIF/MDL fusion proteins. Three independent luciferase complementation imaging assays were performed. The blot shown was performed from one of these experiments. X
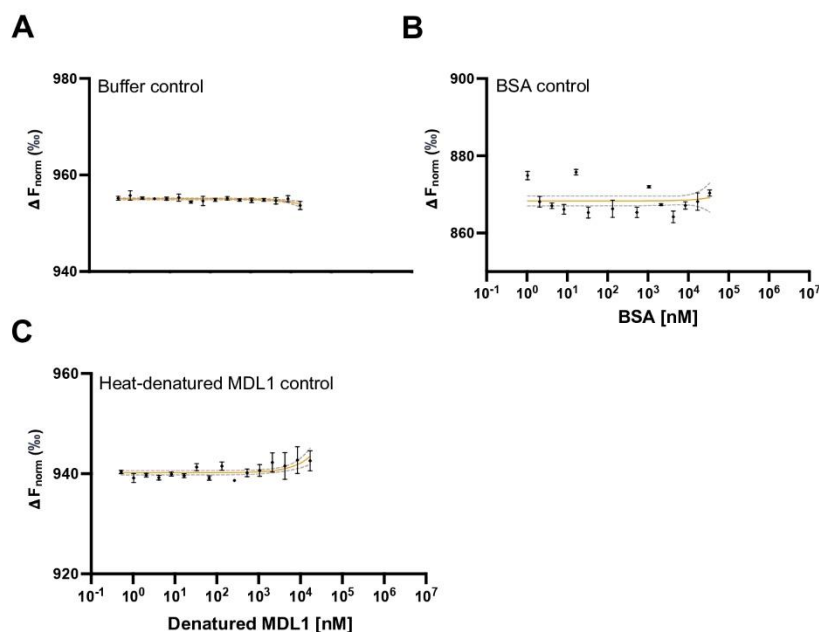
Fig. S8. Microscale thermophoresis (MST) control experiments. RED-NHS-MIF was tested in MST in different control conditions: (**A**) buffer control**,** (**B**) bovine serum albumin (BSA) as an unrelated control protein instead of MDL, and (**C**) heat-denatured MDL1 as a negative control for folded MDL1 protein. Settings and buffer conditions were the same as for the MIF-MDL experiments (20 mM sodium phosphate buffer, pH 7.2, containing 0.2% Tween-20). Values shown represent means ± SD as obtained from at least 3 biological replicates (n≥3). Data analysis and K_D-fitting was performed using NanoTemper MOcontrol software, visualization was done by non-linear fitting using Graphpad Prism.
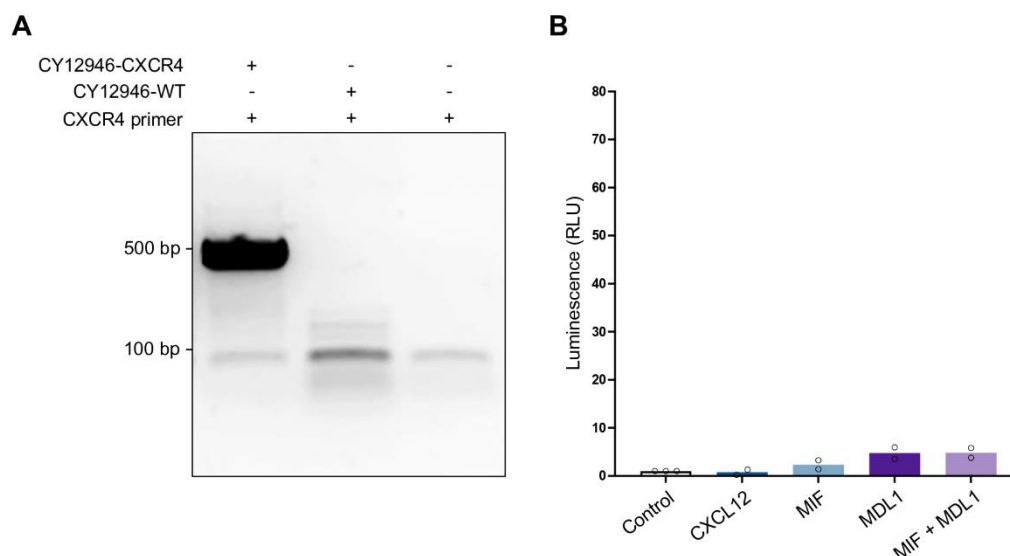
Fig. S9. A plasmid loss assay confirms the specificity of MIF and MDL effects in the yeast-based reporter system. The plasmid loss assay for the CXCR4-encoding plasmid was carried out as described in the Materials and Methods. (**A**) PCR confirms loss of the CXCR4-encoding plasmid from the yeast hCXCR4 clone (CY12946-CXCR4). The new clone lacking CXCR4 is designated CY12946-WT. (**B**) Control experiment with clone CY12946-WT, generated according to (A). Thirty minutes after addition of test proteins to the yeast system, luminescence (in relative light units, RLU) due to *lacZ* reporter gene activation was measured. MIF and MDL1 were used individually at 20 µM or in combination (10 µM each). Only minimal unspecific activation of the lacZ reporter pathway was observed in the yeast cells that have lost the CXCR4-encoding plasmid, confirming the specificity of the effects measured in the CXCR4 yeast reporter system. The effect with the cognate CXCR4 ligand CXCL12 (tested at 2 µM) is shown for comparison. Values shown represent means as obtained from two independent experiments (n=2), with RLUs of each experiment assessed in technical duplicates and normalized to untreated controls. Individual data points are indicated by white circles.
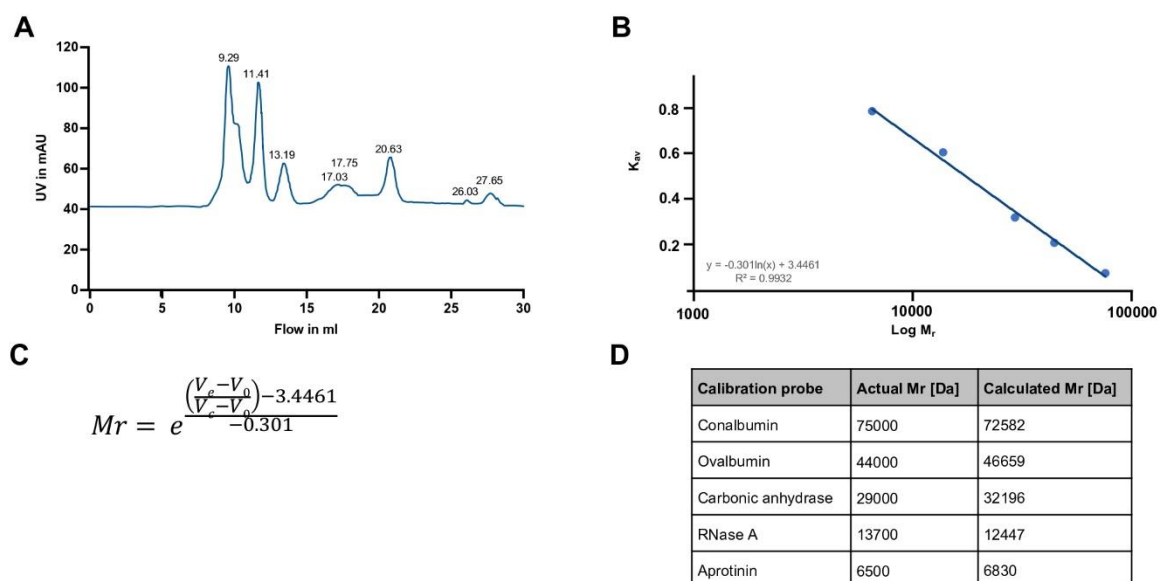
A

CXCR4

Luminescence (RLU)

| MDL1 [µM] | - | 0.01 | 0.1 | 1 | 2 | 4 | 10 |
| MIF [1 µM] | + | + | + | + | + | + | + |

B

CXCR4

Luminescence (RLU)

| MDL1 [µM] | - | 0.01 | 0.1 | 1 | 2 | 4 | 10 |
| MIF [1 µM] | + | + | + | + | + | + | + |

C

CXCR4 – 1 µM MIF
EC_{50} = 3.2 µM MDL1

Luminescence (RLU)

MDL1 [µM]

D

CXCR4 – 1 µM MIF
EC_{50} = 2.4 µM MDL1

Luminescence (RLU)

MDL1 [µM]

Fig. S10. Additional biological replicates showing synergistic CXCR4 activation by MIF and MDL1 in the yeast-based reporter system. Shown are two additional biological replicates of the concentration-response experiments (Fig. 3, H and I). (**A and B**) The bar diagrams show luminescence (in RLU) due to *lacZ* reporter gene activation upon the addition of a sub-threshold concentration of 1 μM MIF and increasing concentrations (0 - 10 μM) of MDL1. The effect of the cognate CXCR4 ligand CXCL12 (at 1 μM) is shown for comparison. (**C and D**) Concentration-response curves for MIF-MDL1 interaction in the CXCR4 reporter system according to (A) and (B), respectively, assuming a non-linear fit. From those fits, a half-maximal effective ('synergistic') concentration (EC_{50}) of 3.2 and 2.4 μM MDL1, respectively, was derived. Each experiment was carried out in technical triplicates. White circles indicate individual data points.
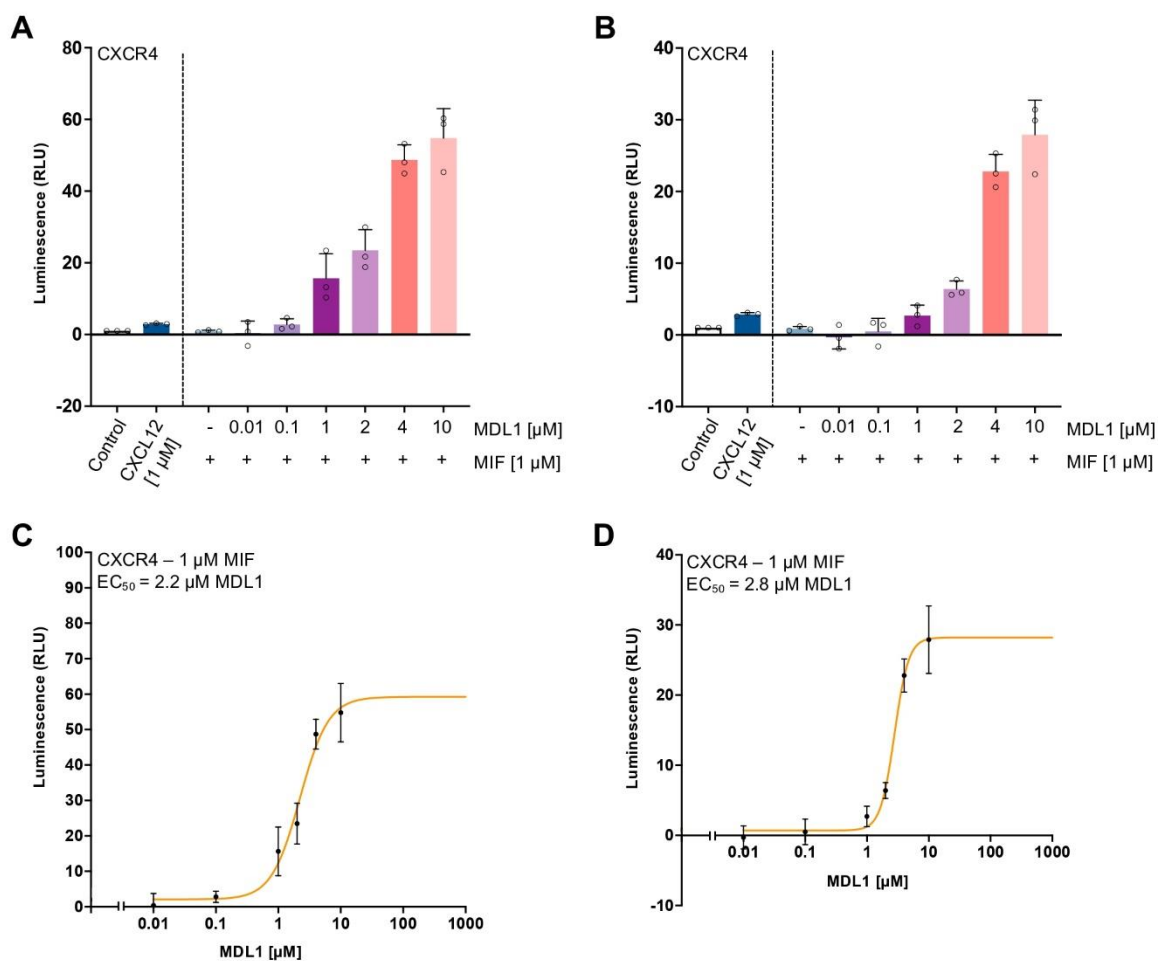
Fig. S11. Subtraction of the effect of MDL1 alone from experiments showing synergistic CXCR4 activation by MIF and MDL1 in the yeast-based reporter system. Shown are two biological replicates of the concentration-response experiment with combinations of constant MIF and increasing MDL1 concentrations (fig. S10, A to D), with the respective MDL1-alone values subtracted. (**A and B**) Bar diagrams show luminescence (RLU) due to *lacZ* reporter gene activation upon addition of a sub-threshold concentration of 1 µM MIF and increasing concentrations (0 - 10 µM) of MDL1. Luminescence of MDL1-alone at 0.01, 0.1, 1, 2, 4, 10 µM (measured separately) was deducted from values observed for the respective MIF + MDL1 combinations. Negative RLU values for combinations of MIF and low MDL1 concentration are due to this subtraction. The effect of the cognate CXCR4 ligand CXCL12 (at 1 µM) is shown for comparison. (**C and D**) Concentration-response curves for MIF-MDL1 interaction in the CXCR4 reporter system according to (A) and (B), respectively, assuming a non-linear fit. From those fits, a half-maximal effective ('synergistic') concentration (EC_{50}) of 2.2 and 2.8 µM MDL1, respectively, was derived. Each experiment was carried out in technical triplicates. White circles indicate individual data points.

A

B

C

$$Mr = e^{\frac{\left(\frac{V_e - V_0}{V_c - V_0}\right) - 3.4461}{-0.301}}$$

D

Calibration probe	Actual Mr [Da]	Calculated Mr [Da]
Conalbumin	75000	72582
Ovalbumin	44000	46659
Carbonic anhydrase	29000	32196
RNase A	13700	12447
Aprotinin	6500	6830

Fig. S12. Establishing a calibration curve and a standard equation for the Superdex 75 10/300 SEC column. The GE Healthcare Gel Filtration Calibration Kit was used to establish a standard curve and equation for the following conditions: 20 mM sodium phosphate buffer including 20 mM sodium chloride, pH 7.2, flow rate 0.5 mL/min. (**A**) Standard proteins with known molecular masses were prepared, mixed according to manufacturer's instructions and run over the column under the aforementioned conditions. The chromatogram shows the elution profile of the standard proteins with their corresponding elution volumes. (**B**) Standard curve generated from the known molecular mass and the observed elution volume for each of the test proteins. Notice the logarithmic x-axis. (**C**) Standard equation to calculate the molecular mass (Mr) of a protein according to its elution volume (**V_e**). V_0 = column volume, e = Euler's number. (**D**) Comparison of the known molecular masses of test proteins to their calculated mass based on their elution volumes (V_e) and the standard equation shown in (**C**).
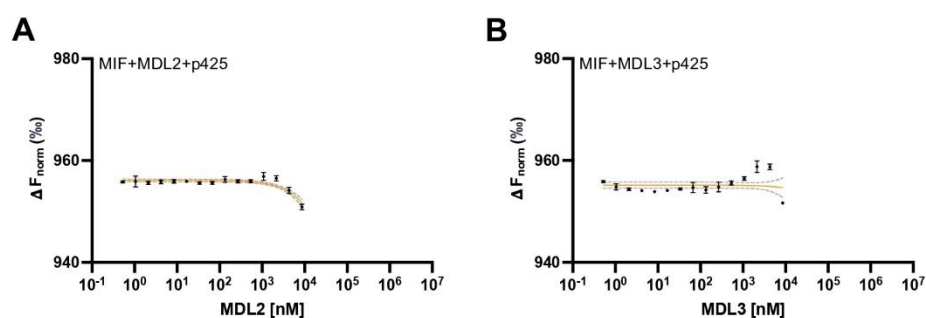
Fig. S13. p425 blocks the interaction between MIF and MDL2 or MDL3. The interaction between RED-NHS-MIF and different concentrations of (**A**) MDL2 or (**B**) MDL3 in the presence of the MIF allosteric inhibitor p425 was determined by microscale thermophoresis (MST). Values shown represent means ± SD as obtained from at least 3 biological replicates (n≥3). Data analysis and K_D-fitting was performed using NanoTemper MOcontrol software, visualization was done by non-linear fitting using Graphpad Prism.
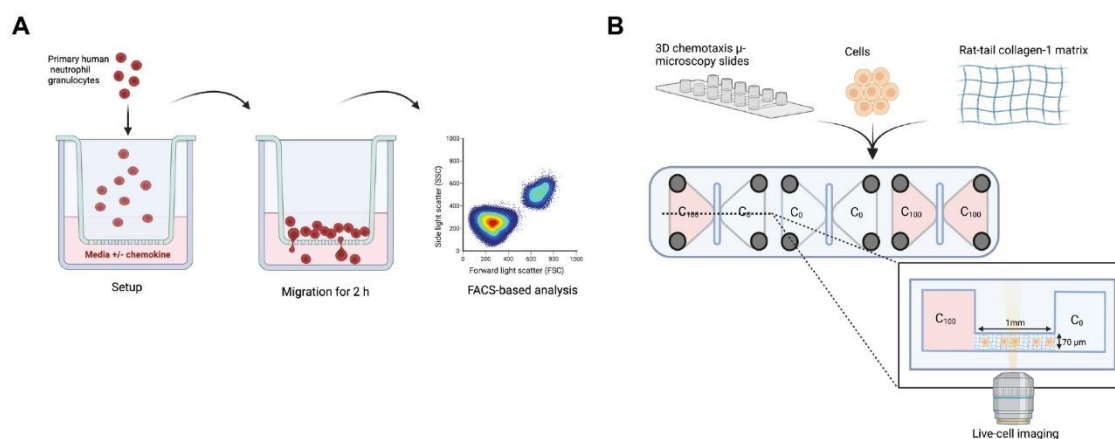
Fig. S14. Schematic illustrations of experiments used to study the chemotactic movement of primary human neutrophils. (**A**) Schematic illustration of the Transwell migration assay. Neutrophils migrating across the filter towards a chemotactic stimulus were quantified by flow cytometry. (**B**) Schematic illustration of the 3D collagen matrix migration assay using time-lapse live-cell microscopy and individual cell tracking, using the 3D-chemotaxis µ-Slide system from Ibidi GmbH. Migration along this gradient was observed using time-lapse imaging for 1 h at 37 °C on a Leica inverted DMi8-Life Cell Imaging system.
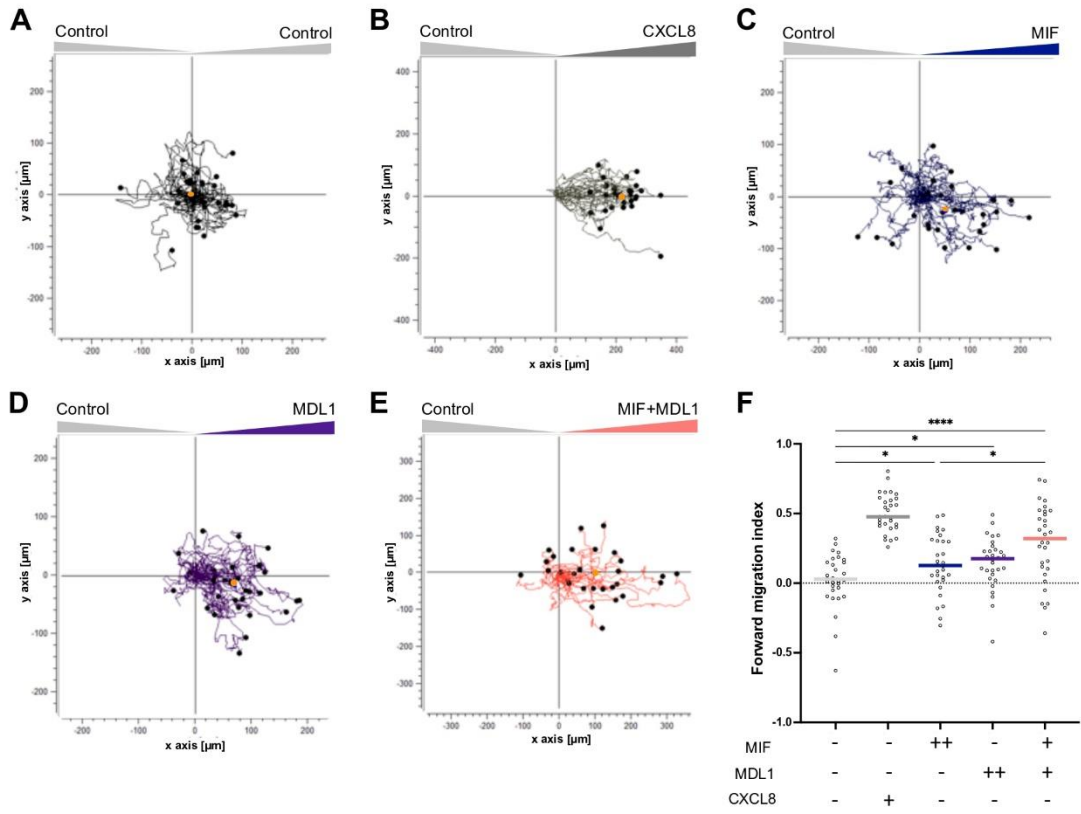
Fig. S15. MDLs promote human neutrophil chemotaxis and augment the chemotactic effect of human MIF. Chemotaxis was assessed by 3D chemotaxis of primary human neutrophils applying live-cell microscopy of single-cell migration tracks in x/y direction in μm. **(A to E)** Representative experiments showing 3D chemotaxis of primary human neutrophils towards (**A**) buffer control (gray), indicating random motility; (**B**) CXCL8 (1 μM); (**C**) MIF (500 ng/mL); (**D**) MDL1 (500 ng/mL); or (**E**) a 1:1 mixture of MIF and MDL1 (250 ng/mL each). Orange dots represent the center of mass in each experiment. (**F**) Quantification of (A to E). The migration tracks of 30 randomly selected cells per treatment group (n=30) were recorded and the forward migration index plotted. This is an independent biological replication of the experiment shown in the main text (Fig. 5, C to H). Statistical analysis was performed using one-way ANOVA with Tukey's posthoc multiple comparison between the buffer control and the treatment groups (* $p < 0.05$, **** $p < 0.0001$).
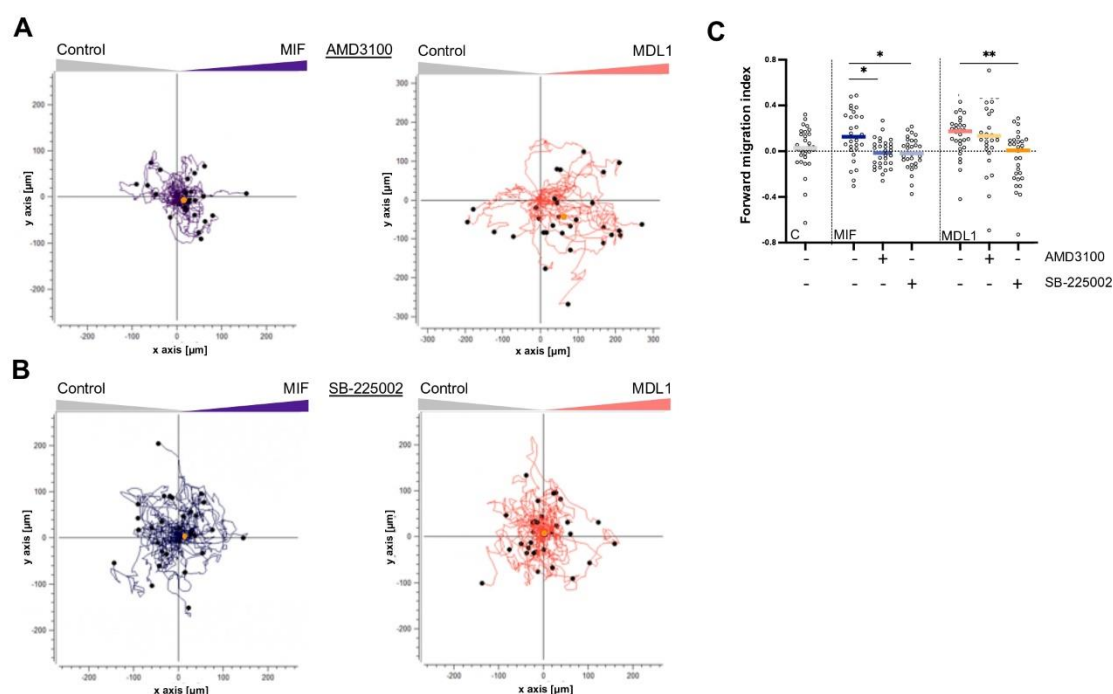
Fig. S16. MDL1-mediated neutrophil chemotaxis is inhibited by SB-225002 but not by AMD3100. 3D chemotaxis of primary human neutrophils as assessed by live-cell microscopy of single-cell migration tracks in x/y direction in μm. (**A and B**) Representative experiments showing 3D chemotaxis of primary human neutrophils. Shown is the comparison between migration towards MIF (500 ng/mL) or MDL1 (500 ng/mL) in the presence of either the CXCR4 I nhibitor AMD3100 (A); or the CXCR2 inhibitor SB225002 (B). Orange dots represent the center of mass for each experiment. (**C**) Quantification of (B) and (C) plus experiments performed in the absence of the inhibitors. The migration tracks of 30 randomly selected cells per treatment group were recorded and the forward migration index plotted. This is an independent biological replication of this experiment is shown in the main text (Fig. 6, B to D). Statistics were performed using one-way ANOVA with Tukey's posthoc multiple comparison (* $p < 0.05$, ** $p < 0.01$).
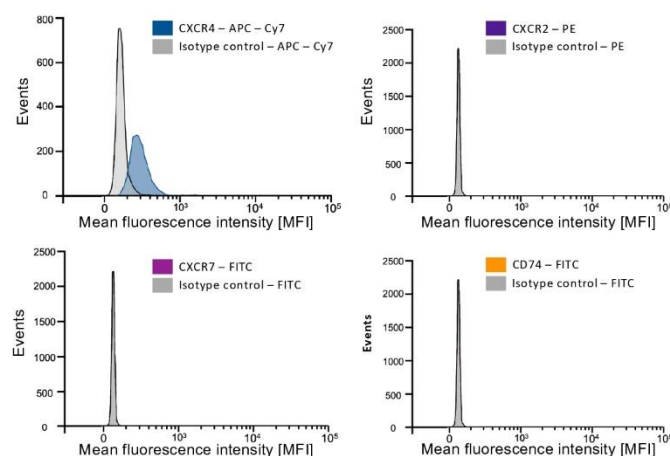
Fig. S17. MIF receptor expression in A549 lung epithelial cells and the CXCR4-PI3K-AKT signaling pathway. (A) Surface CXCR4 on A549 lung epithelial cells as assessed by flow cytometry. The histogram represents the mean fluorescence intensity (MFI) on the x-axis and the number of fluorescent events on the y-axis. Antibody staining for CXCR4 (APC-Cy7), CXCR2 (PE), CXCR7 (FITC), CD74 (FITC) as well as staining with the corresponding isotype control (IgG control, grey) are shown. Data are representative of n = 3 independent experiments. (**B**) Schematic illustration of the CXCR4 receptor (a typical GPCR) and PI3K (phosphoinositid-3-kinase) as well as the AKT pathway as one of its downstream signaling cascades known to be involved in cell proliferation and migration. MIF or MDL1 binding to CXCR4 results in activation of the pathway as indicated.

8. References

1.   Diercks, G. F. H., and Kluin, P. M. (2016) Basic principles of the immune system and autoimmunity. In *Autoimmune Bullous Diseases: Text and Review* (Jonkman, M. F., ed) pp. 3-12, Springer International Publishing, Cham

2.   Parkin, J., and Cohen, B. (2001) An overview of the immune system. *The Lancet* **357**, 1777-1789

3.   Pennock, N. D., White, J. T., Cross, E. W., Cheney, E. E., Tamburini, B. A., and Kedl, R. M. (2013) T cell responses: naive to memory and everything in between. *Adv Physiol Educ* **37**, 273-283

4.   Rivera, A., Siracusa, M. C., Yap, G. S., and Gause, W. C. (2016) Innate cell communication kick-starts pathogen-specific immunity. *Nat Immunol* **17**, 356-363

5.   Varn, F. S., Mullins, D. W., Arias-Pulido, H., Fiering, S. N., and Cheng, C. (2017) Adaptive immunity programmes in breast cancer. *Immunology* **150**

6.   Sette, A., and Crotty, S. (2021) Adaptive immunity to SARS-CoV-2 and COVID-19. *Cell* **184**, 861 - 880

7.   Andersen, M. H., Schrama, D., Thor Straten, P., and Becker, J. C. (2006) Cytotoxic T cells. *J Invest Dermatol* **126 1**, 32-41

8.   Yoshimura, A., Ito, M., Chikuma, S., Akanuma, T., and Nakatsukasa, H. (2018) Negative regulation of cytokine signaling in immunity. *Cold Spring Harb Perspect Biol* **10 7**

9.   Dong, C. (2021) Cytokine regulation and function in T cells. *Annu Rev Immunol* **39**, 51-76

10.   Altan-Bonnet, G., and Mukherjee, R. (2019) Cytokine-mediated communication: a quantitative appraisal of immune complexity. *Nat Rev Immunol* **19**, 205-217

11.   Calandra, T., and Roger, T. (2003) Macrophage migration inhibitory factor: a regulator of innate immunity. *Nat Rev Immunol* **3**, 791-800

12.   Sumaiya, K., Langford, D., Natarajaseenivasan, K., and Shanmughapriya, S. (2022) Macrophage migration inhibitory factor (MIF): A multifaceted cytokine regulated by genetic and physiological strategies. *Pharmacol Ther* **233**, 108024

13.   Zhu, J., Yamane, H., and Paul, W. E. (2010) Differentiation of effector CD4 T cell populations (*). *Annu Rev Immunol* **28**, 445-489

14.   Haabeth, O. A. W., Fauskanger, M., Manzke, M., Lundin, K. U., Corthay, A., Bogen, B., and Tveita, A. A. (2018) CD4(+) T-cell-mediated rejection of MHC class II-positive tumor cells is dependent on antigen secretion and indirect presentation on host APCs. *Cancer Res* **78**, 4573-4585

15.   Zhou, L., Chong, M. M., and Littman, D. R. (2009) Plasticity of CD4+ T cell lineage differentiation. *Immunity* **30**, 646-655

16.   DuPage, M., and Bluestone, J. A. (2016) Harnessing the plasticity of CD4(+) T cells to treat immune-mediated disease. *Nat Rev Immunol* **16**, 149-163

17.   Anderson, G., and Jenkinson, E. J. (2001) Lymphostromal interactions in thymic development and function. *Nat Rev Immunol* **1**, 31-40

18.   von Boehmer, H., Teh, H. S., and Kisielow, P. (1989) The thymus selects the useful, neglects the useless and destroys the harmful. *Immunol Today* **10**, 57-61

19.   Germain, R. N. (2002) T-cell development and the CD4-CD8 lineage decision. *Nat Rev Immunol* **2**, 309-322

20.   Williams, O., Tanaka, Y., Bix, M., Murdjeva, M., Littman, D. R., and Kioussis, D. (1996) Inhibition of thymocyte negative selection by T cell receptor antagonist peptides. *Eur J Immunol* **26**, 532-538

21. Klein, L., Kyewski, B., Allen, P. M., and Hogquist, K. A. (2014) Positive and negative selection of the T cell repertoire: what thymocytes see (and don't see). *Nat Rev Immunol* **14**, 377-391

22. Pozzi, L. A., Maciaszek, J. W., and Rock, K. L. (2005) Both dendritic cells and macrophages can stimulate naive CD8 T cells in vivo to proliferate, develop effector function, and differentiate into memory cells. *J Immunol* **175**, 2071-2081

23. Guéry, J. C., and Adorini, L. (1995) Dendritic cells are the most efficient in presenting endogenous naturally processed self-epitopes to class II-restricted T cells. *J Immunol* **154**, 536-544

24. Schrezenmeier, H., and Fleischer, B. (1988) A regulatory role for the CD4 and CD8 molecules in T cell activation. *J Immunol* **141**, 398-403

25. Mueller, D. L., and Jenkins, M. K. (1995) Molecular mechanisms underlying functional T-cell unresponsiveness. *Curr Opin Immunol* **7**, 375-381

26. Lanier, L. L., O'Fallon, S., Somoza, C., Phillips, J. H., Linsley, P. S., Okumura, K., Ito, D., and Azuma, M. (1995) CD80 (B7) and CD86 (B70) provide similar costimulatory signals for T cell proliferation, cytokine production, and generation of CTL. *J Immunol* **154**, 97-105

27. Orabona, C., Grohmann, U., Belladonna, M. L., Fallarino, F., Vacca, C., Bianchi, R., Bozza, S., Volpi, C., Salomon, B. L., Fioretti, M. C., Romani, L., and Puccetti, P. (2004) CD28 induces immunostimulatory signals in dendritic cells via CD80 and CD86. *Nat Immunol* **5**, 1134-1142

28. van Kooten, C., and Banchereau, J. (2000) CD40-CD40 ligand. *J Leukoc Biol* **67**, 2-17

29. Mahajan, S., Cervera, A., MacLeod, M., Fillatreau, S., Perona-Wright, G., Meek, S., Smith, A., MacDonald, A., and Gray, D. (2007) The role of ICOS in the development of CD4 T cell help and the reactivation of memory T cells. *Eur J Immunol* **37**, 1796-1808

30. Dong, C., Juedes, A. E., Temann, U. A., Shresta, S., Allison, J. P., Ruddle, N. H., and Flavell, R. A. (2001) ICOS co-stimulatory receptor is essential for T-cell activation and function. *Nature* **409**, 97-101

31. Weissmüller, S., Semmler, L. Y., Kalinke, U., Christians, S., Müller-Berghaus, J., and Waibler, Z. (2012) ICOS-LICOS interaction is critically involved in TGN1412-mediated T-cell activation. *Blood* **119**, 6268-6277

32. Wen, T., Bukczynski, J., and Watts, T. H. (2002) 4-1BB ligand-mediated costimulation of human T cells induces CD4 and CD8 T cell expansion, cytokine production, and the development of cytolytic effector function. *J Immunol* **168**, 4897-4906

33. Tivol, E. A., Borriello, F., Schweitzer, A. N., Lynch, W. P., Bluestone, J. A., and Sharpe, A. H. (1995) Loss of CTLA-4 leads to massive lymphoproliferation and fatal multiorgan tissue destruction, revealing a critical negative regulatory role of CTLA-4. *Immunity* **3**, 541-547

34. Krummel, M. F., and Allison, J. P. (1995) CD28 and CTLA-4 have opposing effects on the response of T cells to stimulation. *J Exp Med* **182**, 459-465

35. Balagopalan, L., Ashwell, B. A., Bernot, K. M., Akpan, I. O., Quasba, N., Barr, V. A., and Samelson, L. E. (2011) Enhanced T-cell signaling in cells bearing linker for activation of T-cell (LAT) molecules resistant to ubiquitylation. *Proc Natl Acad Sci U S A* **108**, 2885-2890

36. Schmidl, C., Delacher, M., Huehn, J., and Feuerer, M. (2018) Epigenetic mechanisms regulating T-cell responses. *J Allergy Clin Immunol* **142**, 728-743

37. Cibrián, D., and Sánchez-Madrid, F. (2017) CD69: from activation marker to metabolic gatekeeper. *Eur J Immunol* **47**, 946-953

38. Smith-Garvin, J. E., Koretzky, G. A., and Jordan, M. S. (2009) T cell activation. *Annu Rev Immunol* **27**, 591-619

39. Poloni, C., Schonhofer, C., Ivison, S., Levings, M. K., Steiner, T. S., and Cook, L. (2023) T-cell activation-induced marker assays in health and disease. *Immunol Cell Biol* **101**, 491-503

40. Wu, H., Witzl, A., and Ueno, H. (2019) Assessment of TCR signal strength of antigen-specific memory CD8(+) T cells in human blood. *Blood Adv* **3**, 2153-2163

41. Shatrova, A. N., Mityushova, E. V., Vassilieva, I. O., Aksenov, N. D., Zenin, V. V., Nikolsky, N. N., and Marakhova, II. (2016) Time-dependent regulation of IL-2R α-Chain (CD25) expression by TCR signal strength and IL-2-induced STAT5 signaling in activated human blood T lymphocytes. *PLoS One* **11**, e0167215

42. Wolf, T., Jin, W., Zoppi, G., Vogel, I. A., Akhmedov, M., Bleck, C. K. E., Beltraminelli, T., Rieckmann, J. C., Ramirez, N. J., Benevento, M., Notarbartolo, S., Bumann, D., Meissner, F., Grimbacher, B., Mann, M., Lanzavecchia, A., Sallusto, F., Kwee, I., and Geiger, R. (2020) Dynamics in protein translation sustaining T cell preparedness. *Nat Immunol* **21**, 927-937

43. Szeto, C., Bloom, J. I., Sloane, H., Lobos, C. A., Fodor, J., Jayasinghe, D., Chatzileontiadou, D. S. M., Grant, E. J., Buckle, A. M., and Gras, S. (2020) Impact of HLA-DR Antigen Binding Cleft Rigidity on T Cell Recognition. *Int J Mol Sci* **21**

44. Luckheeram, R. V., Zhou, R., Verma, A. D., and Xia, B. (2012) CD4+T cells: differentiation and functions. *Clin Dev Immunol* **2012**, 925135

45. Daniels, M. A., and Teixeiro, E. (2015) TCR Signaling in T Cell Memory. *Front Immunol* **6**, 617

46. Zhang, K., Chen, L., Zhu, C., Zhang, M., and Liang, C. (2023) Current knowledge of Th22 cell and IL-22 functions in infectious diseases. *Pathogens* **12**

47. Vignali, D. A., Collison, L. W., and Workman, C. J. (2008) How regulatory T cells work. *Nat Rev Immunol* **8**, 523-532

48. Mosmann, T. R., Cherwinski, H., Bond, M. W., Giedlin, M. A., and Coffman, R. L. (1986) Two types of murine helper T cell clone. I. Definition according to profiles of lymphokine activities and secreted proteins. *J Immunol* **136**, 2348-2357

49. Swain, S. L., Weinberg, A. D., English, M., and Huston, G. (1990) IL-4 directs the development of Th2-like helper effectors. *J Immunol* **145**, 3796-3806

50. Bradley, L. M., Yoshimoto, K., and Swain, S. L. (1995) The cytokines IL-4, IFN-gamma, and IL-12 regulate the development of subsets of memory effector helper T cells in vitro. *J Immunol* **155**, 1713-1724

51. Hsieh, C. S., Macatonia, S. E., Tripp, C. S., Wolf, S. F., O'Garra, A., and Murphy, K. M. (1993) Development of TH1 CD4+ T cells through IL-12 produced by Listeria-induced macrophages. *Science* **260**, 547-549

52. Del Prete, G. F., De Carli, M., Mastromauro, C., Biagiotti, R., Macchia, D., Falagiani, P., Ricci, M., and Romagnani, S. (1991) Purified protein derivative of Mycobacterium tuberculosis and excretory-secretory antigen(s) of Toxocara canis expand in vitro human T cells with stable and opposite (type 1 T helper or type 2 T helper) profile of cytokine production. *J Clin Invest* **88**, 346-350

53. Del Prete, G. F., De Carli, M., D'Elios, M. M., Maestrelli, P., Ricci, M., Fabbri, L., and Romagnani, S. (1993) Allergen exposure induces the activation of allergen-specific Th2 cells in the airway mucosa of patients with allergic respiratory disorders. *Eur J Immunol* **23**, 1445-1449

54. Kanhere, A., Hertweck, A., Bhatia, U., Gökmen, M. R., Perucha, E., Jackson, I., Lord, G. M., and Jenner, R. G. (2012) T-bet and GATA3 orchestrate Th1 and Th2 differentiation through lineage-specific targeting of distal regulatory elements. *Nat Commun* **3**, 1268

55. Hwang, E. S., Szabo, S. J., Schwartzberg, P. L., and Glimcher, L. H. (2005) T helper cell fate specified by kinase-mediated interaction of T-bet with GATA-3. *Science* **307**, 430-433

56. Szabo, S. J., Sullivan, B. M., Stemmann, C., Satoskar, A. R., Sleckman, B. P., and Glimcher, L. H. (2002) Distinct effects of T-bet in TH1 lineage commitment and IFN-gamma production in CD4 and CD8 T cells. *Science* **295**, 338-342

57. Zheng, W., and Flavell, R. A. (1997) The transcription factor GATA-3 is necessary and sufficient for Th2 cytokine gene expression in CD4 T cells. *Cell* **89**, 587-596

58. Zhang, D. H., Cohn, L., Ray, P., Bottomly, K., and Ray, A. (1997) Transcription factor GATA-3 is differentially expressed in murine Th1 and Th2 cells and controls Th2-specific expression of the interleukin-5 gene. *J Biol Chem* **272**, 21597-21603

59.   Pai, S. Y., Truitt, M. L., and Ho, I. C. (2004) GATA-3 deficiency abrogates the development and maintenance of T helper type 2 cells. *Proc Natl Acad Sci U S A* **101**, 1993-1998

60.   Zhu, J., Min, B., Hu-Li, J., Watson, C. J., Grinberg, A., Wang, Q., Killeen, N., Urban, J. F., Jr., Guo, L., and Paul, W. E. (2004) Conditional deletion of Gata3 shows its essential function in T(H)1-T(H)2 responses. *Nat Immunol* **5**, 1157-1165

61.   Zhu, J., Yamane, H., Cote-Sierra, J., Guo, L., and Paul, W. E. (2006) GATA-3 promotes Th2 responses through three different mechanisms: induction of Th2 cytokine production, selective growth of Th2 cells and inhibition of Th1 cell-specific factors. *Cell Res* **16**, 3-10

62.   Park, H., Li, Z., Yang, X. O., Chang, S. H., Nurieva, R., Wang, Y. H., Wang, Y., Hood, L., Zhu, Z., Tian, Q., and Dong, C. (2005) A distinct lineage of CD4 T cells regulates tissue inflammation by producing interleukin 17. *Nat Immunol* **6**, 1133-1141

63.   Weaver, C. T., Hatton, R. D., Mangan, P. R., and Harrington, L. E. (2007) IL-17 family cytokines and the expanding diversity of effector T cell lineages. *Annu Rev Immunol* **25**, 821-852

64.   Zhou, L., Ivanov, II, Spolski, R., Min, R., Shenderov, K., Egawa, T., Levy, D. E., Leonard, W. J., and Littman, D. R. (2007) IL-6 programs T(H)-17 cell differentiation by promoting sequential engagement of the IL-21 and IL-23 pathways. *Nat Immunol* **8**, 967-974

65.   Korn, T., Bettelli, E., Gao, W., Awasthi, A., Jäger, A., Strom, T. B., Oukka, M., and Kuchroo, V. K. (2007) IL-21 initiates an alternative pathway to induce proinflammatory T(H)17 cells. *Nature* **448**, 484-487

66.   Ivanov, II, McKenzie, B. S., Zhou, L., Tadokoro, C. E., Lepelley, A., Lafaille, J. J., Cua, D. J., and Littman, D. R. (2006) The orphan nuclear receptor RORgammat directs the differentiation program of proinflammatory IL-17+ T helper cells. *Cell* **126**, 1121-1133

67.   Chi, X., Jin, W., Zhao, X., Xie, T., Shao, J., Bai, X., Jiang, Y., Wang, X., and Dong, C. (2022) RORγt expression in mature T(H)17 cells safeguards their lineage specification by inhibiting conversion to T(H)2 cells. *Sci Adv* **8**, eabn7774

68.   Yang, X. O., Pappu, B. P., Nurieva, R., Akimzhanov, A., Kang, H. S., Chung, Y., Ma, L., Shah, B., Panopoulos, A. D., Schluns, K. S., Watowich, S. S., Tian, Q., Jetten, A. M., and Dong, C. (2008) T helper 17 lineage differentiation is programmed by orphan nuclear receptors ROR alpha and ROR gamma. *Immunity* **28**, 29-39

69.   Tesmer, L. A., Lundy, S. K., Sarkar, S., and Fox, D. A. (2008) Th17 cells in human disease. *Immunol Rev* **223**, 87-113

70.   Wilke, C. M., Bishop, K., Fox, D., and Zou, W. (2011) Deciphering the role of Th17 cells in human disease. *Trends Immunol* **32**, 603-611

71.   Chen, W., Jin, W., Hardegen, N., Lei, K. J., Li, L., Marinos, N., McGrady, G., and Wahl, S. M. (2003) Conversion of peripheral CD4+CD25- naive T cells to CD4+CD25+ regulatory T cells by TGF-beta induction of transcription factor Foxp3. *J Exp Med* **198**, 1875-1886

72.   Shevach, E. M., and Thornton, A. M. (2014) tTregs, pTregs, and iTregs: similarities and differences. *Immunol Rev* **259**, 88-102

73.   Freeborn, R. A., Strubbe, S., and Roncarolo, M. G. (2022) Type 1 regulatory T cell-mediated tolerance in health and disease. *Front Immunol* **13**, 1032575

74.   de Waal Malefyt, R., Haanen, J., Spits, H., Roncarolo, M. G., te Velde, A., Figdor, C., Johnson, K., Kastelein, R., Yssel, H., and de Vries, J. E. (1991) Interleukin 10 (IL-10) and viral IL-10 strongly reduce antigen-specific human T cell proliferation by diminishing the antigen-presenting capacity of monocytes via downregulation of class II major histocompatibility complex expression. *J Exp Med* **174**, 915-924

75.   Göschl, L., Scheinecker, C., and Bonelli, M. (2019) Treg cells in autoimmunity: from identification to Treg-based therapies. *Semin Immunopathol* **41**, 301-314

76.   Crotty, S. (2011) Follicular helper CD4 T cells (TFH). *Annu Rev Immunol* **29**, 621-663

77.   Schmitt, E., Klein, M., and Bopp, T. (2014) Th9 cells, new players in adaptive immunity. *Trends Immunol* **35**, 61-68

78. Rivera Vargas, T., Humblin, E., Végran, F., Ghiringhelli, F., and Apetoh, L. (2017) T(H)9 cells in anti-tumor immunity. *Semin Immunopathol* **39**, 39-46

79. Végran, F., Apetoh, L., and Ghiringhelli, F. (2015) Th9 cells: a novel CD4 T-cell subset in the immune war against cancer. *Cancer Res* **75**, 475-479

80. Lu, Y., Hong, S., Li, H., Park, J., Hong, B., Wang, L., Zheng, Y., Liu, Z., Xu, J., He, J., Yang, J., Qian, J., and Yi, Q. (2012) Th9 cells promote antitumor immune responses in vivo. *J Clin Invest* **122**, 4160-4171

81. Angkasekwinai, P. (2019) Th9 Cells in Allergic Disease. *Curr Allergy Asthma Rep* **19**, 29

82. Eyerich, S., Eyerich, K., Pennino, D., Carbone, T., Nasorri, F., Pallotta, S., Cianfarani, F., Odorisio, T., Traidl-Hoffmann, C., Behrendt, H., Durham, S. R., Schmidt-Weber, C. B., and Cavani, A. (2009) Th22 cells represent a distinct human T cell subset involved in epidermal immunity and remodeling. *J Clin Invest* **119**, 3573-3585

83. Duhen, T., Geiger, R., Jarrossay, D., Lanzavecchia, A., and Sallusto, F. (2009) Production of interleukin 22 but not interleukin 17 by a subset of human skin-homing memory T cells. *Nat Immunol* **10**, 857-863

84. Trifari, S., Kaplan, C. D., Tran, E. H., Crellin, N. K., and Spits, H. (2009) Identification of a human helper T cell population that has abundant production of interleukin 22 and is distinct from T(H)-17, T(H)1 and T(H)2 cells. *Nat Immunol* **10**, 864-871

85. Yeste, A., Mascanfroni, I. D., Nadeau, M., Burns, E. J., Tukpah, A. M., Santiago, A., Wu, C., Patel, B., Kumar, D., and Quintana, F. J. (2014) IL-21 induces IL-22 production in CD4+ T cells. *Nat Commun* **5**, 3753

86. Missé, D., Yssel, H., Trabattoni, D., Oblet, C., Lo Caputo, S., Mazzotta, F., Pène, J., Gonzalez, J. P., Clerici, M., and Veas, F. (2007) IL-22 participates in an innate anti-HIV-1 host-resistance network through acute-phase protein induction. *J Immunol* **178**, 407-415

87. Cobleigh, M. A., and Robek, M. D. (2013) Protective and pathological properties of IL-22 in liver disease: implications for viral hepatitis. *Am J Pathol* **182**, 21-28

88. Pociask, D. A., Scheller, E. V., Mandalapu, S., McHugh, K. J., Enelow, R. I., Fattman, C. L., Kolls, J. K., and Alcorn, J. F. (2013) IL-22 is essential for lung epithelial repair following influenza infection. *Am J Pathol* **182**, 1286-1296

89. Khantakova, J. N., and Sennikov, S. V. (2023) T-helper cells flexibility: the possibility of reprogramming T cells fate. *Front Immunol* **14**, 1284178

90. Geginat, J., Paroni, M., Maglie, S., Alfen, J. S., Kastirr, I., Gruarin, P., De Simone, M., Pagani, M., and Abrignani, S. (2014) Plasticity of human CD4 T cell subsets. *Front Immunol* **5**, 630

91. Koh, C. H., Lee, S., Kwak, M., Kim, B. S., and Chung, Y. (2023) CD8 T-cell subsets: heterogeneity, functions, and therapeutic potential. *Exp Mol Med* **55**, 2287-2299

92. Künzli, M., and Masopust, D. (2023) CD4(+) T cell memory. *Nat Immunol* **24**, 903-914

93. Pepper, M., Linehan, J. L., Pagán, A. J., Zell, T., Dileepan, T., Cleary, P. P., and Jenkins, M. K. (2010) Different routes of bacterial infection induce long-lived TH1 memory cells and short-lived TH17 cells. *Nat Immunol* **11**, 83-89

94. Schwendemann, J., Choi, C., Schirrmacher, V., and Beckhove, P. (2005) Dynamic differentiation of activated human peripheral blood CD8+ and CD4+ effector memory T cells. *J Immunol* **175**, 1433-1439

95. LaSalle, J. M., and Hafler, D. A. (1991) The coexpression of CD45RA and CD45RO isoforms on T cells during the S/G2/M stages of cell cycle. *Cell Immunol* **138**, 197-206

96. Okumura, M., Fujii, Y., Inada, K., Nakahara, K., and Matsuda, H. (1993) Both CD45RA+ and CD45RA- subpopulations of CD8+ T cells contain cells with high levels of lymphocyte function-associated antigen-1 expression, a phenotype of primed T cells. *J Immunol* **150**, 429-437

97. Cossarizza, A., Ortolani, C., Paganelli, R., Barbieri, D., Monti, D., Sansoni, P., Fagiolo, U., Castellani, G., Bersani, F., Londei, M., and Franceschi, C. (1996) CD45 isoforms expression

on CD4+ and CD8+ T cells throughout life, from newborns to centenarians: implications for T cell memory. *Mech Ageing Dev* **86**, 173-195

98. Booth, N. J., McQuaid, A. J., Sobande, T., Kissane, S., Agius, E., Jackson, S. E., Salmon, M., Falciani, F., Yong, K., Rustin, M. H., Akbar, A. N., and Vukmanovic-Stejic, M. (2010) Different proliferative potential and migratory characteristics of human CD4+ regulatory T cells that express either CD45RA or CD45RO. *J Immunol* **184**, 4317-4326

99. Mishima, T., Toda, S., Ando, Y., Matsunaga, T., and Inobe, M. (2014) Rapid proliferation of activated lymph node CD4(+) T cells is achieved by greatly curtailing the duration of gap phases in cell cycle progression. *Cell Mol Biol Lett* **19**, 638-648

100. Sinitski, D., Gruner, K., Bernhagen, J., and Panstruga, R. (2020) Studying plant MIF/D-DT-Like genes and proteins (MDLs). *Methods Mol Biol* **2080**, 249-261

101. Sallusto, F., Lenig, D., Förster, R., Lipp, M., and Lanzavecchia, A. (1999) Two subsets of memory T lymphocytes with distinct homing potentials and effector functions. *Nature* **401**, 708-712

102. Geginat, J., Sallusto, F., and Lanzavecchia, A. (2003) Cytokine-driven proliferation and differentiation of human naïve, central memory and effector memory CD4+ T cells. *Pathol Biol (Paris)* **51**, 64-66

103. Teijaro, J. R., Turner, D., Pham, Q., Wherry, E. J., Lefrançois, L., and Farber, D. L. (2011) Cutting edge: Tissue-retentive lung memory CD4 T cells mediate optimal protection to respiratory virus infection. *J Immunol* **187**, 5510-5514

104. Gebhardt, T., Whitney, P. G., Zaid, A., Mackay, L. K., Brooks, A. G., Heath, W. R., Carbone, F. R., and Mueller, S. N. (2011) Different patterns of peripheral migration by memory CD4+ and CD8+ T cells. *Nature* **477**, 216-219

105. Siracusa, F., McGrath, M. A., Maschmeyer, P., Bardua, M., Lehmann, K., Heinz, G., Durek, P., Heinrich, F. F., Mashreghi, M. F., Chang, H. D., Tokoyoda, K., and Radbruch, A. (2018) Nonfollicular reactivation of bone marrow resident memory CD4 T cells in immune clusters of the bone marrow. *Proc Natl Acad Sci U S A* **115**, 1334-1339

106. Harari, A., Vallelian, F., and Pantaleo, G. (2004) Phenotypic heterogeneity of antigen-specific CD4 T cells under different conditions of antigen persistence and antigen load. *Eur J Immunol* **34**, 3525-3533

107. Mojtabavi, N., Dekan, G., Stingl, G., and Epstein, M. M. (2002) Long-lived Th2 memory in experimental allergic asthma. *J Immunol* **169**, 4788-4796

108. McGeachy, M. J. (2013) Th17 memory cells: live long and proliferate. *J Leukoc Biol* **94**, 921-926

109. Sallusto, F., Geginat, J., and Lanzavecchia, A. (2004) Central memory and effector memory T cell subsets: function, generation, and maintenance. *Annu Rev Immunol* **22**, 745-763

110. Sathaliyawala, T., Kubota, M., Yudanin, N., Turner, D., Camp, P., Thome, J. J., Bickham, K. L., Lerner, H., Goldstein, M., Sykes, M., Kato, T., and Farber, D. L. (2013) Distribution and compartmentalization of human circulating and tissue-resident memory T cell subsets. *Immunity* **38**, 187-197

111. Larbi, A., and Fulop, T. (2014) From "truly naïve" to "exhausted senescent" T cells: when markers predict functionality. *Cytometry A* **85**, 25-35

112. Henson, S. M., Macaulay, R., Riddell, N. E., Nunn, C. J., and Akbar, A. N. (2015) Blockade of PD-1 or p38 MAP kinase signaling enhances senescent human CD8(+) T-cell proliferation by distinct pathways. *Eur J Immunol* **45**, 1441-1451

113. Callender, L. A., Carroll, E. C., Beal, R. W. J., Chambers, E. S., Nourshargh, S., Akbar, A. N., and Henson, S. M. (2018) Human CD8(+) EMRA T cells display a senescence-associated secretory phenotype regulated by p38 MAPK. *Aging Cell* **17**

114. Merk, M., Mitchell, R. A., Endres, S., and Bucala, R. (2012) D-dopachrome tautomerase (D-DT or MIF-2): doubling the MIF cytokine family. *Cytokine* **59**, 10-17

115. Bloom, B. R., and Bennett, B. (1966) Mechanism of a reaction in vitro associated with delayed-type hypersensitivity. *Science* **153**, 80-82

116. Weiser, W. Y., Temple, P. A., Witek-Giannotti, J. S., Remold, H. G., Clark, S. C., and David, J. R. (1989) Molecular cloning of a cDNA encoding a human macrophage migration inhibitory factor. *Proc Natl Acad Sci U S A* **86**, 7522-7526

117. Bozza, M., Satoskar, A. R., Lin, G., Lu, B., Humbles, A. A., Gerard, C., and David, J. R. (1999) Targeted disruption of migration inhibitory factor gene reveals its critical role in sepsis. *J Exp Med* **189**, 341-346

118. Donn, R. P., Shelley, E., Ollier, W. E., and Thomson, W. (2001) A novel 5'-flanking region polymorphism of macrophage migration inhibitory factor is associated with systemic-onset juvenile idiopathic arthritis. *Arthritis Rheum* **44**, 1782-1785

119. Yang, J., Li, Y., and Zhang, X. (2015) Meta-analysis of macrophage migration inhibitory factor (MIF) gene -173G/C polymorphism and inflammatory bowel disease (IBD) risk. *Int J Clin Exp Med* **8**, 9570-9574

120. Shin, J. J., Fan, W., Par-Young, J., Piecychna, M., Leng, L., Israni-Winger, K., Qing, H., Gu, J., Zhao, H., Schulz, W. L., Unlu, S., Kuster, J., Young, G., Liu, J., Ko, A. I., Baeza Garcia, A., Sauler, M., Wisnewski, A. V., Young, L., Orduña, A., Wang, A., Ocskay, K., Garcia-Blesa, A., Hegyi, P., Armstrong, M. E., Mitchell, P. D., Bernardo, D., Garami, A., Kang, I., and Bucala, R. (2023) MIF is a common genetic determinant of COVID-19 symptomatic infection and severity. *Qjm* **116**, 205-212

121. Zhang, C., Ramsey, C., Berical, A., Yu, L., Leng, L., McGinnis, K. A., Song, Y., Michael, H., McCormack, M. C., Allore, H., Morris, A., Crothers, K., Bucala, R., Lee, P. J., and Sauler, M. (2019) A functional macrophage migration inhibitory factor promoter polymorphism is associated with reduced diffusing capacity. *Am J Physiol Lung Cell Mol Physiol* **316**, L400-l405

122. Rosengren, E., Bucala, R., Aman, P., Jacobsson, L., Odh, G., Metz, C. N., and Rorsman, H. (1996) The immunoregulatory mediator macrophage migration inhibitory factor (MIF) catalyzes a tautomerization reaction. *Mol Med* **2**, 143-149

123. Bernhagen, J., Mitchell, R. A., Calandra, T., Voelter, W., Cerami, A., and Bucala, R. (1994) Purification, bioactivity, and secondary structure analysis of mouse and human macrophage migration inhibitory factor (MIF). *Biochemistry* **33**, 14144-14155

124. Sun, H. W., Bernhagen, J., Bucala, R., and Lolis, E. (1996) Crystal structure at 2.6-A resolution of human macrophage migration inhibitory factor. *Proc Natl Acad Sci U S A* **93**, 5191-5196

125. David, J. R. (1966) Delayed hypersensitivity in vitro: its mediation by cell-free substances formed by lymphoid cell-antigen interaction. *Proc Natl Acad Sci U S A* **56**, 72-77

126. Jankauskas, S. S., Wong, D. W. L., Bucala, R., Djudjaj, S., and Boor, P. (2019) Evolving complexity of MIF signaling. *Cell Signal* **57**, 76-88

127. Calandra, T., Bernhagen, J., Mitchell, R. A., and Bucala, R. (1994) The macrophage is an important and previously unrecognized source of macrophage migration inhibitory factor. *J Exp Med* **179**, 1895-1902

128. Flieger, O., Engling, A., Bucala, R., Lue, H., Nickel, W., and Bernhagen, J. (2003) Regulated secretion of macrophage migration inhibitory factor is mediated by a non-classical pathway involving an ABC transporter. *FEBS Lett* **551**, 78-86

129. Eickhoff, R., Wilhelm, B., Renneberg, H., Wennemuth, G., Bacher, M., Linder, D., Bucala, R., Seitz, J., and Meinhardt, A. (2001) Purification and characterization of macrophage migration inhibitory factor as a secretory protein from rat epididymis: evidences for alternative release and transfer to spermatozoa. *Mol Med* **7**, 27-35

130. Merk, M., Baugh, J., Zierow, S., Leng, L., Pal, U., Lee, S. J., Ebert, A. D., Mizue, Y., Trent, J. O., Mitchell, R., Nickel, W., Kavathas, P. B., Bernhagen, J., and Bucala, R. (2009) The Golgi-associated protein p115 mediates the secretion of macrophage migration inhibitory factor. *J Immunol* **182**, 6896-6906

131. Baugh, J. A., and Bucala, R. (2002) Macrophage migration inhibitory factor. *Crit Care Med* **30**, S27-35

132. Lue, H., Kleemann, R., Calandra, T., Roger, T., and Bernhagen, J. (2002) Macrophage migration inhibitory factor (MIF): mechanisms of action and role in disease. *Microbes Infect* **4**, 449-460

133. Jones, P. P., Murphy, D. B., Hewgill, D., and McDevitt, H. O. (1979) Detection of a common polypeptide chain in I--A and I--E sub-region immunoprecipitates. *Mol Immunol* **16**, 51-60

134. Momburg, F., Koch, N., Möller, P., Moldenhauer, G., Butcher, G. W., and Hämmerling, G. J. (1986) Differential expression of Ia and Ia-associated invariant chain in mouse tissues after in vivo treatment with IFN-gamma. *J Immunol* **136**, 940-948

135. Kukol, A., Torres, J., and Arkin, I. T. (2002) A structure for the trimeric MHC class II-associated invariant chain transmembrane domain. *J Mol Biol* **320**, 1109-1117

136. Jasanoff, A., Wagner, G., and Wiley, D. C. (1998) Structure of a trimeric domain of the MHC class II-associated chaperonin and targeting protein Ii. *Embo j* **17**, 6812-6818

137. Shachar, I., Elliott, E. A., Chasnoff, B., Grewal, I. S., and Flavell, R. A. (1995) Reconstitution of invariant chain function in transgenic mice in vivo by individual p31 and p41 isoforms. *Immunity* **3**, 373-383

138. Schröder, B. (2016) The multifaceted roles of the invariant chain CD74--More than just a chaperone. *Biochim Biophys Acta* **1863**, 1269-1281

139. Arunachalam, B., Lamb, C. A., and Cresswell, P. (1994) Transport properties of free and MHC class II-associated oligomers containing different isoforms of human invariant chain. *Int Immunol* **6**, 439-451

140. Li, Q. L., Tang, J., Zhao, L., Ruze, A., Shan, X. F., and Gao, X. M. (2022) The role of CD74 in cardiovascular disease. *Front Cardiovasc Med* **9**, 1049143

141. Sung, E., and Jones, P. P. (1981) The invariant chain of murine Ia antigens: its glycosylation, abundance and subcellular localization. *Mol Immunol* **18**, 899-913

142. Naujokas, M. F., Morin, M., Anderson, M. S., Peterson, M., and Miller, J. (1993) The chondroitin sulfate form of invariant chain can enhance stimulation of T cell responses through interaction with CD44. *Cell* **74**, 257-268

143. Leng, L., Metz, C. N., Fang, Y., Xu, J., Donnelly, S., Baugh, J., Delohery, T., Chen, Y., Mitchell, R. A., and Bucala, R. (2003) MIF signal transduction initiated by binding to CD74. *J Exp Med* **197**, 1467-1476

144. Anderson, H. A., Bergstralh, D. T., Kawamura, T., Blauvelt, A., and Roche, P. A. (1999) Phosphorylation of the invariant chain by protein kinase C regulates MHC class II trafficking to antigen-processing compartments. *J Immunol* **163**, 5435-5443

145. Liu, Z., Chu, S., Yao, S., Li, Y., Fan, S., Sun, X., Su, L., and Liu, X. (2016) CD74 interacts with CD44 and enhances tumorigenesis and metastasis via RHOA-mediated cofilin phosphorylation in human breast cancer cells. *Oncotarget* **7**, 68303-68313

146. Hüttl, S., Helfrich, F., Mentrup, T., Held, S., Fukumori, A., Steiner, H., Saftig, P., Fluhrer, R., and Schröder, B. (2016) Substrate determinants of signal peptide peptidase-like 2a (SPPL2a)-mediated intramembrane proteolysis of the invariant chain CD74. *Biochem J* **473**, 1405-1422

147. Anderson, M. S., and Miller, J. (1992) Invariant chain can function as a chaperone protein for class II major histocompatibility complex molecules. *Proc Natl Acad Sci U S A* **89**, 2282-2286

148. Marks, M. S., Blum, J. S., and Cresswell, P. (1990) Invariant chain trimers are sequestered in the rough endoplasmic reticulum in the absence of association with HLA class II antigens. *J Cell Biol* **111**, 839-855

149. Kaufman, J. F., Auffray, C., Korman, A. J., Shackelford, D. A., and Strominger, J. (1984) The class II molecules of the human and murine major histocompatibility complex. *Cell* **36**, 1-13

150. Bijlmakers, M. J., Benaroch, P., and Ploegh, H. L. (1994) Mapping functional regions in the lumenal domain of the class II-associated invariant chain. *J Exp Med* **180**, 623-629

151. Roche, P. A., and Cresswell, P. (1990) Invariant chain association with HLA-DR molecules inhibits immunogenic peptide binding. *Nature* **345**, 615-618

152. Bakke, O., and Dobberstein, B. (1990) MHC class II-associated invariant chain contains a sorting signal for endosomal compartments. *Cell* **63**, 707-716

153. Odorizzi, C. G., Trowbridge, I. S., Xue, L., Hopkins, C. R., Davis, C. D., and Collawn, J. F. (1994) Sorting signals in the MHC class II invariant chain cytoplasmic tail and transmembrane region determine trafficking to an endocytic processing compartment. *J Cell Biol* **126**, 317-330

154. Pieters, J., Horstmann, H., Bakke, O., Griffiths, G., and Lipp, J. (1991) Intracellular transport and localization of major histocompatibility complex class II molecules and associated invariant chain. *J Cell Biol* **115**, 1213-1223

155. Mellins, E. D., and Stern, L. J. (2014) HLA-DM and HLA-DO, key regulators of MHC-II processing and presentation. *Curr Opin Immunol* **26**, 115-122

156. Basha, G., Omilusik, K., Chavez-Steenbock, A., Reinicke, A. T., Lack, N., Choi, K. B., and Jefferies, W. A. (2012) A CD74-dependent MHC class I endolysosomal cross-presentation pathway. *Nat Immunol* **13**, 237-245

157. Becker-Herman, S., Arie, G., Medvedovsky, H., Kerem, A., and Shachar, I. (2005) CD74 is a member of the regulated intramembrane proteolysis-processed protein family. *Mol Biol Cell* **16**, 5061-5069

158. Guncar, G., Pungercic, G., Klemencic, I., Turk, V., and Turk, D. (1999) Crystal structure of MHC class II-associated p41 Ii fragment bound to cathepsin L reveals the structural basis for differentiation between cathepsins L and S. *Embo j* **18**, 793-803

159. Mihelic, M., Dobersek, A., Guncar, G., and Turk, D. (2008) Inhibitory fragment from the p41 form of invariant chain can regulate activity of cysteine cathepsins in antigen presentation. *J Biol Chem* **283**, 14453-14460

160. Annaert, W. G., and Saftig, P. (2009) Regulated intramembrane proteolysis--a story about sheddases and I-CliPs. *Semin Cell Dev Biol* **20**, 125

161. Beisner, D. R., Langerak, P., Parker, A. E., Dahlberg, C., Otero, F. J., Sutton, S. E., Poirot, L., Barnes, W., Young, M. A., Niessen, S., Wiltshire, T., Bodendorf, U., Martoglio, B., Cravatt, B., and Cooke, M. P. (2013) The intramembrane protease Sppl2a is required for B cell and DC development and survival via cleavage of the invariant chain. *J Exp Med* **210**, 23-30

162. Schneppenheim, J., Dressel, R., Hüttl, S., Lüllmann-Rauch, R., Engelke, M., Dittmann, K., Wienands, J., Eskelinen, E. L., Hermans-Borgmeyer, I., Fluhrer, R., Saftig, P., and Schröder, B. (2013) The intramembrane protease SPPL2a promotes B cell development and controls endosomal traffic by cleavage of the invariant chain. *J Exp Med* **210**, 41-58

163. Matza, D., Wolstein, O., Dikstein, R., and Shachar, I. (2001) Invariant chain induces B cell maturation by activating a TAF(II)105-NF-kappaB-dependent transcription program. *J Biol Chem* **276**, 27203-27206

164. Gil-Yarom, N., Radomir, L., Sever, L., Kramer, M. P., Lewinsky, H., Bornstein, C., Blecher-Gonen, R., Barnett-Itzhaki, Z., Mirkin, V., Friedlander, G., Shvidel, L., Herishanu, Y., Lolis, E. J., Becker-Herman, S., Amit, I., and Shachar, I. (2017) CD74 is a novel transcription regulator. *Proc Natl Acad Sci U S A* **114**, 562-567

165. Shi, X., Leng, L., Wang, T., Wang, W., Du, X., Li, J., McDonald, C., Chen, Z., Murphy, J. W., Lolis, E., Noble, P., Knudson, W., and Bucala, R. (2006) CD44 is the signaling component of the macrophage migration inhibitory factor-CD74 receptor complex. *Immunity* **25**, 595-606

166. Gore, Y., Starlets, D., Maharshak, N., Becker-Herman, S., Kaneyuki, U., Leng, L., Bucala, R., and Shachar, I. (2008) Macrophage migration inhibitory factor induces B cell survival by activation of a CD74-CD44 receptor complex. *J Biol Chem* **283**, 2784-2792

167. Sánchez-Zuno, G. A., Bucala, R., Hernández-Bello, J., Román-Fernández, I. V., García-Chagollán, M., Nicoletti, F., Matuz-Flores, M. G., García-Arellano, S., Esparza-Michel, J. A., Cerpa-Cruz, S., Pérez-Guerrero, E. E., and Muñoz-Valle, J. F. (2021) Canonical (CD74/CD44)

and non-canonical (CXCR2, 4 and 7) MIF receptors are differentially expressed in rheumatoid arthritis patients evaluated by DAS28-ESR. *J Clin Med* **11**

168. Yoo, S. A., Leng, L., Kim, B. J., Du, X., Tilstam, P. V., Kim, K. H., Kong, J. S., Yoon, H. J., Liu, A., Wang, T., Song, Y., Sauler, M., Bernhagen, J., Ritchlin, C. T., Lee, P., Cho, C. S., Kim, W. U., and Bucala, R. (2016) MIF allele-dependent regulation of the MIF coreceptor CD44 and role in rheumatoid arthritis. *Proc Natl Acad Sci U S A* **113**, E7917-e7926

169. Voss, S., Krüger, S., Scherschel, K., Warnke, S., Schwarzl, M., Schrage, B., Girdauskas, E., Meyer, C., Blankenberg, S., Westermann, D., and Lindner, D. (2019) Macrophage migration inhibitory factor (MIF) expression increases during myocardial infarction and supports pro-Inflammatory signaling in cardiac fibroblasts. *Biomolecules* **9**

170. Miller, E. J., Li, J., Leng, L., McDonald, C., Atsumi, T., Bucala, R., and Young, L. H. (2008) Macrophage migration inhibitory factor stimulates AMP-activated protein kinase in the ischaemic heart. *Nature* **451**, 578-582

171. Ma, H., Wang, J., Thomas, D. P., Tong, C., Leng, L., Wang, W., Merk, M., Zierow, S., Bernhagen, J., Ren, J., Bucala, R., and Li, J. (2010) Impaired macrophage migration inhibitory factor-AMP-activated protein kinase activation and ischemic recovery in the senescent heart. *Circulation* **122**, 282-292

172. Bernhagen, J., Krohn, R., Lue, H., Gregory, J. L., Zernecke, A., Koenen, R. R., Dewor, M., Georgiev, I., Schober, A., Leng, L., Kooistra, T., Fingerle-Rowson, G., Ghezzi, P., Kleemann, R., McColl, S. R., Bucala, R., Hickey, M. J., and Weber, C. (2007) MIF is a noncognate ligand of CXC chemokine receptors in inflammatory and atherogenic cell recruitment. *Nat Med* **13**, 587-596

173. Günther, S., Fagone, P., Jalce, G., Atanasov, A. G., Guignabert, C., and Nicoletti, F. (2019) Role of MIF and D-DT in immune-inflammatory, autoimmune, and chronic respiratory diseases: from pathogenic factors to therapeutic targets. *Drug Discov Today* **24**, 428-439

174. Westmeier, J., Brochtrup, A., Paniskaki, K., Karakoese, Z., Werner, T., Sutter, K., Dolff, S., Limmer, A., Mittermüller, D., Liu, J., Zheng, X., Koval, T., Kaidashev, I., Berger, M. M., Herbstreit, F., Brenner, T., Witzke, O., Trilling, M., Lu, M., Yang, D., Babel, N., Westhoff, T., Dittmer, U., and Zelinskyy, G. (2023) Macrophage migration inhibitory factor receptor CD74 expression is associated with expansion and differentiation of effector T cells in COVID-19 patients. *Front Immunol* **14**, 1236374

175. Borghese, F., and Clanchy, F. I. (2011) CD74: an emerging opportunity as a therapeutic target in cancer and autoimmune disease. *Expert Opin Ther Targets* **15**, 237-251

176. Starlets, D., Gore, Y., Binsky, I., Haran, M., Harpaz, N., Shvidel, L., Becker-Herman, S., Berrebi, A., and Shachar, I. (2006) Cell-surface CD74 initiates a signaling cascade leading to cell proliferation and survival. *Blood* **107**, 4807-4816

177. Klasen, C., Ohl, K., Sternkopf, M., Shachar, I., Schmitz, C., Heussen, N., Hobeika, E., Levit-Zerdoun, E., Tenbrock, K., Reth, M., Bernhagen, J., and El Bounkari, O. (2014) MIF promotes B cell chemotaxis through the receptors CXCR4 and CD74 and ZAP-70 signaling. *J Immunol* **192**, 5273-5284

178. Han, X., Shi, H., Sun, Y., Shang, C., Luan, T., Wang, D., Ba, X., and Zeng, X. (2019) CXCR2 expression on granulocyte and macrophage progenitors under tumor conditions contributes to mo-MDSC generation via SAP18/ERK/STAT3. *Cell Death Dis* **10**, 598

179. Zhou, S. L., Zhou, Z. J., Hu, Z. Q., Li, X., Huang, X. W., Wang, Z., Fan, J., Dai, Z., and Zhou, J. (2015) CXCR2/CXCL5 axis contributes to epithelial-mesenchymal transition of HCC cells through activating PI3K/Akt/GSK-3β/Snail signaling. *Cancer Lett* **358**, 124-135

180. Goczalik, I., Ulbricht, E., Hollborn, M., Raap, M., Uhlmann, S., Weick, M., Pannicke, T., Wiedemann, P., Bringmann, A., Reichenbach, A., and Francke, M. (2008) Expression of CXCL8, CXCR1, and CXCR2 in neurons and glial cells of the human and rabbit retina. *Invest Ophthalmol Vis Sci* **49**, 4578-4589

181. Sherwood, J., Bertrand, J., Nalesso, G., Poulet, B., Pitsillides, A., Brandolini, L., Karystinou, A., De Bari, C., Luyten, F. P., Pitzalis, C., Pap, T., and Dell'Accio, F. (2015) A homeostatic function of CXCR2 signalling in articular cartilage. *Ann Rheum Dis* **74**, 2207-2215

182. Kraemer, S., Lue, H., Zernecke, A., Kapurniotu, A., Andreetto, E., Frank, R., Lennartz, B., Weber, C., and Bernhagen, J. (2011) MIF-chemokine receptor interactions in atherogenesis are dependent on an N-loop-based 2-site binding mechanism. *Faseb j* **25**, 894-906

183. Weber, C., Kraemer, S., Drechsler, M., Lue, H., Koenen, R. R., Kapurniotu, A., Zernecke, A., and Bernhagen, J. (2008) Structural determinants of MIF functions in CXCR2-mediated inflammatory and atherogenic leukocyte recruitment. *Proc Natl Acad Sci U S A* **105**, 16278-16283

184. Zhang, H., Ye, Y. L., Li, M. X., Ye, S. B., Huang, W. R., Cai, T. T., He, J., Peng, J. Y., Duan, T. H., Cui, J., Zhang, X. S., Zhou, F. J., Wang, R. F., and Li, J. (2017) CXCL2/MIF-CXCR2 signaling promotes the recruitment of myeloid-derived suppressor cells and is correlated with prognosis in bladder cancer. *Oncogene* **36**, 2095-2104

185. Schindler, L., Zwissler, L., Krammer, C., Hendgen-Cotta, U., Rassaf, T., Hampton, M. B., Dickerhof, N., and Bernhagen, J. (2021) Macrophage migration inhibitory factor inhibits neutrophil apoptosis by inducing cytokine release from mononuclear cells. *J Leukoc Biol* **110**, 893-905

186. Gregory, J. L., Morand, E. F., McKeown, S. J., Ralph, J. A., Hall, P., Yang, Y. H., McColl, S. R., and Hickey, M. J. (2006) Macrophage migration inhibitory factor induces macrophage recruitment via CC chemokine ligand 2. *J Immunol* **177**, 8072-8079

187. Dumitru, C. A., Gholaman, H., Trellakis, S., Bruderek, K., Dominas, N., Gu, X., Bankfalvi, A., Whiteside, T. L., Lang, S., and Brandau, S. (2011) Tumor-derived macrophage migration inhibitory factor modulates the biology of head and neck cancer cells via neutrophil activation. *Int J Cancer* **129**, 859-869

188. Chevalier, N., Jarrossay, D., Ho, E., Avery, D. T., Ma, C. S., Yu, D., Sallusto, F., Tangye, S. G., and Mackay, C. R. (2011) CXCR5 expressing human central memory CD4 T cells and their relevance for humoral immune responses. *J Immunol* **186**, 5556-5568

189. Muehlinghaus, G., Cigliano, L., Huehn, S., Peddinghaus, A., Leyendeckers, H., Hauser, A. E., Hiepe, F., Radbruch, A., Arce, S., and Manz, R. A. (2005) Regulation of CXCR3 and CXCR4 expression during terminal differentiation of memory B cells into plasma cells. *Blood* **105**, 3965-3971

190. Aiuti, A., Turchetto, L., Cota, M., Cipponi, A., Brambilla, A., Arcelloni, C., Paroni, R., Vicenzi, E., Bordignon, C., and Poli, G. (1999) Human CD34(+) cells express CXCR4 and its ligand stromal cell-derived factor-1. Implications for infection by T-cell tropic human immunodeficiency virus. *Blood* **94**, 62-73

191. Lavi, E., Strizki, J. M., Ulrich, A. M., Zhang, W., Fu, L., Wang, Q., O'Connor, M., Hoxie, J. A., and González-Scarano, F. (1997) CXCR-4 (Fusin), a co-receptor for the type 1 human immunodeficiency virus (HIV-1), is expressed in the human brain in a variety of cell types, including microglia and neurons. *Am J Pathol* **151**, 1035-1042

192. Balkwill, F. (2004) The significance of cancer cell expression of the chemokine receptor CXCR4. *Semin Cancer Biol* **14**, 171-179

193. Zhou, W., Guo, S., Liu, M., Burow, M. E., and Wang, G. (2019) Targeting CXCL12/CXCR4 axis in tumor immunotherapy. *Curr Med Chem* **26**, 3026-3041

194. Caspar, B., Cocchiara, P., Melet, A., Van Emelen, K., Van der Aa, A., Milligan, G., and Herbeuval, J. P. (2022) CXCR4 as a novel target in immunology: moving away from typical antagonists. *Future Drug Discov* **4**, Fdd77

195. Rajasekaran, D., Gröning, S., Schmitz, C., Zierow, S., Drucker, N., Bakou, M., Kohl, K., Mertens, A., Lue, H., Weber, C., Xiao, A., Luker, G., Kapurniotu, A., Lolis, E., and Bernhagen, J. (2016) Macrophage migration inhibitory factor-CXCR4 receptor Interactions: evidence for partial allosteric agonism in comparison with CXCL12 chemokine. *J Biol Chem* **291**, 15881-15895

196. Döring, Y., Noels, H., van der Vorst, E. P. C., Neideck, C., Egea, V., Drechsler, M., Mandl, M., Pawig, L., Jansen, Y., Schröder, K., Bidzhekov, K., Megens, R. T. A., Theelen, W., Klinkhammer, B. M., Boor, P., Schurgers, L., van Gorp, R., Ries, C., Kusters, P. J. H., van der Wal, A., Hackeng, T. M., Gäbel, G., Brandes, R. P., Soehnlein, O., Lutgens, E., Vestweber, D., Teupser, D., Holdt, L. M., Rader, D. J., Saleheen, D., and Weber, C. (2017) Vascular CXCR4 limits atherosclerosis by maintaining arterial integrity: evidence from mouse and human studies. *Circulation* **136**, 388-403

197. Döring, Y., Pawig, L., Weber, C., and Noels, H. (2014) The CXCL12/CXCR4 chemokine ligand/receptor axis in cardiovascular disease. *Front Physiol* **5**, 212

198. Kontos, C., El Bounkari, O., Krammer, C., Sinitski, D., Hille, K., Zan, C., Yan, G., Wang, S., Gao, Y., Brandhofer, M., Megens, R. T. A., Hoffmann, A., Pauli, J., Asare, Y., Gerra, S., Bourilhon, P., Leng, L., Eckstein, H. H., Kempf, W. E., Pelisek, J., Gokce, O., Maegdefessel, L., Bucala, R., Dichgans, M., Weber, C., Kapurniotu, A., and Bernhagen, J. (2020) Designed CXCR4 mimic acts as a soluble chemokine receptor that blocks atherogenic inflammation by agonist-specific targeting. *Nat Commun* **11**, 5981

199. Lourenco, S., Teixeira, V. H., Kalber, T., Jose, R. J., Floto, R. A., and Janes, S. M. (2015) Macrophage migration inhibitory factor-CXCR4 is the dominant chemotactic axis in human mesenchymal stem cell recruitment to tumors. *J Immunol* **194**, 3463-3474

200. Schwartz, V., Lue, H., Kraemer, S., Korbiel, J., Krohn, R., Ohl, K., Bucala, R., Weber, C., and Bernhagen, J. (2009) A functional heteromeric MIF receptor formed by CD74 and CXCR4. *FEBS Lett* **583**, 2749-2757

201. Tarnowski, M., Grymula, K., Liu, R., Tarnowska, J., Drukala, J., Ratajczak, J., Mitchell, R. A., Ratajczak, M. Z., and Kucia, M. (2010) Macrophage migration inhibitory factor is secreted by rhabdomyosarcoma cells, modulates tumor metastasis by binding to CXCR4 and CXCR7 receptors and inhibits recruitment of cancer-associated fibroblasts. *Mol Cancer Res* **8**, 1328-1343

202. Tillmann, S., Bernhagen, J., and Noels, H. (2013) Arrest Functions of the MIF Ligand/Receptor Axes in Atherogenesis. *Front Immunol* **4**, 115

203. Ishizuka, M., Harada, M., Nomura, S., Ko, T., Ikeda, Y., Guo, J., Bujo, S., Yanagisawa-Murakami, H., Satoh, M., Yamada, S., Kumagai, H., Motozawa, Y., Hara, H., Fujiwara, T., Sato, T., Takeda, N., Takeda, N., Otsu, K., Morita, H., Toko, H., and Komuro, I. (2021) CXCR7 ameliorates myocardial infarction as a β-arrestin-biased receptor. *Sci Rep* **11**, 3426

204. Lounsbury, N. (2020) Advances in CXCR7 Modulators. *Pharmaceuticals (Basel)* **13**

205. Naumann, U., Cameroni, E., Pruenster, M., Mahabaleshwar, H., Raz, E., Zerwes, H. G., Rot, A., and Thelen, M. (2010) CXCR7 functions as a scavenger for CXCL12 and CXCL11. *PLoS One* **5**, e9175

206. Koch, C., and Engele, J. (2020) Functions of the CXCL12 Receptor ACKR3/CXCR7-What Has Been Perceived and What Has Been Overlooked. *Mol Pharmacol* **98**, 577-585

207. Betterman, K. L., and Harvey, N. L. (2014) Decoys and cardiovascular development: CXCR7 and regulation of adrenomedullin signaling. *Dev Cell* **30**, 490-491

208. Levoye, A., Balabanian, K., Baleux, F., Bachelerie, F., and Lagane, B. (2009) CXCR7 heterodimerizes with CXCR4 and regulates CXCL12-mediated G protein signaling. *Blood* **113**, 6085-6093

209. Alampour-Rajabi, S., El Bounkari, O., Rot, A., Müller-Newen, G., Bachelerie, F., Gawaz, M., Weber, C., Schober, A., and Bernhagen, J. (2015) MIF interacts with CXCR7 to promote receptor internalization, ERK1/2 and ZAP-70 signaling, and lymphocyte chemotaxis. *Faseb j* **29**, 4497-4511

210. Bloom, J., Sun, S., and Al-Abed, Y. (2016) MIF, a controversial cytokine: a review of structural features, challenges, and opportunities for drug development. *Expert Opin Ther Targets* **20**, 1463-1475

211. Michelet, C., Danchin, E. G. J., Jaouannet, M., Bernhagen, J., Panstruga, R., Kogel, K. H., Keller, H., and Coustau, C. (2019) Cross-kingdom analysis of diversity, evolutionary history,

and site selection within the eukaryotic macrophage migration inhibitory factor superfamily. *Genes (Basel)* **10**

212. Baeza Garcia, A., Siu, E., Sun, T., Exler, V., Brito, L., Hekele, A., Otten, G., Augustijn, K., Janse, C. J., Ulmer, J. B., Bernhagen, J., Fikrig, E., Geall, A., and Bucala, R. (2018) Neutralization of the Plasmodium-encoded MIF ortholog confers protective immunity against malaria infection. *Nat Commun* **9**, 2714

213. Panstruga, R., Baumgarten, K., and Bernhagen, J. (2015) Phylogeny and evolution of plant macrophage migration inhibitory factor/D-dopachrome tautomerase-like proteins. *BMC Evol Biol* **15**, 64

214. Sinitski, D., Gruner, K., Brandhofer, M., Kontos, C., Winkler, P., Reinstädler, A., Bourilhon, P., Xiao, Z., Cool, R., Kapurniotu, A., Dekker, F. J., Panstruga, R., and Bernhagen, J. (2020) Cross-kingdom mimicry of the receptor signaling and leukocyte recruitment activity of a human cytokine by its plant orthologs. *J Biol Chem* **295**, 850-867

215. Gruner, K., Leissing, F., Sinitski, D., Thieron, H., Axstmann, C., Baumgarten, K., Reinstädler, A., Winkler, P., Altmann, M., Flatley, A., Jaouannet, M., Zienkiewicz, K., Feussner, I., Keller, H., Coustau, C., Falter-Braun, P., Feederle, R., Bernhagen, J., and Panstruga, R. (2021) Chemokine-like MDL proteins modulate flowering time and innate immunity in plants. *J Biol Chem* **296**, 100611

216. Bacher, M., Metz, C. N., Calandra, T., Mayer, K., Chesney, J., Lohoff, M., Gemsa, D., Donnelly, T., and Bucala, R. (1996) An essential regulatory role for macrophage migration inhibitory factor in T-cell activation. *Proc Natl Acad Sci U S A* **93**, 7849-7854

217. Stavitsky, A. B., and Xianli, J. (2002) In vitro and in vivo regulation by macrophage migration inhibitory factor (MIF) of expression of MHC-II, costimulatory, adhesion, receptor, and cytokine molecules. *Cell Immunol* **217**, 95-104

218. Sánchez-Zamora, Y. I., Juarez-Avelar, I., Vazquez-Mendoza, A., Hiriart, M., and Rodriguez-Sosa, M. (2016) Altered macrophage and dendritic cell response in Mif-/- mice reveals a role of Mif for inflammatory-Th1 response in Type 1 Diabetes. *J Diabetes Res* **2016**, 7053963

219. Alibashe-Ahmed, M., Roger, T., Serre-Beinier, V., Berishvili, E., Reith, W., Bosco, D., and Berney, T. (2019) Macrophage migration inhibitory factor regulates TLR4 expression and modulates TCR/CD3-mediated activation in CD4+ T lymphocytes. *Sci Rep* **9**, 9380

220. Koebernick, H., Grode, L., David, J. R., Rohde, W., Rolph, M. S., Mittrücker, H. W., and Kaufmann, S. H. (2002) Macrophage migration inhibitory factor (MIF) plays a pivotal role in immunity against Salmonella typhimurium. *Proc Natl Acad Sci U S A* **99**, 13681-13686

221. Cox, G. M., Kithcart, A. P., Pitt, D., Guan, Z., Alexander, J., Williams, J. L., Shawler, T., Dagia, N. M., Popovich, P. G., Satoskar, A. R., and Whitacre, C. C. (2013) Macrophage migration inhibitory factor potentiates autoimmune-mediated neuroinflammation. *J Immunol* **191**, 1043-1054

222. Das, R., Moss, J. E., Robinson, E., Roberts, S., Levy, R., Mizue, Y., Leng, L., McDonald, C., Tigelaar, R. E., Herrick, C. A., and Bucala, R. (2011) Role of macrophage migration inhibitory factor in the Th2 immune response to epicutaneous sensitization. *J Clin Immunol* **31**, 666-680

223. Choi, S., Kim, H. R., Leng, L., Kang, I., Jorgensen, W. L., Cho, C. S., Bucala, R., and Kim, W. U. (2012) Role of macrophage migration inhibitory factor in the regulatory T cell response of tumor-bearing mice. *J Immunol* **189**, 3905-3913

224. Gajic, D., Koprivica, I., Stojanovic, I., and Saksida, T. (2021) Defective immunosuppressive function of Treg cells in visceral adipose tissue in MIF deficient mice. *Cytokine* **138**, 155372

225. De la Cruz-Mosso, U., García-Iglesias, T., Bucala, R., Estrada-García, I., González-López, L., Cerpa-Cruz, S., Parra-Rojas, I., Gámez-Nava, J. I., Pérez-Guerrero, E. E., and Muñoz-Valle, J. F. (2018) MIF promotes a differential Th1/Th2/Th17 inflammatory response in human primary cell cultures: Predominance of Th17 cytokine profile in PBMC from healthy subjects and increase of IL-6 and TNF-α in PBMC from active SLE patients. *Cell Immunol* **324**, 42-49

226. Trifone, C., Baquero, L., Czernikier, A., Benencio, P., Leng, L., Laufer, N., Quiroga, M. F., Bucala, R., Ghiglione, Y., and Turk, G. (2022) Macrophage migration inhibitory factor (MIF)

promotes increased proportions of the highly permissive Th17-like cell profile during HIV infection. *Viruses* **14**

227. Liu, Z., Li, Z., Yan, G., Lin, C., Luo, Y., Ye, Y., Zeng, X., and Yao, J. (2023) MIF promotes Th17 cell differentiation in Hashimoto's thyroiditis by binding HVEM and activating NF-κB signaling pathway. *Int Immunopharmacol* **121**, 110494

228. Li, J., Mo, H. Y., Xiong, G., Zhang, L., He, J., Huang, Z. F., Liu, Z. W., Chen, Q. Y., Du, Z. M., Zheng, L. M., Qian, C. N., and Zeng, Y. X. (2012) Tumor microenvironment macrophage inhibitory factor directs the accumulation of interleukin-17-producing tumor-infiltrating lymphocytes and predicts favorable survival in nasopharyngeal carcinoma patients. *J Biol Chem* **287**, 35484-35495

229. Mo, H., Monard, S., Pollack, H., Ip, J., Rochford, G., Wu, L., Hoxie, J., Borkowsky, W., Ho, D. D., and Moore, J. P. (1998) Expression patterns of the HIV type 1 coreceptors CCR5 and CXCR4 on CD4+ T cells and monocytes from cord and adult blood. *AIDS Res Hum Retroviruses* **14**, 607-617

230. Bermejo, M., Martín-Serrano, J., Oberlin, E., Pedraza, M. A., Serrano, A., Santiago, B., Caruz, A., Loetscher, P., Baggiolini, M., Arenzana-Seisdedos, F., and Alcami, J. (1998) Activation of blood T lymphocytes down-regulates CXCR4 expression and interferes with propagation of X4 HIV strains. *Eur J Immunol* **28**, 3192-3204

231. Bleul, C. C., Wu, L., Hoxie, J. A., Springer, T. A., and Mackay, C. R. (1997) The HIV coreceptors CXCR4 and CCR5 are differentially expressed and regulated on human T lymphocytes. *Proc Natl Acad Sci U S A* **94**, 1925-1930

232. Feng, Y., Broder, C. C., Kennedy, P. E., and Berger, E. A. (1996) HIV-1 entry cofactor: functional cDNA cloning of a seven-transmembrane, G protein-coupled receptor. *Science* **272**, 872-877

233. Ottoson, N. C., Pribila, J. T., Chan, A. S., and Shimizu, Y. (2001) Cutting edge: T cell migration regulated by CXCR4 chemokine receptor signaling to ZAP-70 tyrosine kinase. *J Immunol* **167**, 1857-1861

234. Yang, L., Kong, Y., Ren, H., Li, M., Wei, C. J., Shi, E., Jin, W. N., Hao, J., Vandenbark, A. A., and Offner, H. (2017) Upregulation of CD74 and its potential association with disease severity in subjects with ischemic stroke. *Neurochem Int* **107**, 148-155

235. Fagone, P., Mazzon, E., Cavalli, E., Bramanti, A., Petralia, M. C., Mangano, K., Al-Abed, Y., Bramati, P., and Nicoletti, F. (2018) Contribution of the macrophage migration inhibitory factor superfamily of cytokines in the pathogenesis of preclinical and human multiple sclerosis: In silico and in vivo evidences. *J Neuroimmunol* **322**, 46-56

236. Kaku, S., Nguyen, C. D., Htet, N. N., Tutera, D., Barr, J., Paintal, H. S., and Kuschner, W. G. (2020) Acute respiratory distress syndrome: etiology, pathogenesis, and summary on management. *J Intensive Care Med* **35**, 723-737

237. Bellani, G., Laffey, J. G., Pham, T., Fan, E., Brochard, L., Esteban, A., Gattinoni, L., van Haren, F., Larsson, A., McAuley, D. F., Ranieri, M., Rubenfeld, G., Thompson, B. T., Wrigge, H., Slutsky, A. S., and Pesenti, A. (2016) Epidemiology, patterns of care, and mortality for patients with acute respiratory distress syndrome in intensive care units in 50 countries. *Jama* **315**, 788-800

238. Wu, C., Chen, X., Cai, Y., Xia, J., Zhou, X., Xu, S., Huang, H., Zhang, L., Zhou, X., Du, C., Zhang, Y., Song, J., Wang, S., Chao, Y., Yang, Z., Xu, J., Zhou, X., Chen, D., Xiong, W., Xu, L., Zhou, F., Jiang, J., Bai, C., Zheng, J., and Song, Y. (2020) Risk factors associated with acute respiratory distress syndrome and death in patients with coronavirus disease 2019 pneumonia in Wuhan, China. *JAMA Intern Med* **180**, 934-943

239. Govender, M., Hopkins, F. R., Göransson, R., Svanberg, C., Shankar, E. M., Hjorth, M., Nilsdotter-Augustinsson, Å., Sjöwall, J., Nyström, S., and Larsson, M. (2022) T cell perturbations persist for at least 6 months following hospitalization for COVID-19. *Front Immunol* **13**, 931039

240.	Kuri-Cervantes, L., Pampena, M. B., Meng, W., Rosenfeld, A. M., Ittner, C. A. G., Weisman, A. R., Agyekum, R. S., Mathew, D., Baxter, A. E., Vella, L. A., Kuthuru, O., Apostolidis, S. A., Bershaw, L., Dougherty, J., Greenplate, A. R., Pattekar, A., Kim, J., Han, N., Gouma, S., Weirick, M. E., Arevalo, C. P., Bolton, M. J., Goodwin, E. C., Anderson, E. M., Hensley, S. E., Jones, T. K., Mangalmurti, N. S., Luning Prak, E. T., Wherry, E. J., Meyer, N. J., and Betts, M. R. (2020) Comprehensive mapping of immune perturbations associated with severe COVID-19. *Sci Immunol* **5**

241.	Laing, A. G., Lorenc, A., Del Molino Del Barrio, I., Das, A., Fish, M., Monin, L., Muñoz-Ruiz, M., McKenzie, D. R., Hayday, T. S., Francos-Quijorna, I., Kamdar, S., Joseph, M., Davies, D., Davis, R., Jennings, A., Zlatareva, I., Vantourout, P., Wu, Y., Sofra, V., Cano, F., Greco, M., Theodoridis, E., Freedman, J. D., Gee, S., Chan, J. N. E., Ryan, S., Bugallo-Blanco, E., Peterson, P., Kisand, K., Haljasmägi, L., Chadli, L., Moingeon, P., Martinez, L., Merrick, B., Bisnauthsing, K., Brooks, K., Ibrahim, M. A. A., Mason, J., Lopez Gomez, F., Babalola, K., Abdul-Jawad, S., Cason, J., Mant, C., Seow, J., Graham, C., Doores, K. J., Di Rosa, F., Edgeworth, J., Shankar-Hari, M., and Hayday, A. C. (2020) A dynamic COVID-19 immune signature includes associations with poor prognosis. *Nat Med* **26**, 1623-1635

242.	Yang, S. C., Tsai, Y. F., Pan, Y. L., and Hwang, T. L. (2021) Understanding the role of neutrophils in acute respiratory distress syndrome. *Biomed J* **44**, 439-446

243.	Liu, Y., Du, X., Chen, J., Jin, Y., Peng, L., Wang, H. H. X., Luo, M., Chen, L., and Zhao, Y. (2020) Neutrophil-to-lymphocyte ratio as an independent risk factor for mortality in hospitalized patients with COVID-19. *J Infect* **81**, e6-e12

244.	Terpos, E., Ntanasis-Stathopoulos, I., Elalamy, I., Kastritis, E., Sergentanis, T. N., Politou, M., Psaltopoulou, T., Gerotziafas, G., and Dimopoulos, M. A. (2020) Hematological findings and complications of COVID-19. *Am J Hematol* **95**, 834-847

245.	Bleilevens, C., Soppert, J., Hoffmann, A., Breuer, T., Bernhagen, J., Martin, L., Stiehler, L., Marx, G., Dreher, M., Stoppe, C., and Simon, T. P. (2021) Macrophage migration inhibitory factor (MIF) plasma concentration in critically Ill COVID-19 patients: a prospective observational study. *Diagnostics (Basel)* **11**

246.	Lai, K. N., Leung, J. C., Metz, C. N., Lai, F. M., Bucala, R., and Lan, H. Y. (2003) Role for macrophage migration inhibitory factor in acute respiratory distress syndrome. *J Pathol* **199**, 496-508

247.	Donnelly, S. C., Haslett, C., Reid, P. T., Grant, I. S., Wallace, W. A., Metz, C. N., Bruce, L. J., and Bucala, R. (1997) Regulatory role for macrophage migration inhibitory factor in acute respiratory distress syndrome. *Nat Med* **3**, 320-323

Acknowledgements

I would like to begin by expressing my deepest gratitude to Univ.-Prof. Dr. rer. nat. Jürgen Bernhagen for granting me the invaluable opportunity to join his laboratory and pursue my PhD studies. Over the past five years, I have grown from an inexperienced newcomer to an independent researcher, and this transformation would not have been possible without his constant support and mentorship. I am sincerely grateful for his profound academic expertise, rigorous work ethic, and sharp scientific insight, which have significantly influenced my growth. I am also deeply appreciative of Dr. med. Adrian Hoffmann. Dr. Hoffmann is a passionate and thoughtful individual, and without his tireless efforts in supporting me on project design, implementation, and problem-solving throughout the course of my PhD, I am certain that my journey would not have been as smooth. His dedication and proactive approach in addressing challenges were instrumental in overcoming obstacles and ensuring the successful completion of my research. I extend my heartfelt thanks to my TAC members, Prof. Dr. med. Patrick Scheiermann and Univ.-Prof. Dr. med. Markus Sperandio, for their invaluable guidance and support in directing the progress of my research.

Being part of the Bernhagen lab has been a privilege and honor, which has truly been a turning point in my life. This international and highly professional environment, filled with talented and welcoming colleagues, has greatly enriched my experience.

On a personal level, I am deeply grateful to Sabrina Lukanovic for her support with administrative, personal, and daily matters. In the daily life of the laboratory, I am especially grateful to Simona Gerra, Maida Avdic, and Roya Batool for their exceptional management of the lab's operations, which ensured a smooth and efficient working environment. Their dedication to crucial tasks such as the production of MIF/DDT and the management of animal care has been essential for the successful continuation of my experiments. I am also thankful to Dr. rer. nat. Omar El Bounkari for his insightful feedback during our group meetings, which has significantly contributed to the progress and advancement of my research.

For the T-cell project, I would like to thank Mathias Holzner for his patient guidance when I first joined the lab. His instruction on basic experimental techniques laid a strong foundation for my subsequent PhD research. I am also grateful to Iris Woltering for her contributions to the project and to Carl-Christian Schäfer, Simon Ebert, and Genta Bushati for their collaborative support. Special thanks go to Dr. rer. nat. Markus Brandhofer, whose technical expertise and patience were invaluable when challenges arose in certain parts of the project.

In my work on the ARDS project, I am grateful for the support provided by Andi Abdyli, and Zhishen Zhang. I also appreciate Chunfang Zan, Yuan Tian and Hao Ji for their valuable insights and assistance.

Beyond my academic endeavors, I am sincerely thankful to Chunfang Zan, Ying Gao, Yuan Tian, and Yue Yuan for their care and encouragement during difficult times. I also extend my heartfelt thanks to Ruibing Xia and Yingdong Wang for their support in daily life, which has brought me immense joy. Additionally, I would like to express my gratitude to Kailing Li and my cat, Lucas, whose companionship has been a great source of happiness and comfort.

Moreover, I would also like to express my gratitude to generative AI- ChatGPT and Claude. As a non-native English speaker, ChatGPT and Claude have been invaluable in refining my writing, significantly enhancing the quality of my work.

Most importantly, I wish to express my deepest gratitude to my parents. Their unconditional support and encouragement have been fundamental to my success over these five years.

Lastly, I am profoundly thankful to all the teachers, colleagues and friends who have supported and guided me throughout this journey. Meeting all of you has been one of the greatest blessings of my life, and your unwavering support has allowed me to overcome numerous challenges, leading to the successful completion of this dissertation.

I once read a quote: "I may not have always been excellent, but I have never given up." I am grateful to myself for persevering through this academic journey and for striving to grow and learn every step of the way.